DOCTOR OF PHILOSOPHY

Regulation of the Lipid Kinase VPS34 by mTOR-Mediated UVRAG Phosphorylation

Munson, Michael

Award date:
2014

REGULATION OF THE LIPID KINASE VPS34 BY MTOR-MEDIATED UVRAG PHOSPHORYLATION

Michael J. Munson

A THESIS SUBMITTED FOR THE DEGREE OF DOCTOR OF PHILOSOPHY,

UNIVERSITY OF DUNDEE

OCTOBER 2014

I. CONTENTS

II. LIST OF FIGURES

III. LIST OF TABLES

IV. ACKNOWLEDGEMENTS

First and foremost I would like to thank Ian for giving me the opportunity to join his laboratory and work on such an intriguing project. Despite the ups and downs of science it has been an extremely rewarding experience to have been able to utilise such a breadth of techniques in the course of my PhD and I sincerely appreciate the support and advice from Ian throughout.

Secondly I would like to thank the members of the Ganley lab, past and present, for their profound science knowledge, support and making the lab such an enjoyable environment to work in. I couldn't imagine a friendlier group of people to work with.

I also owe a huge amount of gratitude to support staff throughout the MRC and DSTT, without whom my project would not have reached the stage it has. I also have to extend my thanks to the rest of the MRC unit and members of the college for their help and suggestions.

Finally, I have to thank my family and Kirstin for their constant support throughout my PhD and particularly in the last couple of months. I also appreciate the concern held by my parents regarding the wellbeing of my cells.

V. DECLARATIONS

I hereby declare that the following thesis is based on the results of investigations conducted by myself and that this thesis is of my own composition. Work other than my own is clearly indicated in the text by reference to the researchers or their publications. This dissertation has not in whole, or in part, been previously presented for a higher degree.

Michael J. Munson

I certify that Michael Munson has spent the equivalent of at least nine terms in research work in the College of Life Sciences, University of Dundee and that he has fulfilled the conditions of the Ordinance General No. 14 of the University of Dundee and is qualified to submit the accompanying thesis in application for the degree of Doctor of Philosophy.

Ian G. Ganley

VI. ABBREVIATIONS

4E-BP1	eIF4E-binding protein 1
ACN	Acetonitrile
ALR	Autophagic lysosome reformation
AMPK	5'AMP-activated protein kinase
AP	Adaptor Protein Complex
APPL1	Adaptor protein, phosphotyrosine interaction PH domain and leucine zipper containing 1
ARF	ADP-Ribosylation Factor
ATG14L	Atg14 like
ATP	Adenosine triphosphate
BATS	Barkor/ATG14L autophagosome targeting sequence
Bif-1	Endophilin-B1
CCD	Coiled-coil domain
CLEAR	Coordinated lysosomal expression and regulation
CMA	Chaperone-mediate autophagy
CME	Clathrin mediated endocytosis
CPY	Carboxypeptidase Y
DEPTOR	DEP domain-containing mTOR-interacting protein
DNA-PK	DNA-dependent protein kinase
DSTT	Division of Signal Transduction Therapy
DTT	Dithiothreitol
EBSS	Earle’s balanced salt solution
ECD	Evolutionary conserved domain
ECL	Enhanced chemiluminescence
EEA1	Early endosome antigen 1
EGF	Epidermal growth factor
EGFR	Epidermal growth factor receptor
ER	Endoplasmic reticulum
FBS	Foetal bovine serum
FYVE	Fab1, YOTB, Vac1 and EEA1 zinc finger binding domain
GAP	GTPase-activating protein
GEF	Guanine nucleotide exchange factor
GFP	Green fluorescent protein
HCQ	Hydroxychloroquine
HRS	Hepatocyte growth factor regulated tyrosine kinase substrate
HSC70	Heat shock cognate protein of 70 kDa
IF	Immunofluorescence
IGF-1	Insulin-like growth factor 1
IP	Immunoprecipitation
IR	Insulin Receptor
ILVs	Intraluminal vesicles
LAMP1	Lysosome associated membrane protein 1
LKA	Lipid kinase assay
LSD	Lysosomal storage disease
M6PR	Mannose-6-phosphate receptor
MEFs	Mouse embryonic fibroblasts
mLST8	Mammalian lethal with SEC13 protein 8

mSIN1	Mammalian stress-activated protein kinase interacting protein
mTOR	Mechanistic target of rapamycin
mTORC1	mTOR complex 1
mTORC2	mTOR complex 2
MVB	Multivesicular body
NCE	Non-clathrin endocytosis
PADK	Z-Phe-Ala-diazomethylketone
PDK1	PtdIns(3,4,5)P3-dependent protein kinase-1
PEI	Polyethylenimine
PH Domain	Plecstrin homology domain
PI	Phosphatidylinositol
PIK	Phosphatidylinositol kinase
PI3K	Phosphatidylinositol-3-kinase
PI3KC1	Phosphatidylinositol-3-kinase class I
PI(3)P	Phosphatidylinositol-3-phosphate
PKB or AKT	Protein kinase B
PKC	Protein kinase C
PMSF	Phenylmethanesulfonyl fluoride
PNS	Post nuclear supernatant
PRAS40	Proline-rich AKT substrate of 40 kDa
PRR	Proline rich region
PtdIns	Phosphatidylinositol
PTEN	Phosphatase and tensin homolog
PX Domain	Phox homology domain
RAPTOR	Regulatory associated protein of mTOR
RHEB	Ras homolog enriched in brain
RICTOR	Rapamycin insensitive companion of mTOR
RTKs	Receptor tyrosine kinases
Rpm	Rotations per minute
S6K or p70	S6 kinase
SEC	Size exclusion chromatography
SGK	Serum and glucocorticoid induce protein kinase
SNARE	Soluble N-ethylmaleimide-sensitive factor attachment protein receptor
SNX	Sorting nexin
TBST	Tris buffered saline and tween 20
TFEB	Transcription factor EB
TGN	Trans-Golgi network
TLC	Thin layer chromatography
TOR	Target of rapamycin
TR	Transferrin receptor
TSC	Tuberous sclerosis complex
ULK1	Unc-51 like autophagy activating kinase 1
UVRAG	UV radiation resistance associated gene
vpl	Vacuolar protein localisation
vps	Vacuolar protein sorting
vpt	Vacuolar protein targeting
XIC	Extracted ion chromatogram

VII. AMINO ACID CODE

Amino acid	Three letter symbol	One letter symbol
Alanine	Ala	A
Arginine	Arg	R
Asparagine	Asn	N
Aspartate	Asp	D
Cysteine	Cys	C
Glutamate	Glu	E
Glutamine	Gln	Q
Glycine	Gly	G
Histidine	His	H
Isoleucine	Ile	I
Leucine	Leu	L
Lysine	Lys	K
Methionine	Met	M
Phenylalanine	Phe	F
Proline	Pro	P
Serine	Ser	S
Threonine	Thr	T
Tryptophan	Trp	W
Tyrosine	Tyr	Y
Valine	Val	V
Any amino acid	Xaa	X

VIII. SUMMARY

The lipid kinase VPS34 is an essential mediator of multiple aspects of intracellular trafficking via the formation of phosphoinositide-3-phosphate (PI(3)P) on membranes, this is critical to mediate efficient trafficking of cargo by endocytosis. In addition, VPS34 kinase activity is essential for inducing autophagy in combination with the protein kinase ULK1. Autophagy acts as a catabolic pathway that is up regulated in response to stress, but is negatively regulated by the master growth protein kinase mTOR. This study sought to identify novel control mechanisms that may mediate the regulation of VPS34 between the pathways of endocytosis and autophagy. During nutrient rich conditions a binding protein of VPS34, UVRAG, was identified to be phosphorylated. Further analysis has identified that phosphorylation is mediated by mTOR and that this occurs at two sites, S550 and S571. Multiple lines of evidence suggest that phosphorylation does not alter the stoichiometry or localisation of the complex nor does it mediate recruitment of additional factors. Phosphorylation of UVRAG acts to increase lipid kinase activity *in vitro* and cellular PI(3)P levels by ~ 2 fold, mutation of S550 and S571 to alanine residues abrogate this increase in activity. Examination of autophagy, receptor mediated endocytosis and recycling have demonstrated no effect of UVRAG phosphorylation upon their rate of trafficking. Mutation of UVRAG phosphorylation sites however leads to a significant lysosome abnormality that is demonstrated by a dispersed phenotype. Preliminary analysis suggests that this may occur due to abnormalities in the process of autophagic lysosome reformation, a process that is dependent upon the activity of mTOR. This suggests a previously uncharacterised role of PI(3)P in lysosomal regulation and adds to current understanding of regulation between VPS34 and mTOR. Additionally data presented here examines a novel PI3KC3 inhibitor that demonstrates profound selectivity over other PI3K isoforms and lipid kinases. This will be important to further examine the functional role of VPS34 and UVRAG.

1 INTRODUCTION

1.1 Endocytosis

1.1.1 The Cell Surface

The plasma membrane defines the edge of a cell and is a dynamic structure that physically acts to separate and protect cellular contents, be it part of a uni- or multicellular organism, from a fluctuating exterior environment. Cells require basic nutrients such as sugars and proteins for survival, when available in excess cells are able to utilise these to grow and divide. The plasma membrane barrier however means that specialised processes are required for the uptake of components from the exterior environment. Multiple mechanisms exist to internalise 'cargo' and can be broadly referred to as the process of 'Endocytosis' (Doherty & McMahon 2009). Traditionally endocytosis was thought simply to traffic cargo to the lysosome, an acidic degradative organelle, to break down material (Duve & Wattiaux 1966). Through intensive study our understanding has vastly increased to appreciate that endocytosis is inextricably linked with intracellular trafficking and signalling to mediate all aspects of cellular logistics (Sigismund et al. 2012). Endocytosis ultimately governs the relationship of a cell with its exterior environment and this is crucial for survival. Alterations in the exterior environment can result in periods where nutrients are no longer freely accessible, it is during these times that the cell must efficiently identify that resources are limited and respond by implementing changes to allow survival until fresh nutrients become available. Part of this process involves reducing anabolic activities whilst simultaneously activating catabolic pathways, failure to do so and continuing growth under these circumstances would be catastrophic and ultimately lead to cell death (Tsukada & Ohsumi 1993). Understanding the interaction of cells with their exterior environment and how this regulates cellular pathways to determine growth is of fundamental importance, particularly as impaired endocytosis and growth signalling are commonly associated with human disease such as cancer.

This chapter will examine further the processes of endocytosis and intracellular transport, in addition the pathways of cell catabolism upon nutrient restriction will be explored. Most importantly, our current understanding of the mechanisms utilised by the cell to modulate and regulate these pathways will be discussed.

1.1.2 The Endocytic Pathway

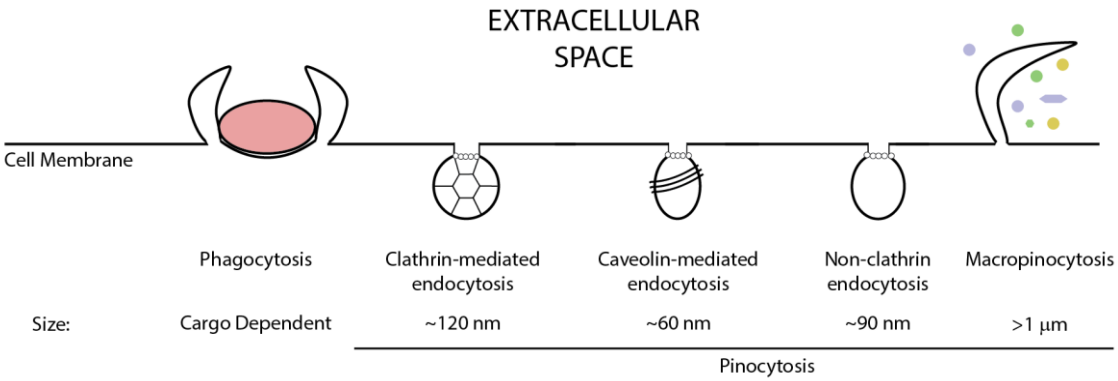

Figure 1.1 - Mechanisms of Endocytosis

Adapted from (Conner & Schmid 2003). Demonstrates the multiple mechanisms utilised by cells to internalise cargo and the size of endocytic vesicle produced.

The process of endocytosis can be divided into two primary groups dependent on whether it mediates the uptake of particles (Phagocytosis – 'Cell eating') or uptake of solutes and fluid (Pinocytosis – 'Cell drinking'). Pinocytosis can be further sub-divided based upon uptake mechanism, whereby fluid-phase endocytosis refers to the non-selective bulk fluid uptake by the cell. Receptor-mediated endocytosis (RME) by comparison utilises high affinity receptors to bind specific ligands (Besterman & Low 1983) and this includes the well characterised epidermal growth factor receptor (EGFR) and the transferrin receptor (TR) (Karin & Mintz 1981; Sullivan et al. 1976). Upon ligand binding, receptors cluster and are internalised by clathrin-mediated endocytosis (CME) into small vesicles. Other forms of cellular uptake include caveolin-mediated endocytosis and non-clathrin endocytosis (NCE) that utilise distinct mechanisms for vesicle formation that also differ in size (Mayor & Pagano 2007).

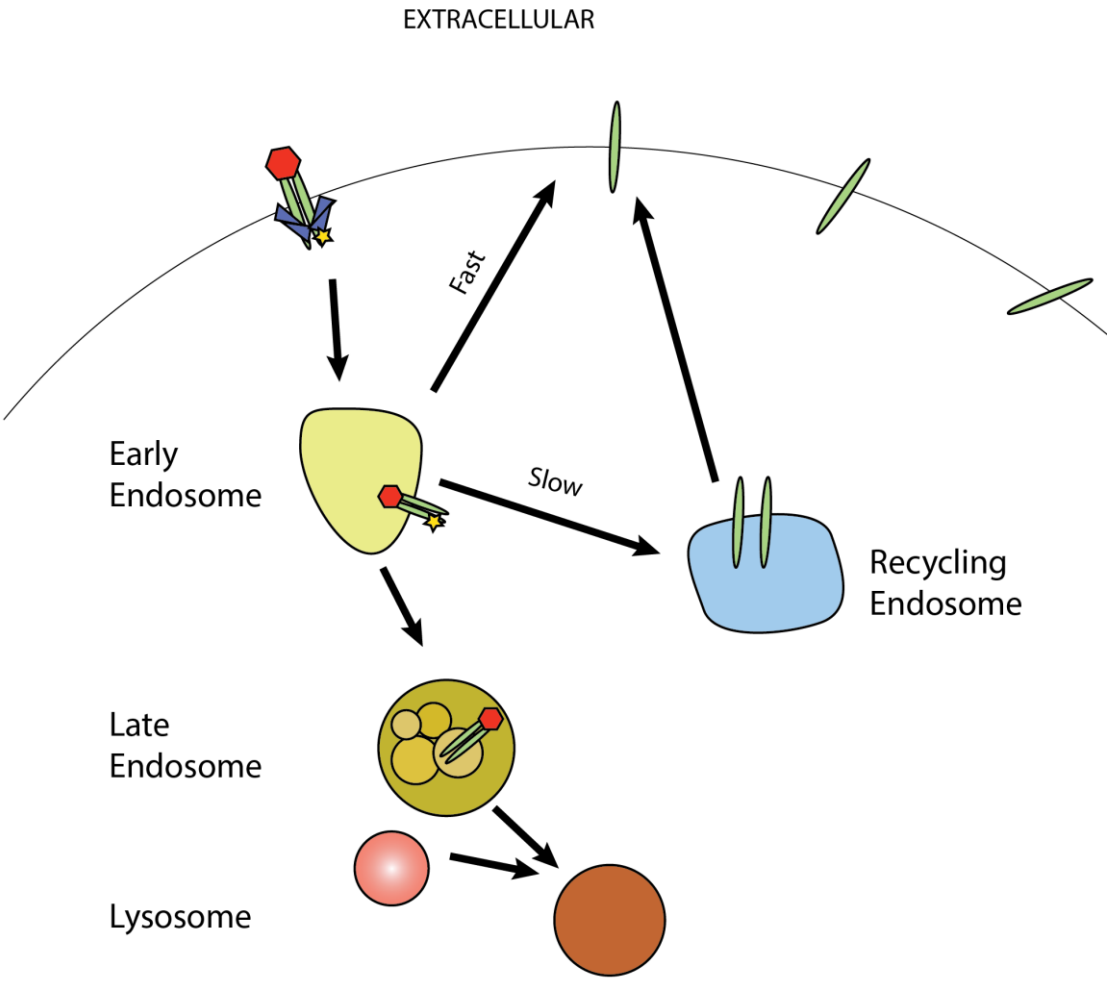

Figure 1.2 - The Endocytic Pathway

Internalisation of activated receptors by CME traffics material to the early endosome where cargo is sorted for recycling or degradation. Material can undergo 'fast' direct recycling to the plasma membrane or 'slow' recycling via a recycling endosome. Further internalisation of cargo into intraluminal vesicles (ILVs) within the late endosome commits the cargo to degradation by fusion with the lysosome.

The breadth of internalisation mechanisms employed by a cell ensures the uptake of numerous cargoes that in some cases display preference for particular internalisation mechanisms (Eyster et al. 2009; Traub 2003). The rate of endocytic processes is also varied between cell types dependent upon their function, macrophages for example extensively utilise phagocytosis for the uptake of large debris or pathogens (Aderem & Underhill 1999).

Internalisation of material by pinocytosis leads to a series of trafficking and sorting steps via vesicular structures known as endosomes to determine material that is to be recycled to the cell

surface or degraded at the lysosome (Steinman et al. 1983). Early endosomal structures that are present near the cell periphery act at the first step of cargo sorting (Steinman et al. 1983), receptors can be rapidly returned to the cell surface by direct trafficking or alternately a slower recycling pathway exists that involves trafficking to a recycling endosome prior to return to the cell surface (van Dam et al. 2002). Whilst at early endosomal structures receptor mediated signalling can still occur as the C-termini is still cytoplasmic facing (Lloyd et al. 2002). Signalling can be terminated by targeting the receptor for degradation by incorporation into intraluminal vesicles (ILVs) that bud inward at the endosome, this leads to the characteristic vesicular appearance of late endosomes also known as multi-vesicular bodies (MVBs) (Futter et al. 2001). Once internalised the receptor can no longer signal as the C-termini no longer contacts the cytoplasm, MVBs then ultimately fuse with lysosomes, causing the breakdown of material by acid hydrolases (Hershko & Ciechanover 1982).

1.1.3 Intracellular Trafficking and the Lysosome

Within the cell multiple distinct trafficking pathways exist that transport material between specific organelles and locations, this is essential to ensure cellular components are located at the regions where they are required for function. Vesicular trafficking is a complex process that requires many proteins, however, the process can be divided into four major steps (Figure 1.3). Adaptor proteins (APs) recognise cargo and recruit coat proteins to induce vesicle budding (Ford et al. 2001), the vesicle then undergoes scission (Bliek & Redelmeier 1993) and is trafficked towards the acceptor membrane (Caviston & Holzbaur 2006). Tethering proteins and Rab GTPases work together (Simonsen et al. 1998) to bring membranes close together that allow membrane fusion mediated by soluble N-ethylmaleimide-sensitive factor attachment protein receptors (SNAREs) (Söllner et al. 1993).

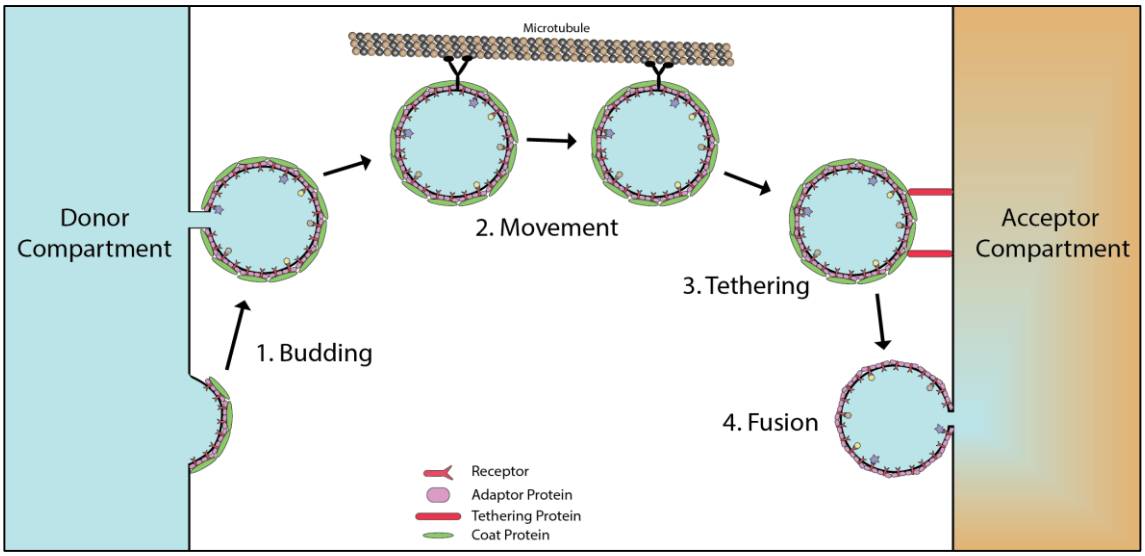

Figure 1.3 - Basic Steps of Vesicular Trafficking

Figure adapted from (Cai et al. 2007). **(1)** Coat proteins are recruited via adaptor proteins (AP) to the donor membrane, APs also bind cargo to be internalised (Ford et al. 2001). The vesicle is released from membrane by Dynamin mediated scission (Hinshaw & Schmid 1995). **(2)** Vesicles are transported to the acceptor membrane by motor proteins and microtubules (Caviston & Holzbaur 2006). **(3)** Tethering factors and Rab GTPases bind vesicles (Simonsen et al. 1998) to reduce the membrane distances to assist with **(4)** membrane fusion mediated by SNARE proteins (Söllner et al. 1993).

Multiple cellular trafficking pathways exist (Figure 1.4) and are often characterised by distinct components. Adaptor protein complex 2 (AP-2) is utilised in transport from the plasma membrane (Gaidarov & Keen 1999) whilst AP-1 mediates Golgi to Endosome transport (Traub et al. 1993). Transport via the Golgi is critical for lysosomal hydrolases that are translocated into the lumen of the endoplasmic reticulum (ER) during synthesis and then subsequently require transport to the lysosome where they become active in the acidic pH of the lumen (Kornfeld 1987). Newly formed hydrolases contain a mannose 6-phosphate tag that, following transport to the trans-Golgi network (TGN), is recognised and bound by mannose-6-phosphate receptors (M6PRs) (Dahms et al. 1989). The M6PR-hydrolase complex is then trafficked to endosomes where the mildly acidic pH triggers the release from the receptor (Kornfeld 1987). Hydrolases remain in the endosome as they mature to assist with proteolytic degradation, meanwhile the vacant M6PRs are transported back to the TGN to repeat this process and prevent the degradation of the receptor by the lysosome (Brown et al. 1986). An equivalent pathway exists

in yeast that transports vacuolar proteases including carboxypeptidase Y (CPY) from the ER via the Golgi to the vacuole (Stevens et al. 1982).

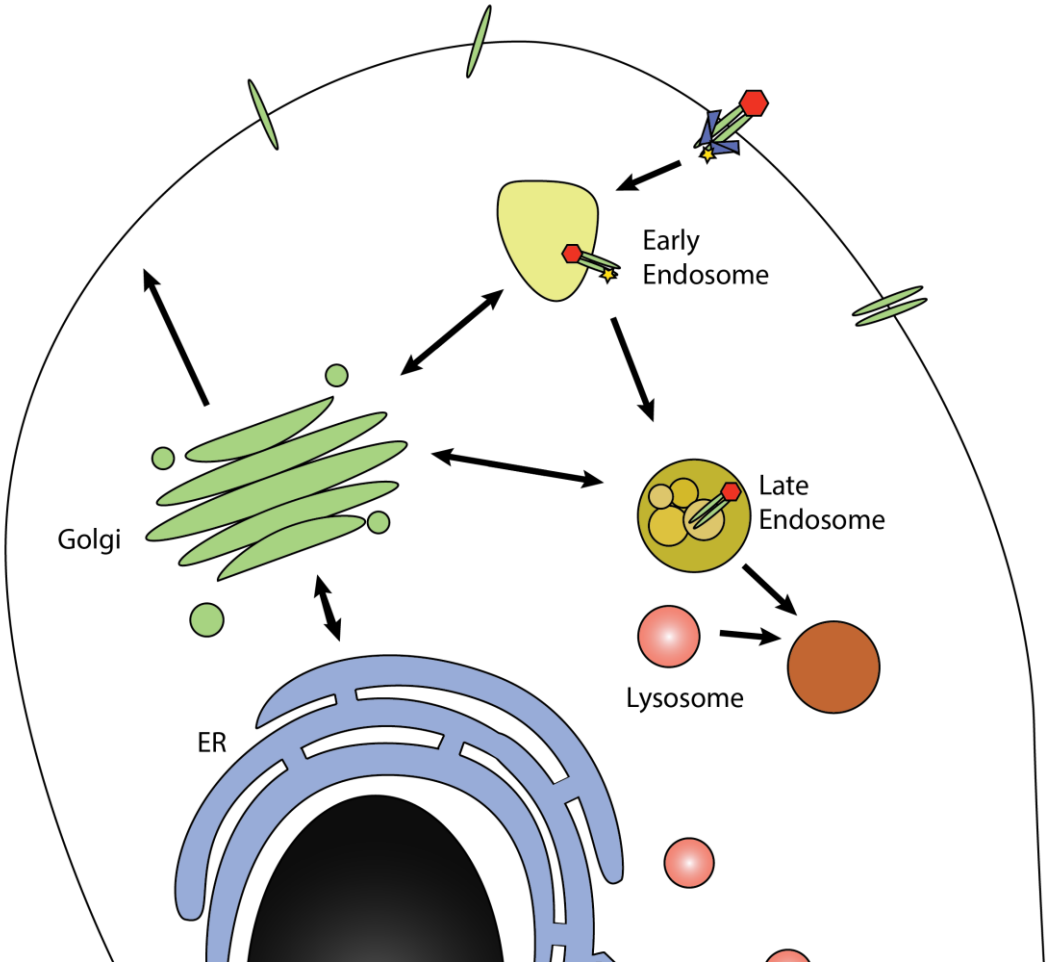

Figure 1.4 - Intracellular Trafficking Pathways

Multiple pathways exist in the cell in addition to the endocytic pathway (recycling not included in this figure). Material internalised is trafficked to the lysosome by the endosomes, but these are interlinked with transport to and from the Golgi. Upon formation, lysosomal hydrolases are delivered to the lysosome via trafficking from the Golgi, which also acts to direct cargo for secretion.

1.1.4 Identification of Vacuolar Protein Sorting (*vps*) Mutants

Several pioneering genetic mutational analyses were carried out in yeast cells that examined the transportation of CPY to determine proteins required for transport to the vacuole. It had previously been identified that over-expression of CPY or mutating the sorting signal caused CPY to be transported from the Golgi to the plasma membrane for secretion instead of localisation to the vacuole (Johnson et al. 1987; Stevens et al. 1986). This phenotype was taken advantage of experimentally as yeast cells that secrete CPY following genetic mutation are likely to be deficient in trafficking to the vacuole and this approach led to the classification of eight vacuolar protein localisation (*vpl*) mutants (Rothman & Stevens 1986). This method was improved by fusing CPY to the enzyme invertase that is normally secreted and allows yeast growth on sucrose (Bankaitis et al. 1986). Fusion to CPY results in delivery to the vacuole that is only reverted to the secretory pathway if transport to the vacuole is impeded (Johnson et al. 1987). This approach improved the identification of vacuolar trafficking mutants as yeast are only viable on sucrose if trafficking is impaired, this led to the identification of vacuolar protein targeting (*vpt*) mutants (Bankaitis et al. 1986)(Robinson et al. 1988). Mutants can be sub-divided into three classes by vacuolar phenotype where class A causes no effect, class B causes vacuole fragmentation and class C yeast exhibit vacuole biogenesis defects (Banta et al. 1988). Further *vpl* mutants were identified by secretion of CPY and compared to previously identified *vpt* mutants or *pep* mutants that have decreased expression of CPY (Jones 1977; Rothman et al. 1989). Significant overlaps were detected between mutants and as such *vpt, vpl* and *pep* mutants were consolidated and renamed as vacuolar protein sorting (vps) mutants. These experiments were critical in establishing an initial list of essential trafficking proteins that we now understand to be involved in all aspects of cellular trafficking and not simply limited to vacuolar protein sorting. Current understanding of the 40 *vps* mutants identified in *vpl* and *vpt* screens is shown in Table 1.

VPS	VPL	VPT	Class	PEP	Mammalian Homolog	Complex	Role
1	1	26	B	-	Dynamin	N/A	Vesicle Scission
2	2	-	A	-	VPS2 (CHMP2)	ESCRT-III	MVB formation
3	3	17	A	6	VPS3	CORVET Complex	Tethering
4	4	10	A	-	VPS4 (SKD1)	VPS4-VTA1 complex	ATPase
5	5	5	B	10	VPS5	Retromer	Endosome to TGN transport
6	6	13	A	-	Syntaxin	SNARE	Q-SNARE
7	7	-	A	15	Unknown	Unknown	Unknown
8	8	8	A	-	VPS8	CORVET Complex	Tethering
9	-	9	A	-	VPS9D1	Rab5 GEF	GEF
10	-	1	A	-	VPS10	CPY Transport TGN -> Vacuole	CPY Receptor
11	9	11	C	5	VPS11	Class C-VPS Complex	Lysosome Fusion
12	-	12	A	-	Unknown	Unknown	Unknown
13	-	2	A	-	VPS13A-D (Chorein)	N/A	Unknown – Possibly TGN to late endosome
14	-	14	A	-	CHMP2A	ESCRT-III	MVB Formation
15	-	15	A	-	VPS15	PI3KC3 Complex	Endocytosis + Autophagy
16	-	16	C	-	VPS16	Class C-VPS Complex	Lysosome Fusion
17	-	3	B	21	VPS17	Retromer	Endosome to TGN transport
18	-	18	C	-	VPS18	Class C-VPS Complex	Lysosome Fusion
19	-	19	A	-	Unknown	Unknown	Unknown
20	10	20	A	-	VPS20 (CHMP6)	ESCRT-III	MVB formation
21	-	21	A	-	Rab5	N/A	Rab
22	14	22	A	-	VPS22 (EAP30)	ESCRT-II	MVB formation
23	15	23	A	-	VPS23 (TSG101)	ESCRT-I	MVB formation
24	-	24	A	-	VPS24 (CHMP3)	ESCRT-III	MVB formation
25	12	25	A	-	VPS25 (EAP20)	ESCRT-II	MVB formation
26	-	4	A	8	VPS26A / B	Retromer	Endosome to TGN transport
27	-	27	A	-	HRS	ESCRT-0	MVB formation
28	13	28	A	12	VPS28	ESCRT-I	MVB formation
29	-	6	A	-	VPS29	Retromer	Endosome to TGN transport
30	-	30	A	-	BECLIN1	PI3KC3 Complex	Endocytosis + Autophagy
31	-	31	A	-	ALIX (AIP1)	N/A	Adaptor protein - MVBs
32	-	32	A	-	SNF7 (CHMP4)	ESCRT-III	MVB formation
33	-	33	C	-	VPS33 (PEP14)	Class C-VPS Complex	Lysosome Fusion
34	-	29	A	-	VPS34	PI3KC3 Complex	Endocytosis + Autophagy
35	-	7	A	-	VPS35	Retromer	Endosome to TGN transport
36	11	-	A	-	VPS36 (EAP45)	ESCRT-II	MVB formation
37	16	-	A	-	VPS37	ESCRT-I	MVB formation
38	17	-	A	-	UVRAG	PI3KC3 Complex	Endocytosis
39	18	-	A	-	VPS39	HOPS Complex	Lysosome Fusion
40	19	-	B	-	Unknown	Unknown	Unknown

Table 1 – Vacuolar Protein Sorting Mutants, Homologues and Function

1.1.5 VPS34 Modulates Trafficking by PI3K Activity

Vps mutants have been studied intently since identification to characterise the mechanisms by which they mediate trafficking. Of these proteins, VPS34 is now known to be an essential mediator of multiple trafficking steps and plays a key role in signalling events directing both endocytosis and autophagy.

Initial characterisation of *Δvps34* yeast cells demonstrated a temperature sensitive growth defect and that Vps34p binds to membrane structures (Herman & Emr 1990). Vps34p has significant homology to the catalytic domain of the lipid kinase PI3Kα and analysis *in vitro* revealed that VPS34 also contains Phosphatidylinositol 3-kinase (PI3K) activity (further examined in 1.1.6)(Schu et al. 1993). The vacuolar phenotype of *Δvps15* and *Δvps34* is very similar and does not cleanly fall into the defined vacuolar class types, suggesting the two proteins may be interlinked (Banta et al. 1988). Vps34p and Vps15p were identified to co-fractionate by density gradient and could also be reciprocally immunoprecipitated with one another, this was later determined to be mediated by the final ~ 30 amino acids at the C-termini of Vps34p (Budovskaya et al. 2002; Stack et al. 1993). Vps15p is a protein kinase and is myristoylated at the N-terminus, a modification that commonly enables membrane binding, however mutation of the myristoylation site had no effect upon membrane association (Herman et al. 1991; Madsen et al. 2010). The mechanism through which Vps15p regulates Vps34p is not entirely understood, although it is clear that Vps34p from *Δvps15* yeast is deficient in membrane binding and lipid kinase activity is severely impaired (Stack et al. 1993). Expression of a Vps15p kinase domain mutant restores Vps34p membrane binding, but does not rescue lipid kinase activity suggesting that Vps15p protein kinase activity mediates lipid kinase activity (Stack et al. 1993). Substrates of Vps15p however have not been identified and the level of Vps34p phosphorylation is not altered between wild-type or *Δvps15* mutants (Stack & Emr 1994). The mammalian homolog VPS34 was identified based upon homology to the yeast Vps34p and is also shown to possess PI3K activity; additionally it has been identified to interact with p150, a

homologue of Vps15p (Volinia et al. 1995). Blockade of PI3K activity by use of inhibitory antibodies impairs the trafficking of platelet-derived growth factor receptor and the formation of ILVs (Siddhanta et al. 1998; Futter et al. 2001). Additionally PI3K inhibition using the inhibitor wortmannin blocks the fusion of early endosomes (Jones & Clague 1995). Although wortmannin is not specific for PI3KC3 inhibition (Arcaro & Wymann 1993; Stack & Emr 1994), taken together the data is highly suggestive that the lipid kinase activity and formation of PI(3)P is critical for mediating trafficking by VPS34. This led to further study and understanding of the regulation of phosphoinositides in trafficking.

1.1.6 Phosphatidylinositol and Phosphoinositides

Phosphatidylinositol (PtdIns or PI) is a glycerolipid composed of two non-polar fatty acid chains connected to a glycerol backbone and phosphate group containing an inositol ring polar head group (Figure 1.5) and represents a minor proportion of eukaryote cellular membranes, contributing to less than 15% of the total lipid composition (van Meer & de Kroon 2011). The polar inositol head contains five hydroxyl groups, where position three, four or five can be phosphorylated either singly or in combination to yield seven distinct lipids referred to as phosphoinositides (Di Paolo & De Camilli 2006). The hydroxyl groups at position two and six are not phosphorylated due to steric hindrance (Figure 1.5).

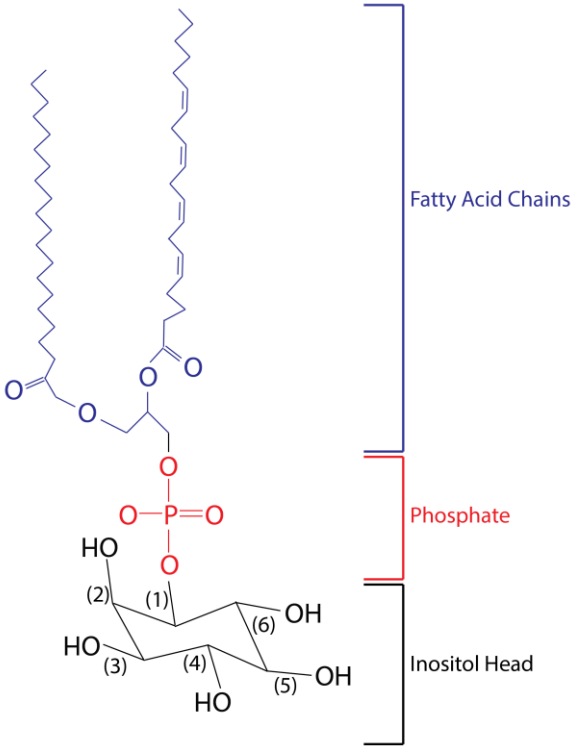

Figure 1.5 - Structure of Phosphatidylinositol

The structure of phosphatidylinositol is shown. Numbers in brackets represent the hydroxyl group number that is utilised for the naming of phosphoinositide species.

All seven phosphoinositides species have been identified in mammalians and are estimated to account for ~ 8 % of cellular PtdIns or ~ 1 % of total lipids (Figure 1.6). The abundance of individual phosphoinositides species varies greatly; $PI(3,5)P_2$ for example is present at concentrations ~ 125 fold lower than that of the most abundant phosphoinositide $PI(4,5)P_2$ (Zolov et al. 2012).

Phosphorylation is catalysed by phosphatidylinositol kinases (PIKs) that are divided into classes based upon their inositol head group target. These are phosphatidylinositol-3-kinases (PI3Ks), phosphatidylinositol-4-kinases (PI4Ks) and phosphatidylinositol-5-kinases (PI5Ks) that phosphorylate inositol position 3,4 and 5 respectively (Fruman et al. 1998). PIKs selectively phosphorylate a single position, therefore the formation of phosphatidylinositol-bis- or tris-phosphate requires sequential kinase activity (Figure 1.6). PI3Ks are further divided into class I, II and III dependent upon their substrate preference *in vivo*. Class I (PI3KC1) enzymes are

shown to produce PI(3,4,5)P_3 (Stephens et al. 1993), class II (PI3KC2) are less understood but appear to catalyse the formation of PI(3)P and PI(3,4)P_2 (Misawa et al. 1998). VPS34 is the sole mammalian class III enzyme and produces the majority of cellular PI(3)P (Devereaux et al. 2013). Several lipid phosphatases also demonstrate specific activity towards individual phosphorylation sites on the inositol ring of phosphoinositides such as the 3'-phosphatase myotubularin (MTM1) that dephosphorylates position 3 from PI(3)P and PI(3,5,)P_2 (Taylor et al. 2000) or the 5'-phosphatase SHIP2 that catalyses PI(3,4,5)P_3 to PI(3,4)P_2 (Ishihara et al. 1999).

The production of phosphoinositides is important for the generation of region specific identity that occurs due to spatial restriction of PIKs and phosphatases. The distribution of phosphoinositides can be demonstrated by utilising specific protein recognition binding domains (see 1.1.7). PI(4)P for example is primarily present in a perinuclear region that corresponds to the Golgi, PI(4,5)P_2 is accumulated at the plasma membrane whilst PI(3)P is mainly observed with endosomes (Figure 1.7) (Gillooly et al. 2000; Hammond et al. 2009).

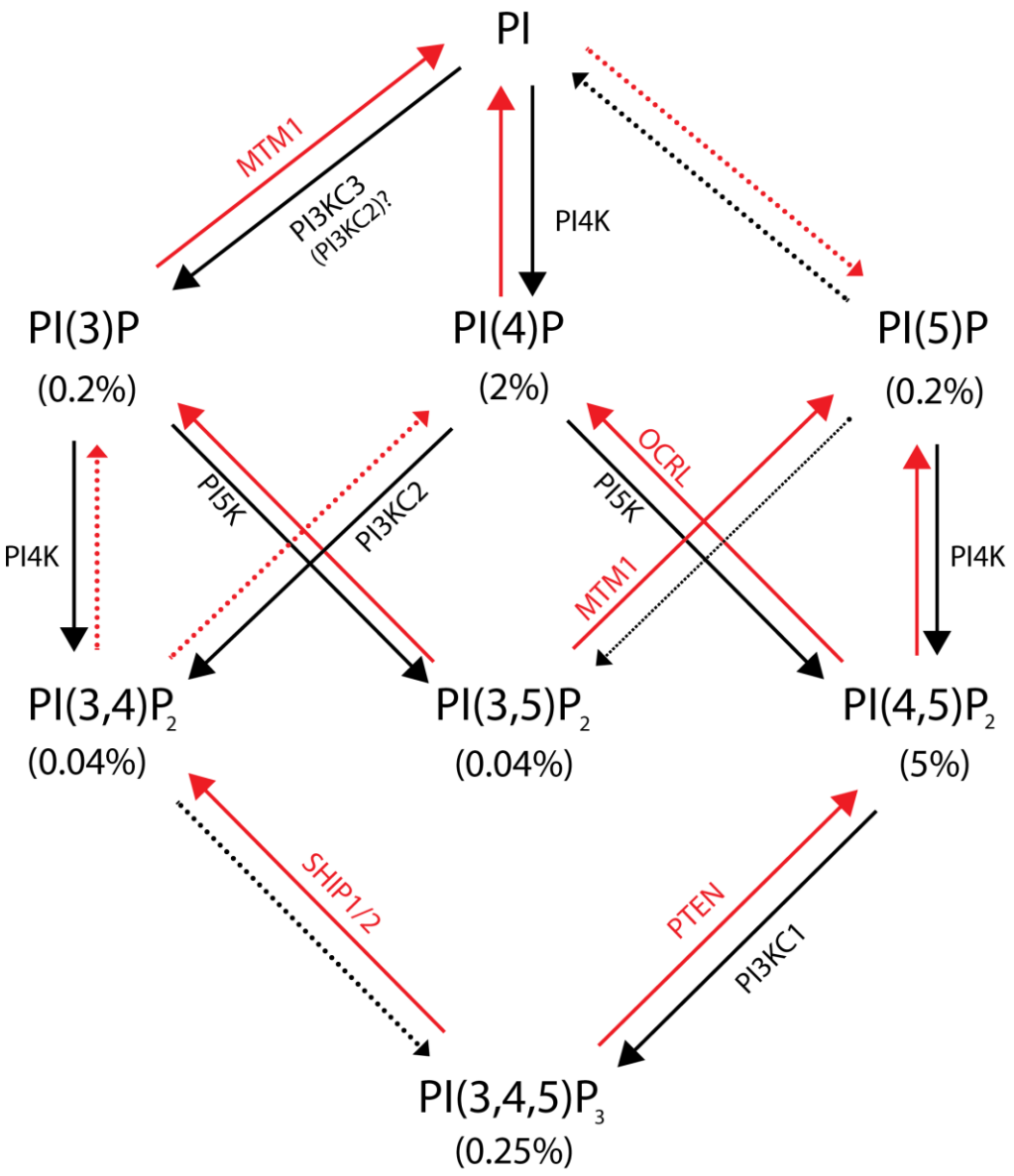

Figure 1.6 - Interconversion of Phosphoinositides

PtdIns can be interconverted between phosphoinositide species by lipid kinase or lipid phosphatase activity. Solid arrows represent activity that has been demonstrated in cells, dashed arrows represents activity that has been shown *in vitro* but not in cells. Arrows represent activity by lipid kinases (black) or lipid phosphatases (red). Values in brackets represent estimated percentage values of total PtdIns in the absence of any stimulatory factors from mammalian cells (Devereaux et al. 2013; Lemmon 2008; Milne et al. 2005; Zolov et al. 2012).

It must be noted that the action of lipid phosphatases is not always to simply counteract lipid kinase action, but can also be important for generation of distinct lipid identity. PI(5)P for example is not formed by phosphorylation of PtdIns in cells, instead it is generated via dephosphorylation of $PI(3,5)P_2$ (Zolov et al. 2012).

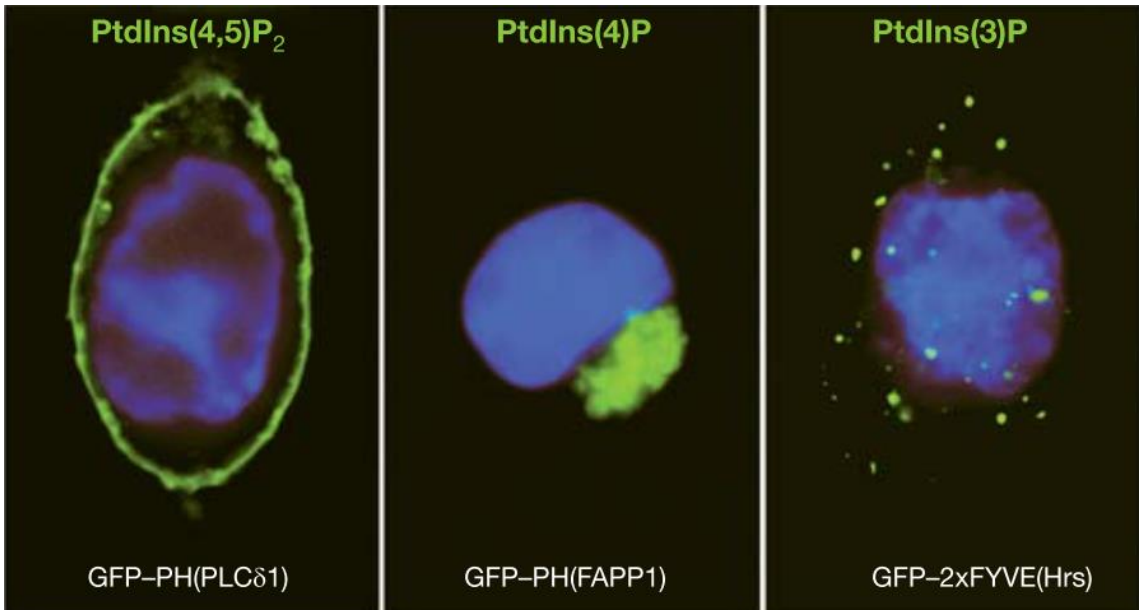

Figure 1.7 - Distinct Localisation of Phosphoinositides

Figure taken from (Di Paolo & De Camilli 2006). The PH Binding domain of PLCδ1 recognises $PI(4,5)P_2$ at the plasma membrane, PH Domain of FAPP1 binds to PI(4)P in the Golgi and a 2xFYVE domain from HRS binds PI(3)P at endosomes. Experiments were carried out in Chinese hamster ovary cells.

The presence of lipid identities allows the recruitment of specific effector proteins via phosphoinositide binding domains for essential functions at that location (1.1.7). Similarly alterations to phosphoinositide composition that may occur due to localisation or activation of PIKs will modulate recruitment of effector proteins and can therefore alter processes at the membrane. This is exemplified by the activation of PI3Kα by growth factors at the plasma membrane that leads to the rapid generation of $PI(3,4,5)P_3$ to recruit downstream factors to mediate growth factor signalling (Stephens et al. 1993).

1.1.7 Phosphoinositide Binding Domains

The pleckstrin homology (PH) domain is found in a large number of proteins and is highly represented amongst proteins involved in signalling and trafficking. The PH domain was identified based upon sequence similarity to the protein Pleckstrin (Haslam et al. 1993). Subsequently a small proportion of these domains were identified to be able to bind to varying phosphoinositide species (Harlan et al. 1994). The PH domains that interact with phosphoinositides generally favour interaction with those containing two adjacent phosphates such as PI(3,4)P_2, PI(4,5)P_2 and PI(3,4,5)P_2 (Lemmon 2007). This is not entirely exclusive however and work has demonstrated that the PH domain of FAPP1 can localise to the Golgi based upon coincident binding of PI(4)P and ADP-Ribosylation factor 1 (ARF1) (Godi et al. 2004).

Advancement in the understanding of trafficking in relation to VPS34 and endocytosis was made by the identification of binding domains that are able to interact specifically with PI(3)P (Table 2). Early endosome antigen 1 (EEA1) was discovered to be localised to early endosomes in a PI3K activity dependent manner (Patki et al. 1997). Analyses identified a zinc-binding finger in EEA1 that was distinct from traditional zinc fingers present in nucleic acid binding proteins and was found in several other trafficking proteins, this was named the **F**ab1, **Y**OTB, **V**ac1 and **E**EA1 (**FYVE**) zinc finger binding domain (Stenmark et al. 1996)**.** The FYVE domain of EEA1 was subsequently identified to bind PI(3)P that localises the protein at endosomal structures (Gaullier et al. 1998). This study also demonstrated for the first time that FYVE domains are highly specific for binding to PI(3)P over other phosphoinositides and that the FYVE domain of hepatocyte growth factor regulated tyrosine kinase substrate (HRS) displayed similar properties to EEA1 (Gaullier et al. 1998). FYVE domains retain a conserved basic motif and eight conserved cysteine residues that co-ordinate two Zn^{2+} ions to stabilise the domain structure (Misra & Hurley 1999). Following this discovery, a phox homology (PX) domain from the vacuolar SNARE protein Vam7 involved in vesicle fusion was also demonstrated to bind PI(3)P (Cheever et al. 2001; Song et al. 2001). The PX domain is found in multiple proteins including the sorting nexin

(SNX) family that were originally identified by their ability to assist with EGFR degradation (Kurten et al. 1996; Haft et al. 1998). Other phosphoinositide binding domains are also present within the cell such as C2 domains that typically require calcium to mediate binding to phospholipids (Sutton et al. 1995). All FYVE domains and a large proportion of PX domain containing proteins are specific for binding to PI(3)P, therefore their function within the cell is largely controlled by the activity of VPS34.

Domain	Lipid Binding	Example protein	Reference
FYVE	PI(3)P	EEA1, HRS, DFCP1	(Gaullier et al. 1998)
PH	$PI(3,4)P_2$	AKT	(Thomas et al. 2002)
	$PI(4,5)P_2$	DYNAMIN	(Achiriloaie et al. 1999)
	$PI(3,4,5)P_3$	GRP1, AKT	(Gray et al. 1999; Thomas et al. 2002)
PX	PI(3)P	P40 PHOX, SNX2, SNX3	(Kanai et al. 2001)
	PI(5)P	SNX13	(He et al. 2011)
	$PI(3,4)P_2$	P47 PHOX	(Kanai et al. 2001)

Table 2 – Example of Phosphoinositide Binding Domains

1.1.8 Cellular Trafficking Mediated by PI(3)P

The dependence of PI(3)P for correct localisation of multiple FYVE domain containing proteins such as EEA1 or HRS has allowed further insight into the regulatory roles PI(3)P plays in the trafficking system (Gaullier et al. 1998). EEA1 is one of the most studied FYVE domain containing proteins and is a large coiled-coil protein that also contains a Rab5 binding domain next to the FYVE domain (Simonsen et al. 1998). Recruitment of EEA1 to membranes requires co-incident binding to Rab5-GTP and PI(3)P and thereby drives very specific EEA1 membrane recruitment (Lawe et al. 2000). EEA1 assists with fusion of Rab5 positive membranes that is thought to occur by tethering to allow SNARE protein pairing (Christoforidis et al. 1999). Determination of the FYVE domain crystal structure (Misra & Hurley 1999) combined with knowledge of the conserved FYVE domain sequence allows targeted mutation of conserved cysteine residues to prevent phosphoinositide binding, this has proven a useful tool for determining the role of PI(3)P binding in protein function (Ridley et al. 2001). One of the most critical advances has been the development of a recombinant double FYVE domain protein probe separated by a linker region

that can bind to PI(3)P in cells with high affinity (Gillooly et al. 2000). Addition of a protein tag or fluorophore to this probe allows determination of cellular PI(3)P levels based upon the level of probe membrane binding, this has been critical for more recent analysis into regulatory mechanisms and pathways that trigger more subtle changes in activity or function of VPS34 (Furuya et al. 2010; Russell et al. 2013; Yuan et al. 2013). Similarly the PX domain from the protein $p40^{phox}$ can also be expressed recombinantly to bind PI(3)P specifically (Kanai et al. 2001).

1.2 Autophagy

1.2.1 Background

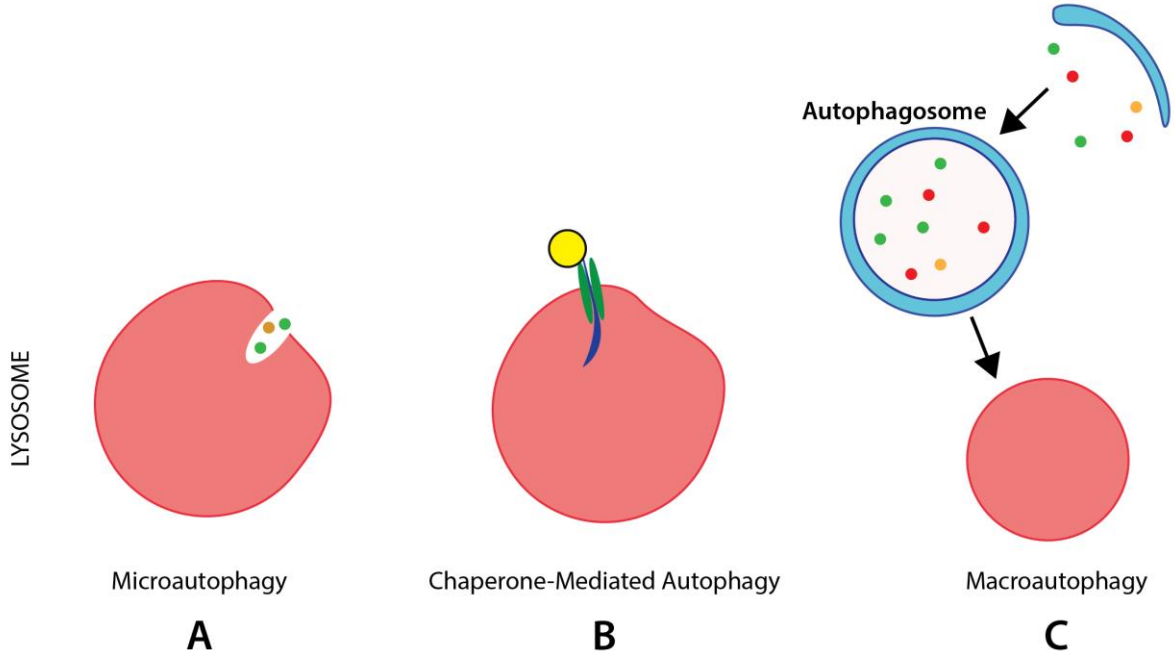

Figure 1.8 - Forms of Autophagy

Three subtypes of autophagy exist. **(A)** Microautophagy is thought to involve the invagination of the lysosome membrane to directly take up material. **(B)** Chaperone-Mediated autophagy involves the specific targeting of proteins by binding to hsc70 and then subsequent transport across the lysosomal membrane. **(C)** Macroautophagy is the most well studied form that involves the uptake of cellular material inside a characteristic double membrane structure that then fuses with the lysosome for degradation.

Autophagy is a catabolic cellular process that degrades intracellular material via the lysosome. There are several forms of autophagy: microautophagy (Figure 1.8A) that is thought to involve direct engulfment of cytoplasmic material by the lysosome (Mijaljica et al. 2011); Chaperone-mediated autophagy (CMA - Figure 1.8B) is a highly specific pathway that utilises heat shock cognate protein of 70 kDa (HSC70) to recognise and bind precise cargo that it then assists in transporting across the lysosomal membrane (Chiang et al. 1989; Dunn 1994); and macroautophagy that encapsulates portions of the cytoplasm in a characteristic double membrane structure for trafficking and delivery to the lysosome (Figure 1.8C). Macroautophagy (herein referred to as autophagy) has been the most studied and characterised form to date.

Autophagy is a highly conserved process that is also found in unicellular eukaryotes such as yeast and amoeba (Goldberg & St. John 1976; Takeshige et al. 1992). Whilst the process of autophagy has been known of since the 1960s (Duve & Wattiaux 1966), it has only been in the last two decades that understanding of the process has really progressed. Autophagy proceeds at a basal rate in cells that assists with the turnover of proteins and organelles, however in response to diverse cellular stresses this process can be rapidly increased (Mortimore & Schworer 1977). Amino acid starvation is one of the most potent inducers of autophagy and it is necessary to prolong cell survival by generating nutrients from the breakdown of cellular components, blockade of autophagy in yeast results in a severe reduction in cell survival upon nitrogen starvation (Tsukada & Ohsumi 1993). Inhibition of yeast vacuolar proteases by addition of the serine protease inhibitor phenylmethanesulfonyl fluoride (PMSF) causes accumulation of autophagic bodies during nitrogen starvation that can be easily identified by light microscopy (Takeshige et al. 1992). The ability to identify accumulation of autophagic structures by light microscopy provides an easy screening method and was utilised to determine autophagy deficient mutants.

1.2.2 Identification of Key Autophagy Proteins

Understanding of proteins required for the autophagy pathway was pioneered by mutational studies in *S. cerevisiae* that identified more than 35 genes that are responsible for deficient autophagy upon nitrogen starvation (Tsukada & Ohsumi 1993; Thumm et al. 1994). These genetic mutational analysis experiments were similar to those carried out previously for the identification of *vpt* and *vpl* mutants (1.1.4). Of the autophagy deficient yeast strains found, ~20 % were due to mutation in the same gene that was termed *apg1,* further analysis identified that Apg1p is a serine-threonine protein kinase and contains homology to UNC-51 of *C. elegans* (Matsuura et al. 1997). This proved a vital stepping stone to linking Apg1p to the human and

mouse homolog Unc-51 like autophagy activating kinase 1 (ULK1) that contains 41 % and 29 % sequence identity to UNC-51 and Apg1p respectively (Kuroyanagi et al. 1998; Yan et al. 1998). Despite this linkage, it took almost another 10 years to confirm that knockdown of ULK1 impairs mammalian autophagy (Chan et al. 2007). From the *apg* mutants identified in yeast, Apg1p/ULK1 has been the only kinase identified. Further study in yeast identified that Apg1p overexpression can rescue the autophagy defect of *apg13* mutant yeast and that they form a complex required for cell viability upon starvation (Funakoshi et al. 1997). A third component, Atg17, was identified as an additional binding partner required for autophagy (Cheong et al. 2005; Kabeya et al. 2005). Homologs of these components have subsequently been identified in mammalian cells as ATG13 and FIP200 and found to form a complex with ULK1 that is required for autophagy (Ganley et al. 2009; Hosokawa et al. 2009; Jung et al. 2009).

Intriguingly, analysis of the interaction between two *apg* proteins, Apg14p and Apg6p, revealed that a*pg6* mutants are deficient in both autophagy and CPY trafficking to the vacuole whilst *apg14* is only defective in autophagy (Kametaka et al. 1998). Structural analysis identified Apg6p to be the same protein as Vps30p identified through earlier vacuolar protein screens (1.1.4) (Kametaka et al. 1998). Further analysis of Vps30p interacting proteins identified binding to Apg14p, Vps15p, Vps34p and Vps38p (Kihara, Noda, et al. 2001). One of the most interesting aspects is that Apg6p/Vps30p, Vps34p and Vps15p all cause combined CPY and autophagy defects in yeast whilst Apg14p and Vps38p are only defective in autophagy and CPY trafficking respectively (Kihara, Noda, et al. 2001). Immunoprecipitation of Vps38p and Apg14p individually are unable to interact with one another but retain a common core binding complex of Vps15p, Vps34p and Apg6p/Vps30p (Figure 1.9) (Kihara, Noda, et al. 2001). This study demonstrated for the first time that VPS34 can form two distinct complexes, one primarily associated with autophagy (Apg14p – Complex I) and another primarily associated with vacuolar trafficking (Vps38p – Complex II).

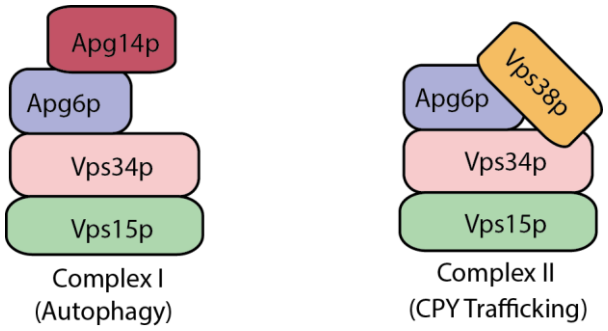

Figure 1.9 - VPS34 Complex Formation in Yeast

1.2.3 The Mammalian VPS34 Complex

Following the identification of Apg6p/Vps30p, the mammalian homologue BECLIN1 was identified based upon ~25 % sequence homology and the ability to complement the autophagy deficiency of *apg6* mutants (Liang et al. 1999). BECLIN1 binds to VPS34 by a conserved region from yeast to mammals termed the evolutionary conserved domain (ECD) (Furuya et al. 2005) and BECLIN1 is suggested to be a haploinsufficient tumour suppressor as it is mono-allelically deleted in 40-75 % of sporadic breast and ovarian cancers (Liang et al. 1999). In addition, BECLIN1 -/+ mice have a high incidence of spontaneous tumour generation (Qu et al. 2003). Immunoprecipitation experiments of BECLIN1 identified UV radiation resistance associated gene (UVRAG) as an interacting protein via interaction of their coiled-coil domains (CCDs) (Liang et al. 2006). UVRAG was later attributed as a Vps38p homologue in a study by Itakura et al. (2008) that also identified a homologue of Apg14p now termed Atg14 like (ATG14L). ATG14L and UVRAG both contain <15 % sequence homology with their yeast counterparts but retain >30 % sequence similarity (Itakura et al. 2008). Akin to yeast, ATG14L and UVRAG are found in mutually distinct complexes that retain a common VPS15, VPS34, BECLIN1 (Apg6) core (Itakura et al. 2008; Kihara, Noda, et al. 2001). ATG14L also possesses a CCD that mediates binding with the CCD of BECLIN1, it is by this requirement for the same binding site between UVRAG and ATG14L that leads to the formation of mutually exclusive complexes (Sun et al. 2008). The domain structure of VPS34 complex proteins is demonstrated in Figure 1.10. ATG14L is required for autophagy

similar to yeast Apg14p as knock-down drastically impairs autophagosome formation and autophagy (Itakura et al. 2008; Matsunaga et al. 2009). A specific region at the C-termini of ATG14L termed the Barkor/ATG14L autophagosome targeting sequence (BATS) has been determined to target the VPS34 complex to the ER by recognition of membrane curvature and PI(3)P in a positive feedback mechanism (Fan et al. 2011). The binding of UVRAG to BECLIN1 increases VPS34 PI3K activity *in vitro* by ~2-4 fold (Liang et al. 2006; Sun et al. 2010) and knock-down of UVRAG,BECLIN1, VPS34 or VPS15 all cause defects in the trafficking and degradation of the EGFR (Thoresen et al. 2010).

Homologues of yeast complex I and II are therefore found in mammalian cells and are able to fulfil similar trafficking roles as those defined in yeast. Further complexity is added in the mammalian system however by interaction of further proteins with the VPS34 complex.

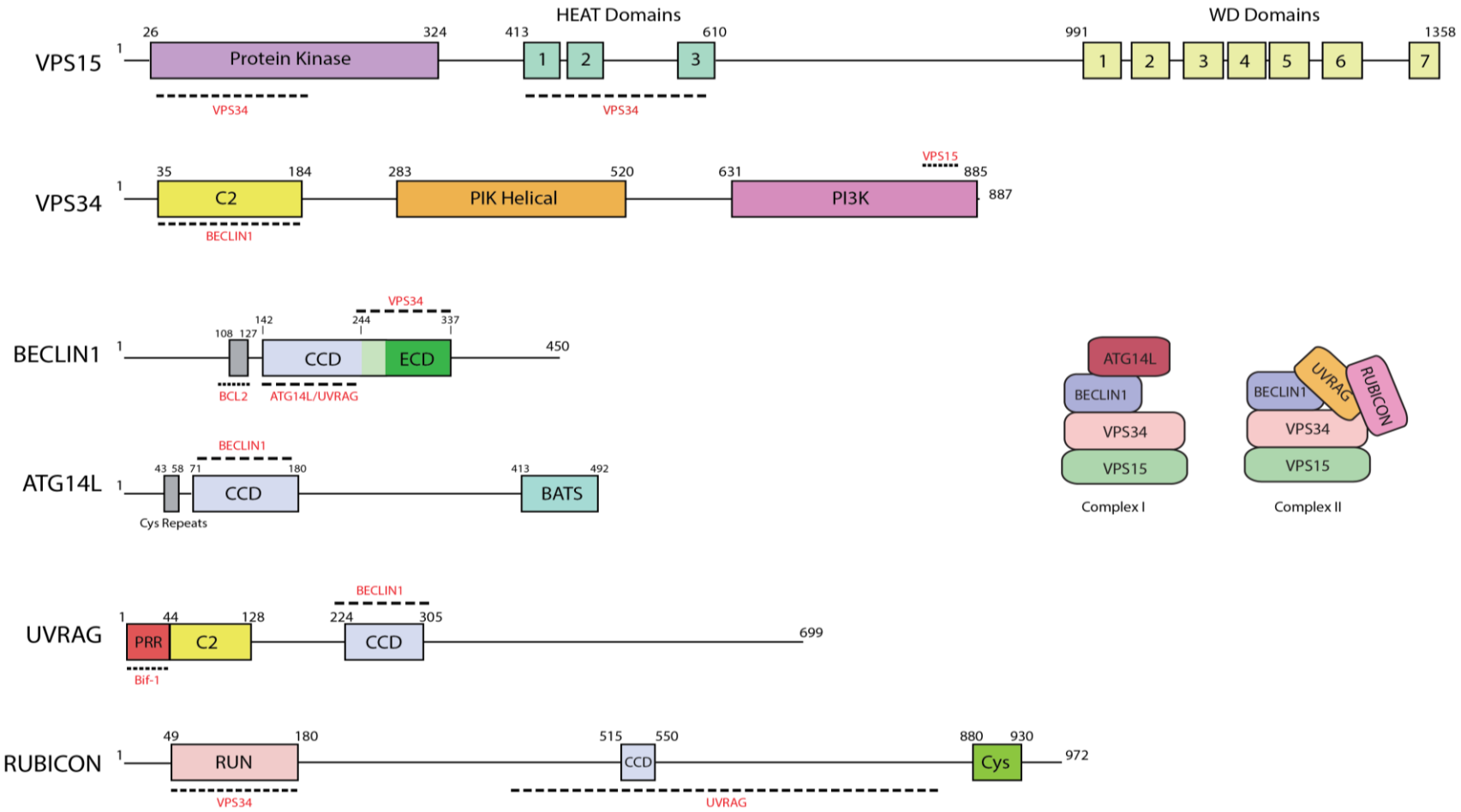

Figure 1.10 - Domain Structure of the VPS34 Complex

Domain structure of VPS34 complex components where numbers indicate amino acid residues, dashed lines and protein names in re d indicate defined protein interacting regions. Domain abbreviations: CCD = Coiled coil domain, ECD = Evolutionary conserved domain, BATS = Barkor/ATG14L autophagosome targeting sequence, PRR = Proline rich region.

1.2.4 The Role of UVRAG

The protein UVRAG was first identified by its ability to promote survival in xeroderma pigmentosum cells upon exposure to ultraviolet irradiation and it is presumed to be a haploinsufficient tumour suppressor as it is frequently found monoallelically deleted or mutated in colon cancers (Ionov et al. 2004; Teitz et al. 1990). UVRAG contains an N-terminal proline rich region (PRR), a C2 domain, a CCD and a large C-terminal domain with no defined domain structure (Figure 1.10). Very little was known regarding the function of UVRAG until it became implicated in binding to BECLIN1 via the CCD and reported to induce autophagy upon expression (Liang et al. 2006), however subsequent studies have failed to recapitulate an autophagic phenotype upon expression or depletion (Itakura et al. 2008; Knævelsrud et al. 2010). UVRAG is also bound by 'RUN domain protein as Beclin-1 interacting and cysteine-rich containing' (RUBICON) that acts as a negative regulator to reduce VPS34 lipid kinase activity and subsequently EGFR trafficking (Matsunaga et al. 2009; Sun et al. 2010). The PRR of UVRAG contains non-repetitive repeats, a particular class of PRR that often bind to SH3 domains of other proteins (Williamson 1994). UVRAG has been reported to bind to the SH3 domain of Endophilin-B1 (Bif-1), an N-BAR containing protein that can induce membrane curvature and is thought to promote autophagy (Takahashi et al. 2007; Takahashi et al. 2009). UVRAG has also been reported to bind to VPS11 and VPS16 as part of the class C-VPS complex that assists with membrane fusion at the lysosome (Table 1) (Liang et al. 2008). UVRAG is widely expressed throughout cells exhibiting co-localisation determined by immunofluorescence with multiple endosome markers (EEA1, Rab9, LAMP1), Golgi markers (GM130, TGN46), ER markers (Calnexin, Dsred-ER), nuclear damage markers (γ-H2AX) and also the centrosome (CEP63) that suggests UVRAG possesses a wide range of cellular functions beyond the established role of Vps38p in yeast (He et al. 2013; Itakura et al. 2008; Matsunaga et al. 2009; Zhao et al. 2012).

1.2.5 Induction of Autophagy

The small ubiquitin like molecule microtubule-associated protein 1 light chain 3 (LC3 - atg8 in yeast) is conjugated to phosphatidylethanolamine to form LC3-II that is recruited to autophagosomal membranes and therefore correlates with the autophagosome abundance (Kabeya et al. 2000). Once the autophagosome is sealed, the LC3-II retained inside is subject to degradation alongside the other autophagic cargo by the lysosome. Cellular LC3 levels are dynamic due to the constant synthesis and degradation by autophagy, inhibitors that block lysosomal acidification prevent LC3-II degradation but do not affect autophagosome formation (Yamamoto & Tagawa 1998). Therefore LC3-II that would normally be degraded accumulates and this is higher in cells actively undergoing autophagy, measurement of LC3-II before and after lysosome inhibition is commonly used as an assay to compare autophagic rate (Klionsky & Abdalla 2012). This has been utilised extensively to study factors that modulate autophagy.

The activation of autophagy requires the activity of both the lipid kinase VPS34 and protein kinase Apg1/ULK1 at primary stages for successful formation of autophagosomes (Chan et al. 2007; Kihara, Noda, et al. 2001). Autophagy can be activated in response to multiple cellular stresses that includes amino acid starvation (Mortimore & Schworer 1977), glucose starvation (Kotoulas et al. 2006), hypoxia (Tracy et al. 2007) and infection (Suzuki et al. 2007) . Precisely how all these stress pathways feed in to induce autophagy is still poorly understood.

The discovery that inhibiting target of rapamycin (TOR) in yeast leads to the activation of autophagy was a significant step forward in understanding the pathways involved in regulating autophagy (Noda & Ohsumi 1998). It was subsequently found that TOR inhibits Apg1 activity by hyperphosphorylation of Apg13 to prevent interaction with Apg1 (Kamada et al. 2000). In mammalian cells ULK1 and ATG13 are both phosphorylated by mTOR, but this does not affect their binding (Hosokawa et al. 2009). The phosphorylation does however correlate with reduced ULK1 kinase activity and autophagy (Ganley et al. 2009; Jung et al. 2009).

5’AMP-activated protein kinase (AMPK) also plays a critical role in sensing energy status in response to ADP and AMP levels (Hardie 2011). It has also been identified to phosphorylate ULK1 to stimulate autophagy in response to glucose starvation (Kim et al. 2011). AMPK however has also been suggested to negatively regulate ULK1 by inhibitory phosphorylation that is relieved upon amino acid starvation (Shang et al. 2011).

It is now apparent that ULK1 is heavily phosphorylated within cells and it is possible that this represents connections to multiple stress pathways (Alers et al. 2012). Further work is required to determine the upstream kinases to many of these sites and elucidate the functional consequences of ULK1 phosphorylation.

1.3 The Mechanistic Target of Rapamycin

1.3.1 mTOR complexes

The mechanistic target of rapamycin (mTOR) is a serine threonine protein kinase that is homologous to yeast TOR and forms the active core of two distinct complexes, mTOR complex 1 (mTORC1) and mTOR complex 2 (mTORC2). Distinction has been drawn between the two complexes based upon their sensitivity to the inhibitor rapamycin, where mTORC1 is inhibited and mTORC2 is resistant analogous to TOR complex 1 and 2 in yeast (Loewith et al. 2002). mTORC1 is regulated by nutrient status and growth factor signalling and when activated promotes growth by phosphorylation of downstream targets including p70 S6 Kinase (S6K) and eIF4E-binding protein 1 (4E-BP1) that act to improve protein translation (Hara et al. 1997; Price et al. 1992). eIF-4E binds to the mRNA cap to enhance protein synthesis (Gingras et al. 1999) but 4E-BP1 can bind and sequester eIF-4E to inhibit translation (Rousseau et al. 1996). Phosphorylation of 4E-BP1 by mTORC1 releases eIF-4E and thereby promotes growth (Beretta et al. 1996). Simultaneously mTORC1 acts to repress catabolic pathways by inhibitory phosphorylation, such as described previously with ULK1 or transcription factor EB (TFEB) (Ganley et al. 2009; Peña-Llopis et al. 2011). TFEB positively regulates the expression of genes belonging to the coordinated lysosomal expression and regulation (CLEAR) network and autophagy proteins (Sardiello et al. 2009; Settembre et al. 2011). Phosphorylation of TFEB by mTORC1 prevents nuclear localisation and therefore represses transcription of autophagic and lysosomal genes (Roczniak-Ferguson & Petit 2012; Settembre et al. 2012). Co-ordinated positive regulation of anabolic and negative regulation of catabolic processes therefore acts to promote cellular growth when mTORC1 is active (Kim et al. 2002).

The signalling and regulation of mTORC2 is less understood, but it is known to have major roles in the regulation of the actin cytoskeleton and mediates protein kinase B (PKB or AKT), protein

kinase C (PKC) and serum and glucocorticoid induced protein kinase (SGK) phosphorylation (Ikenoue et al. 2008; Sarbassov et al. 2004).

The complexes are differentiated by additional binding proteins, mTORC1 is primarily defined by binding of the **r**egulatory **a**ssociated **p**rotein of m**TOR** (**RAPTOR**) that plays an important role in substrate recognition and is the rapamycin sensitive component (Hara et al. 2002; Kim et al. 2002). mTORC1 also contains the proline-rich Akt substrate of 40 kDa (PRAS40) that binds directly to RAPTOR to inhibit kinase activity, activation of growth factor signalling however leads to phosphorylation of PRAS40 by Akt that causes dissociation from RAPTOR (Sancak et al. 2007; Vander Haar et al. 2007). In contrast mTORC2 is primarily defined by binding to the **r**apamycin-**i**nsensitive **c**ompanion of m**TOR** (**RICTOR**) that is required for mTORC2 activity (Jacinto et al. 2004; Sarbassov et al. 2004). Other unique components of mTORC2 include mammalian stress-activated protein kinase interacting protein (mSIN1) that helps to stabilise RICTOR and contributes to activatory phosphorylation of AKT (Jacinto et al. 2006; Yang et al. 2006). Additionally PROTOR-1 binds to RICTOR but it is not required for mTORC2 stability but affects the phosphorylation of SGK1 (Pearce et al. 2011). mTORC1 and mTORC2 complexes contain the protein DEP domain-containing mTOR-interacting protein (DEPTOR) that negatively reduces activity (Peterson et al. 2009). In addition, both complexes contain the protein mammalian lethal with SEC13 protein 8 (mLST8) that is required for mTORC2 function yet has no effect upon mTORC1 activity (Guertin et al. 2006). The composition of mTORC1 and mTORC2 is demonstrated in Figure 1.11.

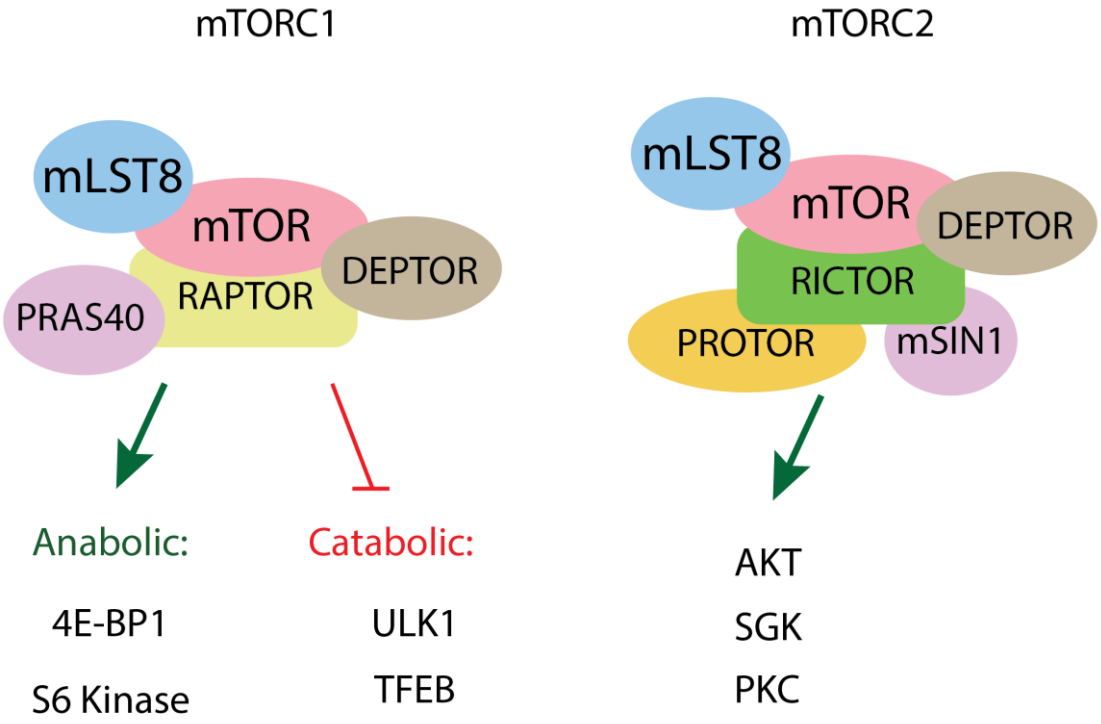

Figure 1.11 - Mammalian mTOR complexes

Components of mTORC1 and mTORC2 are demonstrated. mTORC1 contributes to anabolic process via phosphorylation of 4E-BP1 and S6 Kinase whilst inhibiting catabolic processes by phosphorylation of ULK1 and TFEB. Less is known regarding mTORC2 regulation and substrates, however established substrates include AKT, SGK and PKC.

1.3.2 Regulation of mTORC1

The activity of mTORC1 is modulated by the small G-protein Ras homolog enriched in brain (RHEB) that increases S6K and 4E-BP1 substrate phosphorylation (Inoki et al. 2003; Tee et al. 2003). RHEB is reported to interact with the mTOR complex independently of GDP/GTP binding state, however only RHEB-GTP is able to increase mTORC1 activity (Long et al. 2005). The interaction of mTORC1 and RHEB occurs at the lysosome and is modulated by two distinct nutrient dependent pathways that connect mTOR activity to cellular nutrient status (Flinn et al. 2010).

Receptor tyrosine kinases (RTKs) such as the EGFR or insulin receptor (IR) are activated upon growth factor binding and causes autophosphorylation of the cytoplasmic tail (Schmidt-Ullrich et al. 1997). This subsequently activates PI3Kα that utilises $PI(4,5)P_2$ at the plasma membrane to

form PI(3,4,5)P_3 (Stephens et al. 1993). In turn, PtdIns(3,4,5)P_3-dependent protein kinase-1 (PDK1) and its substrate AKT are recruited to the plasma membrane via their PH lipid binding domains and AKT is activated by PDK1 mediated phosphorylation (Alessi et al. 1997). Alongside relieving mTORC1 of inhibition by removing PRAS40 (Sancak et al. 2007; Vander Haar et al. 2007), AKT also plays a key role in modulating the tuberous sclerosis complex (TSC). TSC1 and TSC2 form a heterodimer that act as a GTPase activating protein (GAP) for RHEB, driving it to the inactive RHEB-GDP state (Garami et al. 2003; Inoki et al. 2003). Active AKT however phosphorylates TSC2 (Potter et al. 2002) and causes the release of TSC1-TSC2 from the lysosome, thereby promoting the RHEB-GTP state (Menon et al. 2014).

In addition to growth factor signalling, the level of amino acids also impacts upon mTORC1 activation. Four Rag GTPases termed RagA-D exist as heterodimers of RagA/RagB and RagC/RagD and are tethered to the lysosome via a protein complex termed the Ragulator (Sancak et al. 2008). In the absence of amino acids Rags are present as RagA/B-GDP and RagC/D-GTP, stimulation with amino acids causes the state to change and is dependent upon the vacuolar H^+ ATPase, leading to RagA/B-GTP and RagC/D-GDP (Zoncu et al. 2011). The Ragulator acts as a guanine nucleotide exchange factor (GEF) in a vacuolar H^+ ATPase dependent manner that promotes RagA/B-GTP (Bar-Peled et al. 2012). The active Rag heterodimer then interacts and recruits RAPTOR to the lysosomal membrane (Sancak et al. 2010). This is key to recruitment of the mTORC1 complex to the lysosome to allow co-localisation with RHEB, as such, withdrawal of amino acids impairs mTORC1 activity in response to growth factor stimulation as mTORC1 does not localise with active RHEB (Smith et al. 2005).

The amino acid and growth factor pathways thereby alter mTORC1 activity by modulating access to RHEB-GTP and are demonstrated in Figure 1.12. Activation of both pathways is required for maximal mTORC1 activity (Sengupta et al. 2010). Active mTORC1 is assumed to remain bound to the lysosomal membrane, however active mTORC1 correlates with peripheral lysosomal positioning that is thought to assist with substrate phosphorylation (Korolchuk et al. 2011). Upon

withdrawal of nutrients the Rag GTPases recruit TSC2 to the membrane to inactivate RHEB and causes mTORC1 release from the lysosome (Demetriades et al. 2014).

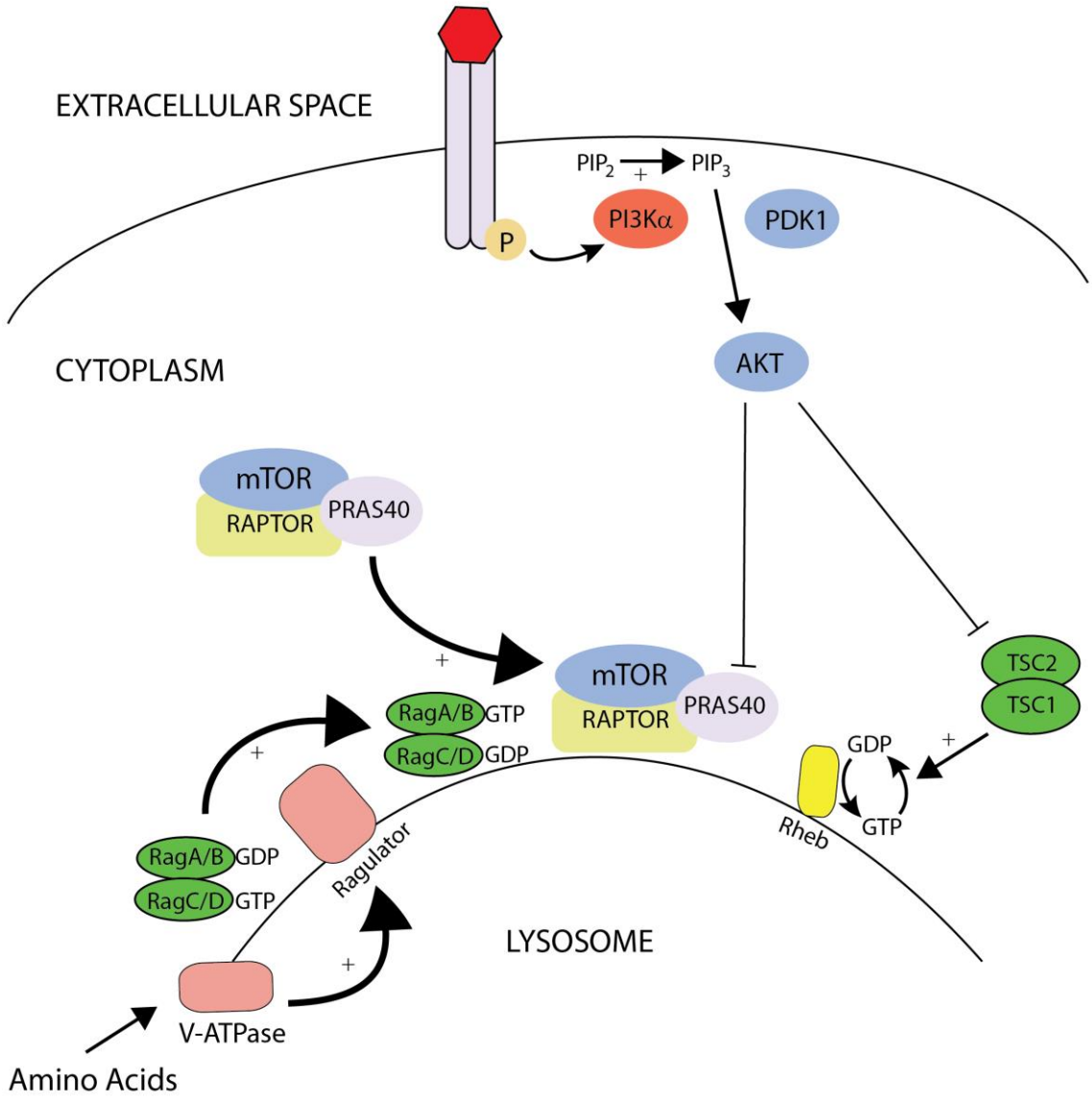

Figure 1.12 - Regulation of mTORC1 Activity

mTORC1 is dependent upon two distinct pathways for activation. Growth factor signalling leads to the formation of PIP_3 at the cell surface by PI3Kα activity, this recruits PDK1 and leads to AKT phosphorylation and activation. AKT removes the negative mTORC1 regulator PRAS40 by phosphorylation and causes dissociation of TSC1-TSC2 from the lysosome to prevent GAP activity towards RHEB. Amino acids impact upon the vacuolar ATPase that promotes GEF activity of the Ragulator complex, forming RagA/B-GTP and RagC/D-GDP. This recruits the mTORC1 complex to the lysosome via interaction with RAPTOR.

1.3.3 Signalling, Trafficking and Human Disease

Growth factor signalling plays a vital role in communicating the presence of nutrients and conveying growth in cells. It is perhaps not surprising therefore that mutations that cause dysregulation of this pathway are responsible for driving many human diseases, particularly cancer(Easton & Houghton 2006; Vivanco & Sawyers 2002).

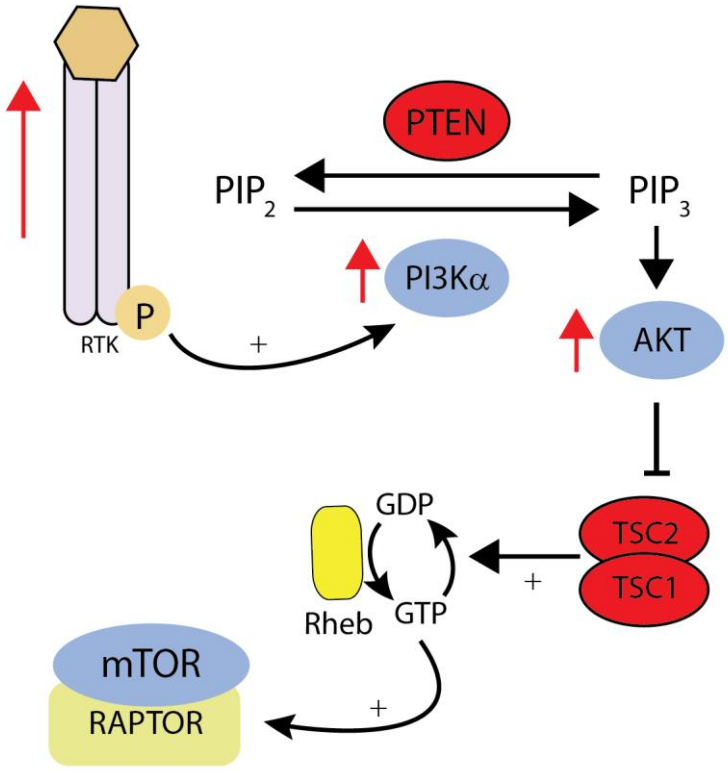

Figure 1.13 - Aberrant Growth Factor Signalling

Many components in the receptor tyrosine kinase (RTK) mediated PI3K-AKT growth factor signalling pathway are mutated in human cancers. Hyperactive signalling is achieved by upregulation or constitutive activation of components indicated by red arrows. Alternately loss of function or decreased expression of negative regulators indicated in red can lead to heightened signalling.

Defects in components of the PI3K-AKT signalling pathway can lead to hyperactive growth signalling (Figure 1.13) and many mutations have been identified in human cancers. Increased formation of PI(3,4,5)P_3 at the plasma membrane is often observed and this can occur through several means. Amplification of the PI3Kα catalytic subunit p110 gene that forms PI(3,4,5)P_3 from PI(4,5)P_2 is detected in many cancers including ~40 % of ovarian cancers (Shayesteh et al.

1999). Alternately loss of function mutations in phosphatase and tensin homolog (PTEN), a 3'-phosphatase that counteracts PI3Kα formation of $PI(3,4,5)P_3$, is also observed in a multitude of cancers (Li et al. 1997; Steck et al. 1997). The expression of HER-2, a growth factor receptor related to EGFR, is increased in ~30 % of breast cancer tumours (Slamon et al. 1987). Increased expression of HER-2 is sufficient to promote malignant transformation (Di Fiore et al. 1987). Mutations in AKT that lead to constitutive activation are also demonstrated to transform cells and induce leukaemia in mice (Carpten et al. 2007). Similarly, tuberous sclerosis complex is caused by mutations and loss of function in the TSC1 or TSC2 gene that consequently enhances mTOR signalling and leads to the formation of multiple benign tumours (Kenerson et al. 2002). Upregulation of the PI3K-AKT pathway is therefore clearly affiliated with the pathogenesis of cancer. PI3K-AKT signalling is mediated through mTORC1 and therefore drugs targeting mTORC1 seems an attractive target to prevent aberrant signalling. Indeed inhibition of mTOR has proven to be beneficial in the treatment of PTEN null cell lines i*n vitro* and tumours from mouse models *in vivo* (Neshat et al. 2001; Podsypanina et al. 2001). Clinical trials with rapamycin analogues however have demonstrated limited efficacy, this may in part be due to the pro-survival mechanism of autophagy that we now understand to be activated by mTOR inhibition (Benjamin et al. 2011). The lysosomal inhibitor hydroxychloroquine (HCQ) (Fedorko et al. 1968) was licensed for use in malaria in 1955 (Hoekenga 1955) and is currently the only FDA approved inhibitor that disrupts autophagy. Combination of mTOR inhibitors with HCQ have demonstrated synergistic effects upon cell death in melanoma cell lines by inducing apoptosis (Xie et al. 2013). Data from phase I clinical trials have indicated that the combination of mTOR inhibition and HCQ prolongs the stable disease period of advanced melanoma compared to mTOR inhibition alone but potentially more potent autophagy inhibition could further improve patient outcome (Rangwala et al. 2014). The consequences of clinical administration of more potent lysosomal inhibitors however is unknown and may lead to increased toxicity, particularly as the lysosome is central to multiple pathways beyond autophagy. The debilitating effects of impaired lysosomal processing is clearly apparent in individuals affected by lysosomal storage

diseases (LSDs). LSDs are a group of over 50 genetic diseases caused by deficiencies in lysosome enzymes or transport proteins that are characterised by the progressive accumulation of material within the lysosome due to aberrant function (Neufeld 1991). The combined prevalence of LSD is ~ 1 in every 7700 live births (Meikle et al. 1999) and cause ranging symptoms with varying severity dependent upon the affected protein. Symptoms include kidney failure, hearing loss, movement disorders and delays in development (Grabowski 2008; van der Ploeg & Reuser 2008; Zarate & Hopkin 2008). Caution must therefore be taken in attempts to pharmacologically target and impair lysosome function as a therapeutic strategy. Positively modulating lysosomes may prove beneficial for treatment of certain diseases that accumulate protein such as LSDs or use in Alzheimer's and Huntington's that are characterised by accumulation of β-amyloid and Huntingtin protein aggregates respectively (DiFiglia et al. 1997; Masters & Simms 1985). Z-Phe-Ala-diazomethylketone (PADK) increases the formation and activity of Cathepsin B and has been demonstrated to reduce the β-amyloid aggregates in an Alzheimer's mouse model (Butler et al. 2011).

The importance of functional autophagy and endocytosis are clearly demonstrated in knockout mouse models. Impairment of autophagy in knockout mice causes death shortly after birth (Komatsu et al. 2005) whilst endocytosis is even more fundamental with VPS34 and BECLIN1 knock-out mice dying during embryogenesis (~E7.5) (Yue et al. 2003; Zhou et al. 2011). Alternative drugs that selectively target the autophagy pathway without affecting the lysosome and endocytic pathways could improve clinical efficacy and carry a lower risk of side effects. However an improved understanding of the co-regulation of autophagy and endocytosis will be required to identify appropriate targets for such drugs.

Interestingly, whilst mTORC1 has been established to regulate autophagy induction via ULK1 (1.2.5), the regulation of VPS34 in this context is unclear. The formation of PI(3)P at early autophagosome sites (the omegasome) is increased upon starvation, demonstrating that activity or localisation of VPS34 is regulated (Axe et al. 2008). Attempts to establish regulatory

roles between VPS34 and mTOR to date have produced contradictory results. Inhibition of VPS34 activity by inhibitory antibodies causes a decrease in the phosphorylation of the mTOR substrate S6K (Byfield et al. 2005), suggesting VPS34 acts upstream. In contrast amino acid starvation and inhibition of mTOR has been demonstrated to decrease the level of cellular PI(3)P (Nobukuni et al. 2005) suggesting VPS34 is regulated by mTOR. Difficulty undoubtedly arises from the interconnection between VPS34 mediated pathways and mTORC1 with the lysosome. Additionally growth factor signalling activates mTORC1 but is subject to regulation by VPS34 as RTK signalling can be terminated by incorporation into MVBs and receptor degradation (1.1.3).

This study aims to identify possible regulatory mechanisms of VPS34 that mediates distinction between endocytosis and autophagy. Improvements in the understanding of how intracellular pathways are connected and regulated is key for the development of future therapies. Recently nanomedicines have been of particular interest with over 70 in clinical trials for cancer alone, endocytosis is one mechanism by which drug internalisation can be achieved (Duncan & Richardson 2012) . Understanding the effect of disease and cancer driving mutations on endocytosis is key as this may be advantageous for targeted delivery of therapeutic compounds, similarly a defect in endocytosis may limit the uptake and impair drug efficacy. A greater understanding of endocytosis and trafficking is therefore essential for generating future therapeutic approaches.

2 MATERIALS AND METHODS

2.1 Materials

2.1.1 Chemicals

Acetone, ethanol, formic acid, glycerol, glycine, 4-(2-Hydroxyethyl)piperazine-1-ethanesulfonic acid (Hepes), Isopropanol, methanol, 2-mercaptoethanol, potassium chloride, sodium chloride, sodium ethylenediaminetetraacetic acid (EDTA), magnesium acetate, sodium ethylene glycol tetra acetic acid (EGTA), sodium fluoride, sodium, β-glycerophosphate, sodium orthovanadate, adenosine 5'-triphosphate sodium salt (ATP), ammonium bicarbonate, ammonium persulphate (APS), bovine serum albumin (BSA), bromophenol blue, dimethyl sulphoxide (DMSO), iodoacetamide, phenylmethanesulphonylfluoride (PMSF), Ponceau S, sodium dodecyl sulphate (SDS), sodium tetraborate, N'-tetramethylethylenediamine (TEMED), triethylammonium bicarbonate, Nonidet P40 and Tween 20 were from Sigma-Aldrich (Poole,UK). Sucrose and Tris (hydroxymethyl)methylamine (Tris) were from BDH (Lutterworth, UK). Precision Plus protein markers, Bradford reagent and Transfectin™ were from BioRad (Herts, UK). 3-[(3-Cholamidopropyl)dimethylammonio]-1-propanesulfonate (CHAPS) was from Calbiochem (Merck Biosciences, Nottingham,UK). Insulin-like growth factor (IGF1) was from Cell Signaling Technology (New Biolabs, Herts, UK). Dialysed foetal bovine serum (FBS) was from Biowest (Nuaillé, France). 6, 24 and 96 well tissue culture plates, cell culture dishes, cryovials and Spin-X columns were from Corning Incorporated (NY, USA). siRNA and buffer was from Dharmacon. 40% (w/v) 29:1 Acrylamide: Bis-Acrylamide solution was from Flowgen Bioscience. Protein G-sepharose, Glutathione-sepharose, Enhanced chemiluminescence (ECL) kit, Hyperfilm MP and ^{32}P-labelled γ-ATP were purchased from GE Healthcare (Piscataway, USA). Dulbecco's modified eagle medium (DMEM), Opti-MEM reduced serum media, Foetal bovine serum (FBS), Dulbecco's Phosphate buffered serum (PBS), Trypsin/EDTA solution and L-glutamine were from GIBCO (Paisley, UK). Precast NuPAGE Novex SDS polyacrylamide 4-12% Bis-Tris gels, NuPAGE MES and

MOPS running buffer (20X), ProLong Gold and Silver Quest stain were from Invitrogen (Paisley, UK). Photographic developer (LX24) and liquid fixer (FX40) were from Kodak (Liverpool, UK). X-ray films were from Konica Corporation (Japan). Polyethylenimine (PEI) was from Polysciences (Warrington, PA). Skimmed milk (Marvel) was from Premier Beverages (Stafford, UK). Plasmid Maxi kits were from Qiagen Ltd (Crawley, UK). Acetonitrile (HPLC grade) and trifluoroacetic acid (TFA) were from Rathburn Chemicals (Walkerburn, UK). Protran BA nitrocellulose membrane was purchased from Schleicher and Schuell (Anderman and Co.Ltd., Surrey, UK).

2.1.2 Buffers

The buffers utilised for experiments in this study are detailed in Table 3.

Buffer	DTT	PMSF	PI	β-Me	Composition
Acid Strip					20 mM Acetic Acid, 500 mM NaCl
Blocking Buffer					5 % (w/v) Milk Powder, TBST
BSA Antibody Buffer					5 % (w/v) BSA, TBST, 0.02 % (w/v) Sodium Azide
CHAPS lysis buffer	X	X	X		20 mM Tris pH 7.4, 137 mM NaCl, 2 mM EDTA, 10 % (v/v) Glycerol, 2 % (w/v) CHAPS
Dialysis Buffer	X				25mM Hepes pH 7.4, 50mM KCl
Formaldehyde Buffer					3.7 % (w/v) Formaldehyde, 200 mM Hepes pH 7.4
Fractionation Buffer	X	X	X		20 mM Hepes pH 7.4, 250 mM Sucrose, 1 mM EDTA
Gel Filtration Buffer	X	X	X		50 mM Hepes pH 7.4, 150 mM NaCl, 1 mM EDTA
Glutamate Buffer					25 mM Hepes pH 7.4, 25 mM KCl, 2.5 mM Mg-Acetate, 5 mM EGTA, 150 mM K-Glutamate
GST Elution Buffer				0.1 %	(50 mM Tris pH 7.5, 250 mM NaCl, 0.1 mM EDTA, 0.3 % (v/v) Brij-35, 40 mM Glutathione) pH 8
IF Blocking Buffer					PBS, 1 % (w/v) BSA
Kinase Buffer					25 mM Hepes pH 7.4, 50 mM KCl
Lipid Kinase Assay Buffer					10 mM $MnCl_2$, 20 mM Tris pH 7.5, 67 mM NaCl, 0.02 % (w/v) CHAPs
Milk Antibody Buffer					5 % (w/v) Milk powder, TBST, 0.02 % (w/v) Sodium Azide
mTORC lysis buffer	X	X	X		40 mM Hepes pH 7.4, 120 mM NaCl, 1 mM EDTA, 0.3 % (w/v) CHAPS
NP-40 (0.5 %) lysis buffer	X	X	X		50 mM Hepes pH 7.4, 150 mM NaCl, 1 mM EDTA, 10 % (v/v) Glycerol, 0.5 % (v/v) NP-40
NP-40 (1 %) lysis buffer	X	X			50 mM Hepes pH 7.4, 150 mM NaCl, 1 mM EDTA, 10 % (v/v) Glycerol, 1 % (v/v) NP-40
Opti-prep buffers					10-45% (v/v) Opti-prep, 20 mM Hepes pH 7.4, 1mM EDTA
Permeabilisation buffer					PBS, 0.2 % (v/v) NP-40
Phosphatase Inhibitor Cocktail (100x)					115 mM Sodium Molybdate, 400 mM Sodium Tartrate, 1 M β-Glycerophosphate, 100 mM Sodium Fluoride, 100 mM Sodium Orthovanadate
Ponceau					5 % (v/v) Acetic Acid, 0.1 % (w/v) Ponceau S
Potassium Oxalate Buffer					1 % (w/v) Potassium Oxalate, 5 mM EDTA, 50 % (v/v) Methanol
Running Buffer (1x)					25 mM Tris, 51.7 mM Glycine, 3.47 mM SDS
Sample Buffer (4x)				10 %	250 mM Tris pH 6.8, 8 % (w/v) SDS, 40 % (v/v) Glycerol, 0.02 % (w/v) Bromophemol Blue
Sample Buffer (5x)				12.5 %	300 mM Tris pH 6.8, 10 % (w/v) SDS, 50 % (v/v) Glycerol, 0.025 % (w/v) Bromophenol Blue
TBST (1x)					20 mM Tris, 150 mM NaCl, 0.1 % (v/v) Tween- 20
Transfer Buffer (1x)					48 mM Tris, 39 mM Glycine, 1.3 mM SDS, 10 % (v/v) Methanol

Table 3 – Buffers Utilised in this Study.

Where indicated 1mM DTT, 1mM PMSF, 1x Phosphatase Inhibitor cocktail and β-mercaptoethanol (β-Me) were added fresh before use.

2.1.3 Inhibitors

Inhibitors utilised in this study and their working concentrations are indicated in Table 4.

Name	Target	IC50	Working Concentration	Reference	Company	Cat Number	CAS Number
Bafilomycin A1	V-ATPase	0.6 - 1.5 nM	50 nM	(Yoshimori et al. 1991)	Enzo life sciences	BML-CM110	88899-55-2
KU0063794	mTOR	10 nM	1 µM	(García-Martínez et al. 2009)	Tocris	3725	938440-64-3
Rapamycin	mTORC1	50 pM	100 nM – 1 µM	(Hara et al. 2002)	Merck Millipore	553210	53123-88-9
VPS34-IN1	VPS34	25 nM	1 µM	(Bago et al. 2014)	Novartis	N/A	N/A
VPS34-IN2	VPS34	6 nM	1 µM	N/A	Novartis	N/A	N/A
Wortmannin	PI3K	3 µM	10 µM	(Stack & Emr 1994)	Enzo life sciences	BML-ST415	19545-26-7
YM201636	PIKfyve	33 nM	1 µM	(Jefferies et al. 2008)	Biovision	2045-1	371942-69-7

Table 4 – Inhibitors Utilised and IC_{50} Values

2.1.4 Antibodies (In-House)

Antibodies were generated and purified by the Division of Signal Transduction Therapy (DSTT), University of Dundee and are detailed in Table 5.

Name	Estimated MW (kDa)	Species	Ref	WB Conc	WB buffer
LC3	14/16	Sheep	S400D	1 µg/ml	Milk
mTOR	260	Sheep	S683B	1 µg/ml	Milk
PRAS40	40	Sheep	S115B	1 µg/ml	Milk
RAPTOR	150	Sheep	S682B + S260D	1 µg/ml	Milk
RICTOR	192	Sheep	S654B	1 µg/ml	Milk
UVRAG	95	Sheep	S323D	1 µg/ml	Milk
UVRAG P-550	95	Sheep	S307D	1 µg/ml	Milk
UVRAG P-571	95	Sheep	S451D	1 µg/ml	Milk
VPS34	100	Sheep	S672B	1 µg/ml	Milk

Table 5 - In-House Antibodies Utilised

2.1.5 Antibodies (Commercial)

Commercial antibodies utilised for western blotting and immunofluorescence are detailed in Table 6.

Target	~MW (kDa)	Species	Company	Cat Number	WB Conc	IF Conc	WB Buffer	Comments
4E-BP1	20	Rabbit	CST	9452	1:1000		BSA	
4E-BP1 P-T37/46	20	Rabbit	CST	9459	1:1000		BSA	
Akt P-T308	60	Rabbit	CST	4056	1:1000		BSA	
Akt P-S473	60	Rabbit	CST	9271	1:1000		BSA	
APPL1	80	Rabbit	CST	3858	1:1000	1:500	BSA	
Anti-Mouse	-	Goat	Thermo		1:5000		Milk	HRP conjugate
Anti-Rabbit	-	Goat	Thermo		1:5000		Milk	HRP conjugate
Anti-Sheep	-	Rabbit	Thermo		1:5000		Milk	HRP conjugate
ATG13	55	Rabbit	Sigma	SAB4200100	1:1000		Milk	
ATG13 S318	55	Rabbit	Abnova	PAB19948	1:1000		Milk	
ATG14L	70	Rabbit	MBL	PD026	1:1000		BSA	
BECLIN1	55	Rabbit	MBL	PD017	1:4000		BSA	
Beclin2-HRP	50	HRP	Novus Biologicals	NB110-60982H	1:1000		Milk	
DNA-PK	250	Rabbit	CST	4602	1:1000		BSA	
EEA1	170	Rabbit	CST	2411	1:1000	1:500	BSA	
EGFR	150	Rabbit	Santa Cruz	sc-03	1:1000		BSA	
ERK1/2	44/42	Rabbit	CST	4695	1:1000		BSA	
P-ERK1/2	44/42	Rabbit	CST	4376	1:1000		BSA	
FLAG-HRP	-	HRP	Sigma	A8592	1:2000		Milk	
FYCO1	200	Mouse	Abnova	H00079443-A01	1:1000	1:500	BSA	
FYVE-CENT	260	Rabbit	CST	8532	1:1000	1:500	BSA	
GFP	-	Mouse	Roche	11814460001	1:3000		BSA	WB Only
GFP	-	Rabbit	Life Technologies	A11122	-	1:1000		IF Only
GSK3 a/b	51/46	Mouse	Invitrogen	44610	1:500		BSA	
GSK3 P-S9/21	51/46	Rabbit	CST	9331	1:1000		BSA	
GST-HRP	-	HRP	Abcam	Ab3416	1:2000		Milk	
LAMP1	100	Mouse	Santa Cruz	sc-20011 (H4A3)	1:1000	1:1000	Milk	Detects Human
LAMP1	100	Rat	Santa Cruz	sc-19992 (1D4B)	1:1000	1:1000	Milk	Detects Mouse
LC3	14/16	Rabbit	CST	4108	1:1000		Milk	WB Only
LC3	14/16	Mouse	MBL	M152-3		1:1000		IF Only
mCherry	-	Mouse	Clontech	632543	1:1000		Milk	
mTOR	250	Rabbit	CST	2983	1:1000	1:500	BSA	
P70 S6K	70	Rabbit	CST	2708	1:1000		BSA	
p70 (S6K) P-T389	70	Rabbit	CST	9205	1:1000		BSA	
RAB5	~25	Rabbit	CST	2143	1:1000		BSA	
RAB7	~25	Rabbit	CST	9367	1:1000		BSA	
RAB11a	~25	Rabbit	CST	2413	1:1000		BSA	
RUBICON	130	Rabbit	CST	8465	1:1000		BSA	
α-TUBULIN	52	Mouse	Calbiochem	CP06	1:2500		BSA	
α-TUBULIN	52	Rabbit	CST	2125	1:3000		Milk	
Transferrin Receptor	95	Mouse	Invitrogen	136800	1:1000		BSA	
TSC2	200	Rabbit	CST	3990	1:1000		BSA	
TSC2 P-T1462	200	Rabbit	CST	3611	1:1000		BSA	
ULK1	130	Rabbit	Sigma	A7481	1:1000		Milk	
ULK1 P-757	130	Rabbit	CST	6888	1:1000		BSA	
UVRAG	95	Mouse	MBL	M160-3	1:1000		BSA	

Table 6 - Commercial Antibodies utilised in this study.

Western Blot (WB) and Immunofluorescence (IF) antibody concentrations are as indicated. CST = Cell Signaling Technologies, MBL = MBL International Corporation.

2.1.6 cDNA Constructs

cDNA constructs utilised for experiments in this study are highlighted in Table 7.

Protein	Tag (Terminus)	Vector	Genbank ID	Species	Mammalian Selection	DU Number	Comments
ATG14L	GST (N)	pEBG6P	NM_014924.4	H	N/A	40296	
BECLIN1	FLAG (N)	pBabe	AAH10276.1	H	Puro	35123	
DFCP1	GFP (N)	pBabe	NP_067083.1	H	Hyg	40185	
HRS	GFP (N)	pBabe	AF020308.1	M	Puro	40523	2xFYVE domain (147-223 with linker)
HRS	GST (N)	pGEX6P	AF020308.1	M	N/A	45781	2xFYVE domain (147-223 with linker)
LAMP1	GFP (C)	pBabe	NM_005561.3	H	Puro	40445	
LAMP1	mCherry (C)	pBabe	NM_005561.3	H	Puro	49491	
p40 phox	GST (N)	pGEX6P	AB025219.1	H	N/A	45823	M1-R148
p70 (S6K)	GST (N)	pEBG6P	NP_003152.1	H	N/A	32609	D236A (Kinase Dead)
UVRAG	FLAG (N)	pBabe	AAH64837.1	H	Hyg	35051	
UVRAG	FLAG (N)	pBabe	AAH64837.1	H	Hyg	40448	S550A+S571A
UVRAG	GFP (N)	pBabe	AAH64837.1	H	Puro	40482	siRNA Resistant
UVRAG	GFP (N)	pBabe	AAH64837.1	H	Puro	40467	siRNA Resistant, S550A+S571A
UVRAG	GST (N)	pEBG6P	AAH64837.1	H	N/A	36657	
UVRAG	GST (N)	pEBG6P	AAH64837.1	H	N/A	40451	S550A
UVRAG	GST (N)	pEBG6P	AAH64837.1	H	N/A	40452	S571A
UVRAG	GST (N)	pEBG6P	AAH64837.1	H	N/A	40453	S550A + S571A
UVRAG	shRNA	pSuper	AAH64837.1	H + M	Puro	36747	ORF1 site - GGACAAAGGAAGTGCATTT
UVRAG	shRNA	pSuper	AAH64837.1	H + M	Puro	36749	5'UTR site - GTAATATGGCTCTTCCTTA
SGK	GST (N)	pEBG6P	XP_037046	H	N/A	125	K127A

Table 7 – cDNA Constructs used in this study.

Human (H), Mouse (M), Hygromycin (Hyg), Puromycin (Puro). DU Number is the clone reference as recorded by the Division of Signal Transduction Therapy, Dundee.

2.2 Cell Culture

Cell culture media for growth and treatment of cells is detailed in Table 8, all procedures were carried out under aseptic conditions meeting biological safety requirements. For growth, cell lines were maintained in a complete media which included Dulbecco's modified eagles medium (DMEM) and 10 % (v/v) foetal bovine serum (FBS). Cells were grown at 37 °C with 5 % CO_2 in a water-saturated incubator. For passaging, cells were washed once with Dulbecco's phosphate buffered saline (DPBS) prior to incubation with Trypsin + 0.05 % EDTA for 3-5 min at 37 °C to detach cells and split at 1:6 for maintaining growth.

Media Name	Composition of Media
Complete Media	DMEM, 10 % (v/v) FBS, 2 mM L-Glutamine, 100 units/ml penicillin, 0.1 mg/ml streptomycin.
EGF Media	DMEM, 10 mM Hepes pH 7.4, 0.1 % (w/v) BSA
IF Complete Media	DMEM, 10 % (v/v) FBS, 2 mM L-Glutamine, 100 units/ml penicillin, 0.1 mg/ml streptomycin 20 mM Hepes pH 7.4 (No phenol red)
IF Quench Media	DMEM, 10mM Hepes pH 7.4
IF Starvation Media	EBSS, 20mM Hepes pH 7.4 (No phenol red)
Serum Starve Media	DMEM
Starvation Media	EBSS
TFR Media	DMEM, 20mM Hepes pH 7.4, 0.1% (w/v) BSA

Table 8 - Composition of Media used for cell culture and experiments.

Details of media utilised for tissue culture cell growth and experiments where IF = Immunofluorescence.

2.2.1 Induction of Autophagy

Autophagy was induced in cells either by amino acid starvation or chemically via mTOR inhibition (1.2.5). For the former, cells were washed twice and incubated in Earle's balanced salt solution (EBSS) to deprive the cells of amino acids and serum. Alternatively the dual mTORC1 and mTORC2 ATP-competitive inhibitor KU0063794 was used to directly inhibit mTOR activity (García-Martínez et al. 2009). The induction of autophagy was confirmed by addition of the lysosomal inhibitor Bafilomycin A1 to monitor LC3 flux (1.2.5), further details of treatments are noted in figure legends.

2.2.2 Retroviral Generation of Stable Cell Lines

Stable cell lines were generated via retroviral infection in accordance with biological safety regulations. The cDNA of interest (6 µg) was co-transfected into 293FT cells with 3.8 µg GAG/POL and 2.2 µg VSV-G expression plasmids (Clontech) per 10 cm dish for retrovirus production using Lipofectamine® 2000 (Invitrogen) as per manufacturer's protocol. The growth medium was changed at 16 h post-transfection and subsequently harvested at 40 h post-transfection, passed through a 0.45 µm filter, and applied directly on to target cells in the presence of 10 µg/ml polybrene to assist with viral infection (Hesse et al. 1978). Following 24 h of retrovirus exposure, the growth media was changed to include selection with 10 µg/ml puromycin (Sigma) or 100 µg/ml hygromycin B (Source Bioscience) dependent upon cDNA resistance marker (as indicated in Table 7). Successfully transfected cells were utilised for experiments following complete death of non-viral exposed cells in response to selection.

2.2.3 siRNA Knockdown

Endogenous UVRAG was knocked down primarily utilising the siRNA GGACAAAGGAAGTGCATTT as previously described (Liang et al. 2006). All siRNAs were obtained from Dharmacon.

Name	Target Region	Sequence
UVRAG ORF1	Protein Coding	GGACAAAGGAAGTGCATTT
UVRAG ORF2	Protein Coding	ACTCCAGACTTGAGGCAAA
UVRAG 5'UTR	5' Untranslated Region	GTAATATGGCTCTTCCTTA

Table 9 - siRNA Sequences

Cells were reverse transfected using Lipofectamine® RNAIMAX or TransFectin™ as per manufacturer's instructions. Cells were counted using a Countess® automated cell counter (Invitrogen) and $1x10^6$ cells were plated per transfection in a 6 cm dish. Cells were incubated with siRNA in OptiMem for 16 h prior to changing to complete media and the cells were passaged at ~24 h post-transfection, they were then utilised for desired experiments between 40-70 h post-transfection. For forward transfection, protocol was the same utilising adherent cells.

2.3 Cell Lysis and Sample Preparation

Following treatment of cells as described in figure legends, cells were lysed and prepared for subsequent analysis. Cells were moved onto ice and washed twice with ice-cold PBS; all remaining PBS was removed before the addition of lysis buffer (Table 3). Cells were scraped and transferred to eppendorfs for clarification by centrifugation at 21,000 x g for 10 min at 4 °C, supernatants were retained for use in analysis. The protein concentration of samples was determined via Bradford assay (Bradford 1976) to allow normalisation between samples for subsequent analysis.

2.3.1 Western Blotting

Samples to be analysed by western blot were diluted and normalised in 4x sample buffer to create 1x samples for separation by SDS-PAGE. Typically 25-40 µg of protein was loaded per sample alongside Precision Plus Protein™ All Blue Standards (Bio-Rad) and separated by a poly-acrylamide gel in 1x running buffer (Table 3). Samples were transferred to PVDF (Imobilon P – Millipore) membrane at 350 mA for 50 min in 1x transfer buffer (Table 3) and membranes were stained using ponceau (Table 3) to check the quality of transfer before cutting the membrane appropriately to probe for proteins of interest. Membranes were incubated in blocking buffer for 20 min at RT to block membranes and reduce non-specific antibody binding. Membranes were washed twice with TBST (Table 3) prior to incubation in primary antibody for 16 h at 4 °C using concentrations indicated in 2.1.4/2.1.5 in either Milk or BSA antibody buffer. The primary antibody was removed and membranes washed three times for 10 min with TBST prior to addition of secondary HRP conjugated antibodies (Thermo) for 1 h in blocking buffer. Membranes were washed a further three times whilst rocking for 10 min at RT with TBST. Membranes were incubated with Amersham™ enhanced chemiluminescence (ECL) substrate according to manufacturer's protocol and exposed to X-ray film or high sensitivity Amersham™ Hyperfilm™ dependent upon signal and developed using an automatic film developer (SRX-101A – Konica Minolta).

2.3.2 Protein Immunoprecipitation

Following determination of protein concentration by Bradford assay, a specific protein or complex of interest could be selectively isolated by immunoprecipitation (IP). For endogenous proteins, 3 µg of antibody was added per mg of protein lysate and 20 µl of protein G-sepharose per sample. For exogenous tagged proteins, FLAG agarose, GFP-TRAP agarose, GST Sepharose or S-protein agarose beads were used

as appropriate. An input from each lysate was also taken, usually 2-10% of total IP concentration to compare and allow determination of IP efficiency. Samples were incubated for 2 h rotating at 4 °C, beads were pelleted by centrifugation at 1000 x g for 1 min at 4 °C and washed three times with lysis buffer (Table 3). After the final wash, remaining buffer was aspirated to waste and 1x sample buffer was added to beads to precipitate off bound proteins from the beads. IPs could then be analysed by western blot as detailed previously (2.3.1).

2.3.3 Crude Membrane Fractionation

To compare the cytosol to membrane distribution of proteins, cells were crudely fractionated by ultra-centrifugation. Cells were treated as described in figure legends then moved onto ice and washed twice in ice-cold PBS, all PBS was removed before addition of fractionation buffer (Table 3). Cells were scraped and transferred to an Eppendorf, samples were homogenised in the absence of detergent by repeatedly passing through a narrow gauge needle to burst cells. The efficiency of breakage was confirmed by light microscope. Unbroken cells and nuclei were removed by centrifugation at 500 x g for 5 min at 4 °C. Part of the sample was retained as a post-nuclear supernatant (PNS), the remaining sample was then split into cytosol and membrane components by subsequent centrifugation at 100,000 x g for 1 h at 4 °C. The supernatant (cytosol) was removed and diluted in 4x sample buffer. The pellet (membrane) was resuspended in 1x sample buffer at an equal volume to that of the cytosol, this allowed 1:1 (cytosol:membrane) comparison of proteins when loaded equally by western blot.

2.3.4 Mass Spectrometry Sample Preparation

Samples to be analysed by mass spectrometry were first separated by SDS-PAGE as described previously (2.3.1). Acrylamide gels were stained for protein using either Instant Blue™ coomasssie (Expedeon) or SilverQuest ™ silver staining kit (Invitrogen) as per manufacturer's guidelines. To minimise contamination, mass spectrometry samples were handled and processed in a laminar flow hood during sample preparation. Protein bands to be analysed were diced into small cubes (~1 mm) and transferred to a clean Eppendorf per band. Gel pieces underwent sequential washes (0.5 ml for 10 min each on a vibrating platform) with water, 50 % acetonitrile (ACN), 100 mM Ammonium Bicarbonate (NH_4HCO_3) and 50 % ACN/50 mM NH_4HCO_3. Samples were alkylated in gel by addition of 75 µl 10 mM dithiothreitol (DTT) in

0.1 M ammonium bicarbonate for 45 min at 65°C. The supernatant was removed and 75 µl 50 mM Iodoacetamide in 0.1 M ammonium bicarbonate was added and incubated for 20 min at RT. Gel pieces were washed with 0.5 ml for 10 min with 50 mM ammonium bicarbonate and then 50 mM ammonium bicarbonate + 50 % (v/v) ACN. Gel pieces were then incubated with 0.3 ml ACN for 15 min at RT, which was removed by centrifugal evaporation (SpeedVac™, Thermo Scientific) to dry the gel pieces. To digest proteins, 30 µl of 25 mM Triethylammonium bicarbonate containing 5 µg/ml Trypsin was added to gel pieces and incubated shaking for 30 min at RT. Water was added if required to completely cover gel pieces and samples were left shaking at 1100 rpm for 16 h at RT in a Thermomixer® (Eppendorf) to digest peptides. An equal volume of ACN was then added to the gel pieces to extract peptides and incubated at 1100 rpm for 15 min at RT; the supernatant was removed and dried by centrifugal evaporation. During this time 100 µl formic acid buffer was added to the gel pieces and shaken at 1100 rpm at RT. The supernatant was added to the initial dried extract and dried once more by centrifugal evaporation. Once completed, samples were submitted to the MRC proteomics and mass spectrometry team for analysis by LC-MS/MS using an Orbitrap™ Classic mass spectrometer (Thermo Scientific). Proteins and phosphorylation sites were identified from peptides by Mascot software (Matrixscience). Phosphorylation sites were represented by comparison of the extracted-ion chromatogram (XIC) between samples.

2.4 *In vitro* Kinase Assay

2.4.1 Protein Purification

Recombinant proteins for use in mTORC1 kinase assays were exogenously expressed and purified from HEK293 cells. Cells were transfected in 15 cm dishes at ~60 % confluency. Transfection was carried out by incubating 25 µg of DNA per dish in 0.5 ml of Optimem, 50 µg of Polyethylenimine (PEI) was added to a separate 0.5 ml of Optimem. Following a 5 min incubation, solutions were combined to allow coating of DNA with PEI. PEI condenses DNA into positively charged particles that can be internalised by cells via endocytosis, following which the DNA can escape (possibly by osmotic swelling and vesicle bursting) and reach the nucleus (Boussif et al. 1995). Following a further 20 min incubation the DNA-PEI solution was added directly to HEK293 cells in complete media and incubated for 18 h. The media was changed and cells grown for a further 24 h. Cells were then treated (~42h post-transfection) by washing twice and incubating in EBSS for 1 h to inactivate and dephosphorylate mTOR sites; Cells were moved onto ice, washed twice with PBS and lysed in 1% NP-40 lysis buffer lacking phosphatase inhibitors (Table 3). Lysates

were clarified by centrifugation at 3300 x g for 30 min at 4 °C, the cleared supernatant was used for immunoprecipitation with GST-sepharose beads rotating for 2 h at 4 °C. Beads were washed twice with 1% NP-40 lysis buffer + NaCl (1M final) and twice with 1% NP-40 lysis buffer. Beads were then incubated with 20 µl GST elution buffer per harvested plate with occasional shaking (10s every 60s) in a Thermomixer® for 1 h at 4 °C. Elution buffer was removed by passing through a Spin-X® centrifuge column (0.22µm filter, CLS8162, Corning® Costar® - Sigma) at 2000 x g for 1 min at 4 °C. Beads were used for a second and third round of eluting as previous, except using 25% less elution buffer for each elution. All elutions were then dialysed overnight in dialysis buffer. Elutions were then checked by SDS-PAGE and stained with Instant Blue™ coomassie (Expedeon) as per manufacturer's instructions to examine the abundance and purity. Elutions were then snap frozen in liquid nitrogen until required for use.

2.4.2 mTORC1 *in vitro* Kinase Assay

Endogenous mTORC1 was immunoprecipitated from HEK293 cells and used for *in vitro* kinase assays. Cells were grown in complete media and stimulated with 50 ng/ml insulin-like growth factor 1 (IGF1) for 30 min to hyper-activate mTOR prior to lysis in mTORC lysis buffer (Table 3). Endogenous mTORC1 was immunoprecipitated using 3 µg of anti-raptor antibody (S682B or S260D) per mg of HEK293 lysate and 20 µl Protein G Sepharose per sample rotating for 2 h at 4 °C. The beads were pelleted by centrifugation at 1000 x g for 1 min at 4 °C and washed twice with mTORC lysis buffer + NaCl (0.5 M NaCl total), twice with mTORC lysis buffer and finally twice with kinase buffer (Table 3), all washes were 1 ml. After the final wash step, the total IP was split equally between reactions and ~10 µl kinase buffer was left on beads. Per reaction, ~1 µg of substrate was added in 20 µl of kinase buffer prior to the final addition of 10 µl ATP Mix [10 mM $MnCl_2$, 20 µM ATP, 1 µCi ^{32}P γ-ATP per reaction diluted in kinase buffer]. Reactions were agitated in a Thermomixer® at 1100 rpm for 30 min at 30 °C and terminated by the addition of 10 µl 5x Sample Buffer. Samples were ran by SDS-PAGE and transferred to PVDF membrane as previously described (2.3.1), membranes were then exposed to Amersham™ Hyperfilm™ to detect the incorporation of ^{32}P phosphate into protein substrates. Following autoradiography PVDF membranes were incubated in blocking buffer for 20 min at RT and analysed by western blot to control for protein levels between separate reactions.

2.4.3 VPS34 *in vitro* Kinase Assay

Cells were treated as described in figure legends prior to lysis in 0.5% NP-40 lysis buffer (Table 3). UVRAG in complex with VPS34 was immunoprecipitated via GFP-TRAP or FLAG agarose in exogenous expression experiments or alternatively endogenously utilising an anti-UVRAG antibody (S323D). UVRAG was IP'd by rotating lysate for 2 h at 4 °C, beads were then pelleted at 1000 x g for 1 min at 4 °C between washes. Beads were washed twice with 0.5 % NP-40 lysis buffer + NaCl (0.5 M final), twice with 0.5 % NP-40 lysis buffer and finally twice with lipid kinase assay (LKA) buffer (Table 3). VPS34 activity was assayed *in vitro* with a final reaction concentration of 10 µg phosphatidylinositol (PI) liposomes (bovine liver PI, extruded through a 100 nm filter – Avanti® Mini-Extruder), 5 µM ATP + 7.5 µCi ^{32}P γ-ATP in LKA buffer. Alternatively for kinase inhibitor assays, 100 nM recombinant VPS34/15 (DU8692) was used in place of immunoprecipitated kinase. Reactions were agitated in a Thermomixer™ at 1100 rpm for 30 min at 30 °C before centrifugation through a Spin-X® column to separate beads, addition of 500 µl Methanol:Chloroform:Hydrochloric Acid (200:100:3.5) terminated the reaction. 1x sample buffer was added to the beads removed by Spin-X column and retained to analyse by western blotting as a loading control for VPS34 levels immunoprecipitated and to normalise data. Subsequently 180 µl of chloroform and 300 µl of 0.1 M hydrochloric acid was added to the solvent of each sample and centrifuged at 1000 x g for 1 min at RT to phase split components. The chloroform lipid containing lower layer was transferred to a fresh Eppendorf and dried by centrifugal evaporation. Thin layer chromatography (TLC) silica 60 plates (Merck-Millipore) were treated with potassium oxalate buffer (Table 3) and dried to assist with phospholipid separation (Gonzalez-Sastre & Folch-Pi 1968). Dried lipids were resuspended in 50 µl chloroform, spotted onto treated TLC plates and then ran using a methanol:chloroform:water:ammonium hydroxide (47:60:11.2:2) solvent system to separate phosphoinositol products. Once complete the TLC plate was dried and the incorporation of ^{32}P into lipids was analysed using a Fujifilm Image Reader (FLA-2000). Recombinant VPS34/15 (DU8692) was used as a positive control to identify and determine PI(3)P product formation. Quantitation was carried out using AIDA image analyzer (Raytest).

2.5 EGFR Degradation Assay

To monitor cellular endocytic function, the uptake and degradation of the epidermal growth factor receptor (EGFR) was examined. Tissue culture cells were serum starved by washing twice and incubating in DMEM only for 2h or 4h to accumulate EGFR on the cell surface. At time-point 0, 30 μg/ml cycloheximide was added to inhibit protein synthesis (Ennis & Lubin 1964) and 50 ng/ml EGF was added to stimulate EGFR activation. Cells were moved back into the incubator and at time points indicated, moved onto ice and lysed in 0.5 % NP-40 lysis buffer as described (2.3.1). Samples were immunoblotted for EGFR across time-points and the abundance of the EGFR plotted relevant to time.

2.6 DNA Transformation and Plasmid Purification

E.coli DH5α competent bacteria (Life technologies – Invitrogen) were utilised to increase yield of DNA. For each transformation, 20-50 ng of plasmid DNA was added to 25 µl of competent DH5α on ice for 15 min. Uptake of DNA was induced by heat-shock at 40 °C for 45 seconds and returning to ice for 2 min [Modified from (Cohen et al. 1972)]. LB Broth (250 µl) was added to each reaction and streaked out immediately onto LB agar plates containing 100 µg / ml ampicillin. Plates were inverted and incubated for 16 – 20 h at 37 °C to allow colony growth. A single colony was picked and used to inoculate a culture of 250 ml LB Broth containing 100 µg/ml Carbenicillin in an Erlenmayer flask. Cultures were incubated at 180 rpm for 18 h at 30 °C in a Multitron (Infors HT) bacterial shaker. Plasmid DNA was purified from bacterial cultures utilising a plasmid maxiprep kit (Qiagen) as per manufacturer's protocol. Isolated DNA was analysed using a NanoDrop 1000 spectrophotometer (Thermo Scientific) to confirm sample yield and purity.

2.7 Lambda Phosphatase Treatment

Lambda (λ) phosphatase has a wide range of activity against serine, threonine and tyrosine phosphorylation sites in a manganese dependent manner (Cohen & Cohen 1989). Cells were lysed in 0.5% NP-40 lysis buffer (Table 3) and clarified by centrifugation at 21,000 x g for 10 min at 4 °C, the supernatant was supplemented with 10 µg Lambda Phosphatase and 5mM $MnCl_2$ in the presence or absence of phosphatase inhibitor cocktail (used at 10x final). Samples were incubated at 1100 rpm for 30 min at 30 °C in a Thermomixer® and reactions terminated by the addition of 4x sample buffer. Samples were then analysed by western blotting to determine whether the mobility of proteins are affected, indicative of phosphorylation.

2.8 Opti-Prep Gradient Separation

To separate cell lysates by density, Opti-prep™ density gradient was used (D1556 – Sigma). Following treatment, cells were moved onto ice and scraped in membrane fractionation buffer (Table 3) before passing through a narrow gauge needle to homogenise cells. Nuclei and intact cells were removed by centrifugation at 500 x g for 5 min at 4 °C. Density gradients were prepared by sequential layering of 40 % to 10 % Opti-prep™ (Table 3) in 5 % intervals inside thick-wall polycarbonate ultracentrifuge tubes with the cell lysate layered on top as the final addition. Samples underwent centrifugation at 100,000 x g

for 16 h at 4 °C. Layers were removed sequentially and added to 4x sample buffer for analysis by western blotting.

2.9 Size Exclusion Chromatography

Samples to be separated by size exclusion chromatography were treated as described and lysed on ice in 0.5 % NP-40 lysis buffer. Samples were clarified by centrifugation at 21,000 x g for 10 min at 4 °C, the supernatant was then filtered through a 0.22 µm filter to remove any remaining protein precipitates. A Superose 6 column (GE Healthcare) was equilibrated in Gel filtration buffer prior to injection of 0.5 ml of protein lysate. Fractions were collected every 0.5 ml and western blotted as indicated, the approximate molecular weight of eluted proteins was subsequently determined by running a gel filtration chromatography standard (151-1901 – Bio-Rad).

2.10 Immunofluorescence

For fixed immunofluorescence experiments, cells were seeded out onto 22x22 mm glass coverslips. Coverslips were first washed in 100 % ethanol before allowing to air dry in a 6-well plate inside a biological safety cabinet. Once dry, trypsinised cells were added on top and grown for a minimum of 16 h to ensure cells had adhered and settled sufficiently onto the glass. Cells were then utilised for immunofluorescence experiments as described further below. Imaging was carried out on a Nikon Eclipse Ti widefield microscope using NIS Elements.

2.10.1 Cell Fixation, Staining and Mounting

Following treatments, cells require fixation to terminate cell processes and preserve the sample for subsequent microscopy analysis:

2.10.1.1 - Formaldehyde Fixation

In most cases following the desired cell treatment, coverslips were washed twice in PBS before fixing with formaldehyde buffer (Table 3) for 20 min at RT. The formaldehyde was then removed and quenched by washing twice and incubating for 10 min in IF Quench Media (Table 8). If cells were to be stained using antibodies, they were treated as described (2.10.1.3). Otherwise, cells were washed twice in PBS and dipped into ddH_2O briefly before mounting onto coverslides using Prolong® Gold Mountant (with DAPI). Slides were covered and left at RT overnight to allow mountant to dry completely before imaging.

2.10.1.2 - Methanol Fixation

Where indicated, cells were fixed and permeabilised with methanol. Following treatment, coverslips were washed twice briefly in PBS before incubating in -20 °C methanol for 2 min on ice. Coverslips were washed twice further in PBS to remove trace methanol before incubating in IF blocking buffer (Table 8). Antibody staining was then continued as described in 2.10.1.3 (without permeabilisation step).

2.10.1.3 – Antibody Staining

For staining with antibodies, after fixation coverslips were washed once with PBS and then incubated in permeabilisation buffer (Table 8) for 3 min to make intracellular antigens accessible. Coverslips were then washed twice and incubated for 15 min with IF blocking buffer (Table 8) to reduce non-specific epitope binding. The primary antibody was prepared in IF blocking buffer (Table 8) at concentrations indicated in 2.1.5 (typically 1:500 – 1:1000) and added directly onto coverslips and incubated for 1 h at 37 °C. Unbound antibody was removed by washing three times for 10 min in IF blocking buffer. Secondary Alexa-Fluor conjugated antibodies (Life Technologies, Thermo) were added to coverslips (1:500) in IF blocking buffer and incubated for 30 min at RT; surplus antibody was removed by three further washes for 10 min each in IF blocking buffer. Coverslips were briefly dipped into ddH_2O prior to mounting onto coverslides with ProLong gold® antifade mountant (with DAPI, Life Technologies). Coverslides were covered and left at RT overnight to fully dry before imaging.

2.10.2 Transferrin Recycling Assay

Cells were washed twice and incubated with TFR media containing 5 µg/ml transferrin Alexa-Fluor-594 conjugate for 1 h at 37 °C to pre-load the cells. Cells were then washed twice and incubated with complete media containing 100 µg/ml holo-transferrin to prevent re-uptake of labelled transferrin. Coverslips were stopped at multiple time-points to monitor the turnover of transferrin. At each time-point end cells were washed once with acid strip buffer before fixing with formaldehyde buffer and mounting as described in 2.10.1.1.

2.10.3 Phospholipid Staining

2.10.3.1 – PX and FYVE domain probe - PI(3)P

To create specific probes for PI(3)P within cells, the PX Domain of $p40^{phox}$ (DU45823) and 2xFYVE domain of HRS (DU45781) were utilised. Proteins were cloned, expressed and purified by the DSTT (University of Dundee). The probes were then conjugated to Alexa-Fluor 488 (A30006 – Life Technologies) or Alexa-Fluor-594 (A30008 – Life Technologies) as per manufacturer's protocol. The labelled proteins were stored at 1 mg/ml in 50 % (v/v) Glycerol at -80 °C.

2.10.3.2 – PI(3)P Staining Protocol

Cells were treated as described in figure legends, cells were then moved onto ice and washed once with ice-cold PBS. Coverslips were washed twice with ice-cold glutamate buffer prior to brief snap freezing with liquid N_2, coverslips were then thawed and washed twice with glutamate buffer. Coverslips were then fixed with formaldehyde for 30 min at RT, changing the formaldehyde once at 10 min. The formaldehyde was quenched by washing twice and incubating in IF quench media for 10 min. Cells were then washed twice and incubated with IF blocking buffer for 15 min at RT. Coverslips were then incubated with 2xFYVE or PX Domain Alexa-Fluor probes at 1:200 in IF blocking buffer for 1 h at RT. Coverslips were washed twice with IF blocking buffer prior to dipping into ddH_2O and mounting onto microscope slides with prolong® gold mounting solution.

2.10.4 Live Cell Imaging

For live cell imaging experiments, cells were seeded onto glass bottom dishes (627870 – Greiner Bio One) a minimum of 16 h prior to allow cells to settle flat onto coverslips. Treatments were carried out utilising phenol red free DMEM or EBSS to reduce background fluorescence and buffered with 20 mM Hepes pH 7.4 to prevent acidification of the media in the absence of CO_2. Imaging was carried out by widefield deconvolution microscopy (Deltavision Elite, GE Healthcare) in a heated environment chamber using softWoRx® 5.0 (Applied Precision, GE Healthcare) for image acquisition and deconvolution.

2.10.5 Immunofluorescence Quantitation

Immunofluorescence experiments were quantified by NIS Elements (Nikon) or by Fiji (Schindelin et al. 2012) for parameters described in figure legends. Co-localisation experiments were quantified by determining the Manders' coefficients (Manders et al. 1993).

2.11 Statistical Analysis

Statistical analysis and post-hoc tests were carried out as described in figure legends using GraphPad Prism® v5.0. The statistical significance of data is denoted on graphs by asterisks (*) where * = $p < 0.05$, ** = $p < 0.01$, *** = $p < 0.001$ or n.s = not significant.

2.12 CLS Services

Some materials and procedures described in this section were provided by departments within the College of Life Sciences, University of Dundee. All cDNA constructs and in-house antibodies were produced by the Division of Signal Transduction Therapy (DSTT). DNA sequencing and the majority of DNA maxi preps were carried out by DNA Sequencing & Services. LB broth and plates were provided by Central Technical Services. Live cell imaging was carried out utilising equipment in the Centre for Advanced Scientific Technologies (CAST). Mass spectrometry samples were ran by the MRC Proteomics and Mass Spectrometry team.

3 PHOSPHORYLATION OF UVRAG BY MTOR

3.1 Introduction

Intracellular trafficking is fundamental for many aspects of cellular function (1.1.3). Through continued study, new proteins and functions continue to emerge which highlight the diverse nature of trafficking. Increasing complexity however demands efficient control mechanisms, as a lack of regulation has the propensity to drive disease. This is most strikingly represented by the demonstration that alterations in endocytic genes are ~2-5 fold more likely to cause monogenic disease compared to other human genes (Sigismund et al. 2012). While many studies have identified proteins or regulation mechanisms that are uniquely required for individual trafficking pathways, it is essential to recognise that these distinct trafficking pathways are intricately linked with one another and hence further research is required to fully understand the consequences of alterations in one pathway relative to another. For example, the lysosome acts as the terminal destination for several trafficking pathways such as macroautophagy that when induced causes a rapid increase in the delivery of intracellular material to the lysosome. For this to proceed efficiently requires mechanisms to ensure lysosomes remain 'primed' and able to digest incoming material whilst at the same time recycling components. Precisely how other intracellular pathways are regulated to adjust for this remains unclear. Work examining the transcription factor TFEB has shown it is critical for the upregulation of lysosomal genes and also increases bulk-flow endocytosis following autophagy induction, however this response can take several hours and it is likely that more immediate steps may be required (Sardiello et al. 2009). The VPS34 complex is essential for endocytosis as well as autophagy induction; it could therefore be an immediately attractive target to trigger a change in pathway balance until later acting transcriptional processes such as TFEB take effect.

For this reason the VPS34 complex was examined to determine whether the induction or suppression of autophagy modified the complex in any manner that may lead to regulation of other trafficking pathways.

3.2 Results

3.2.1 UVRAG is Phosphorylated in a Nutrient Dependent Manner

To explore possible regulation mechanisms the VPS34 complex was examined under nutrient rich conditions or during an autophagic response. Autophagy was induced either by nutrient deprivation (EBSS) or via direct chemical inhibition of mTOR with KU0063794 (García-Martínez et al. 2009) in U2OS, Hela and Mouse Embryonic Fibroblasts (MEFs, see Figure 3.1A). Nutrient depletion and inhibitor treatment blocked mTOR activity as demonstrated by the mobility shift of 4E-BP1 indicating dephosphorylation in addition to the reduction in ULK1 S757 phosphorylation, both known substrates of mTORC1. Furthermore the kinase activity of ULK1 is enhanced as judged by an increase in ATG13 S318 phosphorylation, indicating the induction of an autophagic response. Upon examination of the VPS34 complex no notable change was observed in any component except for the protein UVRAG, which exhibited a mobility shift in the presence of nutrients. As a mobility shift by SDS-PAGE can be indicative of post-translational modifications, cell lysates from MEFs grown in nutrient rich conditions were utilised to determine if UVRAG was modified by phosphorylation. Incubation of cell lysate with λ phosphatase, which has broad non-specific phosphatase activity (Zhuo et al. 1993), abolished the observed mobility shift but this was prevented in the presence of phosphatase inhibitors (Figure 3.1B). This demonstrates that UVRAG undergoes phosphorylation in the presence of nutrients. To further examine the requirement of nutrients for UVRAG phosphorylation, MEFs were incubated in the presence of serum alone, amino acids alone, serum and amino acids or with neither. As is shown in Figure 3.1C, both amino acids and serum together elicited the greatest mobility shift. Incubation of either alone results in a partial shift in comparison to without nutrients or with mTOR inhibition. In addition the use of a specific VPS34 kinase inhibitor (VPS34-IN1) does not impair the UVRAG mobility shift suggesting it is not dependent upon VPS34 complex activity (Examination of VPS34-IN1 specificity and action is shown in Chapter 6).

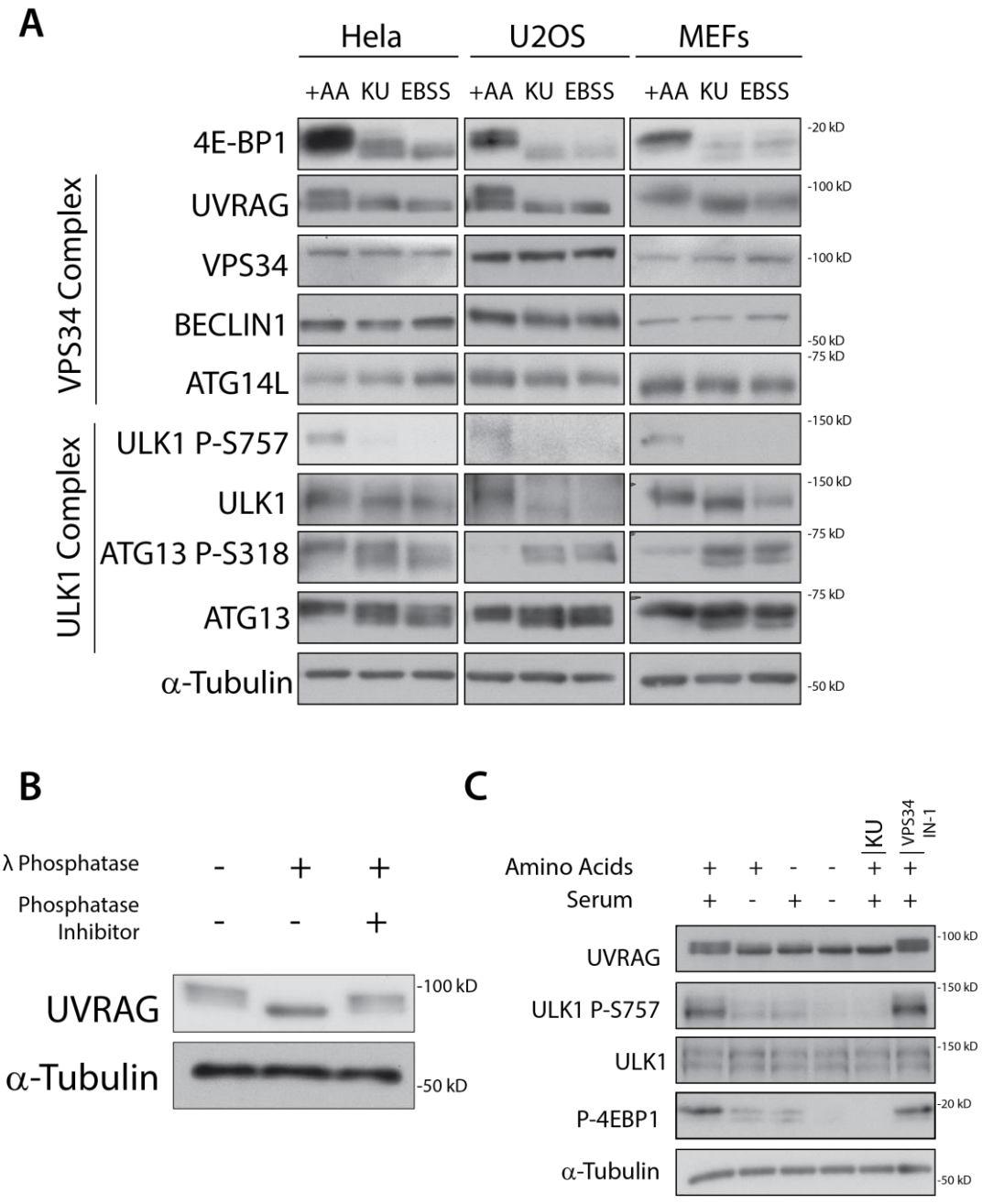

Figure 3.1 - UVRAG is phosphorylated under nutrient rich conditions.

(A) Cells were treated for 1 h (MEFs) or 2 h (U2OS and Hela) in complete media (+AA), 1uM KU0063794 (KU) or starvation media (EBSS). **(B)** MEF cell lysates from cells treated for 1 h in complete media (+AA) were split into three and treated with lambda phosphatase as indicated. **(C)** Wild-type MEFs were incubated for 1 h in the presence of serum and amino acids (complete media), amino acids only (serum starve media), serum only (EBSS + 10 % FBS), without serum or amino acids (starvation media), treated with 1 µM KU0063794 (KU) or 1µM VPS34-IN1 for 1 h prior to lysis. **(A-C)** All samples were lysed in 0.5 % NP-40 lysis buffer.

To examine the loss of UVRAG phosphorylation in a time-dependent manner during nutrient deprivation, MEFs were monitored across multiple time-points (Figure 3.2A). A complete downshift of UVRAG was observed by 45 min which interestingly correlated with that of the mTOR substrate 4E-BP1. Replacement of nutrients (serum and amino acids) caused a rapid reappearance of UVRAG and mTOR substrate phosphorylation within 15 min. The mTOR ATP-competitive inhibitor KU0063794 caused a more rapid inhibition of ULK1 S757 and UVRAG phosphorylation within 10 min when added to cells in nutrient rich conditions (Figure 3.2B). Removal of the inhibitor by washout allowed rapid re-phosphorylation by 5 min. The phosphorylation of UVRAG therefore correlates with nutrient status in an mTOR dependent manner, as the presence of nutrients alone is not sufficient for UVRAG phosphorylation if mTOR is specifically inhibited. The difference in recovery of UVRAG or mTOR substrate phosphorylation following nutrient depletion compared to mTOR inhibition is likely due to the requirement for signalling to occur prior to mTOR reactivation. In comparison the upstream signalling remains intact in the presence of KU0063794 and mTOR activity therefore rapidly recovers following drug washout.

The loss of UVRAG phosphorylation correlates with autophagy induction as both nutrient depletion and mTOR inhibition induce autophagy as indicated by an increase in LC3-II flux, demonstrated by the addition of the lysosomal inhibitor Bafilomycin A1 (BafA1; Figure 3.2C&D). The mTOR inhibitor KU0063794 inhibits both mTORC1 and mTORC2 as it binds to the ATP binding domain of mTOR (García-Martínez et al. 2009). It was of interest to establish whether UVRAG phosphorylation is dependent specifically on mTORC1 or mTORC2, therefore selective mTORC1 inhibitor rapamycin was used (Sarbassov et al. 2004). A partial decrease in the UVRAG mobility shift was observed upon rapamycin treatment whilst mTORC2 activity was unaffected as shown by AKT S473 phosphorylation (Figure 3.2E). The inhibition of mTORC1 by rapamycin is very selective but not complete for all substrates; p70 T389 phosphorylation was ablated completely but 4E-BP1 was only partially down-shifted (Choo et al. 2008). Recent work has demonstrated that rapamycin has differential effects upon mTORC1 substrates dependent upon

their interaction strength, with phosphorylated serines generally more resistant than threonines to rapamycin inhibition (Kang et al. 2013). It is difficult to determine whether the remaining partial mobility shift in UVRAG is due to rapamycin insensitivity (as with 4E-BP1) or whether this suggests a role for mTORC2 mediated phosphorylation. To determine whether mTORC2 was implicated in UVRAG phosphorylation, *Rictor* deficient MEFs which are unable to form mTORC2 were utilised. No difference in the UVRAG mobility shift was observed with *Rictor* -/- MEFs. Rapamycin treatment induced a partial downshift in UVRAG similar to wild-type MEFs that was fully abolished with the mTORC1 and 2 inhibitor KU0063794 (Figure 3.2F). This suggests that mTORC2 is not implicated in UVRAG phosphorylation and that mTORC1 activity is responsible.

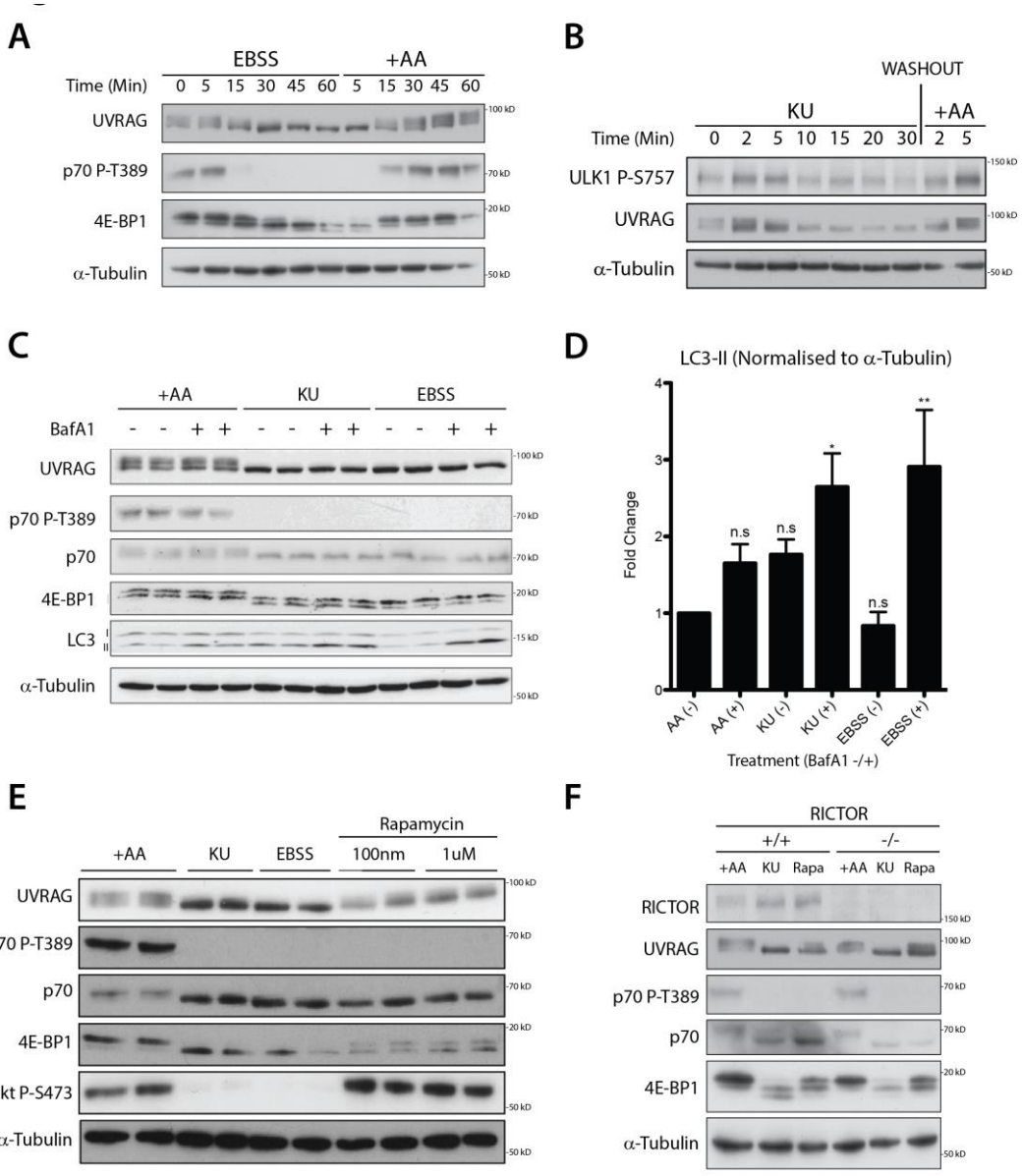

Figure 3.2 - Characterisation of UVRAG phosphorylation in response to nutrients

(A) Wild-type MEFs were washed and incubated in starvation media (EBSS) for 1 h and then changed to complete media (+AA) for 1 h, time-points were taken as indicated. **(B)** Wild-type MEFs were treated with 1 µM KU0063794 (KU) for 30 min, cells were washed twice and incubated in complete media for 5 min with time-points taken as indicated. **(C)** Wild-type MEFs were grown either in complete media (+AA), starvation media (EBSS) or treated with 1 µM KU0063794 (KU) in the presence or absence of 100 nM Bafilomycin A1 (BafA1). **(D)** Quantitation of (C), bars represent mean LC3-II ± SEM of n = 4 independent experiments. Statistical analysis was carried out by one-way analysis of variance using Dunnett's multiple comparison test and comparing to the +AA control where * = $p < 0.05$, ** = $p < 0.01$ or *n.s* = not significant **(E)** Wild-type MEFs were incubated in complete media (+AA), starvation media (EBSS), treated with 1 µM KU0063794 (KU) or treated with 100 nM or 1 µM Rapamycin as indicated for 1 h. **(F)** RICTOR +/+ and -/- MEFs were incubated in complete media (+AA) and treated with 1 µM KU0063794 or 100 nM Rapamycin for 1 h. **(A-F)** All samples were lysed in 0.5 % NP-40 lysis buffer.

3.2.2 mTOR Mediates UVRAG Phosphorylation

The data presented here thus far suggests a dependence upon mTORC1 or its downstream effectors for the phosphorylation of UVRAG under nutrient rich conditions. Given the previously established direct inhibitory role of mTORC1 phosphorylation of ULK1 in the regulation of autophagy (1.2.5). It was examined whether mTORC1 could also directly phosphorylate UVRAG. The mTORC1 or mTORC2 complexes can be selectively isolated by immunoprecipitation (IP) of mTOR complex specific components, for example RAPTOR (mTORC1), SIN1 or RICTOR (mTORC2). As demonstrated in Figure 3.3A, an endogenous mTOR IP was able to immunoprecipitate both mTORC1 and mTORC2 but endogenous RAPTOR or RICTOR IPs were complex specific. In comparison to direct mTOR IP, IP of RAPTOR yielded less mTOR, however a critical factor for substrate phosphorylation is recognition and binding. mTORC1 activity is directed by binding substrates through RAPTOR (Hara et al. 2002) and as such, IP of RAPTOR demonstrated superior phosphorylation of the mTORC1 substrate p70-S6Kinase (p70) *in vitro* in comparison to IP of mTOR (Figure 3.3B). To examine whether mTORC1 can directly phosphorylate UVRAG or other components of the VPS34 complex, an *in vitro* kinase assay was carried out. Endogenous mTORC1 was immunoprecipitated via RAPTOR and incubated with GST-UVRAG, GST-ATG14L or FLAG-BECLIN1 (Figure 3.3C). As a control GST-p70 D236A was also included in the *in vitro* kinase assay. GST-p70 D236A is mutated in the critical kinase DFG motif that orientates the γ-phosphate of ATP for transfer to substrates (Hanks & Hunter 1995), therefore preventing kinase activity. This ensures that incorporation of ^{32}P γ-phosphate into GST-p70 cannot occur via autophosphorylation and therefore any phosphorylation observed purely represents the activity of other kinases. A strong phosphorylation of GST-UVRAG was observed in comparison to GST-p70 D236A; additionally GST-ATG14L was weakly phosphorylated whilst FLAG-BECLIN1 demonstrated no modification. Critically, phosphorylation of p70 or UVRAG was severely ablated if the assay was carried out in the presence of KU0063794 (Figure 3.1Figure 3.3D), suggesting the incorporation of ^{32}P is dependent on mTOR kinase activity. To examine whether mTORC2 could phosphorylate UVRAG *in vitro*, endogenous RAPTOR or RICTOR were

immunoprecipitated and assayed against GST-p70 D236A, GST-UVRAG or GST-Serum and glucocorticoid induced protein kinase 1 (SGK1) K127A (Figure 3.3E). SGK1 is an established mTORC2 target phosphorylated at S422 in the hydrophobic motif and mutation of the ATP binding domain K127A is known to ablate kinase activity (Kobayashi & Cohen 1999; García-Martínez & Alessi 2008). UVRAG and p70 were phosphorylated when incubated *in vitro* with mTORC1 but not with mTORC2. UVRAG is therefore only phosphorylated *in vitro* by mTORC1 and not mTORC2. It should be noted that SGK phosphorylation could not be observed by autoradiography but could be detected by use of phospho-specific antibodies. An increase in SGK S422 phosphorylation was observed with mTORC2 in comparison to IgG, confirming that mTORC2 was active. However, SGK1 S422 phosphorylation was also observed with mTORC1; previous data has demonstrated that mTORC1 can phosphorylate SGK at S422 *in vitro* but mTORC2 is the key kinase in the cellular environment (Hong et al. 2008).

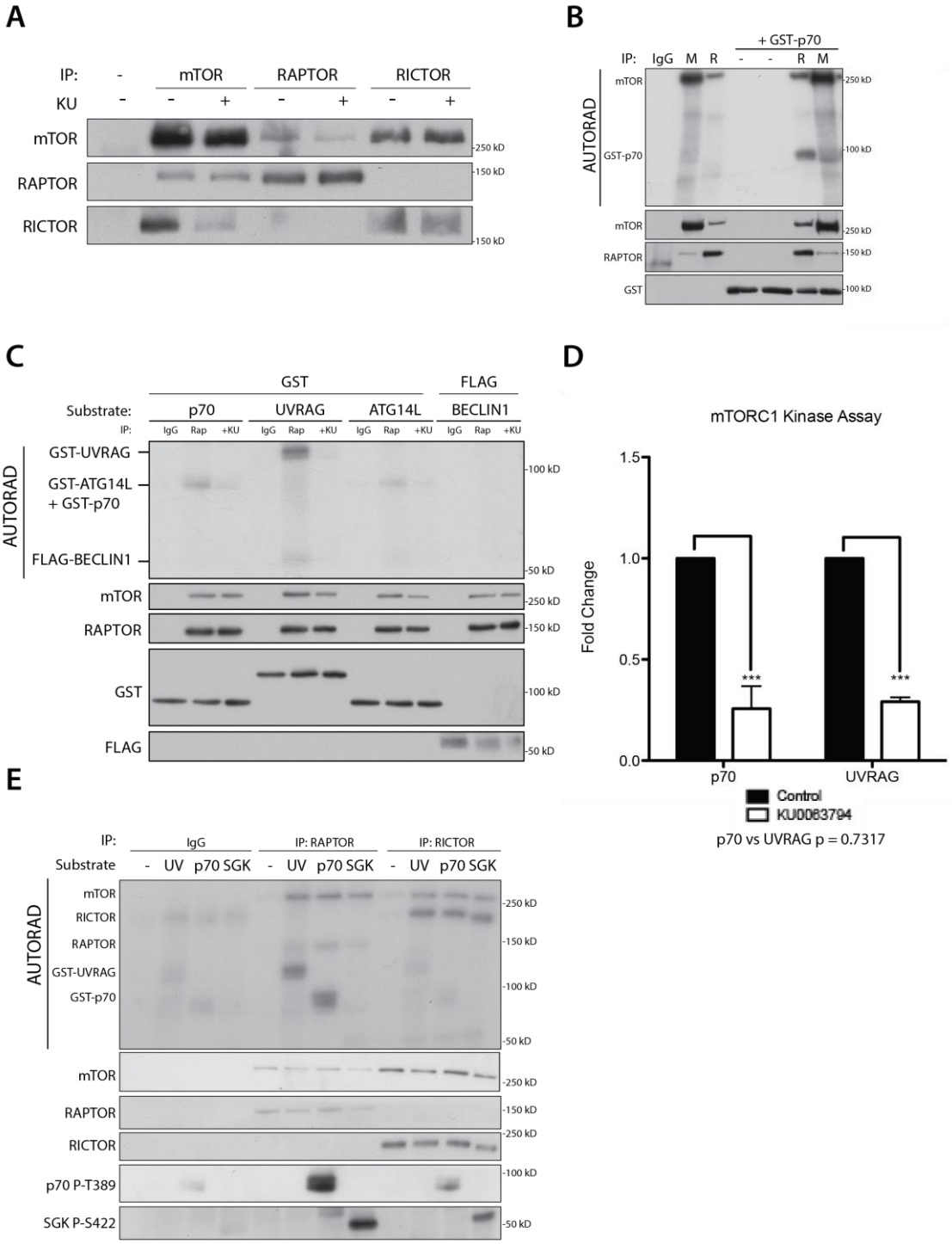

Figure 3.3 – UVRAG and mTOR *in vitro* kinase assay

(A) Antibodies raised against RAPTOR (S682B), RICTOR (S654B) or mTOR (S673B) were used respectively to immunoprecipitate mTORC1, mTORC2 or both from HEK293 cells. **(B)** mTOR (M) and RAPTOR (R) were immunoprecipitated from HEK293 cells and used for an *in vitro* kinase assay with GST-p70 D236A. **(C)** mTORC1 was selectively immunoprecipitated from HEK293 cells using a RAPTOR antibody and utilised for an *in vitro* kinase assay. mTORC1 was incubated with GST-p70 D236A, GST-UVRAG, GST-ATG14L or FLAG-BECLIN1 in the presence or absence of 1 µM KU0063794. **(D)** Quantitation of (C), bars represent mean substrate ^{32}P incorporation ± SEM of n = 4 independent experiments. Statistical analysis was carried out by two-way analysis of variance using Bonferroni's post-test where *** = $p < 0.001$. **(E)** RAPTOR or RICTOR antibodies were used for immunoprecipitation of mTORC1 and mTORC2 from HEK293 cells for *in vitro* kinase assay analysis with GST-UVRAG, GST-p70 D236A and GST-SGK K127A. **(A-E)** All samples were lysed in mTORC lysis buffer.

3.2.3 Identification of UVRAG Phosphorylated Residues

To determine the location of phosphorylation sites on UVRAG two approaches were undertaken. MEFs stably expressing FLAG-UVRAG were grown in nutrient rich conditions or treated with KU0063794 and immunoprecipitated using FLAG agarose. Additionally, GST-UVRAG was incubated *in vitro* with endogenous mTOR and phosphorylated in a non-radioactive kinase assay in the absence or presence of KU0063794. In each experiment samples were separated by SDS-PAGE, the UVRAG band was excised for protease digestion and used for phospho-peptide analysis by mass spectrometry. Phosphorylated peptides identified between experiments are detailed in Table 10. Five unique singly phosphorylated peptides were identified from FLAG-UVRAG immunoprecipitated from cells. Three of these sites were abolished upon mTOR inhibition. Two major single phosphorylated peptides were identified from GST-UVRAG following *in vitro* kinase assay with mTOR that were both sensitive to KU0063794. Notably, these phospho-peptides were also identified upon FLAG-UVRAG IP. The two common peptides were K543-K559 (S548 or S549 or S550 predicted phosphorylation site) and K564-R595 (S571 predicted site). A third L514-R542 (T518 or S522 predicted site) peptide was observed, however this was only observed in a half of experiments and usually presented with a low ion score. The extracted-ion chromatograms (XICs) for K543-K559 and K564-R595 peptides from the *in vitro* kinase assay are shown in Figure 3.4A&B. In both XICs, the phosphorylated peptide species was only observed following a kinase reaction with mTOR, and not in the presence of KU0063794 or with an IgG control IP. To determine the precise residues phosphorylated within UVRAG, a radioactive kinase assay was carried out with endogenous mTORC1 and GST-UVRAG. Trypsin was used to digest UVRAG and peptides were separated by liquid chromatography as shown in Figure 3.4C. The incorporation of ^{32}P was too low to allow Edman degradation to identify phosphorylated residues (Edman & Begg 1967), however two distinct radioactive peaks were eluted by liquid chromatography which may suggest there are two major phosphorylated peptides within UVRAG following an *in vitro* kinase assay. Repeating the non-radioactive *in vitro* kinase assay of UVRAG with mTORC1 (IP: RAPTOR) or mTORC2 (IP: RICTOR) and analysis by mass

spectrometry demonstrated that the phosphorylated K543-K559 peptide was only seen with mTORC1. No phospho-peptides were identified following kinase assay reaction with mTORC2, further suggesting that mTORC2 does not phosphorylate UVRAG (Figure 3.4D). Analysis of GST-UVRAG phosphorylated *in vitro* by mTOR was repeated with several proteases (Trypsin, Chymotrypsin and ASP-N) to increase the sequence coverage of UVRAG. Approximately 92 % of the total UVRAG sequence was identified by mass spectrometry (Figure 3.5A) and two distinct phosphorylated peptide peaks were seen by liquid chromatography (Figure 3.4C). Taken together the above data clearly indicates that mTORC1 mediates phosphorylation at two distinct sites. The domain structure of UVRAG is represented in Figure 3.5B with an alignment of Human UVRAG 501-620, the region where phosphorylated residues were identified. Mass spectrometry was unable to accurately predict which residue of S548-550 is phosphorylated, however the S550 and S571 residues both are positioned with a +1 leucine residue which is favourable for mTOR mediated phosphorylation sites (Figure 3.5C)(Hsu et al. 2011).

Possible Site	**Peptide (P-site)**	**UVRAG IP (from Cells)**		**mTOR Kinase Assay (*in vitro*)**	
		+AA	**KU0063794**	**Control**	**KU0063794**
S498	R.QSSIFGGADVGFSGGIP**S**PDKGHR.K + P	+	+	*n.p*	*n.p*
S508/S509	R.A**SS**ENERLQYK.T + P	+	*n.p*	*n.p*	*n.p*
T518/S522	R.LQYK**T**PPP**S**YNSALAQPVTTVPSMGETER.K + P	+	+	Φ	Φ
S548-S550	R.KITSL**SSS**LDTSLDFSK.E + P	+	*n.p*	+	*n.p*
S571	R.KGEDLVG**S**LNGGHANVHPSQEQGEALSGHR.A + P	+	*n.p*	+	*n.p*

Table 10 – UVRAG Phosphorylated Peptides

List of phosphorylated identified in UVRAG immunoprecipitation or in vitro kinase assays in the presence or absence of mTOR inhibitor KU0063794. Identified peptide for each site is shown with the predicted phosphorylated residue. (+) Denotes that peptide was identified and phosphorylated, (n.p) peptide was identified but not phosphorylated or (Φ) peptide was identified but not consistently phosphorylated across experiments.

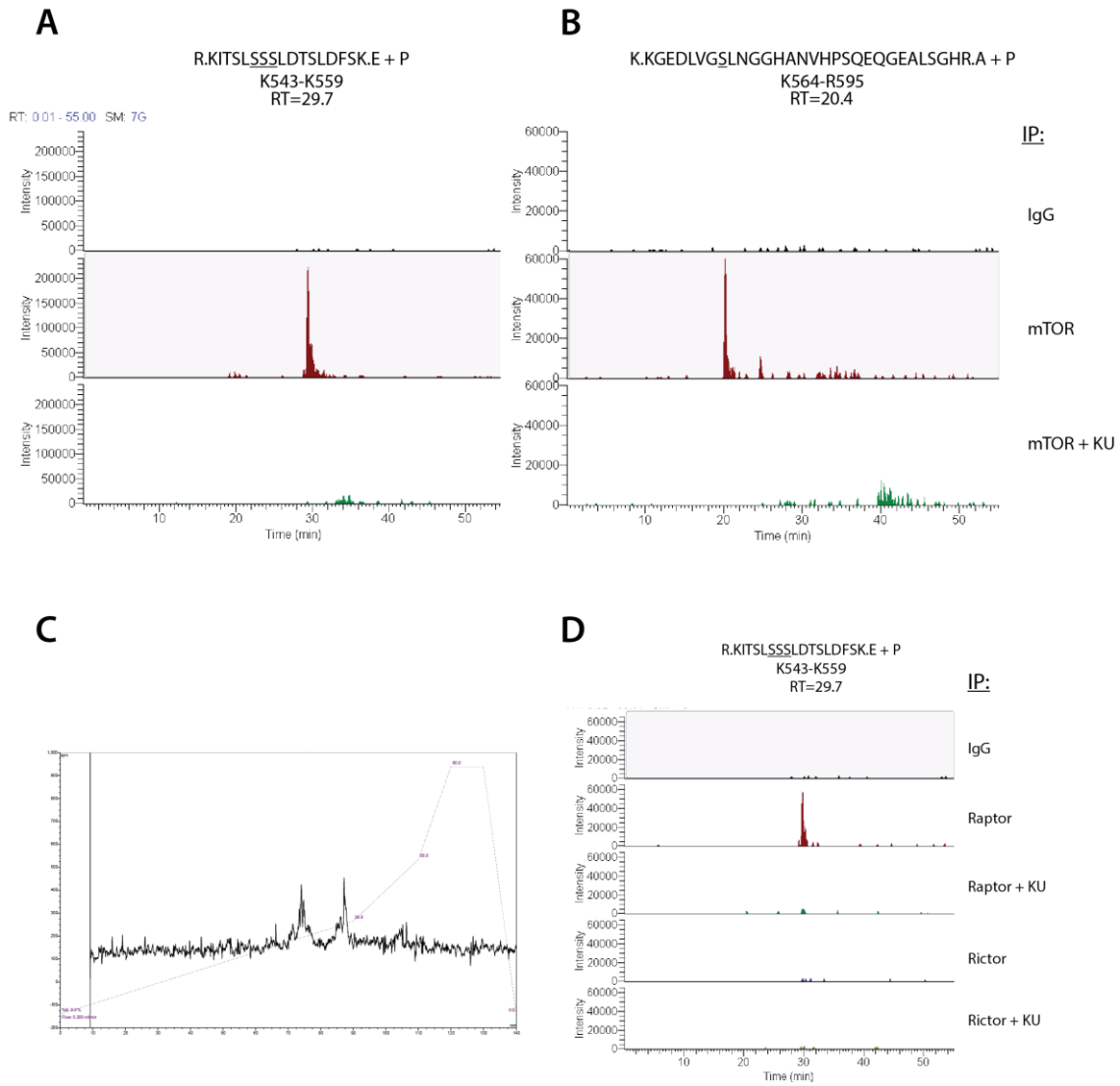

Figure 3.4 – Extracted Ion Chromatograms (XICs) of phosphorylated peptides.

(A-B) mTOR (S683B) was immunoprecipitated from HEK293 cells and incubated with GST-UVRAG in a non-radioactive kinase assay in the presence or absence of 1 µM KU0063794. Peptides were analysed by mass spectrometry following protein digest. XIC of phosphorylated peptides identified **(A)** K543-K559 and **(B)** K564-R595. **(C)** mTOR immunoprecipitated from HEK293 cells was used to carry out a radioactive kinase assay with GST-UVRAG. UVRAG was cleaved by tryptic digest and peptides were separated by liquid chromatography whilst monitoring counts per minute (cpm) of eluted fractions. **(D)** RAPTOR (S260D) or RICTOR (S654B) was immunoprecipitated from HEK293 cells and incubated with GST-UVRAG in a non-radioactive kinase assay in the presence or absence of 1 µM KU0063794. Peptides were analysed by mass spectrometry following protein digest, the XIC of phosphorylated K543-K559 is shown.

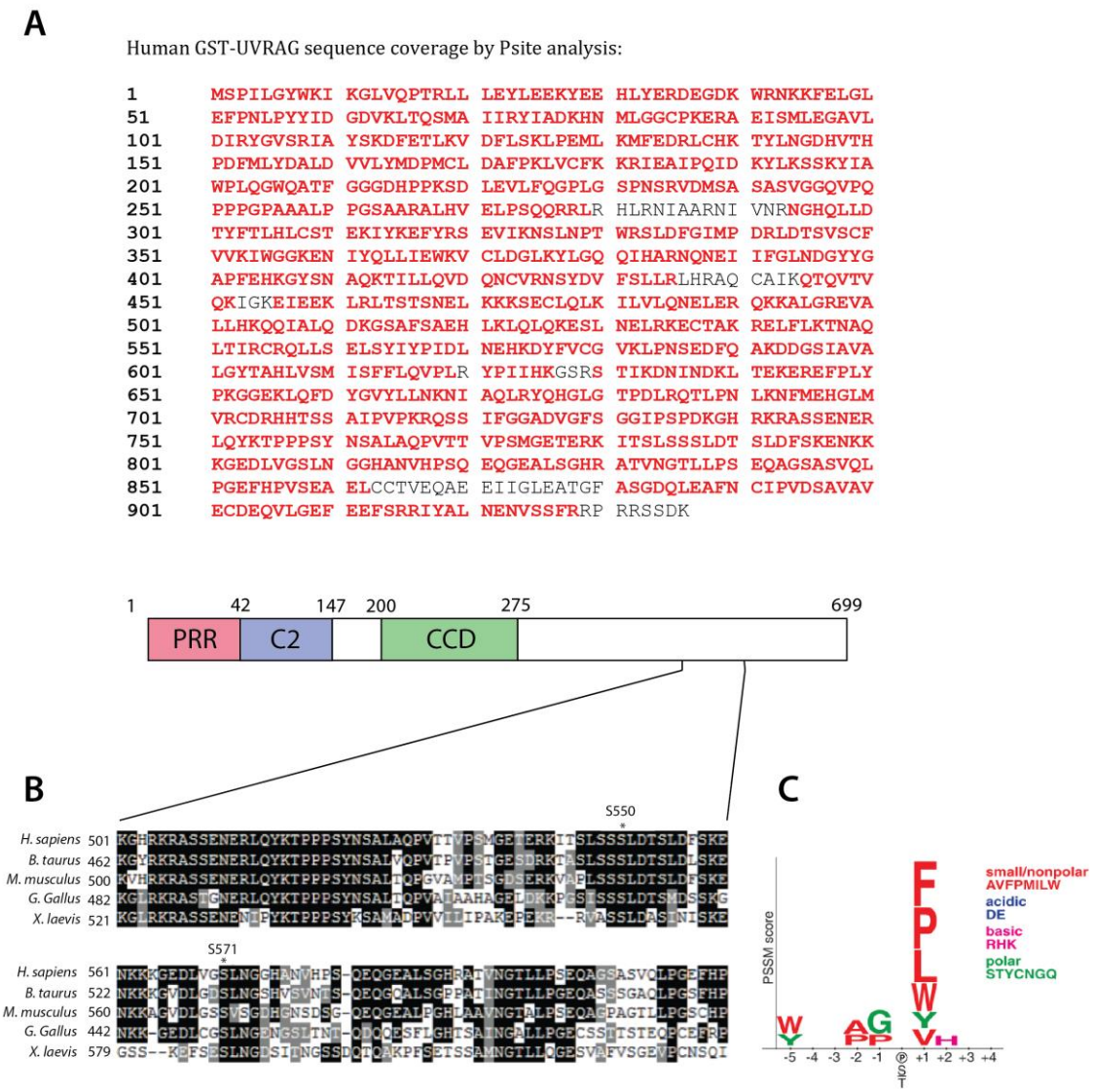

Figure 3.5 - Mass Spectrometry UVRAG Coverage.

(A) Full GST-UVRAG sequence (1-237 = GST). Peptides covering residues highlighted in red were identified by mass spectrometry, 94% of GST-UVRAG was identified (92% of UVRAG). **(B)** Domain structure of UVRAG showing the proline rich region (PRR), C2 Domain (C2) and coiled-coil domain (CCD). Alignment of UVRAG amino acids 501-620 (Human) between species, black boxes signify conserved residues whilst grey represents similar residues. Identified phosphorylation sites indicated with an asterisk (*). Alignment was carried out using ClustalW alignment software (EMBL-EBI) with sequences from UniProt (www.uniprot.org). **(C)** Consensus sequence for mTORC1 directed phosphorylation from (Hsu et al. 2011).

To confirm whether phosphorylation does occur at S548-550 or S571 residues, the serine residues were mutated to alanine residues that cannot be phosphorylated as they lack a hydroxyl group. The GST-UVRAG alanine mutants were incubated *in vitro* with endogenous mTORC1 that was immunoprecipitated via RAPTOR. Mutation of S548, S549 and S550 all to alanine (AAA) caused reduced phosphorylation *in vitro.* This was also seen with S550A but not S549A or S548A (Figure 3.6A), suggesting that S550A is the phosphorylated residue of the K543-K559 peptide. Mutation of UVRAG S571A also caused a decrease in phosphorylation and change in mobility. Expressing UVRAG with S550A and S571A together resulted in an additive loss of ^{32}P incorporation (Figure 3.6B), reducing levels to ~30 % as is also seen when using the mTOR inhibitor KU0063794 (Figure 3.6C). This suggests that S550 and S571 are the primary mTORC1 mediated phosphorylation sites. The residual ^{32}P incorporation of UVRAG was insensitive to the mTOR inhibitor KU0063794 and consequently may result from the activity of contaminating kinases.

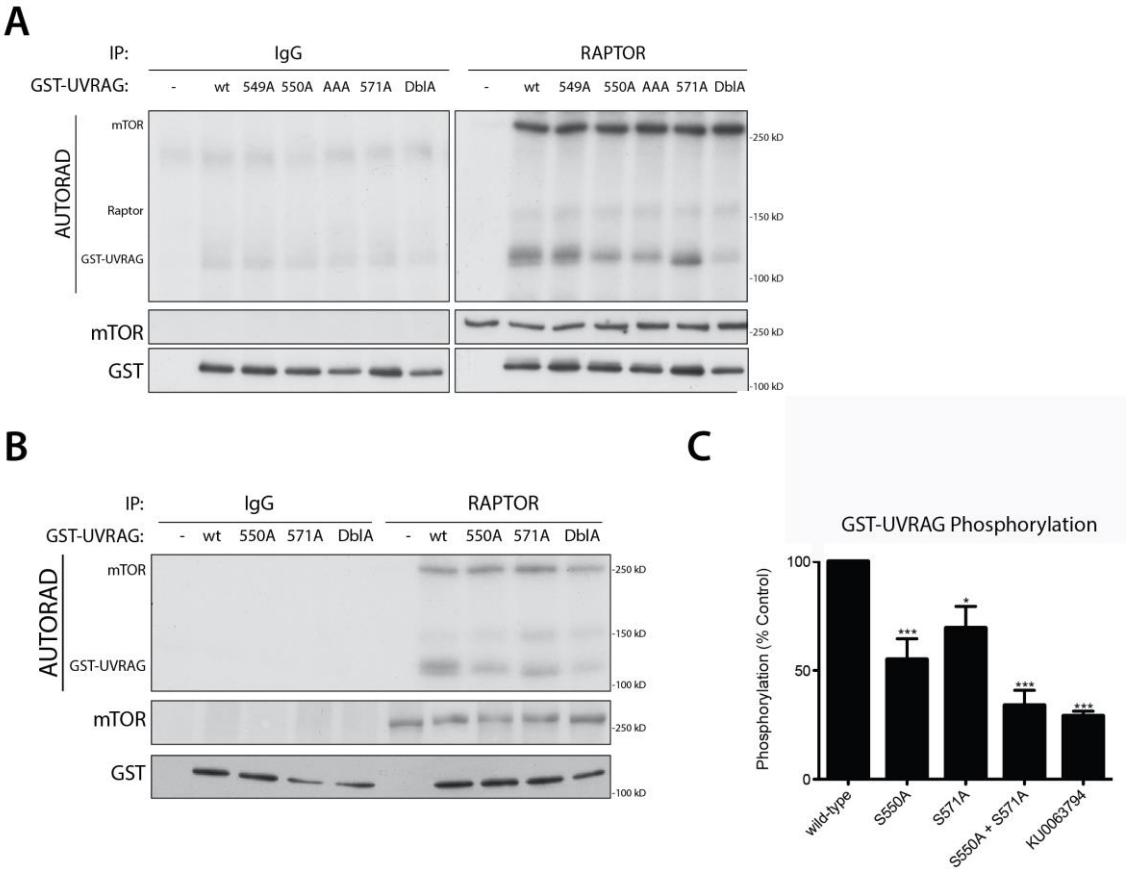

Figure 3.6 - UVRAG Alanine Mutants *in vitro* Kinase Assay

(A+B) HEK293 cells were lysed in mTORC lysis buffer and mTORC1 was immunoprecipitated using a RAPTOR antibody (S260D) and incubated with GST-UVRAG and alanine site mutations (wt= wild-type, AAA = S548A+S549A+S550A, DblA = S550A + S571A) in an *in vitro* kinase assay. **(C)** Quantitation of (B), bars represent mean substrate ^{32}P incorporation ± SEM of n = 4 independent experiments. Statistical analysis was carried out by one-way analysis of variance and Dunnett's multiple comparison test to the wild-type control where * = $p < 0.05$ and *** = $p < 0.001$

3.2.4 Characterisation of UVRAG Phosphorylation Sites

The mutation of S550A and S571A prevented UVRAG phosphorylation *in vitro*, however the mutation to alanine residues may disrupt site recognition by mTOR. To confirm that UVRAG was phosphorylated at S550 and S571, specific phospho-antibodies to each site were raised in sheep and purified by the Division of Signal Transduction Therapy (DSTT), University of Dundee. This allowed further examination and characterisation of these phosphorylation sites in cells endogenously.

GST-UVRAG wild-type or S571A phosphorylated *in vitro* by endogenously immunoprecipitated mTORC1 was recognised by the S550 phospho-specific antibody but as expected the S550A and S550A+S571A mutants were not recognised (Figure 3.7A). Exogenous FLAG-UVRAG immunoprecipitated from MEFs under nutrient rich conditions was also recognised by the S550 phospho-specific antibody; this was ablated upon nutrient starvation or if FLAG-UVRAG S550A was immunoprecipitated instead (Figure 3.7B). Analysis of cell lysates from several cell lines using the S550 phospho-specific antibody also demonstrated that endogenous UVRAG was phosphorylated at S550 in a nutrient dependent manner in multiple cell lines and between species (Figure 3.7C). Incubation of MEFs in serum and amino acid free media caused a loss of S550 phosphorylation with similar kinetics to that of 4E-BP1 (Figure 3.7D). Development of a S571 phospho-specific antibody confirmed that the S571 site is also phosphorylated in response to nutrients. IP of GFP-UVRAG clearly shows S550 and S571 phosphorylation in the presence of nutrients but not upon nutrient starvation or upon mutation of S550A and S571A (Figure 3.7E). The use of phospho-specific antibodies therefore clearly corroborates earlier experiments that S550 and S571 of UVRAG were phosphorylated in response to nutrients.

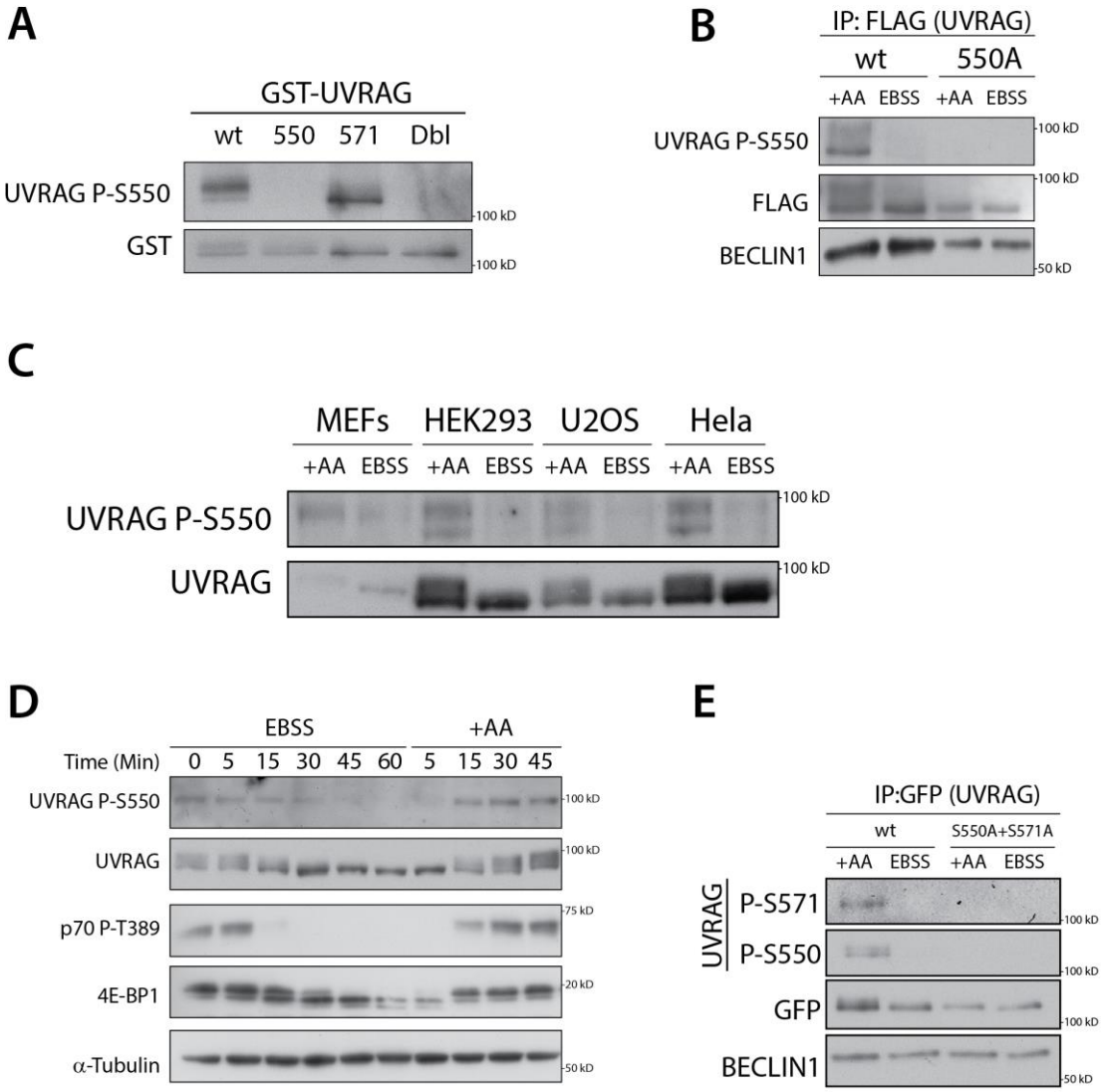

Figure 3.7 – Development of UVRAG S550 and S571 phospho-antibodies

(A) HEK293 were lysed in mTORC lysis buffer and mTORC1 was immunoprecipitated using a RAPTOR antibody (S260D). mTOR was incubated with GST-UVRAG or alanine site mutants (DblA = S550A+S571A) as a substrate in a non-radioactive kinase assay. Samples were blotted using a S550 phospho-specific antibody (S323D). **(B)** U2OS cells stably expressing FLAG-UVRAG wild-type or S550A mutant were incubated in complete media (+AA) or starvation media (EBSS) for 2 h. Anti-FLAG agarose was used to immunoprecipitate FLAG-UVRAG and blotted as shown. **(C)** Cells were incubated in complete media (+AA) or starvation media (EBSS) for 1 h (MEFs) or 2 h (HEK293, U2OS, Hela) and blotted as shown. **(D)** Wild-type MEFs were washed and incubated in starvation media (EBSS) for 1 h and then changed to complete media (+AA) for 45 min, time-points were taken as indicated. **(E)** U2OS cells stably expressing GFP-UVRAG wild-type or S550A+S571A mutant were incubated in complete media (+AA) or starvation media (EBSS) for 2 h. Anti-GFP sepharose was used to immunoprecipitate GFP and blotted as shown. **(B-E)** All samples were lysed in 0.5 % NP-40 lysis buffer.

3.2.5 Cellular Distribution of Phosphorylated UVRAG

Following identification and confirmation of mTOR regulated phosphorylation sites in UVRAG, the effect upon interaction with canonical binding partners was examined. Two distinct VPS34 complexes are present within mammalian cells (Figure 3.8A) and it is possible that phosphorylation of UVRAG may alter complex formation. Endogenous VPS34 was immunoprecipitated and showed equal UVRAG binding between nutrient rich conditions or during autophagy induction by mTOR inhibition or nutrient starvation (Figure 3.8B). Importantly, UVRAG demonstrated a clear mobility shift confirming that phosphorylation was not occluding the protein from interacting with the VPS34 complex. Similarly, direct IP of endogenous UVRAG did not show any difference in VPS34 complex stoichiometry between phosphorylation states (Figure 3.8C). IP of exogenous mCherry-S-BECLIN1, GFP-RUBICON or mCherry-S-ATG14L (Figure 3.8D-F) from MEFs similarly showed no change in the stoichiometry of the complex between conditions. No UVRAG was detected following IP of ATG14L under any treatment as expected due to their mutually exclusive binding to the same coiled-coil domain of BECLIN1 (Itakura et al. 2008). Equally no ATG14L was observed in complex with UVRAG or RUBICON as has previously been demonstrated (Matsunaga et al. 2009). Excluding the IP of ATG14L, in all instances the phosphorylated form of UVRAG interacted under nutrient rich conditions and exhibited no change in component stoichiometry indicating that phosphorylation does not occlude or enhance binding of UVRAG or other canonical components to the VPS34 complex. Despite previously published work suggesting UVRAG interacts with Endophilin B1 (Takahashi et al. 2007), it was not possible to confirm interaction with UVRAG under nutrient rich or depleted conditions (Figure 3.8G).

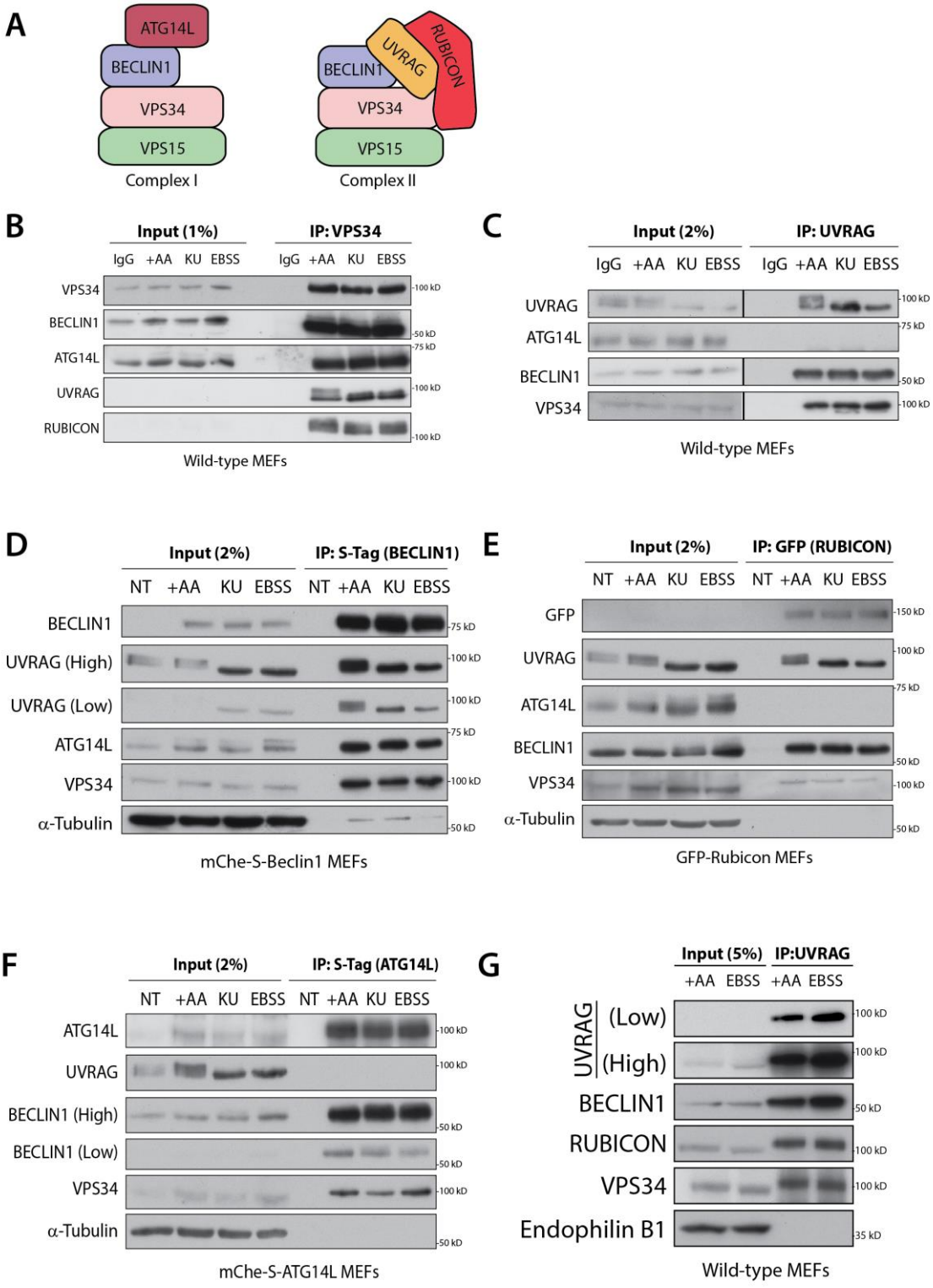

Figure 3.8 - Phosphorylated UVRAG is not occluded from the VPS34 complex

(A) Schematic representation of the two predominant mammalian VPS34 complexes. MEFs were incubated in complete media (+AA), starvation media (EBSS) or treated with 1 μM KU0063794 (KU) for 1 h prior to lysis in 0.5 % NP-40 lysis buffer. S-tag sepharose, GFP sepharose, Protein-G sepharose or FLAG agarose were used as appropriate to IP **(B)** VPS34 (S672B), **(C)** UVRAG (S323D), **(D)** mCherry-S-BECLIN1, **(E)** GFP-Rubicon or **(F)** mCherry-S-ATG14L. **(G)** Wild-type MEFs were incubated in complete media (+AA) or starvation media (EBSS) for 1 h and lysed in CHAPs lysis buffer. UVRAG was IP'd (S323D) and blotted as indicated.

3.2.6 Pursuit of Novel UVRAG Interacting Proteins

Changes in UVRAG complex formation were further examined by size-exclusion chromatography (SEC) on a Sephadex G6 column. Whilst there was no change in established VPS34 complex components (Figure 3.8), it is possible that previously uncharacterised interactions may be altered upon UVRAG phosphorylation; if this is true then this could affect the UVRAG-VPS34 complex molecular weight and elution profile by SEC. MEFs were grown in nutrient rich or nutrient depleted conditions and then analysed by SEC. As is shown in Figure 3.9, UVRAG co-fractionated with VPS34 and BECLIN1 across a wide elution peak with little change between cell treatments. ATG14L was found in a higher weight peak with small amounts of BECLIN1 and VPS34, but this partially shifted to a lower weight peak, correlating with more VPS34, upon autophagy induction. No obvious change in the fractionation profile of UVRAG was evident, however given the wide elution peak it would be difficult to determine changes in the interaction of low molecular weight proteins.

To attempt to identify possible uncharacterised UVRAG interacting proteins, GST-UVRAG wild-type or S548A/S549A/S550A (S548-550A) were immunoprecipitated from MEFs under nutrient rich conditions and separated by SDS-PAGE. Peptides were generated by protease digestion and analysed by mass spectrometry to identify co-immunoprecipitating proteins. A curated list of identified proteins are shown in Table 11, a full list can be found in Appendix A. Many proteins were conserved between both samples including VPS34, VPS15 and RAPTOR. In addition peptides from tubulin, motor proteins and clathrin coat components were found in both samples. Several proteins unique to each pull-down were identified that will require further examination to confirm the interaction and whether binding occurs in a phosphorylation dependent manner.

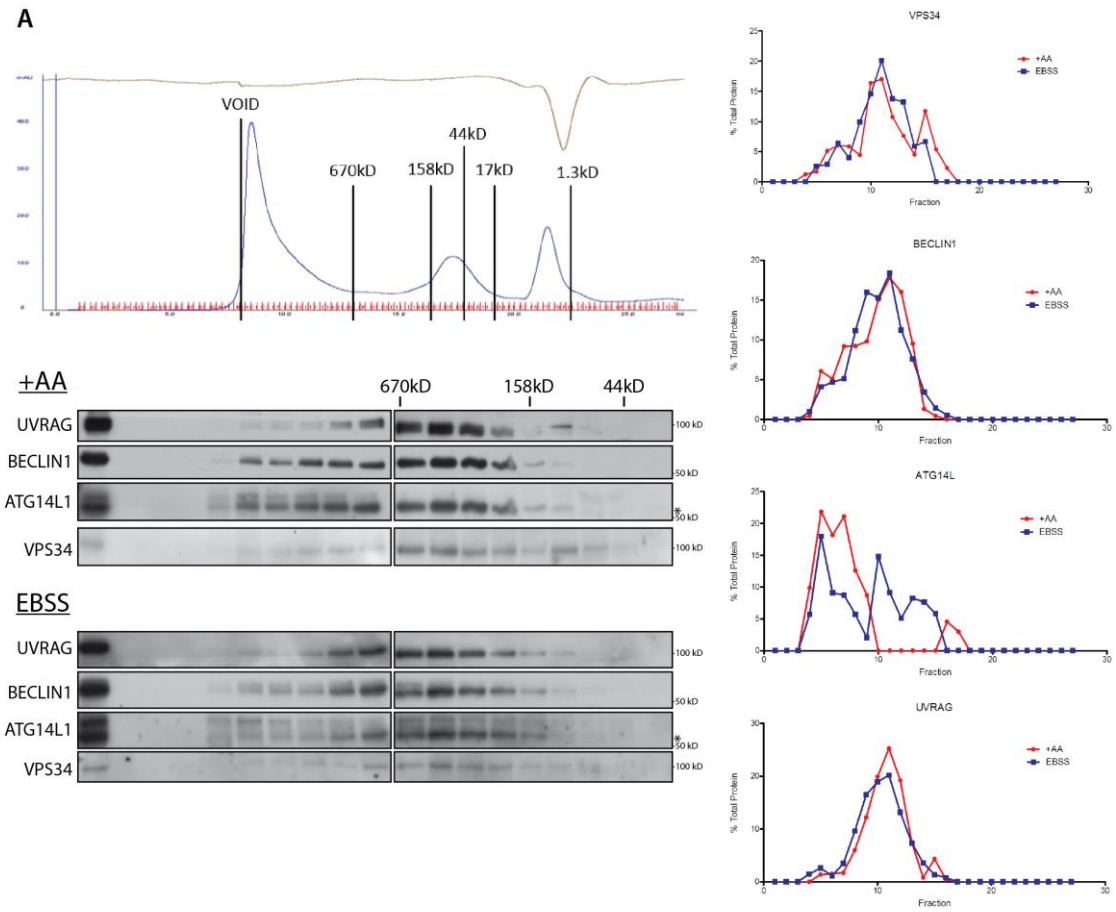

Figure 3.9 - Gel filtration of UVRAG

(A) Wild-type MEFs were incubated in complete media (+AA) or starvation media (EBSS) for 1 h and separated by gel filtration on a Superose 6 column. Estimated molecular weight of fractions was determined by gel filtration chromatography standards. (*) Represents a non-specific band. **(B)** The distribution of each protein between fractions was analysed by densitometry and plotted.

REF	WILD-TYPE UVRAG			S548-550A UVRAG			GENE	NAME
	Score	Peptides	Coverage	Score	Peptides	Coverage		
Q9P2Y5	3391	253	71%	6405	434	72%	UVRAG	UV radiation resistance-associated gene protein
P68363	1150	53	54%	2010	85	62%	TUBA1B	Tubulin alpha-1B chain
Q9BVA1	589	28	46%	2046	88	58%	TUBA2B	Tubulin beta-2B chain
Q8N122	173	13	9%	227	19	14%	RPTOR	Regulatory-associated protein of mTOR
P63167	170	5	37%	161	5	37%	DYNLL1	Dynein light chain 1, cytoplasmic
Q99570	135	16	9%	193	15	10%	PIK3R4	Phosphoinositide 3-kinase regulatory subunit 4
P53675	102	8	4%	95	5	1%	CLTCL1	Clathrin heavy chain 2
Q8NEB9	68	6	6%	78	4	3%	PIK3C3	Phosphatidylinositol 3-kinase catalytic subunit type 3
P33176	65	8	8%	119	5	5%	KIF5B	Kinesin-1 heavy chain
Q9UBP0	32	4	3%	39	6	6%	SPAST	Spastin
O95071	132	9	3%		-		UBR5	E3 ubiquitin-protein ligase UBR5
P61981	108	3	8%		-		YWHAG	14-3-3 protein gamma
Q15836	94	3	24%		-		VAMP3	Vesicle-associated membrane protein 3
Q9Y277	52	4	10%		-		VDAC3	Voltage-dependent anion-selective channel protein 3
Q8TEB1		-		312	14	22%	DCAF11	DDB1- and CUL4-associated factor 11
O14654		-		185	13	12%	IRS4	Insulin receptor substrate 4
Q13263		-		176	10	8%	TRIM28	Transcription intermediary factor 1-beta
P53618		-		69	7	6%	COPB1	Coatomer subunit beta

Table 11 – Curated List of UVRAG Interacting Proteins

Reference for identified proteins is from UniProt, protein score refers to assigned score by MASCOT software. Proteins represent co-immunoprecipitating proteins of GST-UVRAG wild-type or S550A. Full list can be found in Appendix A and Appendix B.

As an alternate approach to enrich for proteins which may selectively interact with the phosphorylated region of UVRAG alone, biotinylated peptides corresponding to S536-S583 of human UVRAG with S550 and S571 both or singly phosphorylated were obtained (DSTT, University of Dundee). The peptides were incubated with cell lysate from HEK293 or MEFs grown in nutrient rich conditions and immunoprecipitated with streptavidin agarose to identify potential phosphorylation specific interactors by mass spectrometry. As is shown in Table 12 the highest scoring interactors of phosphorylated peptides were 14-3-3 proteins, whilst no unique proteins were found to co-immunoprecipitate with the non-phosphorylated peptide.

REF	SCORE	PEPTIDES (UNIQUE)	GENE	NAME	IP IDENTIFIED
P62259	2097	26 (20)	1433E	14-3-3 protein epsilon	Phospho
Q9CQV8	1770	23 (16)	1433B	14-3-3 protein beta/alpha	Phospho
P61982	1631	25 (19)	1433G	14-3-3 protein gamma	Phospho
P68510	1547	19 (16)	1433F	14-3-3 protein eta	Phospho
P63101	1233	19 (14)	1433Z	14-3-3 protein zeta/delta	Phospho
P68254	696	18 (12)	1433T	14-3-3 protein theta	Phospho
P07901	358	6 (5)	HS90A	Heat shock protein HSP 90-alpha	Phospho
P58252	146	8 (5)	EF2	Elongation factor 2	Phospho
P63038	89	3 (3)	CH60	60 kDa heat shock protein, mitochondrial	Phospho
P52480	78	4 (1)	KPYM	Pyruvate kinase isozymes M1/M2	Phospho
P16381	74	3 (2)	DDX3L	Putative ATP-dependent RNA helicase Pl10	Phospho
Q61753	67	3 (2)	SERA	D-3-phosphoglycerate dehydrogenase	Phospho
P17182	61	4 (2)	ENOA	Alpha-enolase	Phospho
P20029	2568	38 (33)	GRP78	78 kDa glucose-regulated protein	Both
P17879	366	7 (5)	HS71B	Heat shock 70 kDa protein 1B	Both
P38647	1290	20 (15)	GRP75	Stress-70 protein, mitochondrial	Both
P11499	155	6 (3)	HS90B	Heat shock protein HSP 90-beta	Both

Table 12 - Curated list of UVRAG biotin peptide interactors

Reference for identified proteins is from UniProt, protein score refers to assigned score by MASCOT software. No unique peptides were identified in the non-phosphorylated peptide with more than two unique peptides. Full uncurated list is shown in Appendix C and Appendix D.

The interaction of 14-3-3 proteins was identified both by biotin peptide and whole protein immunoprecipitation. To examine whether 14-3-3 proteins could interact, GFP-UVRAG wild-type or S550A+S571A was immunoprecipitated and immunoblotted using a pan 14-3-3 antibody that recognises all isoforms. Whilst 14-3-3 appears to interact, this did not appear to occur in a phosphorylation sensitive manner as binding was still observed in the phosphorylation site mutant at a similar level to wild-type protein following normalisation (Figure 3.10). Although the phosphorylation of UVRAG does not alter the binding of the most well established VPS34 complex binding partners, it is possible that the phosphorylation of UVRAG may instead localise the VPS34 complex to a distinct location and this was examined further.

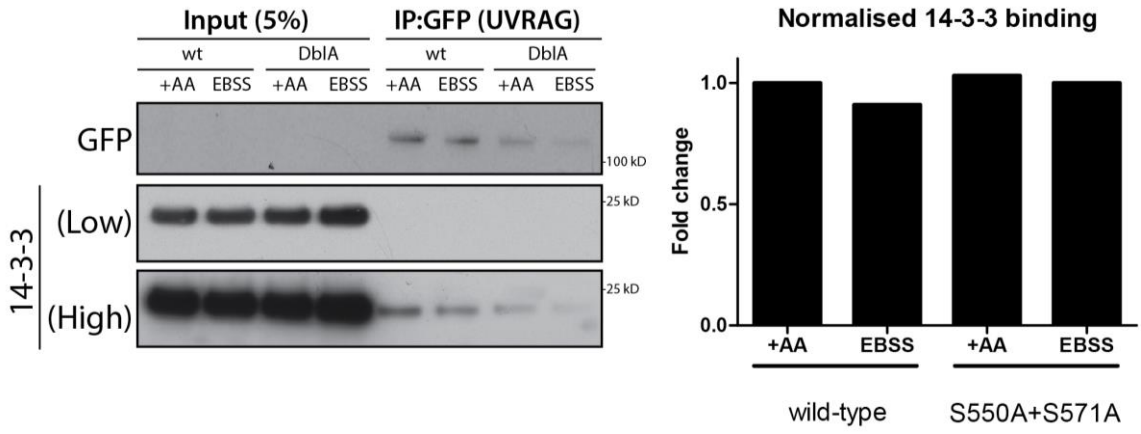

Figure 3.10 - Interaction of UVRAG with 14-3-3 proteins

Wild-type MEFs stably expressing wild-type (wt) or S550A+S571A (DblA) GFP-UVRAG were incubated in complete media (+AA) or starvation media (EBSS) for 1 h and lysed in 0.5 % NP-40 lysis buffer. UVRAG was immunoprecipitated with GFP sepharose and blotted as indicated. Blot was analysed by densitometry and the level of 14-3-3 co-immunoprecipitating normalised to GFP-UVRAG was plotted.

MEFs were homogenised in the absence of detergent and separated by density centrifugation using a gradient of 10-45 % iodixanol. This allows the separation of cellular components based upon their isopycnic point, a technique that is commonly used to differentially separate cellular organelles (Graham et al. 1994). Movement of the UVRAG-VPS34 complex to a distinct cellular location upon phosphorylation may therefore be demonstrated by differences in its isopycnic point. Comparison of nutrient rich or nutrient deprived MEFs however displayed very little change in separation of UVRAG, RUBICON, ATG14L or BECLIN1 (Figure 3.11). A large proportion of total VPS34 however was present in low-density fractions that was distinct from the majority of BECLIN1, UVRAG, RUBICON or ATG14L. This may represent early endosomes as this correlates with the distribution of the early endosome marker EEA1. Upon nutrient starvation the VPS34 distribution shifts to match that of other VPS34 complex components in denser fractions that may represent late endosomes or lysosomes as indicated by the fractionation profile of mTOR. Critically, UVRAG appears to remain in the same fractions regardless of phosphorylation state, but this does not exclude the possibility of a change in localisation between two compartments with similar isopycnic points.

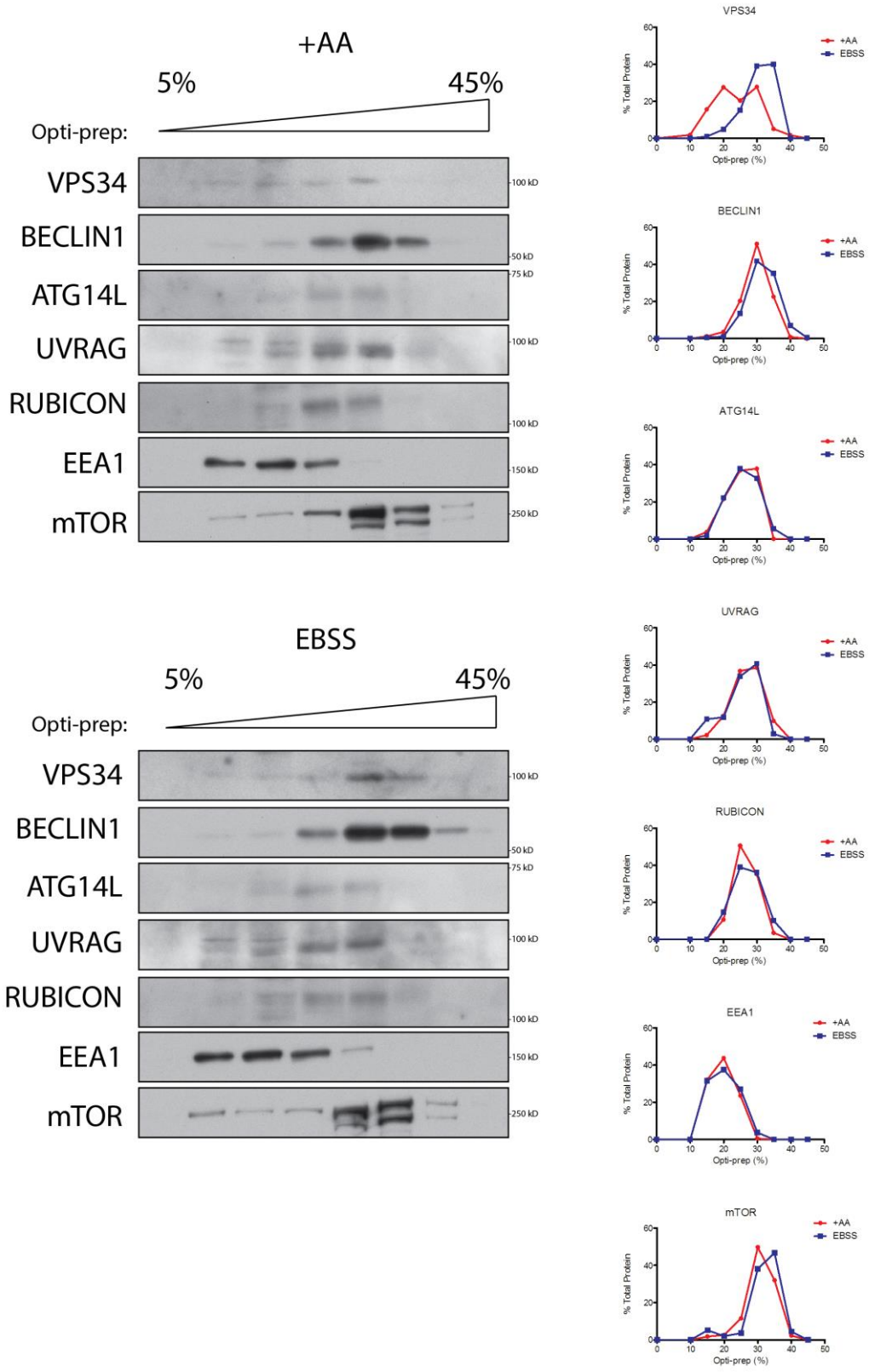

Figure 3.11 - Density gradient separation of VPS34 complex components

(A) Wild-type MEFs were incubated in complete media (+AA) or starvation media (EBSS) for 1 h and separated by iodixanol density gradient, samples were blotted as indicated. **(B)** The distribution of each protein between fractions was analysed by densitometry and plotted.

3.3 Discussion

Data presented in this chapter demonstrates for the first time that UVRAG can be phosphorylated. Moreover the phosphorylation of UVRAG occurs in a nutrient sensitive manner directly by mTORC1 and this may represent part of a co-ordinated control mechanism of key autophagy regulators alongside the ULK1 kinase complex.

Correlation with the activity of mTOR can be undoubtedly seen when assessing UVRAG phosphorylation upon incubation in serum or amino acids alone compared to combined treatment (Figure 3.1C). This clearly demonstrates the requirement of both growth factor and amino acid pathways for the synergistic activation of mTORC1 and phosphorylation of substrates. Induction of autophagy by nutrient deprivation or mTOR inhibition ablated the mobility shift in UVRAG. The inhibitor KU0063794 is a potent and selective ATP-competitive inhibitor of mTORC1 and mTORC2 with an IC_{50} of ~10 nM. Screening against a panel of 76 protein or 7 lipid kinases *in vitro* at 1 μM and 10 μM demonstrates little off-target inhibition (García-Martínez et al. 2009), this gives confidence that the blockage of UVRAG phosphorylation by KU0063794 is due to mTOR or a downstream mTOR effector and not an inhibitor off-target effect. Other structurally distinct dual mTOR inhibitors such as Torin1 are also available that could be utilised to further confirm the specificity of UVRAG phosphorylation by mTOR (Thoreen et al. 2009).

Incubation of mTORC1 but not mTORC2 *in vitro* causes direct phosphorylation of UVRAG. Typically mTORC1 substrates are recognised and bound through the regulatory component RAPTOR to allow phosphorylation. Immunoprecipitation of UVRAG identified several peptides from the RAPTOR protein suggesting that UVRAG interacts with the mTORC1 complex (Table 11). Interestingly a specific TOR signalling (TOS) motif has been identified in p70 and 4E-BP1 that mediates RAPTOR binding and mTOR phosphorylation (Schalm & Blenis 2002). Similar TOS motifs have more recently been found for other mTORC1 substrates such as HIF-1α and PRAS40 (Land & Tee 2007; Oshiro et al. 2007). The motifs identified to date are shown in Figure 3.12,

the most commonly observed motif to date is F.[-].Φ.[-].Φ where F represents phenylalanine, [-] represents negatively charged residues and Φ represents hydrophobic residues (Aasland et al. 2002). Mutation of the phenylalanine in all identified TOS motifs completely abolishes RAPTOR binding and mTORC1 phosphorylation (Schalm & Blenis 2002). Examination of UVRAG sequence however does not appear to have a matching motif with the closest being FEREK or FYTDL. Knowledge to date of the TOS motif however is still preliminary and only based upon several characterised substrates, many other notable mTORC1 substrates including ULK1 and TFEB do not possess a standard TOS motif. TOS motifs so far have primarily been based upon a conserved phenylalanine (F) residue at position 0, however it is possible that other hydrophobic aromatic amino acids such as tyrosine (Y) could function in place of F. Furthermore the negatively charged ([-]) residues could potentially be replaced by serine or threonine residues, with phosphorylation introducing a negative charge. This raises the exciting possibility that RAPTOR binding could be subject to an additional layer of regulation by other kinases phosphorylating the TOS motif, though presence of a serine or threonine at these positions remains to be shown. Further understanding of the RAPTOR recognition motifs in other mTORC1 substrates will allow refinement of the TOS motif and may help identify which region of UVRAG is critical for binding. Alternatively the binding location of RAPTOR could be determined by fragmentation analysis of UVRAG.

Incubation of endogenous mTORC1 *in vitro* with BECLIN1, ATG14L and UVRAG reveals that only UVRAG is strongly phosphorylated in comparison to p70. No phosphorylation is evident with BECLIN1 and ATG14L displays a weak phosphorylation. Phosphorylation *in* vitro was prevented in the presence of KU0063794 indicating this was mediated by mTOR kinase activity. Yuan et al. (2013) have previously demonstrated that ATG14L could be a direct mTORC1 substrate, however this was reliant on tagged and over-expressed RAPTOR and mTOR. In the present investigation using an endogenous mTORC1 assay, ATG14L was weakly phosphorylated in comparison to p70 D236A or UVRAG. For this reason UVRAG was solely focused upon as the data suggested this was likely to be an endogenous substrate of mTORC1.

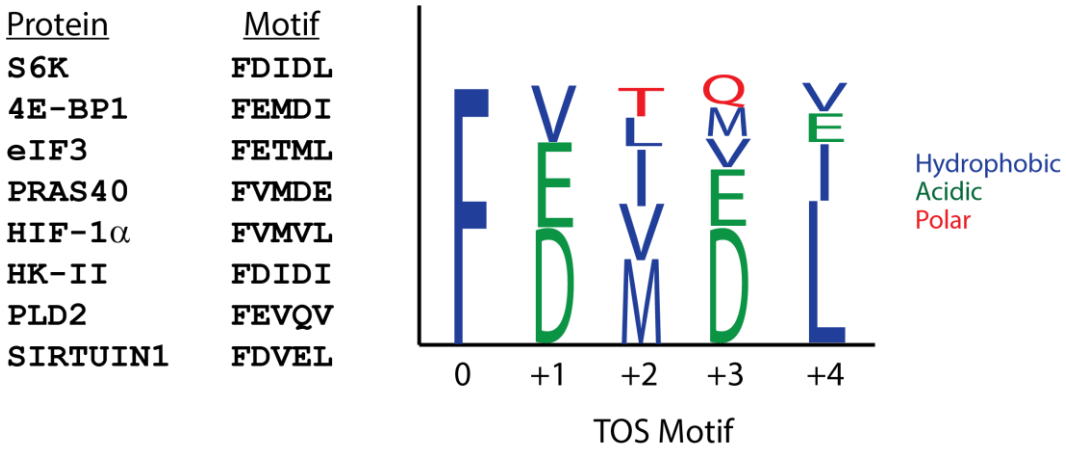

Figure 3.12 - TOR signalling (TOS) motif

Current known TOS motifs are listed alongside their containing protein with the prevalence of each residue in the motif demonstrated. To date TOS motifs have been identified in p70 S6K (Schalm & Blenis 2002), 4E-BP1 (Schalm et al. 2003), eIF3f (Csibi et al. 2010), PRAS40 (Oshiro et al. 2007), HIF-1α (Land & Tee 2007), HEXOKINASE-II (HK-II) (Roberts et al. 2014), PHOSPHOLIPASE D2 (PLD2) (Ha et al. 2006) and SIRTUIN1 (Back et al. 2011).

Analysis by mass spectrometry identified two UVRAG phospho-peptides that were regulated in an mTORC1 dependent manner both in cells and following an *in vitro* kinase assay (Table 10). Large scale proteomic experiments have previously predicted S498, T518 and S548 as potential UVRAG phosphorylation sites (Yu et al. 2011), in this study S498 and T518 were identified but not found to be regulated in an mTOR dependent manner (Table 10). The K543-K559 phospho-peptide corresponding to S548-S550 was identified to be mTOR dependent, S550 is the most favourable mTOR site by consensus sequence (Figure 3.5C) and indeed mutation analysis demonstrated that S550 is the phosphorylated residue (Figure 3.6). S498 or S508 and T518 or S522 may represent inputs from distinct unknown kinases that may also modulate UVRAG function and will require further investigation. Focus was placed upon S550 and S571 as these phosphorylated peptides were consistently identified by mass spectrometry with high scores in an mTOR dependent manner. Whilst higher peptide scores may simply indicate the peptide is more favourable for identification by mass spectrometry, mutation of S550A and S571A caused a complete downshift in UVRAG mobility and reduced ^{32}P incorporation by ~70 % (Figure 3.6)

indicating that these represent major phosphorylation sites in UVRAG. Use of the mTOR kinase inhibitor KU0063794 also reduces ^{32}P incorporation by ~70 %, suggesting that these two sites fully represent mTOR target residues and the remaining phosphorylation occurs due to the presence of contaminating kinases. Due to the fragility of the endogenous mTORC1 complex, IP has to be carried out under weak lysis and wash conditions with CHAPS detergent (Kim et al. 2002) which may increase the propensity for non-specific contaminants.

The location of the identified phosphorylation sites leads to ambiguity over possible functional roles as all sites fall within the C-terminal region of UVRAG with no known domain structure. The majority of characterised UVRAG protein interactions and functions have been correlated with specific protein domains. The coiled-coil domain (CCD, 200-275) for example is the critical mediator of VPS34 complex binding by interacting with a CCD in BECLIN1 (Liang et al. 2006). Phosphorylation of UVRAG does not impede or enhance this interaction as no variation in BECLIN1 binding was observed (Figure 3.8). UVRAG has also been implicated in binding to the N-BAR containing protein Endophilin-B1 (Bif-1) via interaction of an N-terminal proline rich region (PRR) with the SH3 domain of Bif-1 (Takahashi et al. 2007). Membrane insertion of N-BAR domains is sufficient to generate membrane curvature and has been linked to enhancing autophagosome formation (Farsad et al. 2001). Attempts to resolve an interaction by immunoprecipitation of endogenous UVRAG (antibody raised against whole protein) in the same lysis buffer however proved unsuccessful (Figure 3.8D), even under nutrient starvation where the Bif-1 association is reported enhanced (Takahashi et al. 2007). Identification of UVRAG and Bif-1 binding was only demonstrated by exogenous expression of Myc-Bif-1 and FLAG-UVRAG in HEK293T cells. A further independent study resolved an interaction between endogenous UVRAG and HA-Bif-1 (Wong et al. 2011). A true endogenous-endogenous interaction has therefore not truly yet been demonstrated. It is possible that the binding of Bif-1 and UVRAG is weak or transient in nature that is not retained upon IP. The PRR may act to bind other proteins, non-repetitive PRRs such as that in UVRAG are favourable for SH3 domain interactions that are contained in a multitude of proteins. Many of these are membrane-associated proteins and are

often associated with signalling transduction pathways (Williamson 1994). UVRAG also contains a C2 domain that are classically associated with Ca^{2+} interaction and membrane binding (Nalefski & Falke 1996). The co-ordination of calcium can allow phospholipid binding (Sutton et al. 1995) and UVRAG has been shown to interact with PI(3)P for localisation to the endoplasmic reticulum as part of the ER tethering complex (He et al. 2013). The C-terminal region has more recently been identified to interact with several proteins; residues 275-442 for example has been shown to bind the centrosomal protein CEP63 or ER protein RINT-1 whilst residues 442-699 interact with DNA-dependent protein kinase (DNA-PK) (He et al. 2013; Zhao et al. 2012). Binding to CEP63 or DNA-PK is not reported to require the BECLIN1-VPS34 complex for function. Further investigation is required to examine whether binding to these components is affected by UVRAG phosphorylation state.

Separation of cell lysates by density centrifugation or gel filtration did not display any change in the distribution of UVRAG between phosphorylation states. As reported previously however, ATG14L did appear in higher molecular weight fractions than UVRAG demonstrating differences in complex specific binding (Matsunaga et al. 2009) although this was abolished upon autophagy induction. The wide elution peak of UVRAG meant that changes in a possible interaction upon phosphorylation may be easily masked. To look directly for interacting proteins, UVRAG wild-type or S548-550A was immunoprecipitated and analysed by mass spectrometry. BECLIN1 was unable to be identified likely due to the antibody heavy chain present at a similar molecular mass, however both VPS34 and VPS15 were detected. Interestingly peptides corresponding to RAPTOR were also identified in both samples, confirming the involvement of mTORC1 with UVRAG. Tubulin components were highly represented upon UVRAG IP in comparison to a GST control IP and may represent the association of vesicles moving along microtubules given its established role in membrane trafficking. The detection of peptides belonging to motor proteins such as dynein or kinesin however was significantly lower (Table 11). The high score for many tubulin components may in part be explained by the reported binding of UVRAG to the centrosome and CEP63 (Zhao et al. 2012), however neither γ-tubulin nor CEP63 was identified.

CEP63 has a similar mass to BECLIN1 and it is possible it may also have been masked by detection of antibody heavy chain peptides instead. Interestingly the v-SNARE vesicle-associated membrane protein 3 (VAMP3) was identified in only the wild-type immunoprecipitation. VAMP3 in combination with t-SNAREs can mediate vesicle fusion at the plasma membrane, this has been shown to be important in the recycling of integrins for cell motility and also the fusion of granules (lysosome related organelles) from platelets (Riggs et al. 2012; Polgár et al. 2002). VAMP3 is also required for functional retrograde trafficking of mannose-6-phosphate receptors from late endosomes to the trans-golgi network (TGN) (Ganley et al. 2008). Given the low score and number of peptides however this will need further analysis to confirm interaction with UVRAG. DCAF11 and IRS4 were found uniquely in the UVRAG S550A+S571A mutant immunoprecipitation, further experiments are required to examine whether these represent genuine interactions and how they may regulate or interplay with UVRAG function.

To try to improve resolution of phosphorylation specific interacting proteins and reduce non-specific binding, biotin peptides corresponding to Human UVRAG S536-S583 and encompassing both mTORC1 phosphorylation sites were generated (Schulze & Mann 2004). Reducing the whole protein down to a specific peptide region can enrich for proteins that may specifically interact (Gururaja et al. 2003; Hinsby et al. 2004). Synthesis of phosphorylated peptides is also advantageous as it ensures a near homologous phosphorylation state which may help identify interactions, whereas immunoprecipitation of whole protein will likely also contain those that are not phosphorylated at particular residues. The main drawback from the use of peptides however is that the small region may not be sufficient to bind genuine interactors if it is from a region lacking key interacting residues (Schulze & Mann 2004). Use of phosphorylated biotin peptides mainly identified 14-3-3 isoforms (Table 12). 14-3-3 proteins are able to modulate many signalling pathways through their ability to bind phosphorylation sites, thereby preventing them from mediating interactions or fulfilling other functions (Muslin et al. 1996). Analysis of immunoprecipitated UVRAG however demonstrated poor binding of 14-3-3 that was not regulated in a phosphorylation sensitive manner (Figure 3.10). The binding of 14-3-3 may

not be an important interaction for *in vivo* UVRAG, however UVRAG peptides *in vitro* are ideal binding targets for 14-3-3 proteins based upon the residues surrounding each phosphorylated serine residue(Yaffe et al. 1997). Very few other proteins were identified by peptide IP and it is possible that 14-3-3 proteins act to compete off other interactions due to their affinity for the phosphorylation motif. Another approach may be to selectively deplete 14-3-3 isoforms from cell lysates prior to immunoprecipitation, however this also risks losing other potentially important proteins.

In conclusion, the protein UVRAG is phosphorylated by mTORC1 during nutrient rich conditions and this is abolished upon induction of autophagy. ULK1 and VPS34 are the two primary inducers of autophagy downstream of mTOR and it is exciting that they may be regulated co-ordinately with one another. UVRAG remains in complex with VPS34 and does not facilitate any detectable binding of additional components or alter localisation in a manner that impacts upon its isopycnic point. The binding of UVRAG to the VPS34 complex however is known to increase lipid kinase activity. The primary consequence of mTORC1 mediated phosphorylation of ULK1 is a reduction in protein kinase activity to prevent autophagy induction (Ganley et al. 2009; Jung et al. 2009). It may also be possible that mTOR analogously manipulates VPS34 kinase activity via phosphorylation of UVRAG. Additionally post-translational modification of other VPS34 interactors BECLIN1 and ATG14L has previously been shown to regulate lipid kinase activity (Russell et al. 2013; Xia et al. 2014; Yuan et al. 2013). A further examination of VPS34 activity following phosphorylation is therefore critical and is addressed in the following chapter.

4 REGULATION OF VPS34 KINASE ACTIVITY BY MTOR

4.1 Introduction

Phosphatidylinositol kinases (PIKs) regulate cellular signalling via creation of discrete enriched pools of phosphoinositides that recruit effector proteins to drive cellular responses. The phosphatidylinositol 3-kinases (PI3Ks) have been the subject of particularly intense study due to their implication in growth factor signalling, a frequently mutated pathway in disease (Samuels et al. 2004). Notably class I PI3K's (PIK3C1) activity is very low and dependent upon growth factor signalling via receptor tyrosine kinases to induce rapid and significant increases in lipid kinase activity (Stephens et al. 1993). By comparison VPS34 (PIK3C3) does not demonstrate substantial activity changes on the same scale, instead the VPS34 and VPS15 dimer is constitutively active (Stack et al. 1995). Several stimuli have been identified in recent years that are able to modulate VPS34 kinase activity, however the level of activity change is typically 2-4 fold and noticeably much smaller than activity changes observed in PIK3C1. Slight changes in activity however are not inconsequential due to the very nature of phospholipid signalling, the presence of a small enriched pool of phospholipid is sufficient to recruit cellular effectors in a spatial and temporal manner that is critical for correct cellular function. PI(3,5)P_2 for example represents only 0.04 % of the total cellular phosphatidylinositol (PI) but inhibition impairs a diverse set of trafficking pathways (McCartney et al. 2014). Additionally, blocking the formation of one phosphoinositide species can lead to knock-on effects for other lipid species, as many are inter-converted from one species to the next by sequential phosphorylation or phosphatase activity (Figure 1.6).

The binding of regulatory components such as BECLIN1 and UVRAG have been show to increase VPS34 activity (Kihara, Noda, et al. 2001; Liang et al. 2006). Several VPS34 interactors have also been reported to be regulated by post-translational modifications that lead to VPS34 activity changes. Notably BECLIN1 is reported to be phosphorylated and ubiquitinated, both of which

enhance ATG14L-BECLIN1-VPS34 kinase activity and autophagy induction (Russell et al. 2013; Xia et al. 2013). Given that UVRAG is known to modulate VPS34 activity upon complex binding and that phosphorylation of other VPS34 components have been shown to regulate activity, it is possible that UVRAG phosphorylation by mTOR may also act to regulate kinase activity and this was therefore examined further. Additionally, AMPK is reported to co-ordinately regulate the activity of both ULK1 and VPS34 (Kim et al. 2011; Kim et al. 2013), given that mTORC1 is established to regulate ULK1 activity this may represent an analogous control mechanism that also alters VPS34 activity.

4.2 Results

4.2.1 VPS34 activity is regulated by UVRAG phosphorylation.

Endogenous or recombinant VPS34 can be assayed *in vitro* to determine lipid kinase activity. Liposomes created from the VPS34 substrate phosphatidylinositol were incubated in the presence of ^{32}P γ-ATP and Manganese (Mn^{2+}) (Volinia et al. 1995; Whitman et al. 1988); lipid kinase activity of VPS34 catalyses the transfer of γ-phosphate to position three of the inositol ring to create phosphatidylinositol-3-phosphate (PI(3)P) (Schu et al. 1993). The size and consequent curvature of lipid vesicles is an important determinant for the binding of membrane interacting proteins, including VPS34 via the myristoylation of VPS15 (Herman et al. 1991; Madsen et al. 2010). Accordingly, PI was extruded through a polycarbonate membrane to form liposomes with a maximal diameter of 100 nm to reduce substrate variability and improve experimental consistency.

Endogenous UVRAG-BECLIN1-VPS34 complex was selectively analysed by immunoprecipitation of UVRAG. This ensured that UVRAG-bound VPS34 activity was analysed and did not include ATG14L-BECLIN1-VPS34 or unbound VPS34. The UVRAG-BECLIN1-VPS34 kinase activity was examined during nutrient rich conditions or upon autophagy induction by nutrient starvation or mTOR inhibition (KU0063794). A significant drop in VPS34 activity of ~50 % was observed in U2OS cells upon autophagy induction (Figure 4.1A), similarly wild-type MEFs demonstrated a decrease in UVRAG-BECLIN1-VPS34 activity upon nutrient starvation (Figure 4.1B). In comparison the activity of mCherry-S-ATG14L-BECLIN1-VPS34 was examined in MEFs and nutrient starvation displayed no significant change in activity (Figure 4.1C) indicating that the response to nutrient starvation observed is specific to the UVRAG-BECLIN1-VPS34 complex. The UVRAG-BECLIN1-VPS34 lipid kinase activity therefore correlates with changes in the UVRAG phosphorylation state with increased activity when S550 and S571 are phosphorylated.

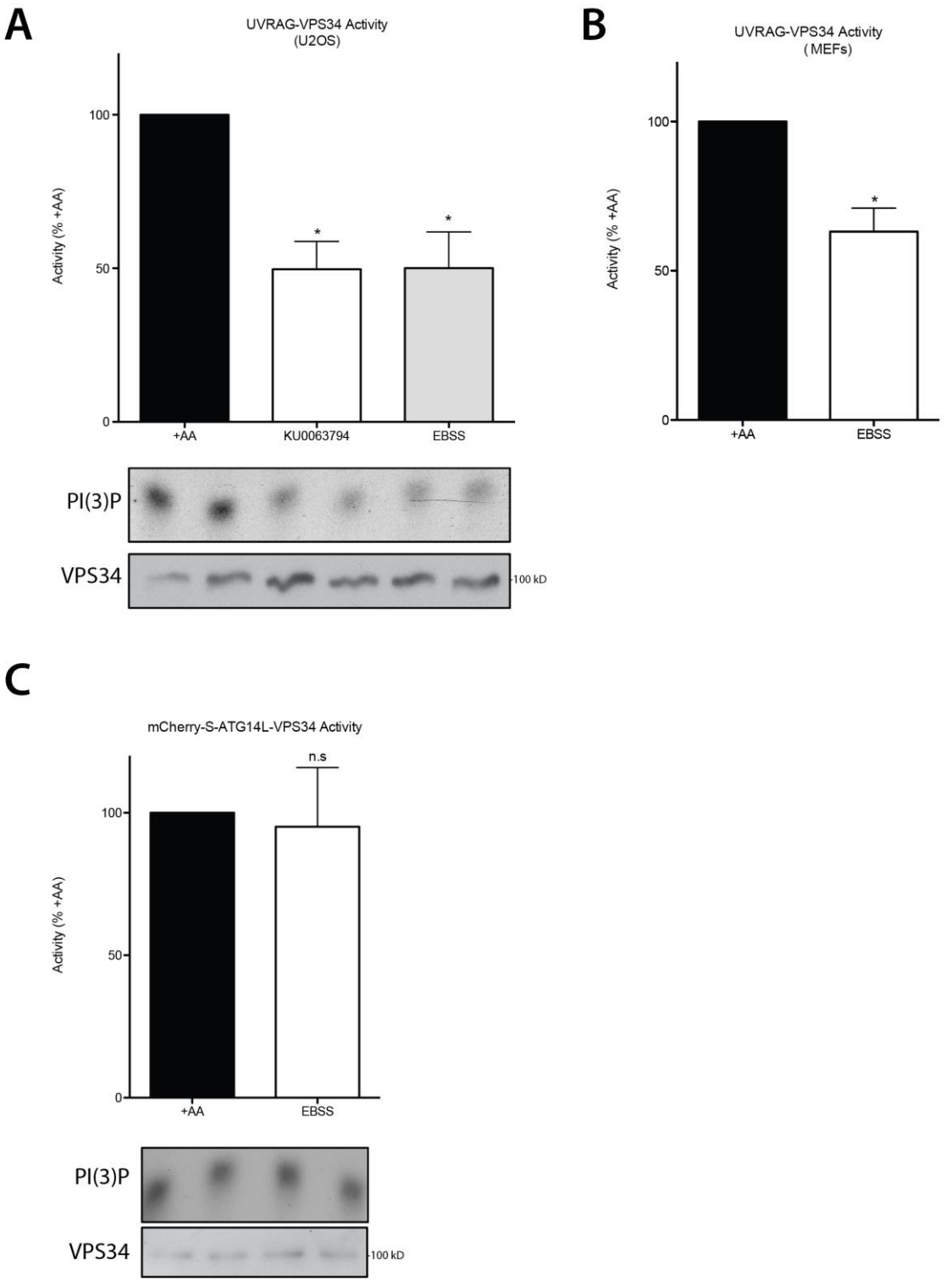

Figure 4.1 – Endogenous VPS34 activity in response to nutrient status

(A+B) Cells were incubated in complete media (+AA), starvation media (EBSS) or treated with 1 µM KU0063794 for 1 h (MEFs) or 2 h (U2OS) before lysis. Endogenous UVRAG was immunoprecipitated (S323D) and co-immunoprecipitated VPS34 was assayed *in vitro*. **(C)** mCherry-S-ATG14L MEFs were incubated in complete media (+AA) or starvation media (EBSS) for 1 h before lysis. ATG14L was immunoprecipitated by S-protein sepharose and assayed for co-immunoprecipitating VPS34 activity. For **(A-C)** samples were lysed in 0.5% NP-40 lysis buffer. Bars in each graph represent mean normalised VPS34 activity ± SEM for n = 3 independent experiments.

To examine whether the kinase activity of VPS34 is directly linked to UVRAG phosphorylation, cells stably expressing near endogenous levels of wild-type or S550A+S571A UVRAG were generated. GFP-UVRAG was immunoprecipitated from MEFs or Hela cells and canonical binding partners were examined to ensure VPS34 complex binding was not impaired (Figure 4.2). Mutation of S550A+S571A had no effect on BECLIN1 or VPS34 binding as was previously predicted (Figure 3.8).

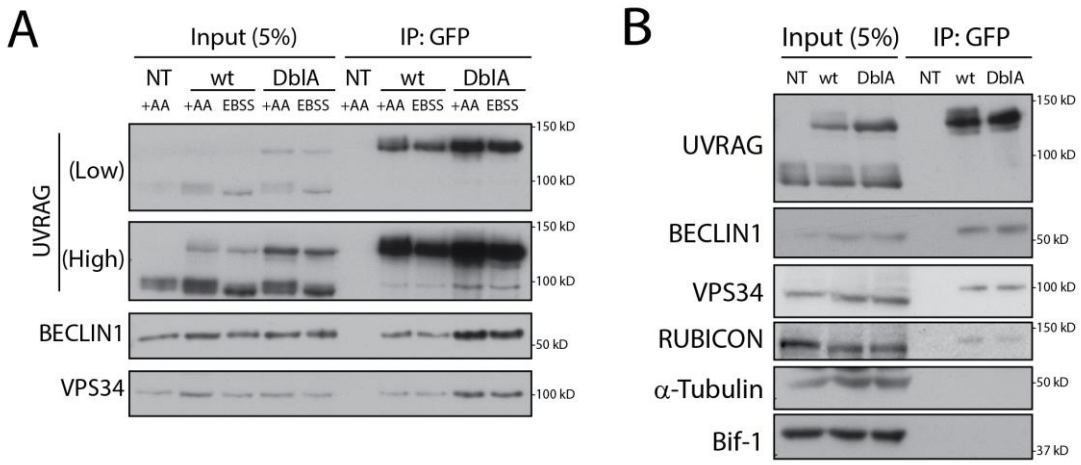

Figure 4.2 - UVRAG S550A + S571A mutant cells

Wild-type MEFs **(A)** or Hela cells **(B)** stably expressing GFP-UVRAG wild-type (wt), S550A+S571A (DblA) or non-transfected (NT) were incubated in complete media (+AA) or starvation media (EBSS) for 1 h (MEFs) or 2 h (Hela). Cells were lysed in 0.5 % NP-40 lysis buffer and GFP-UVRAG was immunoprecipitated with anti-GFP sepharose beads and immunoblotted for associated VPS34 complex proteins.

U2OS cells expressing FLAG-UVRAG wild-type or S550A+S571A were immunoprecipitated and assayed for associated VPS34 activity in the presence or absence of nutrients. FLAG-UVRAG wild-type displayed a similar change in activity to that of endogenous UVRAG, however mutation of S550A+S571A abolished the VPS34 activity increase observed in the presence of nutrients (Figure 4.3A). Mutation of a serine residue to an aspartate can mimic the properties of phosphorylation as it also introduces a negative charge. Analysis of FLAG-UVRAG S550D+S571D bound VPS34 did not display enhanced activity that could be expected if it were

to mimic the phosphorylation phenotype, however it matched that of S550A+S571A (Figure 4.3B). This suggests that whilst unable to mimic the effects of phosphorylation, mutation to a non-phosphorylatable residue still abolishes the increase in complex activity. Investigations utilising MEFs stably expressing GFP-UVRAG also confirmed that mutation of S550A+S571A abolished the enhanced complex activity under nutrient rich conditions (Figure 4.3C).

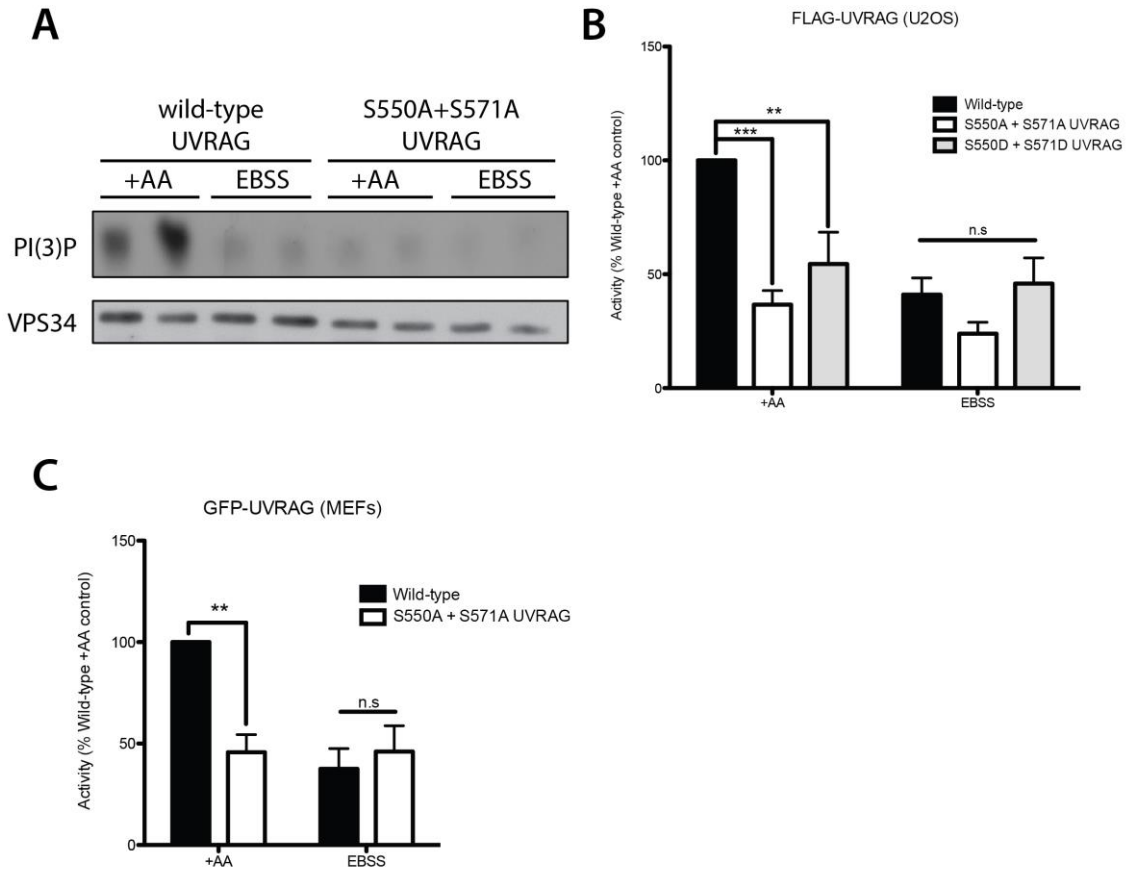

Figure 4.3 - UVRAG S550A+S571A mutant VPS34 kinase activity

(A) U2OS cells stably expressing FLAG-UVRAG wild-type or S550A+S571A were incubated in complete media (+AA) or starvation media (EBSS) for 2 h. UVRAG was immunoprecipitated with FLAG agarose and co-immunoprecipitated VPS34 activity was assayed *in vitro*. **(B)** Quantitation of (A), bars represent the mean normalised VPS34 activity ± SEM for a minimum of n = 4 independent experiments. **(C)** MEFs stably expressing GFP-UVRAG wild-type or S550A+S571A were incubated in complete media (+AA) or starvation media (EBSS) for 1 h. UVRAG was immunoprecipitated with GFP sepharose and co-immunoprecipitated VPS34 activity was assayed *in vitro*. Bars represent mean normalised VPS34 activity ± SEM for n = 3 independent experiments. **(B+C)** Statistical analysis was carried out by two-way analysis of variance and Bonferroni's post-test.

4.2.2 Reconstitution of the VPS34 complex *in vitro*

To rule out the possibility of unknown cellular components influencing the VPS34 complex activity, such as additional binding proteins, a recombinant VPS34 assay was attempted. The VPS34 complex was to be reconstituted *in vitro* and phosphorylated directly with endogenous mTORC1 to reduce external variables. Attempts to reconstitute the VPS34 complex *in vitro* however were unsuccessful due to poor complex formation and high non-specific binding. His-BECLIN1 alone could bind to GST beads non-specifically in the absence of GST-UVRAG whilst the addition of GST-UVRAG did not enhance binding further (Figure 4.4A). Alternatively GST-BECLIN1 was able to successfully bind MBP-UVRAG but His-VPS34-VPS15 was occluded from binding GST sepharose (Figure 4.4B). Interestingly the addition of His-VPS34-VPS15 enhanced the binding of MBP-UVRAG to GST-BECLIN1 but did not bind itself. It may be that these proteins require co-expression to form a functional complex. Alternately it is possible that the presence of tags utilised for protein purification could be detrimental to binding, therefore multiple tag combinations of recombinant proteins were attempted, but without success (data not shown).

Although unclear, assuming the phosphorylation of UVRAG did not facilitate binding of additional components then the increase in activity could potentially be derived from 3D structural changes in the VPS34 complex that impact upon substrate recognition or the ATP hydrolysis rate of VPS34. To determine whether phosphorylation of UVRAG could interact or alter binding with specific VPS34 complex components, biotinylated peptides from UVRAG were utilised. Non-phosphorylated or S550+S571 phosphorylated peptides were incubated with His-VPS34-VPS15, His-VPS34, GST-BECLIN1 or GST-UVRAG. A control peptide of the same charge and length was used for comparison. The phosphorylated UVRAG peptide had a stronger interaction with recombinant proteins than the non-phosphorylated peptide, however this was also observed with the control phosphorylated peptide. The presence of negative charge alone

appears to be favourable for peptide-protein interaction regardless of the sequence and it has been demonstrated that charged proteins are more likely to interact in a system (Xu et al. 2013).

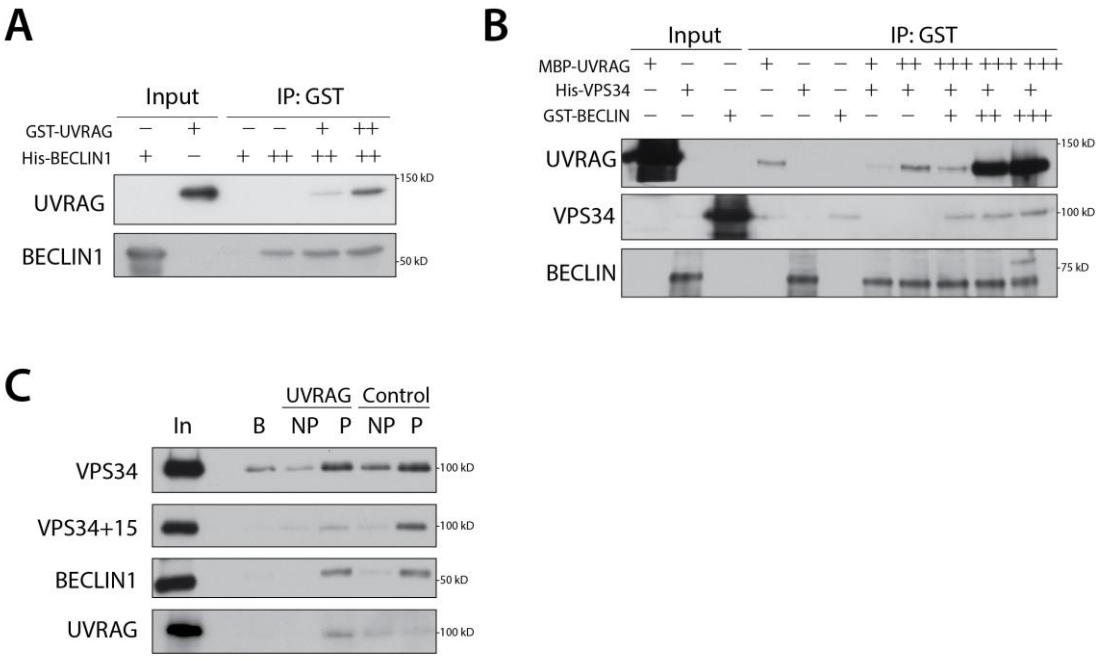

Figure 4.4 - Recombinant VPS34 complex formation

(A) Recombinant GST-UVRAG (DU36724) and His-BECLIN1 (DU40738) or **(B)** Recombinant MBP-UVRAG (DU40944), His-VPS34-VPS15 (DU8692) and GST-BECLIN1 (DU40130) were incubated in 0.5 % NP-40 lysis buffer and immunoprecipitated with GST-Sepharose.**(C)** Biotinylated peptides corresponding to human UVRAG S536-S583 or control peptide were incubated in 0.5 % NP-40 lysis buffer separately with His-VPS34 (DU3303) or His-VPS34-VPS15, His-BECLIN1 or GST-UVRAG. Peptides were immunoprecipitated with streptavidin agarose and analysed by western blot for interaction of recombinant proteins.

4.2.3 Detection of cellular PI(3)P levels

Data obtained *in vitro* indicated that UVRAG phosphorylation at S550+S571 increased VPS34 lipid kinase activity by ~2 fold (Figure 4.3). It is important to ascertain whether the activity change *in vitro* is replicated by cellular changes in the level of the product PI(3)P, particularly as UVRAG-BECLIN1-VPS34 represents a sub-population of total VPS34 within the cell. The cellular PI(3)P level can be estimated by taking advantage of the specific binding properties of FYVE domains. The FYVE domain of HRS exclusively binds to PI(3)P and the binding affinity can be improved by expression of a double (2xFYVE) domain (Gaullier et al. 1998) . The 2xFYVE domain was stably expressed in U2OS cells with a GFP tag, allowing PI(3)P rich membranes to be represented by GFP-positive puncta (Gillooly et al. 2000). However, the expression of GFP-2xFYVE within cells may have adverse effects due to competition with endogenous PI(3)P interacting proteins such as EEA1 (Byfield et al. 2005). This can impair cellular function, therefore, U2OS cells expressing a very low level of GFP-2xFYVE were isolated by single cell cloning to minimise potential artificial cellular effects of probe expression. The punctate expression of GFP-2xFYVE was examined between nutrient rich conditions or autophagy induction either by nutrient depletion or by mTOR inhibition. Additionally the PI3K inhibitor wortmannin was used as a positive control to inhibit PI(3)P production (Arcaro & Wymann 1993; Stack & Emr 1994). No significant change in puncta was observed between conditions except for wortmannin treatment that abolished membrane binding resulting in a diffuse cytosolic location (**Figure 4.5**). This could suggest that UVRAG phosphorylation state has no effect upon cellular PI(3)P levels, contrasting the evidence determined *in vitro* (Figure 4.1). However as described above the expression of an intracellular PI(3)P probe could potentially have adverse effects even at a low expression level and additionally expression that is too low may only label a subset of PI(3)P structures. For these reasons PI(3)P levels were determined by staining following formaldehyde fixation. Recombinant PI(3)P binding domains were purified and conjugated to fluorophores allowing use on fixed cells similar to antibodies.

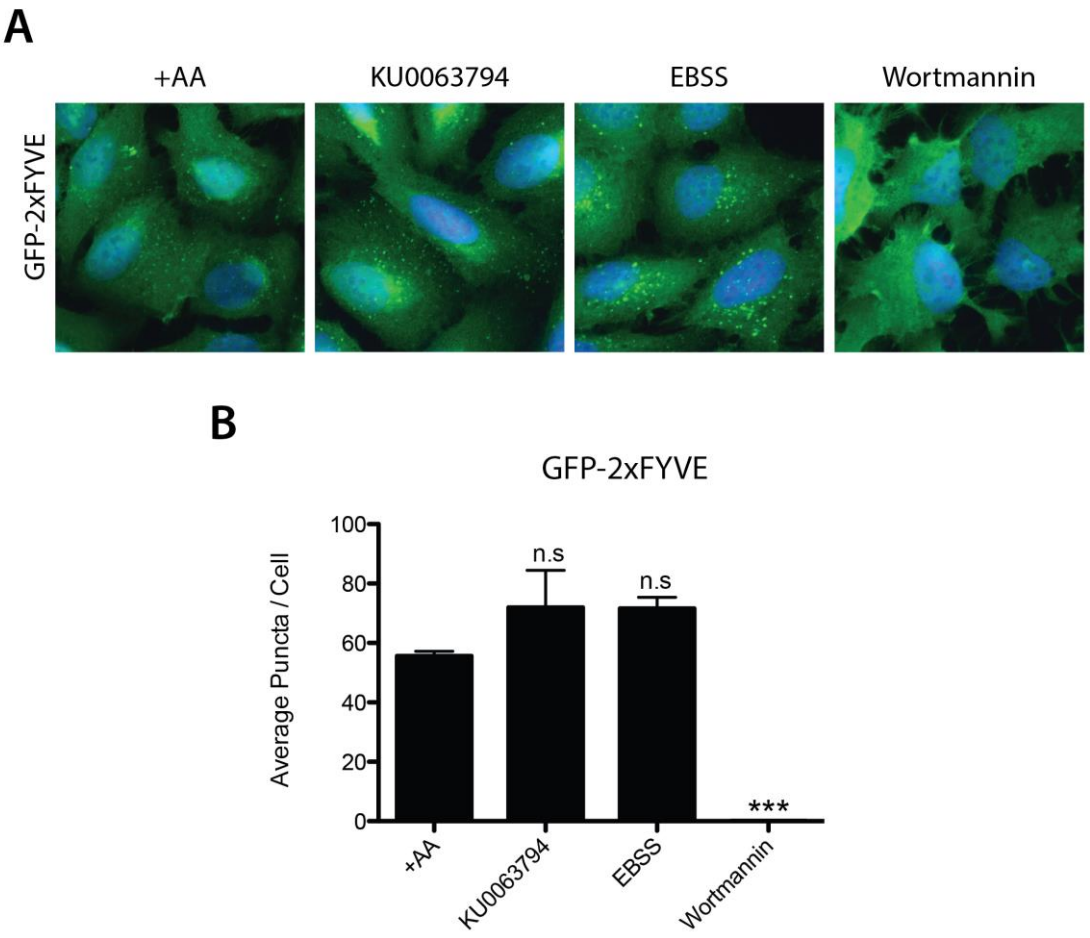

Figure 4.5 – GFP-2xFYVE Staining

(A) Images of U2OS cells stably expressing a GFP-2xFYVE (HRS) PI(3)P binding probe. Cells were washed and incubated in complete media (+AA), starvation media (EBSS), treated with 1 µM KU0063794 or 10 µM Wortmannin for 2 h prior to formaldehyde fixation **(B)** Quantitation of (A), bars represent mean puncta per cell ± SEM for n = 3 independent experiments. Significance was determined by one-way analysis of variance and Dunnet's multiple comparison post-test.

The PX domain from $p40^{phox}$ selectively binds PI(3)P (Kanai et al. 2001); the PX domain conjugated to Alexa Fluor® 555 was a kind gift from N.Ktistakis, Babraham Institute, Cambridge, and was utilised for preliminary experiments. The PX domain was subsequently expressed and purified from bacteria prior to conjugation to Alexa Fluor® 594 (Referred hereafter as PX-594). U2OS cells expressing low levels of GFP-2xFYVE were grown in nutrient rich or depleted conditions and stained with the PX-594 conjugate following fixation. Direct comparison of the two PI(3)P binding domains demonstrated specific PX-594 positive structures that were not labelled with GFP-2xFYVE, particularly in central regions between the cell periphery and nucleus (Figure 4.6A). The punctate staining observed with each probe was not present in cells treated

with wortmannin (Figure 4.5 & Figure 4.7), indicating that the binding of each probe was PI(3)P dependent. This demonstrated that the GFP-2xFYVE stably expressed in U2OS cells (Figure 4.5) was not fully representative of cellular PI(3)P levels. Upon nutrient deprivation and UVRAG dephosphorylation, a ~2 fold decrease in total PX-594 staining was observed that matched VPS34 *in vitro* activity data in comparison to GFP-2xFYVE (Figure 4.6B&C).

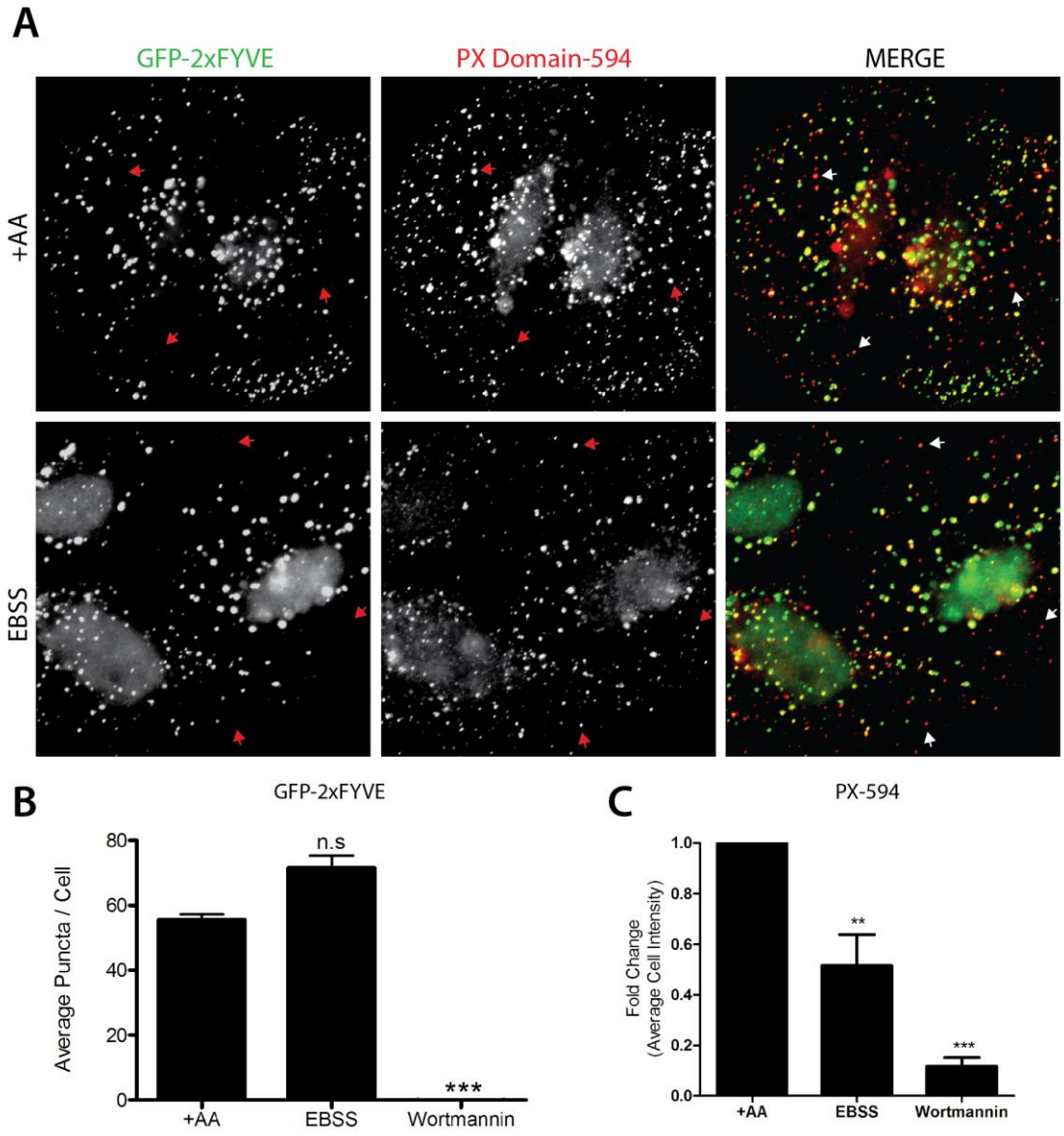

Figure 4.6 - Comparison of PI(3)P Binding Probes.

(A) U2OS cells expressing GFP-2xFYVE were incubated in complete media (+AA) or starvation media (EBSS) for 2 h and fixed with formaldehyde by freeze-thaw. Cells were stained using PX-594 and analysed by microscopy. Arrows indicate examples of distinct PX-594 punctate structures. **(B+C)** Quantitation of (A), bars represent mean value ± SEM for n = 3 independent experiments. Significance was determined by one-way analysis of variance and Dunnet's multiple comparison post-test to the +AA sample where ** = $p < 0.01$, *** = $p < 0.001$ and n.s = not significant.

The co-localisation of PX-594 was assessed with multiple PI(3)P binding proteins. The early endosome markers EEA1 and GFP-WDFY2 bind to PI(3)P via their FYVE domains and displayed significant co-localisation with PX-594 (Figure 4.7,Figure 4.8A) (Hayakawa et al. 2006; Simonsen et al. 1998). In comparison, the early endosomal marker APPL1 interacts with Rab5 in the absence of PI(3)P (Zoncu et al. 2009) and displayed very low co-localisation with PX-594 (Figure 4.8B), thereby demonstrating the selectivity of PX-594 for PI(3)P positive endosomal membranes. Other FYVE domain containing PI(3)P effectors involved in endocytosis showed co-localisation, such as RUFY1 that is present on Rab4 and Rab14 positive endosomes (Figure 4.9A) (Fukuda et al. 2011; Yamamoto et al. 2010) . The motor protein adaptor FYCO1 that is partially dependent upon PI(3)P for membrane binding also displayed small amounts of PX domain co-localisation (Figure 4.9B)(Pankiv et al. 2010). The PX Domain therefore labels a wide selection of known PI(3)P positive compartments.

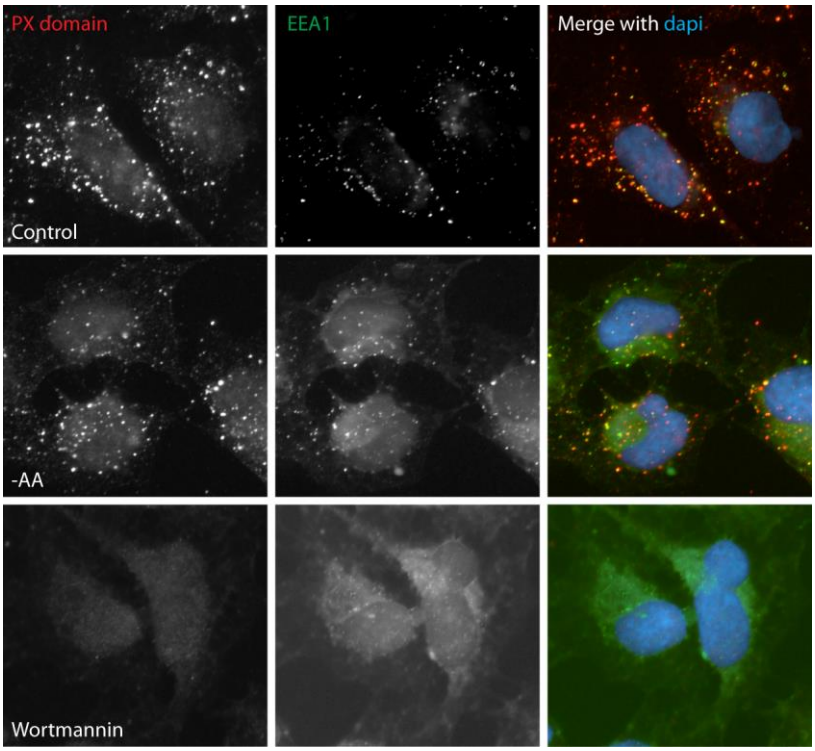

Figure 4.7 - PX Domain and EEA1 Co-localisation

U2OS cells were incubated in complete media (+AA), starvation media (EBSS) or treated with wortmannin (10µM) for 2 h and then fixed by freeze thaw. Cells were stained with PX-594 and anti-EEA antibody using AlexaFluor® 488 secondary antibody.

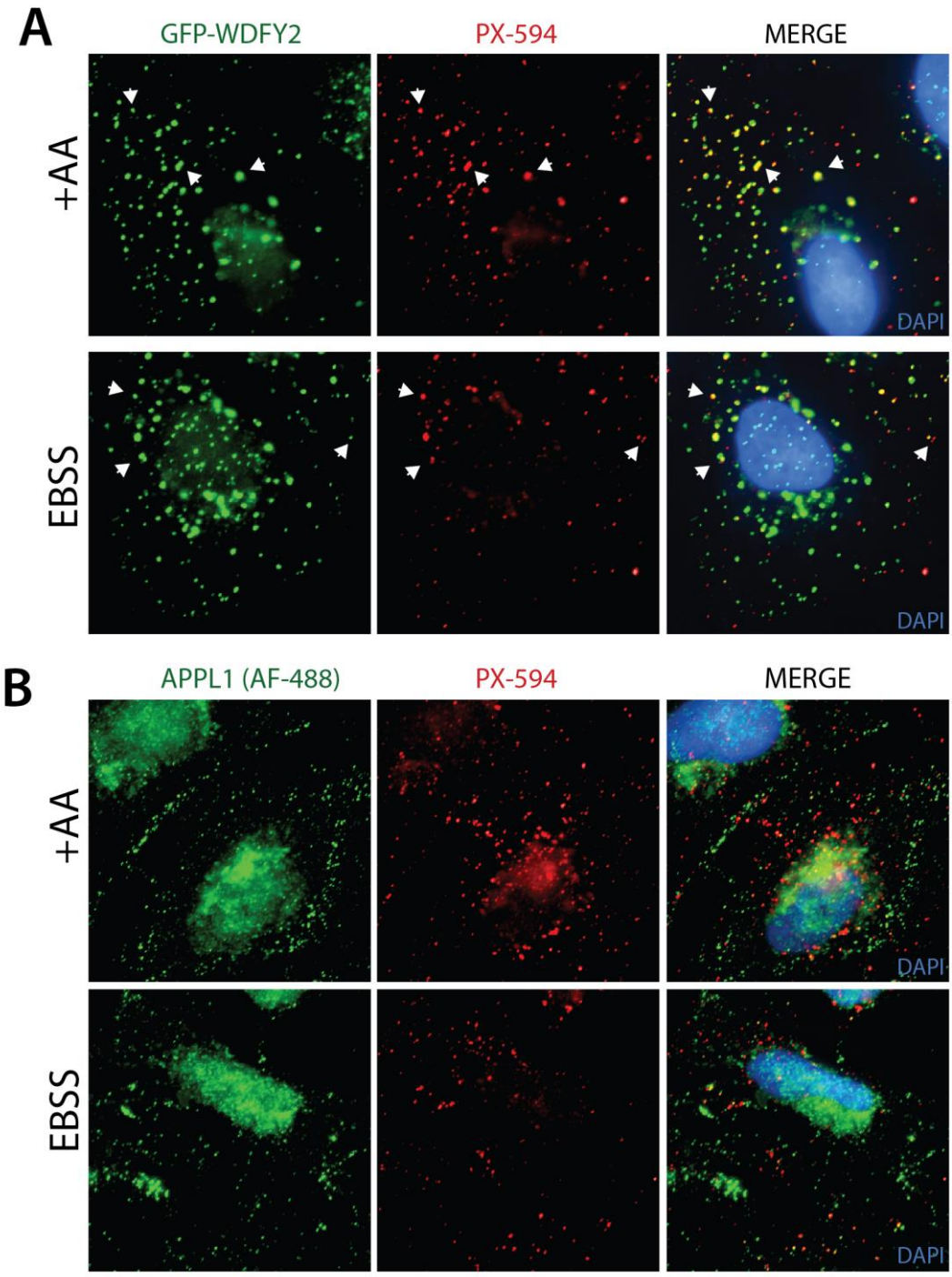

Figure 4.8 - PX Domain co-localisation with WDFY2 and APPL1

U2OS cells **(A)** control or **(B)** transfected with GFP-WDFY2 were incubated in complete media (+AA) or starvation media (EBSS) for 2 h and then fixed by freeze thaw. Cells were stained with PX-594 and **(A)** anti-GFP or **(B)** anti-APPL1 using AlexaFluor® 488 (AF-488) secondary antibody. Arrows indicate example regions of co-localisation.

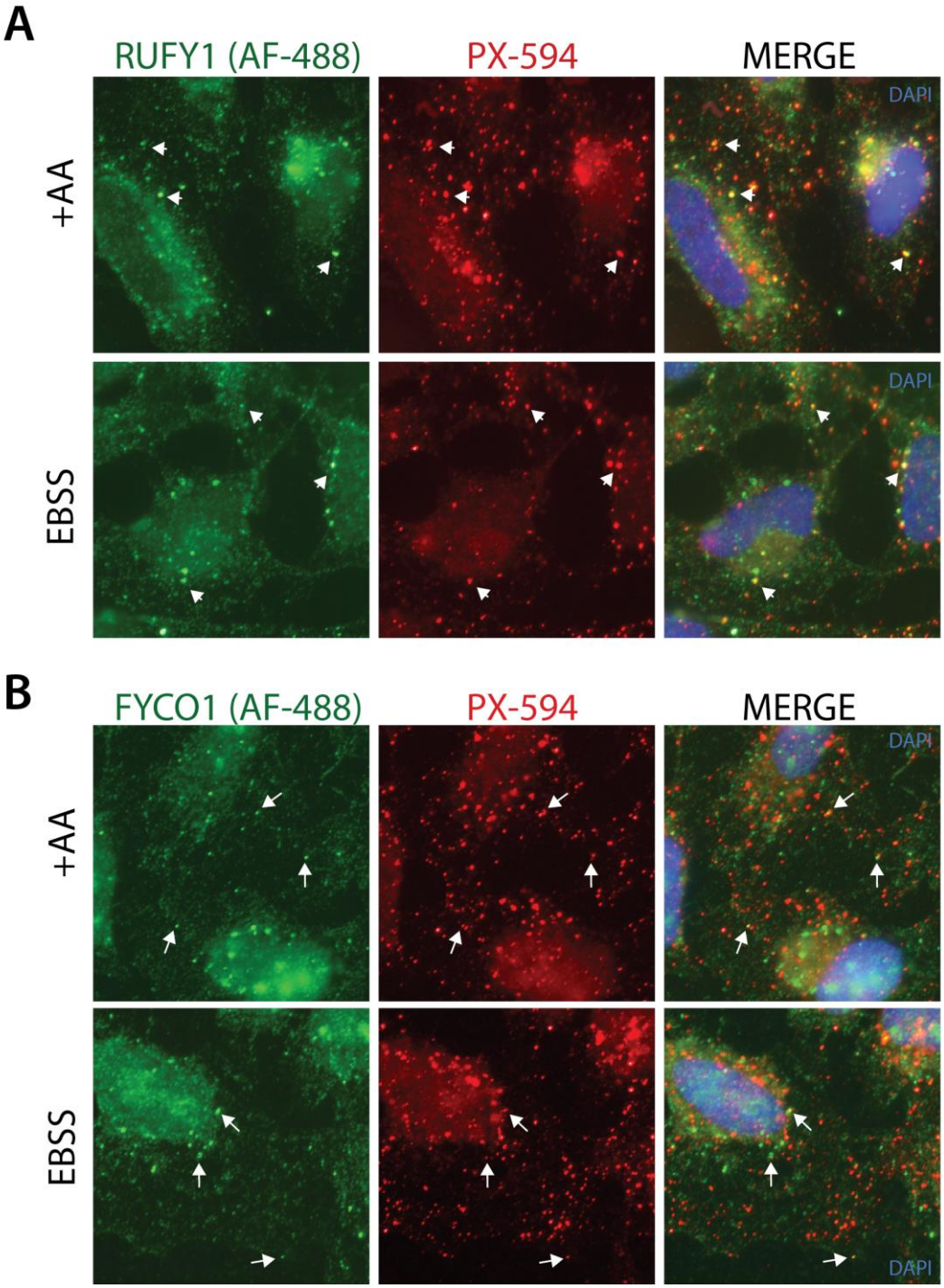

Figure 4.9 - PX Domain and RUFY1 and FYCO1

U2OS cells were incubated in complete media (+AA) or starvation media (EBSS) for 2 h and then fixed by freeze thaw. Cells were stained with PX-594 and **(A)** anti-RUFY1 or **(B)** anti-FYCO1 using AlexaFluor® 488 (AF-488) secondary antibody. Arrows represent examples of co-localisation.

It may appear counter-intuitive that cellular PI(3)P levels dropped upon nutrient starvation, particularly as nutrient starvation is a potent inducer of autophagy and that this is dependent upon VPS34 PI3K activity (Kihara, Noda, et al. 2001). The induction of autophagy and formation of PI(3)P at initial omegasome structures can be monitored by the translocation of the double-FYVE domain containing protein 1 (DFCP1) from the ER (Axe et al. 2008). U2OS cells expressing GFP-DFCP1 were utilised to examine the formation of DFCP1 puncta upon nutrient starvation (Figure 4.10). Upon autophagy induction either by nutrient starvation or mTOR inhibition, the level of punctate structures increased in number and in size (Figure 4.10) concomitantly with a decrease in global cellular PI(3)P levels (Figure 4.6C). Treatment with the PI3K inhibitor wortmannin prevented DFCP1 puncta forming, indicating this was dependent upon PI(3)P. Whilst global PI(3)P levels drop upon nutrient starvation, the staining of DFCP1 clearly demonstrates that the PI(3)P at autophagosomal structures increases.

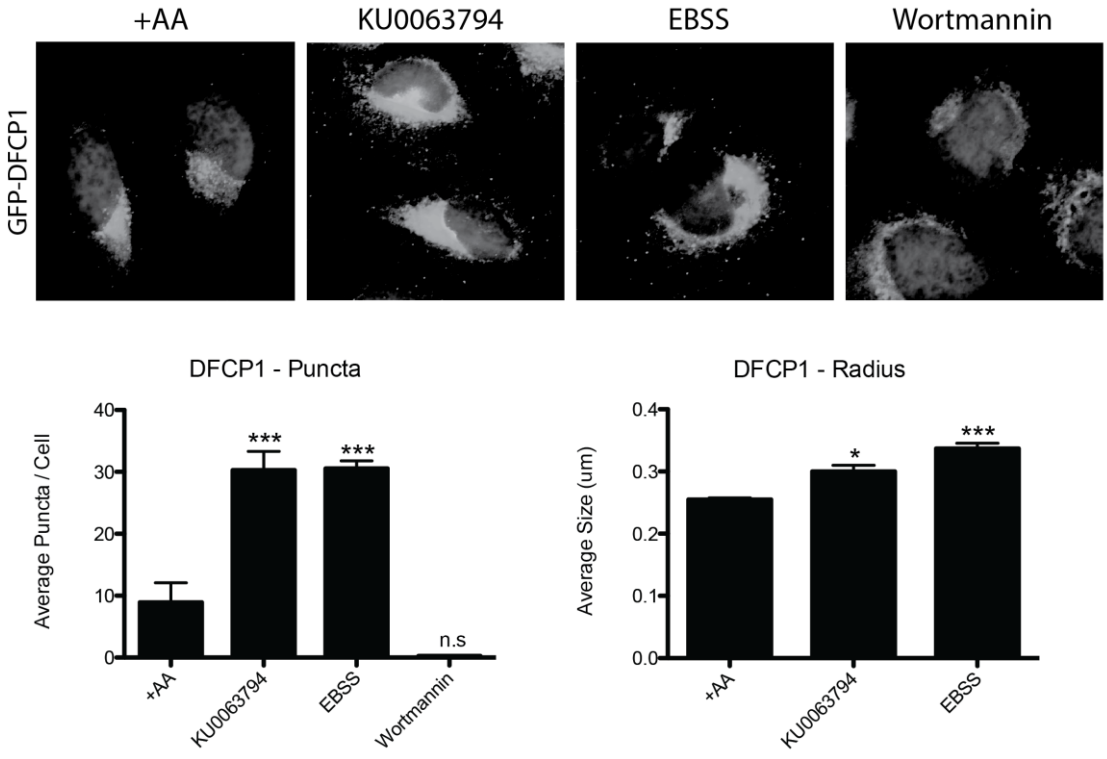

Figure 4.10 - DFCP1 Puncta Increase upon Autophagy Induction

(A) U2OS cells stably expressing GFP-DFCP1 were grown in complete media (+AA), starvation media (EBSS), treated with 1 µM KU0063794 or 10 µM Wortmannin for 2 h prior to formaldehyde fixation. **(B+C)** Graphs represent the mean **(A)** DFCP1 puncta per cell or **(B)** DFCP1 puncta radius ± SEM from n = 3 independent experiments. Statistics were carried out by one-way analysis of variance utilising Dunnett's post-test to compare to +AA control. * = $p < 0.05$, *** = $p < 0.001$, *n.s* = not significant.

4.2.4 Nutrient status governs cellular PI(3)P levels

To examine the role of UVRAG and its phosphorylation further, endogenous UVRAG was depleted by RNA interference (RNAi). Reverse transfection of MEFs with a previously reported siRNA targeting the protein coding region (ORF1) of UVRAG (Liang et al. 2006) caused a significant knockdown of UVRAG within 24h and a peak response at ~48 h (Figure 4.11A&B). Stable transfection of a shRNA targeted against the same region also significantly reduced endogenous UVRAG levels (Figure 4.11C). Other shRNA sequences generated against a separate protein coding region (ORF2) or 5' untranslated region (5'UTR) also caused knockdown of endogenous UVRAG but not as efficiently as ORF1 (Figure 4.11C).

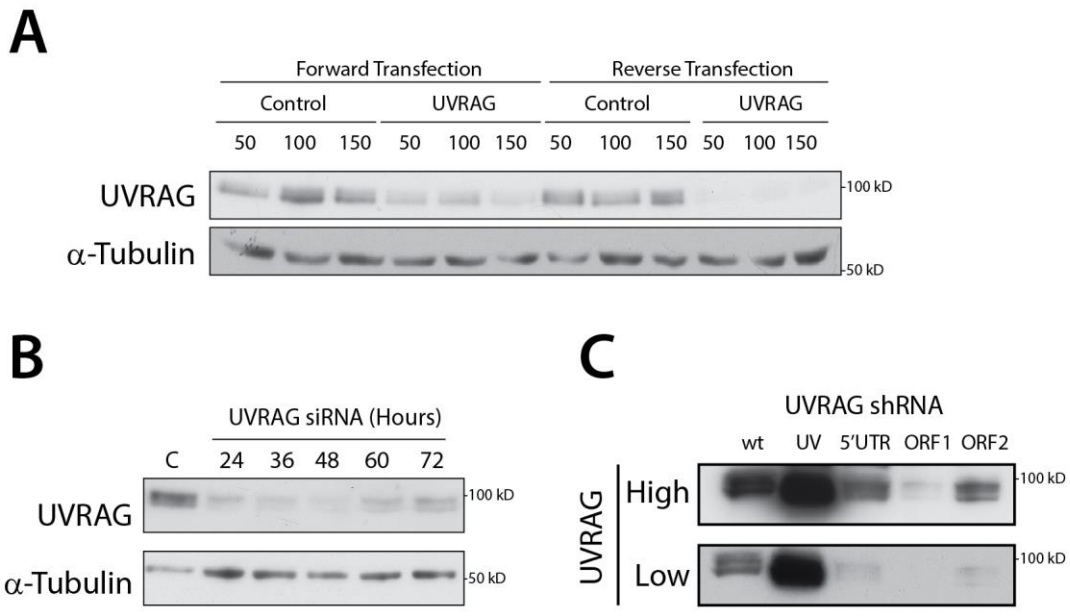

Figure 4.11 - UVRAG siRNA treatment

(A) Wild-type MEFs were transfected with 50-150 nM control or UVRAG ORF1 siRNA (Table 9) by either forward or reverse transfection and lysed and 36 hours post-transfection. **(B)** Wild-type MEFs were reverse transfected with 50 nM ORF1 siRNA and lysed at time-points indicated. **(C)** Wild-type MEFs were stably transfected by retrovirus with the shRNA indicated (Table 7), NT = non-transfected, UV = FLAG-UVRAG over-expression. High and Low refers to western blot exposure. **(A-C)** All samples were lysed in 0.5 % NP-40 lysis buffer.

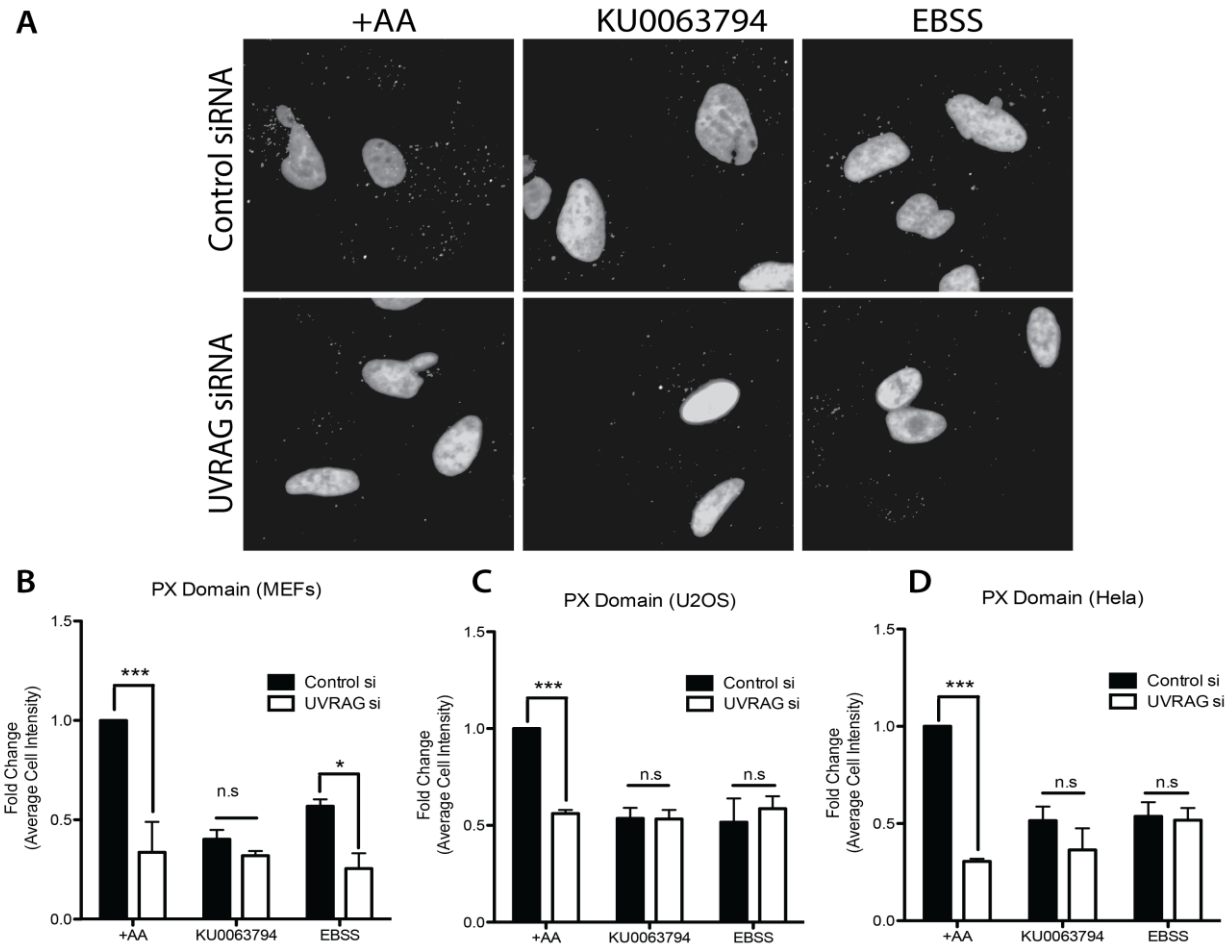

Figure 4.12 - Effect of UVRAG and nutrient status on cellular PI(3)P levels

(A) U2OS cells were transfected with 50 nM control or ORF1 siRNA (Table 9), 40 h post-transfection cells were incubated in complete media (+AA), starvation media (EBSS) or treated with 1 µM KU0063794 for 2 h and fixed by freeze-thaw before staining with PX-594. **(B-D)** Quantitation of experiment carried out as in (A) for **(B)** MEFs, **(C)** U2OS and **(D)** Hela. Bars represent mean fold change in PX Domain staining ± SEM of n=3 independent experiments. Statistical analysis was carried out by two-way analysis of variance with Bonferroni's post-test.

The total level of PX domain staining in U2OS, Hela and MEF cells was examined before and after endogenous UVRAG knockdown. In addition cells were examined between nutrient rich conditions, nutrient depletion or upon mTOR inhibition. Comparison of cell lines demonstrated that cellular PI(3)P levels were lower upon nutrient starvation or mTOR inhibition. In addition, knockdown of UVRAG resulted in lower cellular PI(3)P levels during nutrient rich conditions but equivalent to control siRNA upon nutrient starvation or mTOR inhibition (Figure 4.12). The level of cellular PI(3)P therefore correlates with UVRAG phosphorylation state between cell lines and UVRAG is required for the stimulation seen under nutrient rich conditions. MEFs stably expressing siRNA resistant GFP-UVRAG wild-type or S550A+S571A were next examined to determine whether the nutrient stimulated VPS34 activity was dependent upon UVRAG phosphorylation sites. During nutrient rich conditions, knockdown of UVRAG reduced cellular PI(3)P levels similar to that observed during starvation; expression of GFP-UVRAG wild-type was able to rescue this phenotype whilst GFP-UVRAG S550A+S571A did not (Figure 4.13). The levels of PI(3)P were consistent upon nutrient starvation or mTOR inhibition regardless of UVRAG expression.

This data strongly implicates the importance of phosphorylation at S550 + S571 as critical regulatory sites by mTOR. Phosphorylation at these residues has been demonstrated to increase the VPS34-UVRAG complex activity *in vitro* and also causes a detectable change in cellular PI(3)P levels. Having observed significant changes in the levels of PI(3)P, the precise role of this in cellular function remains to be elucidated.

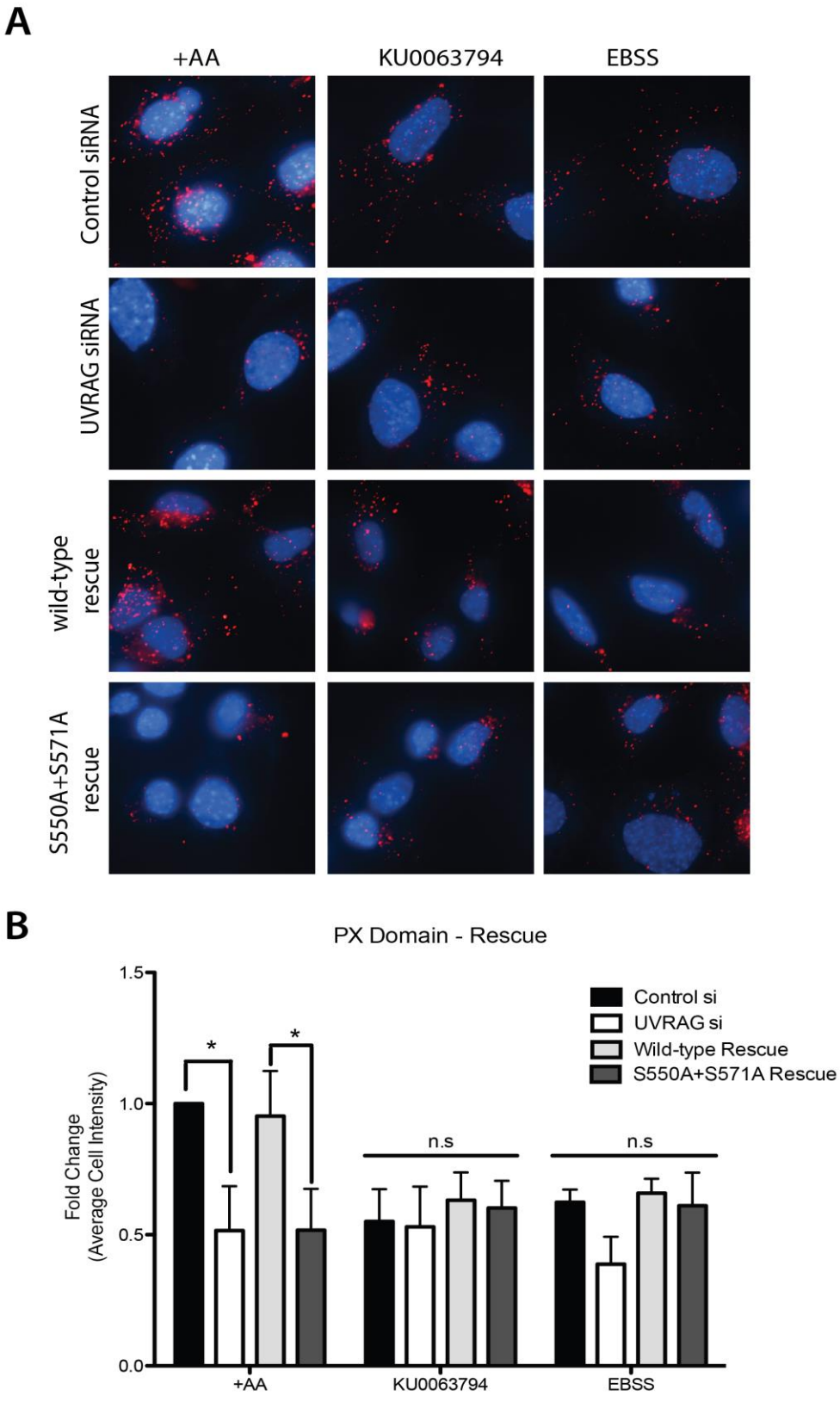

Figure 4.13 – Effect of UVRAG S550A+S571A Upon Cellular PI(3)P

(A) Wild-type MEFS or those stably expressing siRNA resistant GFP-UVRAG wild-type or S550A+S571A were reverse transfected with 100 nM control or ORF1 siRNA. 40 h post-transfection, cells were incubated in complete media (+AA), starvation media (EBSS) or treated with 1 µM KU0063794 for 1 h, fixed by freeze-thaw and stained with PX-594. **(B)** Quantitation of (A), bars represent mean fold change of PX Domain staining ± SEM of n=4 independent experiments. Statistical analysis was carried out using two-way analysis of variance and Bonferonni's post-test where * = $p < 0.05$ and n.s = not significant.

4.3 Discussion

The data presented in this chapter for the first time demonstrate that the phosphorylation of UVRAG directly impacts upon intrinsic VPS34 lipid kinase activity. Furthermore, modulation of VPS34 activity by phosphorylation of UVRAG results in a significant global cellular change in PI(3)P level that may consequently alter cellular function.

Direct examination of endogenous UVRAG-BECLIN1-VPS34 complex activity *in vitro* demonstrates a decrease in activity upon nutrient starvation (Figure 4.1A&B). A reduction in VPS34 activity of ~2.5 fold *in vitro* has previously been observed upon IP of VPS34 or BECLIN1 during amino acid starvation (Byfield et al. 2005; Russell et al. 2013). Analysis of VPS34 or BECLIN1 will likely contain multiple sub-complexes and the proportion of this that is UVRAG-BECLIN1-VPS34 is unclear. A previous report has suggested that ~50 % of VPS34 is bound to BECLIN1 and that UVRAG will likely represent a smaller proportion (Kihara, Kabeya, et al. 2001). In contrast, IP of BECLIN1 co-purified with equivalent stoichiometry of VPS15, VPS34 and UVRAG suggesting a stable 'core' VPS34-BECLIN1-UVRAG complex, whereas levels of ATG14L and Rubicon were lower (Zhong et al. 2009). Given that VPS34, BECLIN1 or UVRAG IP all demonstrate a comparable decrease in activity upon nutrient deprivation it would be expected that this occurs via regulation of a common component. Indeed an analogous situation is present whereby phosphorylation of VPS34 by AMPK has been reported to decrease activity upon glucose starvation (Kim et al. 2013). Binding of ATG14L however prevented inhibitory VPS34 phosphorylation by AMPK but the effect upon UVRAG containing complexes was not fully examined. The increased activity of UVRAG-BECLIN1-VPS34 during nutrient rich conditions was directly dependent upon UVRAG S550 and S571 phosphorylation as mutation to alanine residues abolished this activity (Figure 4.3).

It seems counter-intuitive that the PI(3)P levels decrease upon nutrient starvation due to the requirement of VPS34 activity for autophagy induction (Petiot et al. 2000). Multiple VPS34 complexes are present in the cell and it is the ATG14L containing complex that has primarily

been implicated in autophagy induction (Kihara, Noda, et al. 2001). Importantly, the ATG14L complex is present at a much lower level than the UVRAG complex, estimates from yeast suggest ATG14L is expressed ~15 fold less than BECLIN1 (Kihara, Noda, et al. 2001). The contribution of PI(3)P from ATG14L containing complexes will therefore be a relatively small proportion of total cellular PI(3)P. Indeed analysis of DFCP1 translocation to the omegasome demonstrated a dramatic increase upon autophagy induction indicating that the autophagy specific pool of PI(3)P was increased (Figure 4.10). ATG14L complex activity did not change upon mTOR inhibition, suggesting that the regulatory mechanism that reduces VPS34 activity upon starvation is not present in this complex (Figure 4.1C). An earlier report has suggested that ATG14L-BECLIN1-VPS34 activity is negatively regulated by mTORC1 kinase activity (Yuan et al. 2013). The examination of ATG14L complex activity in this current study utilises exogenous mCherry-S-ATG14L that may reduce phosphorylation stoichiometry and mask regulatory changes. It is worth noting however that *in vitro* kinase reactions of endogenous mTORC1 with ATG14L carried out in this study did not demonstrate strong phosphorylation (Figure 3.3). Regulation of ATG14L complex activity may not be essential to induce autophagy, rather it is suggested that the localisation of the complex to sites of autophagosome formation is critical for autophagosome generation (Fan et al. 2011; Sun et al. 2008). Data shown in (Figure 3.9) demonstrates a change in the ATG14L elution pattern by SEC upon autophagy induction, which may resemble an important regulatory change to allow a very localised pool of PI(3)P generation.

Precisely how the phosphorylation in a separate component of the VPS34 complex can directly affect the lipid kinase activity is intriguing. Assuming the lack of additional protein interactions, it is possible to speculate that introduction of two negative residues causes a global 3D structural change in UVRAG and possibly the whole complex. Site-specific phosphorylation of disordered protein regions has been shown to impact upon secondary and tertiary structure (Garza et al. 2010). Indeed, phosphorylation of S550 and S571 cause large mobility shifts in the native protein by SDS-PAGE that may be in part due to structural changes. Introducing a global structural

change in the VPS34 complex may act to improve lipid substrate or ATP binding, which subsequently improves kinase efficiency. Another possibility could be the manipulation of RUBICON binding. RUBICON binds to the VPS34 complex by extensive contacts with UVRAG and also interacts with VPS34 through a RUN domain to negatively regulate kinase activity (Sun et al. 2010; Zhong et al. 2009). The introduction of negatively charged residues onto UVRAG by phosphorylation could potentially disrupt RUN domain interactions with VPS34 without displacing RUBICON from the complex. Interestingly, RUBICON binding reduces UVRAG complex activity to ~25 % (Sun et al. 2010). Expression of a ΔRUN RUBICON mutant that cannot interact with VPS34 alleviates UVRAG inhibition to ~50 %, a two-fold change that is similar to the observed mTOR phosphorylation induced activity change (Sun et al. 2010). Furthermore, RUBICON has no apparent ancestral homologue in *S. cerevisiae* (Matsunaga et al. 2009) and similarly the unstructured C-terminal domain of UVRAG is absent from the *S. cerevisiae* homolog *vps38.* Use of UVRAG biotin peptides did not show selectivity for peptide sequence, however it clearly demonstrated the binding affinity and preference of proteins for negatively charged peptides (Figure 4.4C). The phosphorylation of S550 and S571 could thereby represent an evolved mechanism to alleviate RUBICON mediated inhibition via the RUN domain, subsequently increasing VPS34 kinase activity. This could allow rapid regulatory changes in VPS34 activity without the requirement for displacement of RUBICON from the complex, allowing further fine tuning of VPS34 complex activity. Critically, the molecular mechanism of S550 and S571 phosphorylation is entirely speculative without further understanding of the VPS34 complex. Crystal structure determination will be key to identifying how components interact and predicting possible C-terminal domain interactions of UVRAG.

Attempts to reconstitute the reaction *in vitro* were unsuccessful through the inability to form a complete complex (Figure 4.4A&B). It is possible that efficient formation may require co-expression or that the combination of tags result in steric hindrance that prevents efficient binding, particularly due to larger tags such as GST or MFP. Purification of recombinant proteins

expressing small (FLAG, V5) or cleavable (TEV, Prescission) tags would likely improve the ability to efficiently form complexes.

Changes in VPS34 complex activity *in vitro* clearly correlated with cellular PI(3)P levels. Examination of GFP2xFYVE expression demonstrated that not all PI(3)P positive structures were being labelled efficiently in comparison with PX-594 (Figure 4.6). PX-594 co-localised with multiple known PI(3)P effectors and also demonstrated a drop in overall intensity upon nutrient starvation. Previous work has also shown that PI(3)P drops upon amino acid starvation with a GST-2xFYVE domain or PI(3)P antibody (Nobukuni et al. 2005; Yuan et al. 2013). The use of PI(3)P detecting 2xFYVE or PX domains still has limitations; not all cellular PI(3)P will be labelled via this method as some will be occluded from recognition and interacting due to binding of endogenous PI(3)P effector proteins. Analysis of the whole cell lipid composition by mass spectrometry would allow the total level of phosphoinositide species relative to one another to be observed. The loss of PI(3)P can potentially have knock-on consequences by impeding the sequential conversion to $PI(3,5)P_2$ that is catalysed by PIK_{FYVE} (Sbrissa et al. 1999; Ikonomov et al. 2001). Analysis of multiple phosphoinositide species would allow greater understanding of how each is regulated in response to nutrient starvation. Alternately, the level of $PI(3,5)P_2$ could be examined by use of mucolipin1 that specifically recognises and binds this phospholipid (Dong et al. 2010).

Depletion of UVRAG causes a decrease in cellular PI(3)P (Figure 4.12), which is perhaps not surprising considering that the binding of UVRAG to VPS34 and BECLIN1 in mammalian cells is reported to increase lipid kinase activity by ~2-4 fold (Liang et al. 2006; Sun et al. 2010). It is surprising however that this is equivalent to the level of PI(3)P observed upon nutrient starvation in cells containing UVRAG, suggesting that under these conditions the presence and binding of UVRAG does not alter PI(3)P formation. In yeast the impact of vps38/UVRAG is more modest, suggesting ~20 % increase in vps34 activity upon binding (Kihara, Noda, et al. 2001). Importantly the stimulation of VPS34 activity observed requires UVRAG and its phosphorylation as mutation of S550 and S571 to alanine blocks the activity increase in the presence of nutrients.

Therefore the phosphorylation of UVRAG drives an increase in VPS34 activity that occurs independently of other complex components. The phosphorylation may cause a structural rearrangement that leads to an increase in lipid kinase activity and significant cellular changes in phospholipid composition. The precise consequences of phosphorylation need to be further examined to understand the role it plays in trafficking. Given the requirement of PI(3)P in trafficking processes, it could be assumed that higher levels of PI(3)P may assist or improve trafficking in the presence of nutrients. The cellular response to alterations in PI(3)P is therefore further examined in the following chapter.

5 FUNCTIONAL CONSEQUENCES OF UVRAG PHOSPHORYLATION

5.1 Introduction

As shown in previous chapters phosphorylation of UVRAG by mTOR caused an increase in VPS34 activity and raised cellular PI(3)P levels (Figure 4.13). To determine possible functional consequences of this regulatory event requires analysis of PI(3)P and UVRAG dependent pathways.

The importance of PI(3)P within cells has predominantly been linked to endocytosis, with multiple stages that are regulated by PI(3)P formation. The production of PI(3)P at early endosomal structures for example plays a key role in recruiting the FYVE domain containing protein EEA1 (Simonsen et al. 1998), EEA1 then acts as a tether to assist with endosome fusion (Christoforidis et al. 1999). VPS34 has also been linked to the formation of intraluminal vesicles (ILVs) that define late endosomes or multi-vesicular bodies (MVBs). The formation of ILVs occurs in a PI(3)P dependent manner and it is thought to be a key regulatory step In defining whether receptors are to be degraded or recycled back to the plasma membrane (Futter et al. 2001). The formation of PI(3)P is also essential as a substrate for PIK_{FYVE} to produce $PI(3,5)P_2$ that is also required for efficient endosome maturation (Jefferies et al. 2008). Aside from endocytosis, VPS34 mediated formation of PI(3)P is also required for the induction of autophagy. The formation of PI(3)P at omegasome sites recruits the FYVE domain containing proteins DFCP1 and WIPI1 and leads to autophagosome formation (Polson et al. 2010). The ATG14L-VPS34 complex is essential for autophagosome formation (Matsunaga et al. 2010), although previous data has suggested that UVRAG may also enhance autophagy induction (Liang et al. 2006).

Given the requirement of PI(3)P for trafficking pathways, it is possible that stimulation of VPS34 by mTOR enhances a distinct pathway or multiple pathways in a manner that assists with cellular function. Several assays of intracellular trafficking were therefore undertaken to determine whether the increase in PI(3)P relates functionally to differences in a pathway.

5.2 Results

5.2.1 Autophagy Induction is unaffected by UVRAG phosphorylation

To examine the function of UVRAG phosphorylation, cells stably expressing GFP-UVRAG wild-type or S550A+S571A were utilised for analysis following depletion of the endogenous protein by RNAi. Whilst primarily the ATG14L containing complex has been linked with autophagy induction, UVRAG has also been implicated in assisting with autophagosome formation and maturation through binding to Bif-1 and mediating fusion of formed autophagosomes with the lysosome (Liang et al. 2006; Liang et al. 2008). Due to the requirement of mTOR activity for phosphorylation at UVRAG S550 and S571, mutation of these residues to alanine should have no effect during an autophagic response as mTOR is inhibited. During nutrient rich conditions UVRAG is phosphorylated and this may affect the rate of basal autophagic flux. Induction of autophagy in MEFs either by mTOR inhibition or by nutrient depletion was noted by an increase in the level of LC3-II formation. Upon comparison to MEFs expressing either of two unique shRNA constructs, no significant difference in the level of LC3-II was observed (Figure 5.1A-D). Expression of GFP-UVRAG wild-type or S550A+S571A did not demonstrate any significant difference with control cells, suggesting that neither UVRAG nor the phosphorylation state impacted upon the induction of autophagy (Figure 5.1E-G). Addition of the lysosomal inhibitor Bafilomycin A1 between cell lines triggered an equivalent increase in LC3-II levels upon depletion of UVRAG, this indicated that LC3-II was constantly being degraded via the lysosome and that autophagosome fusion with lysosomes was not impaired (Figure 5.1).

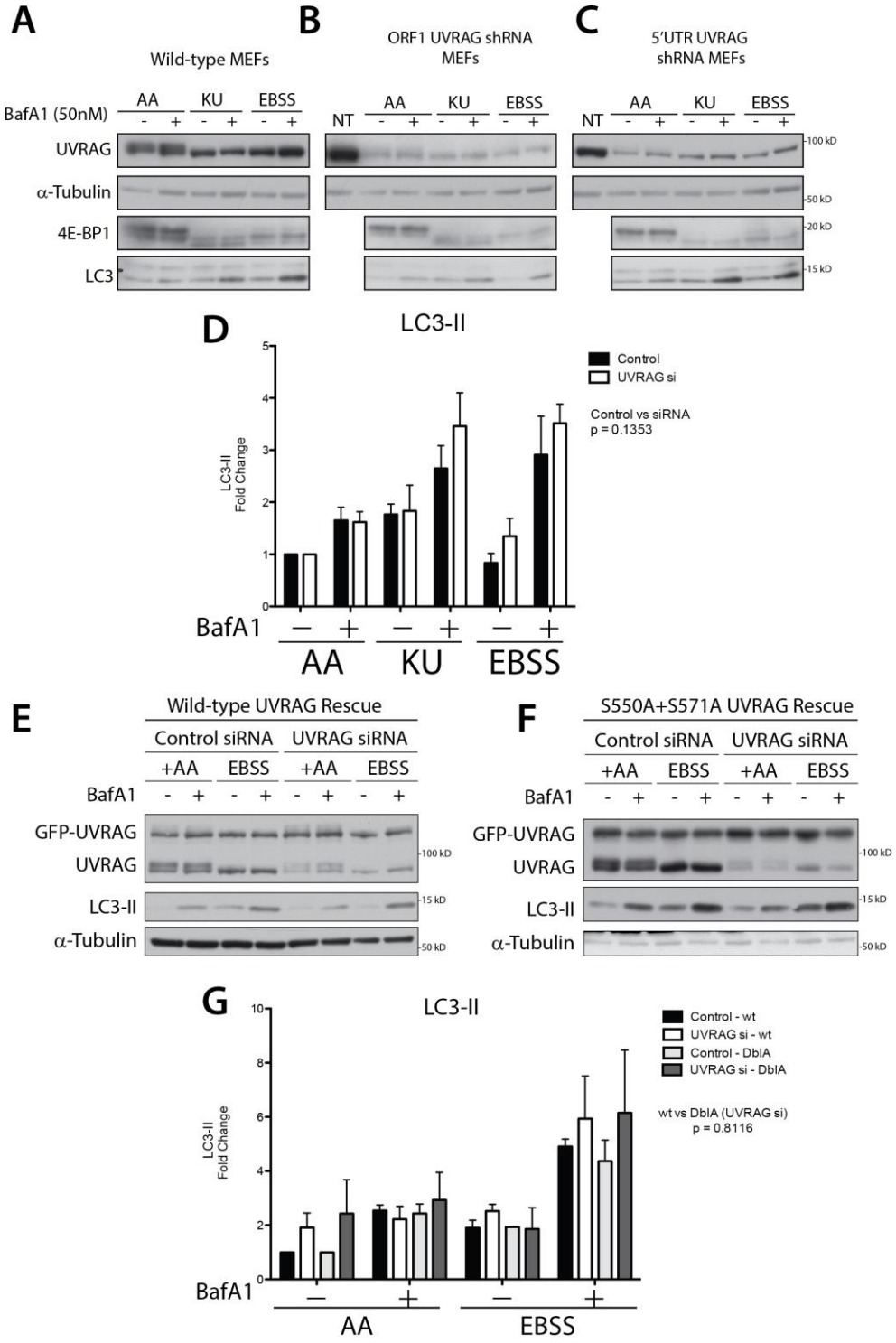

Figure 5.1 - LC3 Flux is unaffected by UVRAG phosphorylation

(A) Wild-type MEFS or those stably expressing **(B)** ORF1 shRNA or **(C)** 5'UTR shRNA (Table 9) were grown in complete media (+AA), starvation media (EBSS) or treated with 1 µM KU0063794 (KU) for 1 h in the presence or absence of 50 nM Bafilomycin A1 (BafA1). NT denotes non-transfected cells. **(D)** Quantitation of A-C where bars represent mean normalised LC3-II values ± SEM of n = 4 independent experiments. MEFs stably expressing siRNA resistant GFP-UVRAG **(E)** wild-type or **(F)** S550A+S571A were reverse transfected with 100 nM control or ORF1 UVRAG siRNA (Table 9). Cells were grown in complete media (+AA) or starvation media (EBSS) for 1 h in the absence or presence of 50 nM Bafilomycin A1 (BafA1). **(G)** Quantitation of E&F where bars represent mean normalised LC3-II values ± SEM of n = 3 independent experiments. Bafilomycin addition is represented by (-) or (+) **(A-F)** All samples were lysed in 0.5 % NP-40 lysis buffer. **(D+G)** Statistics were calculated by two-way analysis of variance and the p-value for each is shown. wt = wild-type, DblA = S550A+S571A

5.2.2 EGFR Degradation is unaffected by UVRAG phosphorylation

The requirement of UVRAG for the trafficking and degradation of the epidermal growth factor receptor (EGFR) was next examined. The EGFR is present at the cell surface where binding of epidermal growth factor (EGF) causes EGFR dimerisation and activation of intrinsic tyrosine kinase activity (Schlessinger 1988). Autophosphorylation of the cytoplasmic C-terminal domain allows binding of downstream effectors to convey growth factor signalling (Lowenstein et al. 1992). Constitutive EGFR signalling by pathway mutations or upregulation plays a pivotal role in cell transformation and progression of multiple carcinomas, it is therefore essential that cells are able to terminate signalling efficiently (Wells et al. 1990). EGFRs are primarily internalised via clathrin mediated endocytosis (CME) but also by non-clathrin endocytosis (NCE) and are trafficked to the lysosome for degradation (Sigismund et al. 2008). The rate of EGFR degradation is commonly used as a marker for analysing the rate of endocytosis as a difference at a single step in the process can cause a measurable change in degradation via the lysosome.

The level of EGFR expression was examined between MEFs, Hela and U2OS cells following differing periods of serum starvation. Serum starvation causes EGFRs to accumulate at the plasma membrane, which is essential to bind EGF. Hela cells displayed very high levels of EGFR in comparison to MEFs or U2OS. The levels of EGFR decreased in U2OS following serum starvation and thus they were not used for further analysis as the protein level was too low to monitor (Figure 5.2A). To examine the rate of EGFR endocytosis and degradation the growth media on cells was changed following serum starvation to complete media including EGF and cycloheximide to inhibit protein translation of further EGFRs (Ennis & Lubin 1964). Additionally the selective mTOR inhibitor KU0063794 was included to assess the impact of mTOR activity upon EGFR degradation. Within two hours ~80 % of the total EGFR pool was degraded in MEFs, however, no significant difference was observed upon inhibition of mTOR activity and subsequently UVRAG phosphorylation (Figure 5.2B). The role of UVRAG in EGFR degradation was examined further by depletion of endogenous UVRAG in MEFs by RNAi.

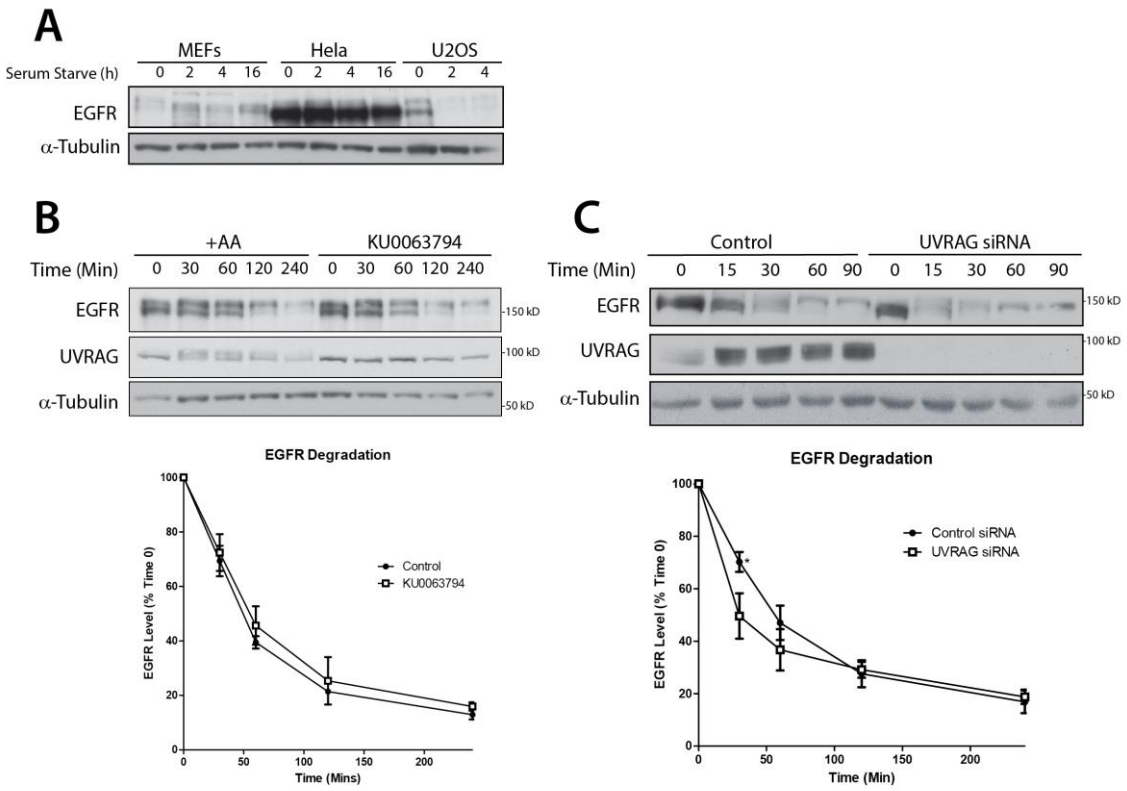

Figure 5.2 - EGFR Degradation with mTOR inhibition and UVRAG depletion

(A) MEFs, Hela and U2OS cells were serum starved for the times indicated in serum starve media. **(B)** MEFs were serum starved for 2 h prior to addition of 50 ng/ml EGF and 30 µg/ml cycloheximide with or without 1 µM KU0063794 in complete media. **(C)** MEFs were reverse transfected with 50 nM control or ORF1 UVRAG siRNA. At ~40 h post-transfection cells were serum starved for 2 h prior to addition of 50 ng/ml EGF and 30 µg/ml cycloheximide in complete media. **(A-C)** All samples were lysed in 0.5 % NP-40 lysis buffer at time-points indicated. Graphs represent the EGFR protein level normalised to α-tubulin and subsequently plotted as a percentage of time 0 h EGFR ± SEM of n = 3 independent experiments. Statistics were determined by Student's t-test comparing each time-point between treatments where * = $p < 0.05$.

Targeting of UVRAG by siRNA demonstrated a modest increase in rate of degradation at earlier time-points and was significantly different at 30 minutes (Figure 5.2C). This is in contrast to previously published data (Liang et al. 2008; Thoresen et al. 2010 - see discussion). Use of an mTOR inhibitor will affect a multitude of downstream targets that could also impact upon trafficking functions and lead to opposing effects. MEFs expressing siRNA resistant GFP-UVRAG wild-type or S550A+571A were utilised to examine possible differences due to UVRAG phosphorylation specifically. No significant change was observed in MEFs when rescued with the S550A+S571A mutant in comparison to GFP-UVRAG wild-type (Figure 5.3A). Examination of Hela cells displayed significantly faster degradation with S550A+S571A at 60 minutes compared

to control siRNA cells. These findings however were not significant in comparison to the wild-type rescue (Figure 5.3B). The use of the mTOR inhibitor KU0063794 is further demonstrated to have no effect upon EGFR degradation upon treatment of UVRAG wild-type or S550A+S571A rescue cells (Figure 5.3C). The protein expression level of EGFR did not demonstrate any significant changes dependent upon UVRAG status (Figure 5.3D).

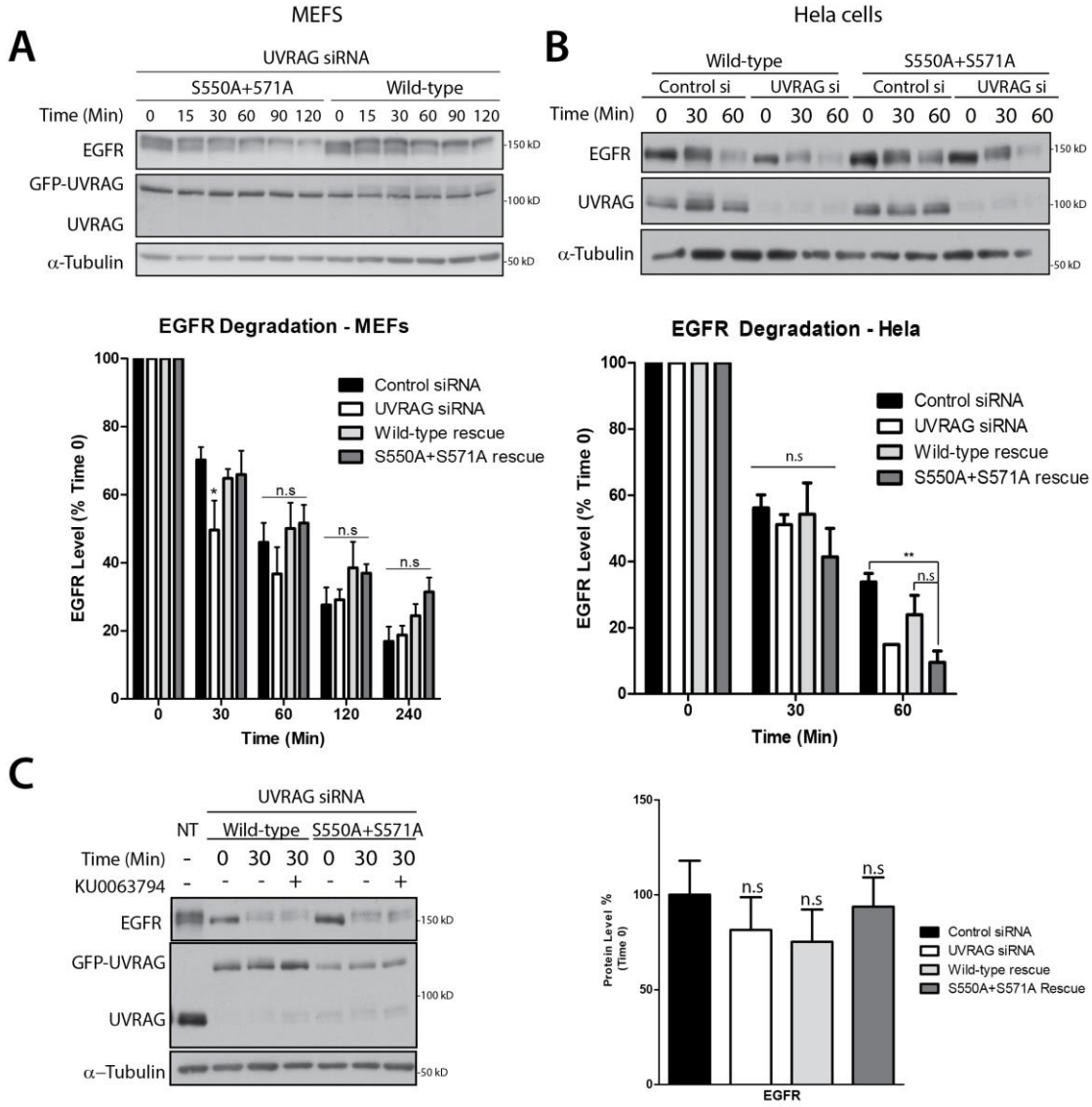

Figure 5.3 - EGFR Degradation is unaffected by UVRAG S550A+S571A

(A-C) GFP-UVRAG wild-type or S550A+S571A were stably expressed in **(A)** MEFs or **(B+C)** Hela cells, NT = Non-transfected. All cells were reverse transfected with 100 nM UVRAG ORF1 siRNA or control siRNA where indicated and utilised for experiments at ~40 h post-transfection. Cells were serum starved for 2 h in serum starvation media. At time 0 cell media was changed to complete media including 50 ng/ml EGF, 30 µg/ml cycloheximide and 1 µM KU0063794 (where indicated). Cells were lysed in 0.5 % NP-40 lysis buffer at each time-point. **(A+B)** Graphs represent mean EGFR level normalised to α-tubulin and plotted as a percentage of time 0 ± SEM for n = 3 independent experiments. **(D)** Quantitation of EGFR levels in Hela cells from (B+C), bars represent mean EGFR level at time 0 relative to control siRNA ± SEM of n = 3 independent experiments.

5.2.3 Transferrin Recycling is unaffected by UVRAG phosphorylation

Uptake of the EGFR does not exclusively lead to degradation as differing levels of EGFR recycling also occurs dependent upon stimulatory conditions (Sigismund et al. 2005), it is important to examine whether the recycling pathway is affected. Transferrin receptors (TR) are exclusively internalised by CME and are almost entirely returned to the plasma membrane via Rab4 and Rab11 recycling endosomes, the trafficking of transferrin can be utilised to examine the recycling pathway (Daro et al. 1996; Ullrich et al. 1996). The transferrin receptor assists with cellular iron uptake by binding the iron storage protein transferrin, upon trafficking to the early endosome iron is released due to the decrease in pH; the receptor and transferrin is then recycled to the plasma membrane to repeat this process (Dautry-Varsat et al. 1983).

To examine the rate of TR recycling, Hela and U2OS cells were incubated in the presence of fluorescently conjugated transferrin to allow cellular uptake and distribution throughout the recycling pathway. Cells were then washed to remove excess transferrin and the rate of TR recycling was monitored in the presence or absence of the mTOR inhibitor KU0063794 (Figure 5.4A&B). The loss of cell fluorescence represented the release of transferrin following successful TR recycling to the surface, re-uptake was reduced due to competition from high concentrations of non-fluorescent transferrin. UVRAG phosphorylation was inhibited upon addition of KU0063794 but no difference was observed in the rate of TR recycling in either Hela or U2OS cells, though the rate between cell lines was notably different (Figure 5.4C&D). MEFs stably expressing GFP-UVRAG wild-type or S550A+S571A were utilised to examine whether UVRAG phosphorylation specifically altered the rate of TR recycling. Within 30 minutes ~60 % of transferrin had been recycled in control MEFs. Depletion of endogenous UVRAG resulted in cells containing higher levels of fluorescent transferrin at time 0 (Figure 5.5A&C), suggestive of either higher rates of uptake or reduced recycling. Immunoblotting indicated that the level of transferrin receptor was increased upon treatment with UVRAG siRNA, particularly in cells lacking GFP-UVRAG rescue (Figure 5.5B). Normalisation of average cell intensity to TR protein

expression level demonstrated that the accumulation of fluorescent transferrin was proportional to receptor level, except for non-rescue UVRAG siRNA cells. Despite higher TR expression level the uptake and turnover rate was slower in UVRAG depleted cells. Control siRNA cells exhibited faster recycling than rescue cells, although crucially there was no difference between the wild-type or S550A+S571A mutant. This indicates that UVRAG is required for transferrin receptor recycling but that this is not dependent upon phosphorylation status.

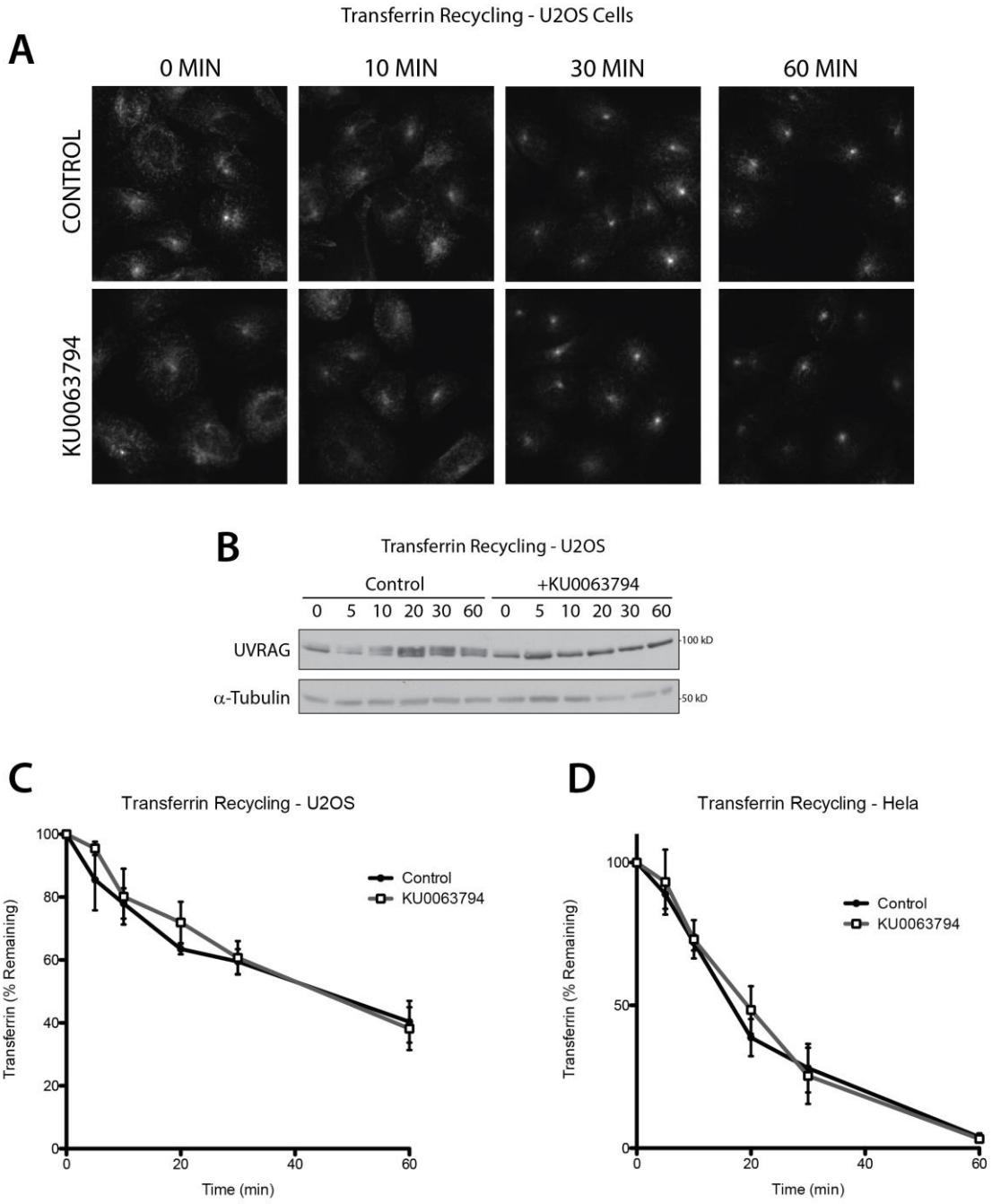

Figure 5.4 - Transferrin Recycling is unaffected by mTOR inhibition

(A) U2OS cells were incubated with 5 µg/ml Transferrin-594 conjugate for 1 h in complete media. Cells were washed and incubated in complete media with 100 µg/ml transferrin and 1 µM KU0063794 where indicated. Cells were formaldehyde fixed at noted time-points and average cell fluorescence was determined. **(B)** U2OS cells were treated as in (A), lysed in 0.5 % NP-40 lysis buffer and immunoblotted as indicated. **(C&D)** Quantitation of experiment as in (A) with **(C)** U2OS or **(D)** Hela cells. Points represent average cell fluorescence normalised to time 0 ± SEM of n = 3 independent experiments.

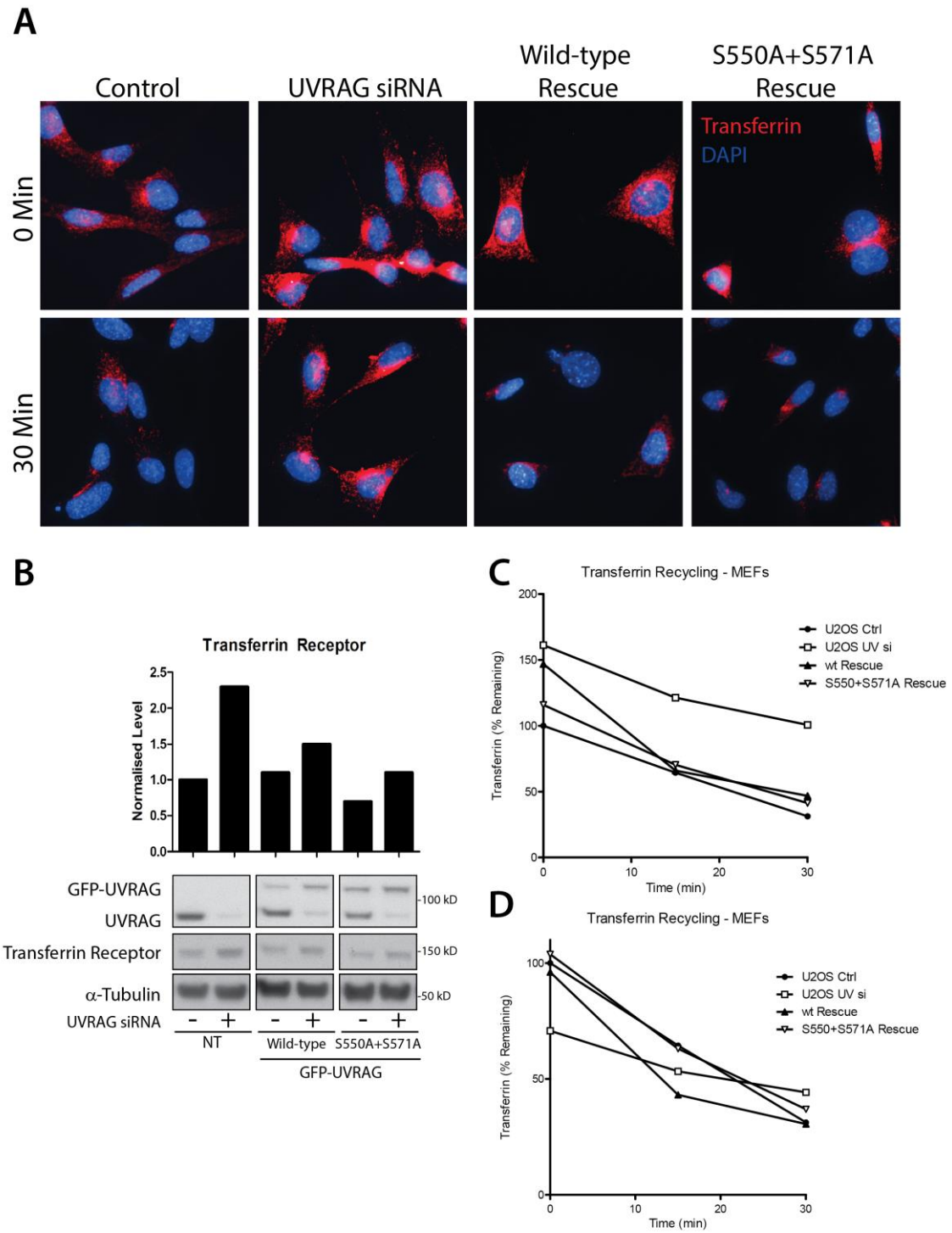

Figure 5.5 - Transferrin Recycling is unaffected by UVRAG S550A+S571A

(A) MEFs or those stably expressing GFP-UVRAG wild-type or S550A+S571A were reverse transfected with 100 nM ORF1 siRNA. ~40 h post-transfection cells were incubated with 5 µg/ml Transferrin-594 conjugate for 1 h. Cells were washed and incubated in complete media with 100 µg/ml transferrin and formaldehyde fixed at time 0 or 30 min. **(B)** MEFs transfected as in (A) were lysed in 0.5 % NP-40 lysis buffer and immunoblotted as indicated. **(C)** Quantitation of (A), points represent average cell intensity normalised to time 0. **(D)** Quantitation of (A) following normalisation of average cellular intensity relative to transferrin receptor expression in (B).

5.2.4 Comparison of PI(3)P binding proteins

Mutation of UVRAG S550A+S571A caused a ~2 fold decrease in cellular PI(3)P during nutrient rich conditions (Figure 4.13), yet no striking phenotype in the rate of EGFR or TR trafficking was observed (Figure 5.2 to Figure 5.5). To query possible effects of PI(3)P loss, multiple interacting proteins from distinct cellular compartments were examined. U2OS cells were fractionated to examine the distribution of proteins between cytosol and membranes during nutrient rich conditions (high PI(3)P) or upon nutrient depletion or mTOR inhibition (low PI(3)P) (Figure 4.6). FYVE domain containing proteins from the early endosome (EEA1 – Rab5 interacting), recycling endosome (RUFY1 – Rab4/11 interacting), late endosome (FYCO1 – Rab7 interacting) or the PX domain containing protein (SNX1 – EGFR and multiple endosomal compartment interacting) all selectively bind PI(3)P and it is a requirement for their membrane localisation (Pankiv et al. 2010; Simonsen et al. 1998; Yamamoto et al. 2010; Zhong et al. 2002). Treatment with the PI3K inhibitor wortmannin blocked PI(3)P formation and consequently abolished membrane binding of EEA1, RUFY1, FYCO1 and SNX1 (Figure 5.6A&B). Reduction of PI(3)P by nutrient depletion or mTOR inhibition in comparison demonstrated no significant change in membrane binding of these proteins.(Figure 5.6A&B) . Analysis of RUFY1, FYCO1 and SNX1 by immunofluorescence did not display any reduction in puncta formation upon nutrient depletion and in some cases was possibly higher (Figure 5.6C), EEA1 was demonstrated previously (Figure 4.7). The reduction in PI(3)P upon nutrient depletion therefore does not impair the binding of these endocytosis markers nor does it significantly alter the rate of receptor trafficking (5.2.2, 5.2.3).

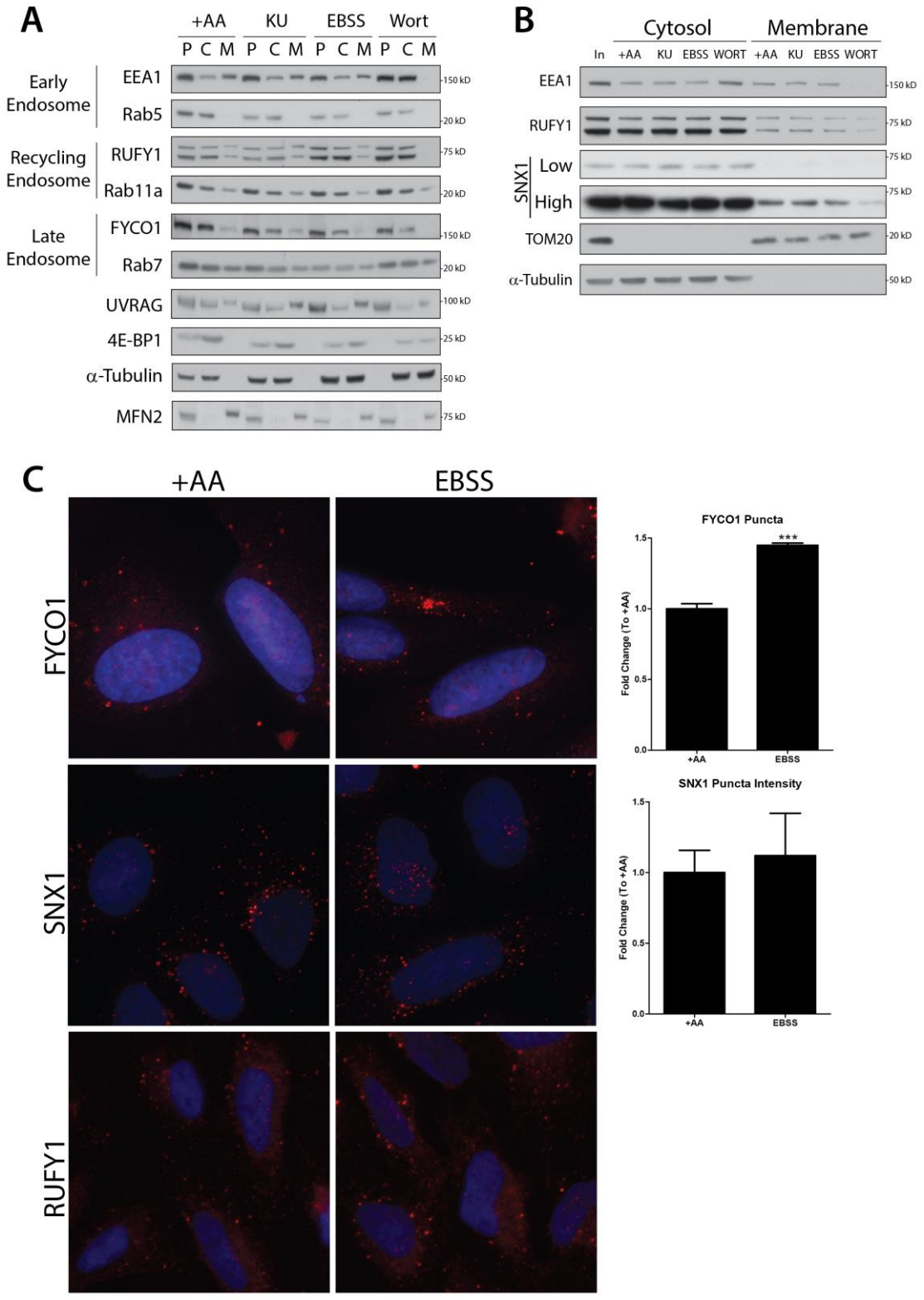

Figure 5.6 - Membrane Binding of PI(3)P Interacting Proteins

(A+B) U2OS cells were grown in complete media (+AA), starvation media (EBSS), treated with 1 µM KU0063794 (KU) or treated with 10 µM Wortmannin (Wort) for 2 h. Cells were homogenised in membrane fractionation buffer and the post-nuclear supernatant (P) underwent ultracentrifugation to split into cytosolic (C) and membrane (M) fractions. **(C)** U2OS cells were grown in complete media (+AA) or starvation media (EBSS) and formaldehyde fixed. Cells were stained as indicated utilising Alexa Fluor®-594 secondary antibody.

5.2.5 Examination of additional UVRAG dependent processes

In addition to autophagy and EGFR degradation, UVRAG has been reported to be implicated in several other processes. Previous studies examining the distribution of UVRAG by immunofluorescence have also demonstrated extensive co-localisation with multiple cellular organelles including the ER, Golgi, Endosomes, Lysosomes and mid-body during cytokinesis (He et al. 2013; Matsunaga et al. 2009; Thoresen et al. 2010). To determine possible effects of UVRAG phosphorylation processes linked to these distinct regions were examined.

UVRAG is reported to interact with the ER-Tethering complex to assist Golgi-ER transport through the protein RINT-1, this interaction is significant as depletion of UVRAG or disruption of RINT-1 binding causes a loss of Golgi integrity leading to fragmentation (He et al. 2013). Examination of the cis-golgi marker GM130 (Nakamura & Rabouille 1995) in U2OS cells treated with UVRAG siRNA demonstrated fragmentation and dispersal as reported (Figure 5.7A). Expression of siRNA resistant GFP-UVRAG wild-type or S550A+S571A were both able to rescue this phenotype suggesting UVRAG phosphorylation does not affect Golgi integrity (Figure 5.7A). UVRAG has also been shown to localise with lysosome associated membrane protein 1 (LAMP1) (Matsunaga et al. 2009), a heavily glycosylated membrane protein that is found primarily in lysosomes (Carlsson et al. 1988). Depletion of endogenous UVRAG caused an increase in LAMP1 positive structures under nutrient rich conditions (Figure 5.7B). Rescue with GFP-UVRAG wild-type reversed this phenotype but mutation of S550A+S571A caused an accumulation of small LAMP1 positive structures (Figure 5.7B). Distinct phenotypes were observed upon UVRAG depletion and S550A+S571A mutation and thus the regulation of lysosomes were examined further. Analysis of other UVRAG functions such as that in cytokinesis are ongoing.

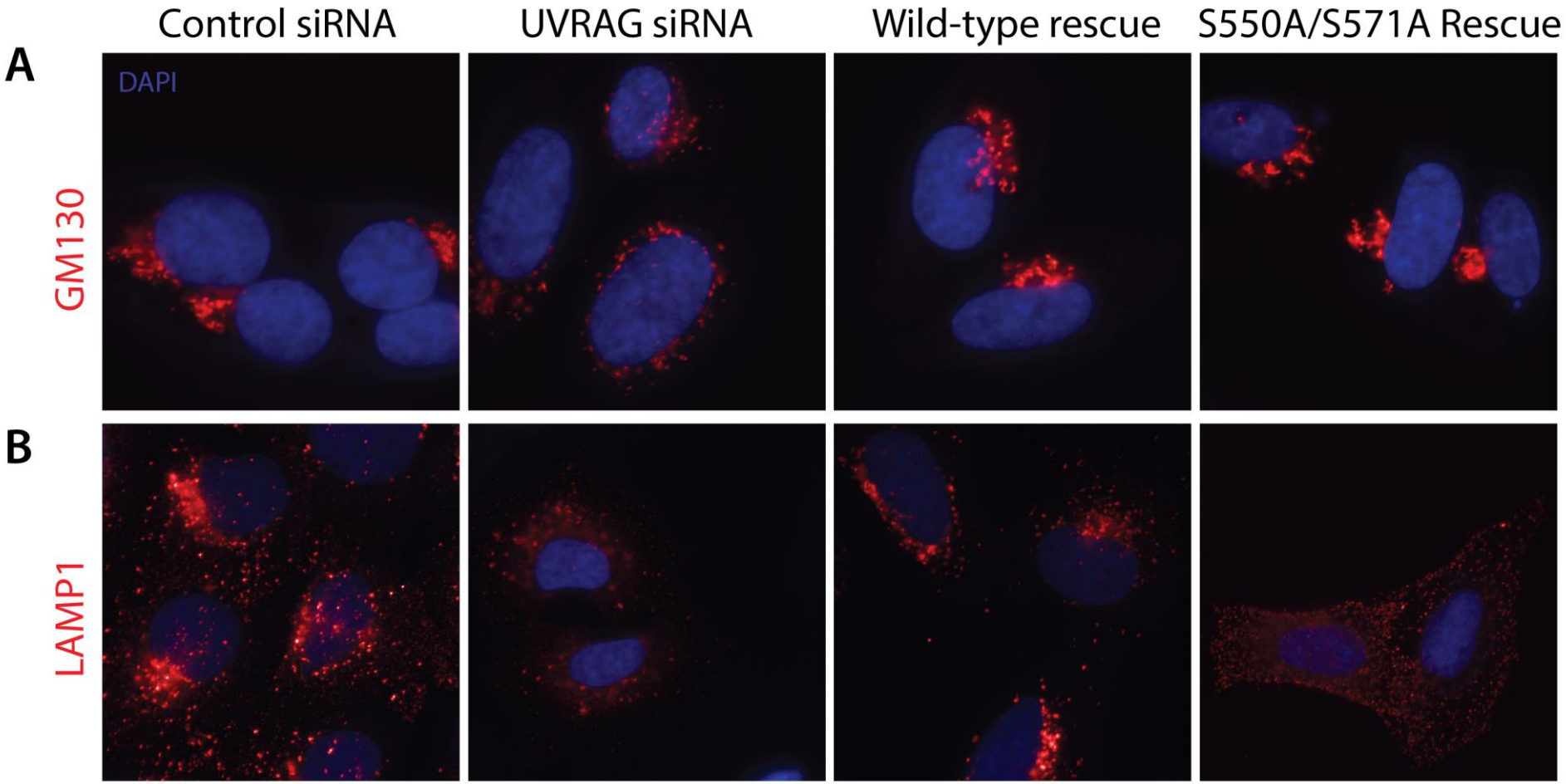

Figure 5.7 - GM130 and LAMP1 in UVRAG S550A+S571A U2OS cells

(A+B) U2OS cells or those stably expressing GFP-UVRAG wild-type or S550A+S571A were reverse transfected with UVRAG ORF1 siRNA (Table 9). 40 h post-transfection cells the growth media was changed and cells were incubated for 1 h in complete media. Cells were fixed with formaldehyde and stained for endogenous (A) GM130 or (B) LAMP1 using Alexa Fluor®-594 secondary antibody.

5.2.6 UVRAG regulates LAMP1 positive structures

The effect of autophagy induction either by mTOR inhibition or nutrient starvation on LAMP1 structures was examined. The activation of autophagy leads to trafficking of autophagosomes towards the lysosome for fusion and degradation of interior contents, consequently LAMP1 positive structures increase in size. Furthermore lysosomes move from the cell periphery to perinuclear locations that is thought to assist with autophagosome fusion (Korolchuk et al. 2011) . Analysis of endogenous LAMP1 in U2OS cells demonstrated an increase in average LAMP1 object size upon autophagy induction (Figure 5.8A&B). Observation of live U2OS cells stably expressing LAMP1-GFP confirmed that LAMP1-GFP structures increased in size but decreased in number in a time-dependent manner following nutrient deprivation. Re-addition of nutrient rich media caused a rapid reversion of phenotype (Figure 5.8C).

The effect of UVRAG upon LAMP1 was further explored in U2OS cells stably expressing GFP-UVRAG wild-type or S550A+S571A by incubation in presence or absence of nutrients (Figure 5.9A). Knockdown of UVRAG resulted in larger lysosomes during nutrient rich conditions whilst rescue with siRNA resistant wild-type UVRAG caused a slight increase in the number of LAMP1 objects that were slightly smaller on average, though neither were significant (Figure 5.9B&C). Expression of GFP-UVRAG S550A+S571A resulted in significantly increased number of LAMP1 positive structures, more than twice that of control siRNA U2OS cells (Figure 5.9C).). The average LAMP1 object size increased upon starvation in all except the UVRAG S550A+S571A mutant that remained significantly smaller and demonstrated no change in size upon starvation (Figure 5.9D). Western blot of cells during growth conditions suggest an increase in the level of LAMP1 expression upon UVRAG siRNA or rescue with UVRAG S550A+S571A (Figure 5.9D)

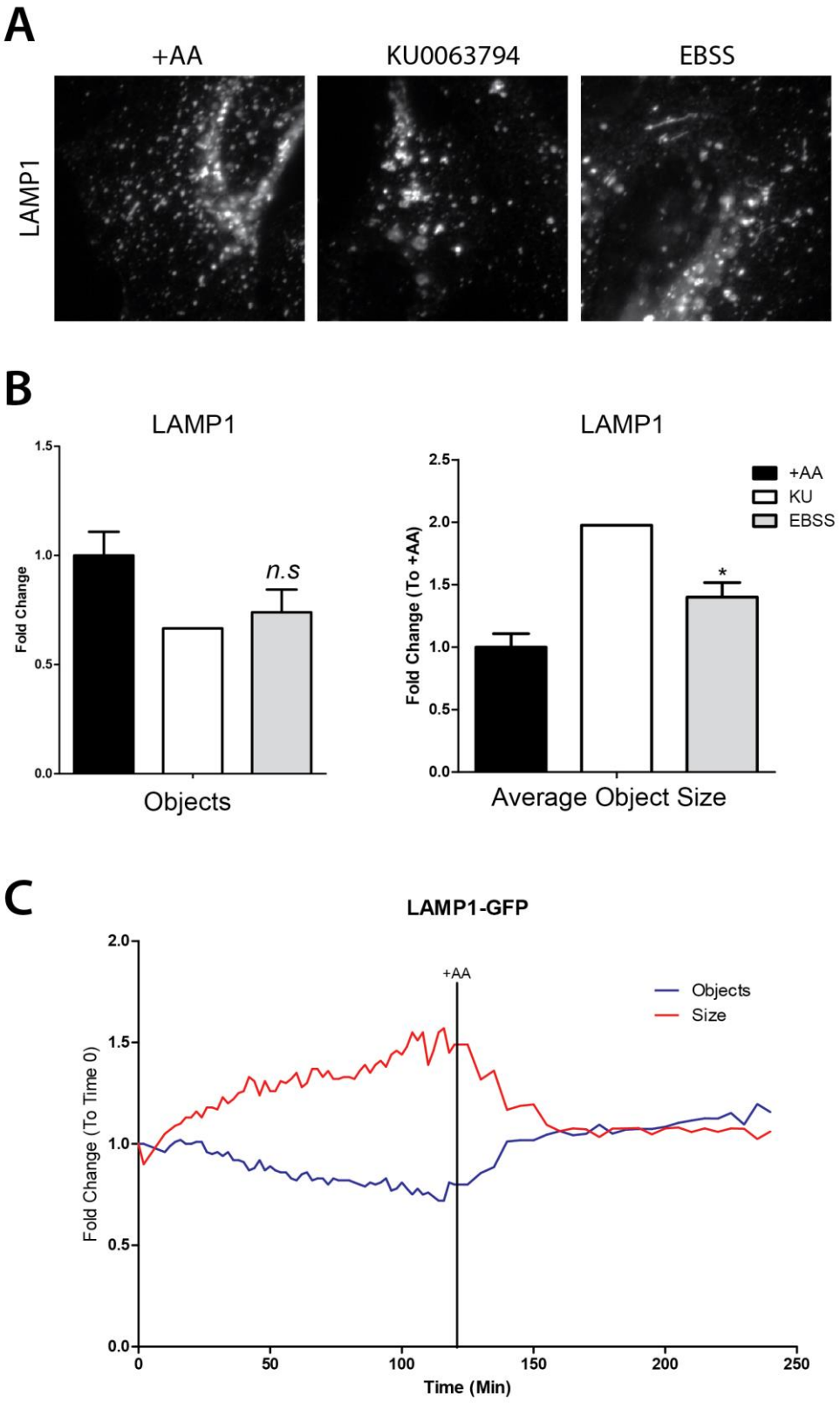

Figure 5.8 - Regulation of LAMP1 Structures By Nutrient Status

(A) U2OS cells were grown in complete media (+AA), starvation media (EBSS) or treated with 1 µM KU0063794 for 2 h prior to formaldehyde fixation and staining for endogenous LAMP1. **(B)** Quantitation of (A) where bars represent mean fold change in object number or object area ± SEM for n = 3 independent experiments (KU0063794 is preliminary data from n = 1). Statistics were determined by Students paired t-test where * = $p < 0.05$. **(C)** LAMP1-GFP expressing U2OS cells were grown in immunofluorescence starvation media for 2 h, cells were then resupplemented with immunofluorescence complete media for 2 h. Graph represents the mean fold change in number of LAMP1-GFP objects or size relative to time 0 for n = 10 cells.

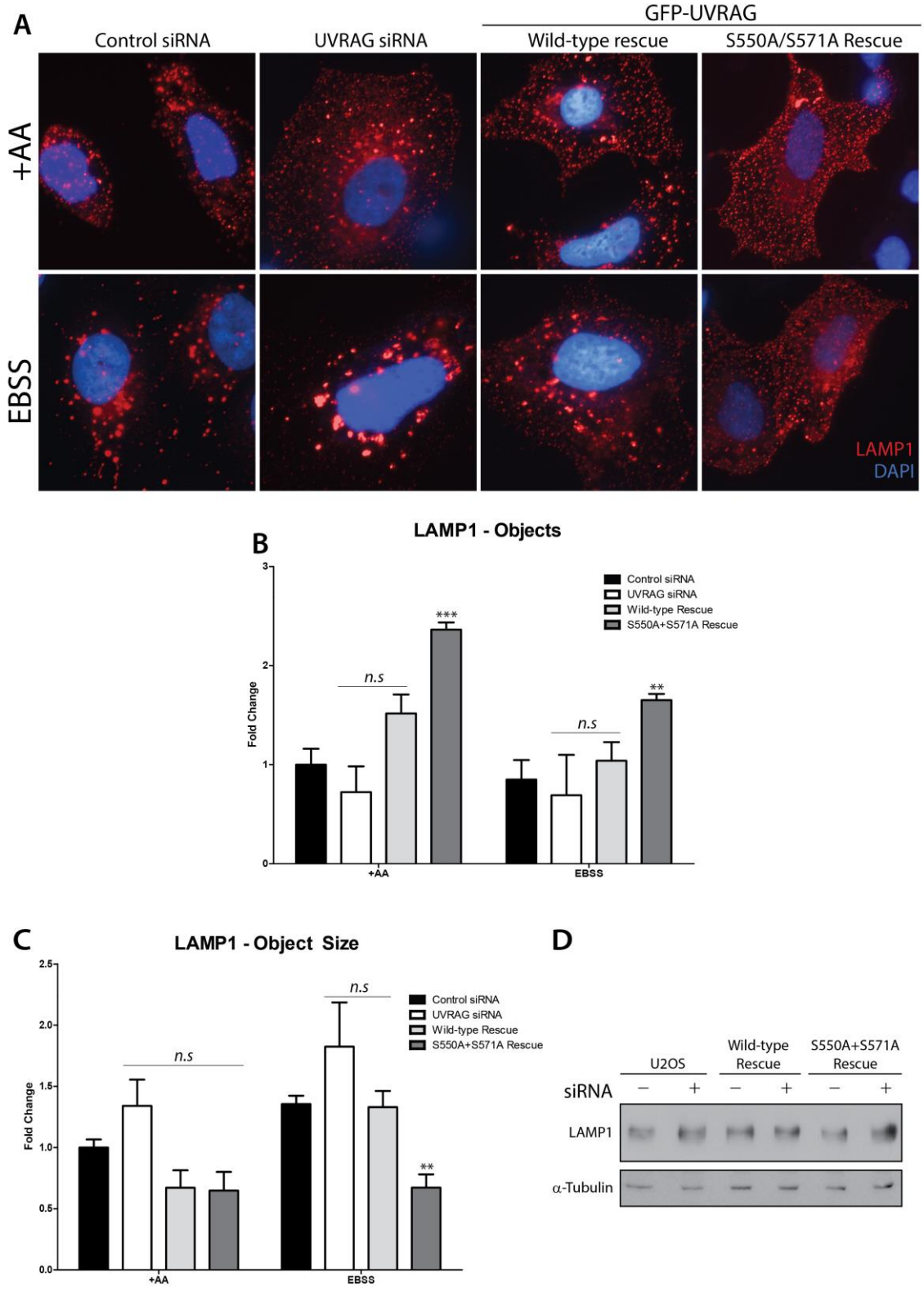

Figure 5.9 - LAMP1 Regulation By UVRAG

(A) U2OS cells or those stably expressing GFP-UVRAG wild-type or S550A+S571A were reverse transfected with 100 nM UVRAG ORF1 siRNA (Table 9). ~40 h post-transfection cells the growth media was changed and cells were incubated for 2 h in complete media (+AA) or starvation media (EBSS). Cells were fixed with formaldehyde and stained for endogenous LAMP1. **(B+C)** Quantitation of (A), bars represent the mean fold change in **(B)** number of objects or **(C)** object size ± SEM for n = 3 independent experiments. Significance was determined by one-way analysis of variance utilising Dunnett's post-test to compare each to the U2OS control siRNA sample where * = $p < 0.05$. ** = $p < 0.01$, *** $p = < 0.001$, *n.s* = not significant. **(D)** Western blot of cells as in (A) grown in complete media (+AA) for 2 h

The depletion of UVRAG or mutation of UVRAG phosphorylation sites resulted in two distinct phenotypes. The localisation of GFP-UVRAG was examined by live cell imaging to confirm whether UVRAG was present at LAMP1 positive structures as had previously been reported (Matsunaga et al. 2009). U2OS cells that stably expressed GFP-UVRAG and LAMP1-mCherry were utilised to determine the extent of co-localisation, GFP-UVRAG displayed extensive co-localisation with mCherry-LAMP1 calculated by Manders co-localisation coefficient (Figure 5.10)(Manders et al. 1993). The co-localisation of LAMP1-mCherry structures was lower with GFP-UVRAG S550A+S571 than GFP-UVRAG wild-type although not significant ($p = 0.0968$). This suggests that no difference in the proportion of GFP-UVRAG binding to LAMP1 structures is observed, but that more LAMP1 structures not containing GFP-UVRAG are present in phospho-mutant cells.

Following confirmation that UVRAG is present at LAMP1 structures, subsequent analysis was important to determine whether other components of the VPS34 complex were also present. Antibodies for immunoblotting VPS34 or BECLIN1 were utilised to examine co-localisation with LAMP1 structures, however, antibody binding proved poor for use by immunofluorescence (data not shown). Instead the localisation of the VPS34 product PI(3)P with LAMP1 structures was examined. PX-594 demonstrated a small proportion of co-staining with LAMP1 structures (Figure 5.11A), additionally known PI(3)P binding proteins including SNX1 and RUFY1 also demonstrated LAMP1 co-localisation suggesting that PI(3)P is present at LAMP1 structures (Figure 5.11B&C).

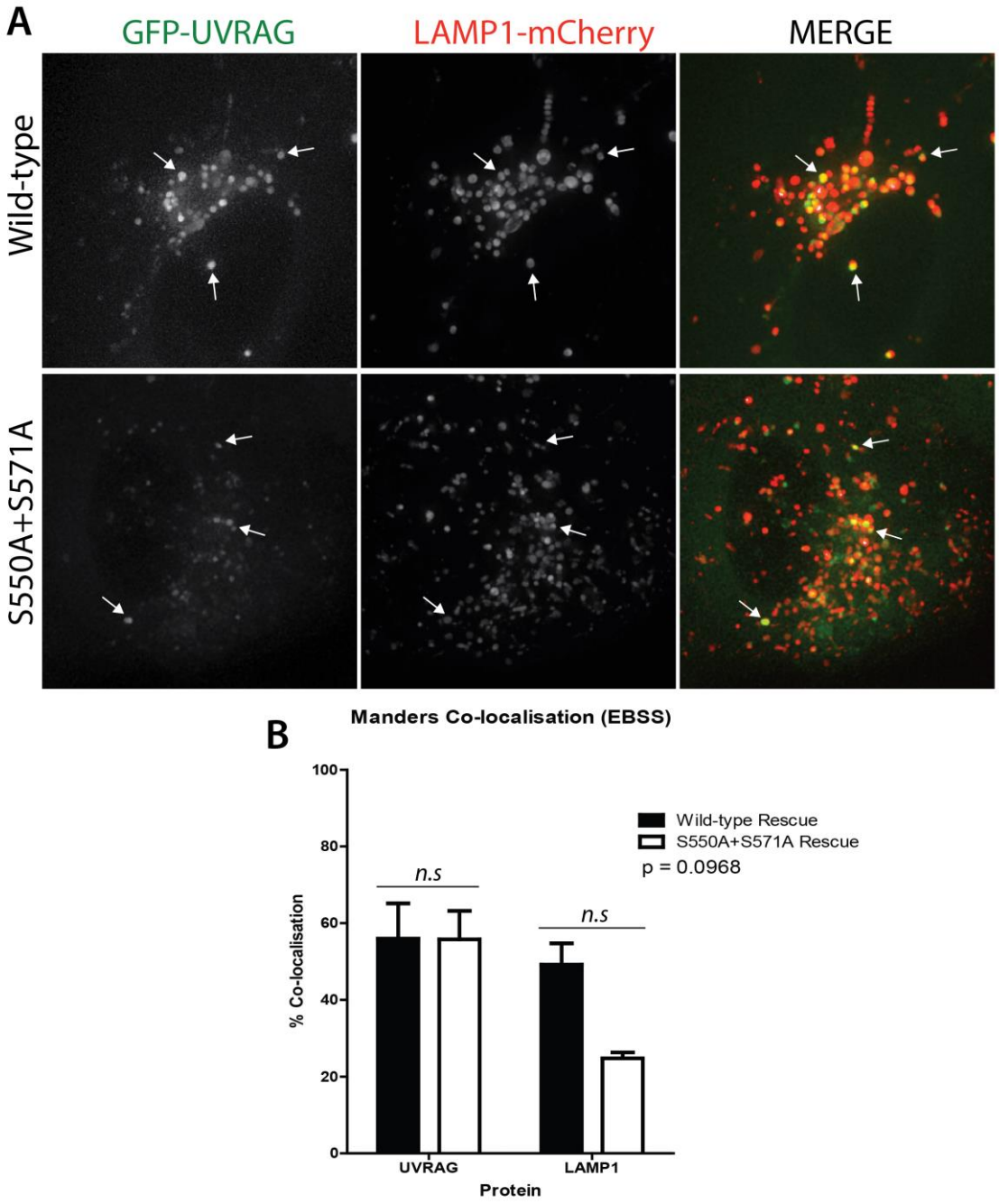

Figure 5.10 – GFP-UVRAG co-localises with LAMP1

(A) U2OS cells stably expressing LAMP1-mCherry and siRNA resistant GFP-UVRAG wild-type or S550A+S571A were reverse transfected with 100 nM ORF1 UVRAG siRNA (Table 9). ~40 h post-transfection cells were grown in immunofluorescence starvation media (EBSS) and images taken at 2 h. Arrows indicate regions of co-localisation. **(B)** Co-localisation of GFP-UVRAG and LAMP1-mCherry was determined by Manders co-localisation coefficient (Manders et al. 1993) ± SEM of n = 3 independent experiments. Statistics were carried out by two-way analysis of variance using Bonferroni's post-test. P-value for wild-type vs S550A+S571A is shown. *n.s* = not significant

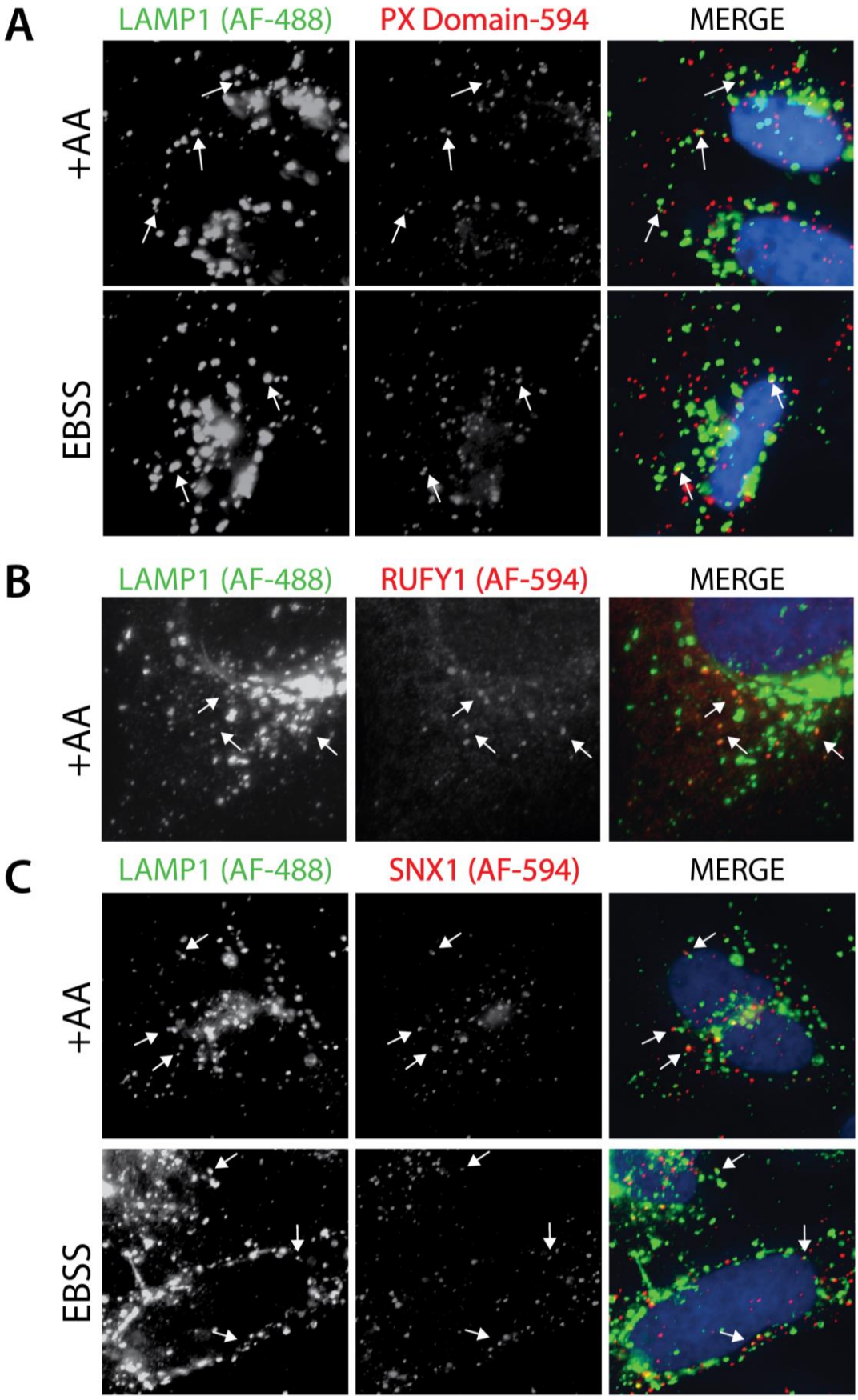

Figure 5.11 - PI(3)P Co-localises with LAMP1

(A-C) U2OS cells were grown in complete media (+AA) or starvation media (EBSS) for 2 h prior to freeze-thaw formaldehyde fixation. Cells were stained for LAMP1 and **(A)** PX-594, **(B)** RUFY1 or **(C)** SNX1 utilising Alexa Fluor® 488 and 594 secondary antibodies as indicated (AF-488 / AF-594)

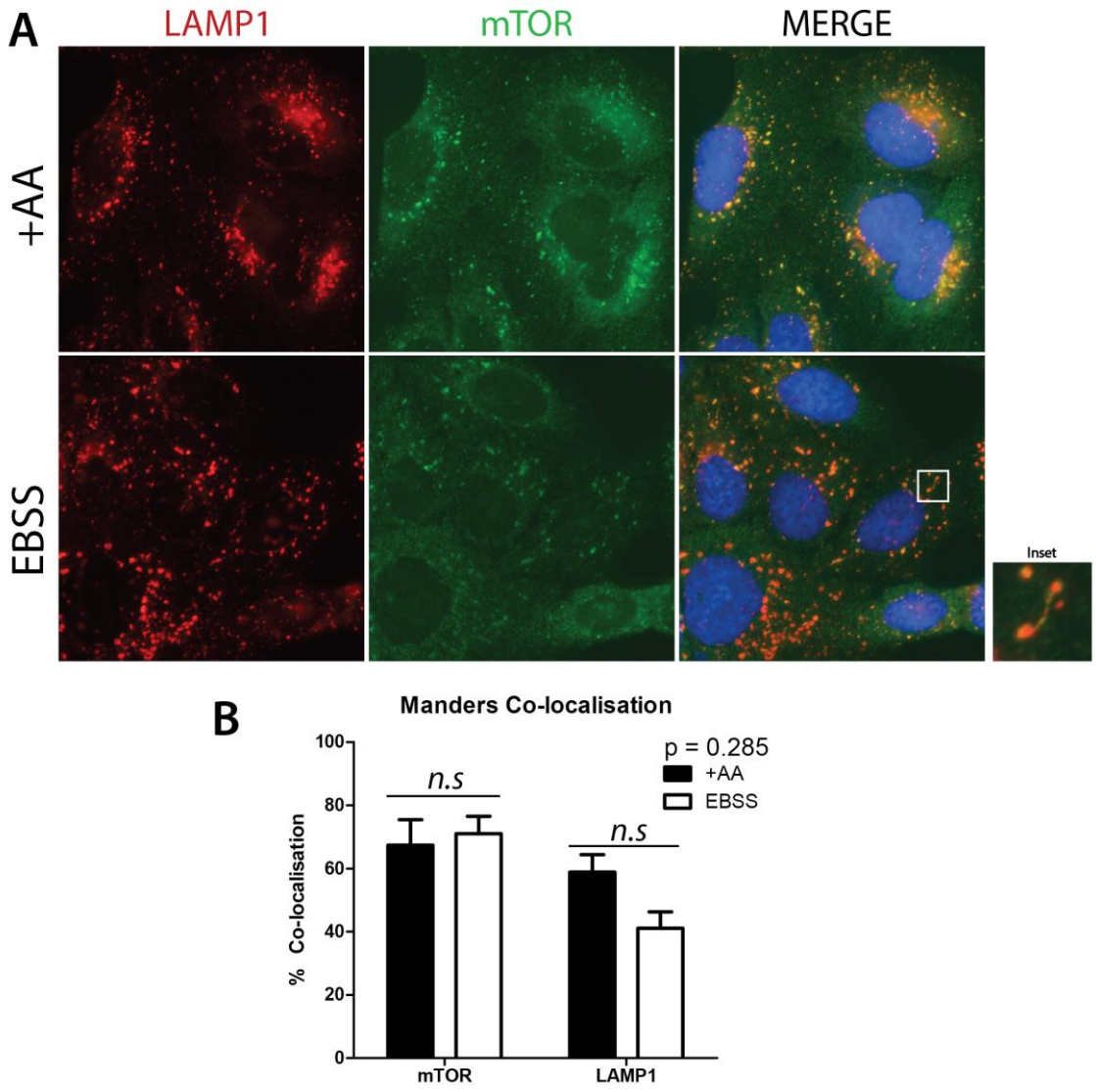

Figure 5.12 - mTOR and LAMP1 co-localisation

(A) U2OS cells were incubated in complete media (+AA) or starvation media (EBSS) for 2 h prior to formaldehyde fixation. Cells were stained for endogenous LAMP1 and mTOR. **(B)** Quantitation of co-localisation in (A) where bars represent mean Manders co-localisation values ± SEM of n = 3 independent experiments. Statistics were determined by two-way analysis of variance and Bonferroni's post-test, *n.s* = not significant. P-value for +AA v EBSS is shown.

Extensive work and literature implicates the requirement of lysosomal localisation for activation of the mTORC1 complex (1.3.2), this thereby raises the possibility that mTORC1 and the novel substrate UVRAG may co-habit the same cellular location. To confirm the localisation of mTOR at LAMP1 structures, U2OS cells were examined between conditions of growth or nutrient starvation (Figure 5.12A). The level of co-localisation between mTOR and LAMP1 was determined by Mander's coefficient (Manders et al. 1993). mTOR exhibited extensive co-localisation with LAMP1 during nutrient rich and deplete conditions (Figure 5.12B).

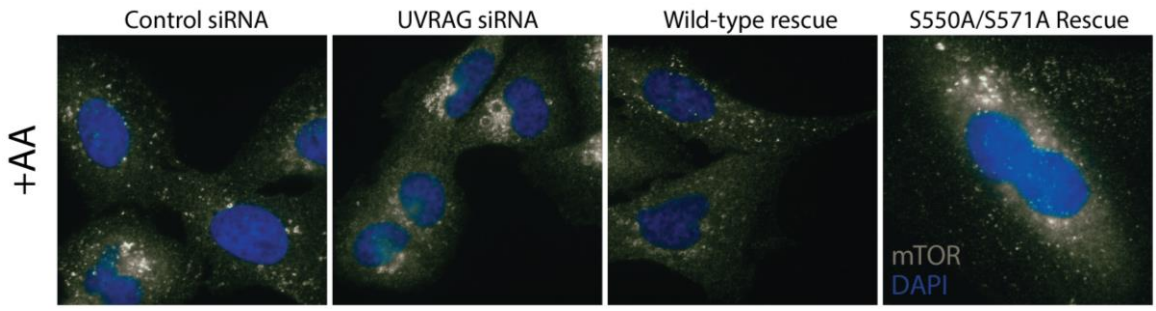

Figure 5.13 - Effect of UVRAG on mTOR distribution

U2OS cells or those stably expressing GFP-UVRAG wild-type or S550A+S571A were reverse transfected with 100 nM ORF1 siRNA (Table 9). ~40 h post-transfection cells were incubated in complete media (+AA) for 1 h prior to formaldehyde fixation and staining for endogenous mTOR.

Depletion of endogenous UVRAG by RNAi resulted in large clustered mTOR structures that could be reverted by expression of GFP-UVRAG wild-type, expression of GFP-UVRAG S550A+S571A caused an increase in smaller structures (Figure 5.13). The staining of mTOR replicates that of LAMP1, which suggests that localisation of mTOR to the lysosome is not affected by UVRAG but reinforces previous data that lysosomal size is altered by UVRAG status (Figure 5.9A).

The regulation of lysosomes has recently been noted to require the presence of phospholipids and has focused upon PI(4)P and PI(4,5)P_2 as critical mediators (Rong et al. 2012; Sridhar et al. 2013). During an autophagic response lysosomal membrane is recycled by a process known as autophagic lysosome reformation (ALR) to ensure consistent formation of competent lysosomes. This process that occurs during autophagy counter-intuitively depends upon mTORC1 activity (Yu et al. 2010). The process of ALR was therefore examined further.

Following a period of starvation, mTOR is re-activated and is required by an unknown mechanism to trigger the budding of tubular structures from lysosomes., tubular structures extend until they are cleaved in a dynamin2 dependent manner (Schulze et al. 2013). The formation of tubules was examined in U2OS cells. A small number of tubules were observed to bud from LAMP1 structures under nutrient rich conditions (Figure 5.14A) whilst nutrient starvation increased the number and length of tubules. Interestingly, addition of the VPS34

inhibitor VPS34-IN1 (Characterised Chapter 6) to cells caused an even greater increase in tubular structures, suggesting that VPS34 and PI(3)P levels are linked to tubule formation and/or turnover.

The requirement of active mTOR and indication that VPS34 is also required strongly suggests that UVRAG-VPS34 complex may be involved in lysosomal regulation. Further investigation is warranted to fully understand the requirement of UVRAG and VPS34 for the process of ALR.

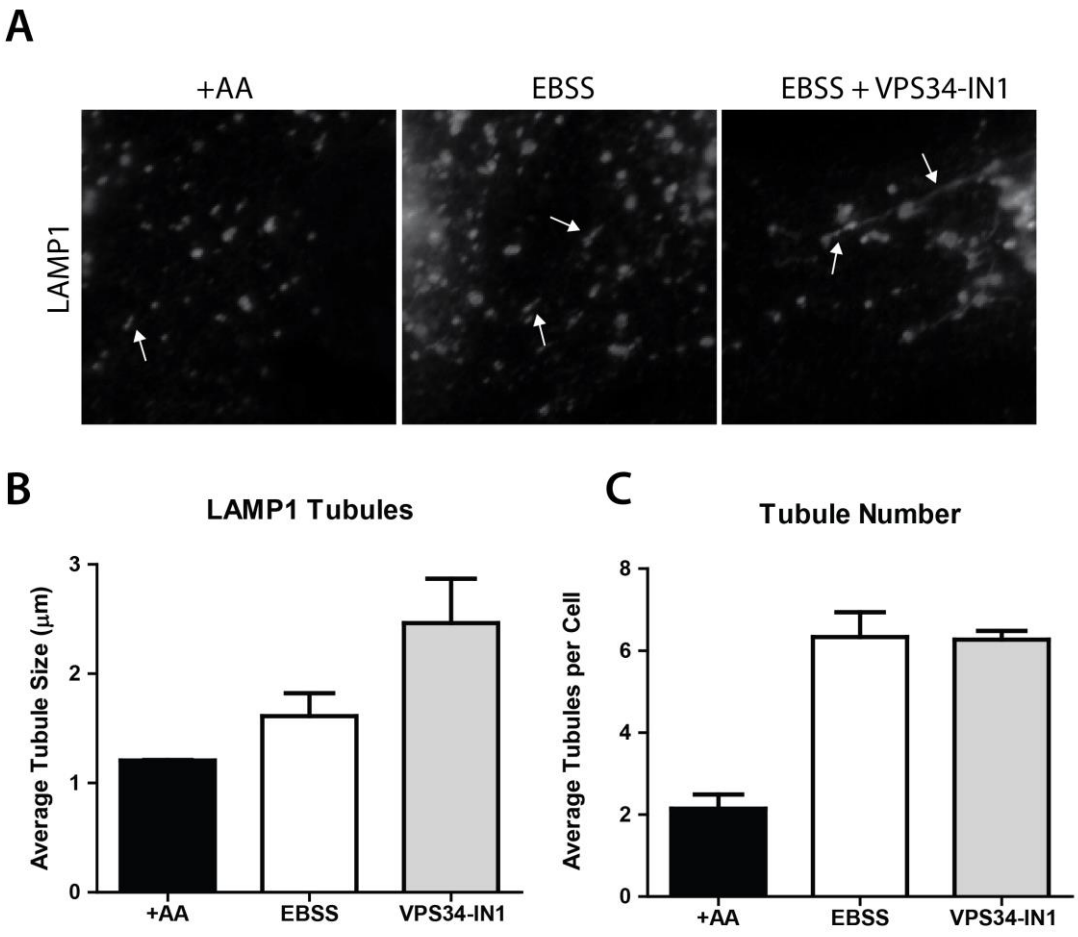

Figure 5.14 - LAMP1 Tubule Formation

(A) U2OS cells were grown in complete media (+AA) or starvation media (EBSS) in the absence or presence of 1 µM VPS34-IN1 for 3 h. Cells were methanol fixed and stained for endogenous LAMP1, arrows highlight tubulated structures. **(B+C)** Quantitation of (A) where bars represent the mean **(B)** tubule length (µm) or **(C)** tubule number ± SD from n = 2 independent experiments.

5.3 Discussion

The role of UVRAG phosphorylation in multiple trafficking processes has been examined and demonstrates a previously unanticipated requirement of VPS34 and PI(3)P for the regulation of lysosomes.

VPS34 plays a fundamental role in the induction of autophagy demonstrated by a blockade of autophagic flux upon depletion in MEFs (Itakura et al. 2008). ATG14L is equally critical as it directs the VPS34 complex to pre-autophagosomal sites via a C-terminal targeting sequence (Fan et al. 2011). The role of UVRAG was originally reported to be required for autophagosome formation in HCT116 cells (Liang et al. 2006), more recent data however has suggested that UVRAG depletion has no effect upon autophagy (Itakura et al. 2008; Knævelsrud et al. 2010). Data presented here agrees with the latter study as no impairment in LC3 flux was observed upon depletion of endogenous UVRAG (Figure 5.1A-D), additionally mutation of UVRAG S550A+S571A had no significant effect upon LC3 flux (Figure 5.1E-G). This data is fitting with the function of vps34 in yeast, where vps38 is required for CPY trafficking but deletion has no effect upon autophagy induction (Kihara, Noda, et al. 2001).

The process of receptor-mediated endocytosis has been shown to be dependent upon PI(3)P as depletion of VPS34 induced by conditional knockout or siRNA causes severe impairment of EGFR degradation (Jaber et al. 2012; Thoresen et al. 2010). Given that UVRAG depletion significantly reduces cellular PI(3)P Figure 4.12 it could be assumed that the trafficking rate would be decreased in a similar manner, analysis upon depletion of UVRAG by RNAi however has unusually shown to increase the rate of EGFR degradation at the 30 min time-point (Figure 5.2C). Previous published data utilising the same siRNA targeting sequence demonstrates conflicting results that depletion of UVRAG impairs EGFR degradation (Liang et al. 2008; Thoresen et al. 2010), the reason for this disparity is unclear. EGFR degradation can be differentially regulated dependent upon stimuli and receptor expression level, although this is still not fully understood despite long-standing knowledge that distinct internalisation mechanisms exist (Lund et al.

1990; Yamazaki et al. 2002). More recently work has demonstrated that treatment with low doses of EGF causes CME mediated internalisation with the majority of receptors recycled back to the plasma membrane (Sigismund et al. 2005). Treatment with high concentrations of EGF (>20 ng/ml) in contrast cause ~40 % of EGFRs to undergo internalisation by non-clathrin endocytosis (NCE) and it is via this pathway that the majority of EGFR degradation occurs (Sigismund et al. 2008). An increase in EGFR degradation may therefore highlight an increased proportion of NCE occurring and reduced recycling. Indeed examination of the transferrin receptor, which exclusively utilises CME, demonstrates impaired recycling upon treatment with UVRAG siRNA (Figure 5.5). A partial defect in CME mediated recycling may consequently increase the proportion of NCE occurring upon EGFR stimulation and explain the increased level of degradation that is observed (Figure 5.2C). The role of UVRAG in CME and recycling requires further investigation and this could be explored by utilising the polyene macrolide Filipin that inhibits NCE (Schnitzer et al. 1994). The use of different cell lines may also be a source of disparity between results, comparison of the human cell lines U2OS and Hela in this study for example display clear differences in recycling rate (Figure 5.4). Care must be taken when utilising cell culture models given the propensity for aberrant endocytosis to drive cancer progression. Mutation of the tumour suppressor p53 for example is thought to occur in ~50 % of all cancers (Vogelstein et al. 2000) and research has demonstrated that this can cause enhanced EGFR and integrin trafficking that promotes growth and cell invasiveness (Muller et al. 2009). Multiple factors may therefore contribute to the discrepancy observed upon UVRAG depletion, importantly, no significant difference of EGFR degradation or transferrin recycling was observed between UVRAG wild-type or S550A+S571A (Figure 5.3, Figure 5.5D) that suggests mTOR regulation is not important for either pathway.

Analysis of multiple PI(3)P interacting proteins representing distinct endosomal compartments demonstrated no change in membrane binding upon nutrient depletion or mTOR inhibition, by comparison use of the PI3K inhibitor blocked membrane binding (Figure 5.6A&B). Furthermore analysis by Immunofluorescence demonstrated no reduction difference in the formation of

punctate structures upon nutrient depletion (Figure 5.6C). As endocytic proteins demonstrated no difference in binding, other processes and cellular locations that UVRAG has been implicated in were examined.

Interaction of UVRAG with the protein RINT-1 has been shown to be important for Golgi integrity (He et al. 2013). Whilst depletion of UVRAG caused fragmentation of the Golgi as determined by GM130 staining, no phenotype was observed following rescue with UVRAG wild-type or S550A+S571A. This is perhaps to be expected as the binding of RINT-1 to UVRAG is reported to be dependent upon UVRAG residues 270-442 (He et al. 2013), distinct from the mTOR mediated phosphorylation sites (Figure 3.5). A previous study indicated that UVRAG localises with LAMP1 positive structures (Matsunaga et al. 2009), examination of LAMP1 by immunofluorescence demonstrated significant differences upon UVRAG depletion or expression of the S550A+S571A mutant (Figure 5.7B). Targeting of UVRAG by siRNA caused an accumulation of large LAMP1 positive structures that appeared similar but not as severe as the vacuolar phenotype observed upon VPS34 kinase inhibition with wortmannin or VPS34 depletion (Futter et al. 2001; Zhou & Wang 2010). Similarly large swollen vacuoles are also observed in yeast by over-expression of the PI(3)P phosphatase MTMR3 (Walker et al. 2001). Blockade of $PI(3,5)P_2$ formation by inhibiting PIK_{FYVE} also yields a strikingly similar phenotype (Jefferies et al. 2008), it appears that $PI(3,5)P_2$ is critical for maturation of endosomes and inhibition of PI(3)P or $PI(3,5)P_2$ generation induces a similar phenotype. In comparison to loss of PI(3)P induced by the aforementioned mechanisms, depletion of UVRAG is still permissive for EGFR and LC3-II degradation suggesting that these structures remain acidic and functional (Figure 5.1 & Figure 5.2). However, it is possible that some endogenous protein remains due to incomplete siRNA knockdown. In contrast to the effect of UVRAG knock-down, expression of GFP-UVRAG S550A+S571A mutant displays a distinct phenotype of numerous small LAMP1 structures (Figure 5.7B).

Following autophagy induction, lysosomes move to the perinuclear region and this is thought to assist with autophagosome fusion and lysosomal size increases (Figure 5.8)(Korolchuk et al.

2011). The size of lysosomes increased and were positioned at the perinuclear region in all cells upon nutrient starvation except for GFP-UVRAG S550A+S571A that exhibited significantly smaller LAMP1 structures throughout (Figure 5.9). The positioning of lysosomes depends upon both passive and active processes, recent research has demonstrated that smaller lysosomes (~500nm) undergo diffusion at approximately two and a half times faster than larger lysosomes (~1.2µm) (Bandyopadhyay et al. 2014). During nutrient starvation conditions lysosomes in control cells were on average twice the size of those in GFP-UVRAG S550A+S571A, passive diffusion may in part explain the diffuse cellular distribution observed upon mTOR site mutation (Figure 5.9). Lysosome transport between the cell periphery and perinuclear region is primarily regulated by the kinesin and dynein motor protein families, siRNA depletion or over-expression of these motor proteins can manipulate lysosome cellular location (Brown et al. 2005; Harada et al. 1998). Treatment of cells with the microtubule depolymerising agent nocodazole (Vasquez et al. 1997) causes a diffuse LAMP1 staining pattern similar to that observed in the GFP-UVRAG S550A+S571A mutant, which could indicate a defect in motor protein binding (Korolchuk et al. 2011). The kinesin family members KIF3, KIF5 and dynein have been demonstrated to regulate lysosome positioning, interestingly peptides corresponding to KIF5 (Kinesin-1) and Dynein were both identified upon mass spectrometry as interactors of GST-UVRAG (Appendix A & B). Peptides were identified upon immunoprecipitation of both UVRAG Wild-type and S550A mutant suggesting that S550 phosphorylation does not mediate or occlude binding. Further analysis is required to determine whether an endogenous interaction occurs and if mutation of both mTOR phosphorylation sites alters binding. Intriguingly the PI(3)P binding protein FYCO1 has been demonstrated to act as an adaptor between autophagosomes, late endosomes or lysosomes and the motor protein kinesin to drive plus-end microtubule movement (Pankiv et al. 2010). Binding to PI(3)P however may first require interaction with LC3 to allow FYVE domain interaction. Over-expression of FYCO1 was observed to increase lysosome fusion and the size of lysosome structures and as such it would be interesting to examine upon mutation of UVRAG S550A+S571A (Pankiv et al. 2010).

UVRAG has been reported to directly mediate lysosome fusion by interaction with VPS11 and VPS16 that form part of the core class C vacuolar protein sorting (Vps) complex (Liang et al. 2008). Immunoprecipitation of GFP-UVRAG S550A however identified several unique peptides from VPS16 by mass spectrometry (Appendix B) suggesting that this interaction was not impeded by mutation of the S550 mTOR site. In addition experiments examining autophagy induction by LC3 flux (Figure 5.1) or endocytosis by EGFR degradation (Figure 5.3) were not significantly impaired indicating successful trafficking to the lysosome. The total level of LAMP1 expression in GFP-UVRAG S550A+S571A cells was higher than control cells and it is possible that this acts as a compensatory mechanism to allow normal trafficking and degradation.

Analysis of GFP-UVRAG and LAMP1-mCherry demonstrated extensive co-localisation and this is in agreement with a previous report that UVRAG is localised to LAMP1 structures (Figure 5.10)(Matsunaga et al. 2009). A Difference in lysosomal phenotype between UVRAG rescue cells was clearly evident upon nutrient starvation, particularly in terms of lysosome size and distribution (Figure 5.10A). Several recently identified functions of UVRAG, such as the double-strand break repair pathway or RINT-1 interaction at the ER, have been determined to occur independently of the VPS34 complex (He et al. 2013; Zhao et al. 2012). Analysis of PX-594, RUFY1 and SNX1 staining with LAMP-1 demonstrated that regions of co-localisation did occur and suggested that PI(3)P is present at the lysosome, which may indicate the UVRAG is bound to the VPS34 complex at lysosomes (Figure 5.11). An important consideration however is that the PI(3)P present may be due to dephosphorylation of other lipid species or that this could be mediated by PI3K class 2 activity (Devereaux et al. 2013). Additionally newly synthesised LAMP1 requires trafficking to the Golgi before continuing to endosomes and lysosomes (Cook et al. 2004; Höning et al. 1996). Furthermore a small proportion of LAMP1 undergoes trafficking separately from the Golgi to the plasma membrane where endocytosis is required for LAMP1 to reach the lysosome (Rohrer et al. 1996). By navigating components of the endocytic trafficking system it is possible that some LAMP1 expression observed by immunofluorescence will not be representative of lysosomes but may co-localise with PI(3)P dependent structures, however this

is unlikely to be significantly accumulated. A recent proteomic experiment of an enriched lysosome fraction from rat liver identified several FYVE domain containing interacting proteins including FYCO1, FYVE-CENT, RUFY3 and ANKFY1; several SNX proteins were also identified that included SNX8, SNX16 and SNX17 (Chapel et al. 2013). The function of many of these proteins is currently uncertain and as such it will be important to examine whether they are indeed localised to lysosomes and if they may regulate lysosome function in a PI(3)P dependent manner.

Immunofluorescence confirmed that mTOR exhibited extensive co-localisation with LAMP1 positive structures in line with previous reports (Figure 5.12) (1.3.2). Depletion of UVRAG or mutation of S550A+S571A did not prevent the formation of mTOR punctate structures, however the distribution and size of structures were visibly altered similar to that observed with LAMP1 staining suggestive that mTOR remains localised to lysosomes (Figure 5.13). Separation of MEF lysates by iodixanol density gradient also showed that UVRAG and mTOR exhibit similar fractionation profiles indicating that mTOR and UVRAG are present at similar density compartments [Figure 3.11]. The cellular distribution of lysosomes can alter mTOR signalling by moving closer to downstream substrate proteins, forcibly directing lysosomes to the periphery by depletion of minus end directed microtubule motor proteins led to an increase in p70-S6K T389 phosphorylation (Korolchuk et al. 2011). The peripheral lysosomal distribution of UVRAG S550A+S571A cells may alter the level of downstream mTOR signalling and should be explored further.

Comparison of LAMP1 staining between wild-type and S550A+S571A UVRAG rescue is particularly striking during nutrient starvation (Figure 5.10), however this is unusual as mTOR is inactive during autophagy and as such UVRAG will not be phosphorylated during this time. More recently however, the importance of mTORC1 activity for autophagic lysosome reformation (ALR) has become apparent (Yu et al. 2010). To continually mediate an autophagic response requires the ability to fuse and degrade autophagosome components whilst simultaneously

recycling membrane, catabolic products and replenishing the degradative ability of lysosomes. This is achieved by re-activation of mTOR following periods of starvation and is dependent on the efflux of nutrients from the lysosome (Rong et al. 2011). Tubular structures bud from LAMP1 positive lysosomes and this is mediated in part by clathrin binding (Rong et al. 2012). Following extension tubules undergo scission mediated by Dynamin2 (Schulze et al. 2013). Formation of tubular LAMP1 positive 'proto-lysosomes' are then thought to undergo maturation to form functional lysosomes. ALR also increases the number or peripheral lysosomes which may assist signalling to mTORC1 substrates as mentioned previously (Korolchuk et al. 2011).

Examination of LAMP1 in U2OS cells demonstrated the formation of tubular structures. Cells grown in nutrient rich conditions were tubulated but these rapidly underwent scission (Figure 5.14). Starvation caused a more observable effect as tubules extended for much longer prior to cleavage from the main LAMP1 structure, inhibition of VPS34 using VPS34-IN1 caused severely extended LAMP1 tubules (Figure 5.14). This implicates PI(3)P directly as a regulator of the scission process. This is distinct from the small punctate staining observed upon UVRAG S550A+S571A mutation, however, it is possible that fixation may disrupt and affect the preservation of some of the tubules. It is therefore important to examine and compare tubule formation by live cell and is currently underway.

Taken together the data presented in this chapter highlights a potentially unanticipated role of PI(3)P in the regulation of lysosomes. Moving forward, work will focus upon delineation of the relationship between PI(3)P and lysosome turnover. The impact of UVRAG S550A+S571A mutation upon tubule length and rate of scission in particular will be examined as this may be critical in driving the dispersed lysosome phenotype that is observed.

6 CHARACTERISATION OF NOVEL SPECIFIC VPS34 INHIBITORS

6.1 Introduction

To date, further understanding of VPS34 has been hampered by a lack of specific tools that can help to delineate functional roles. Disruption of the *VPS34* gene in yeast causes a temperature-sensitive growth defect that was important in establishing a link between Vps34p and protein sorting (Herman & Emr 1990). Further study in mammalian cells however has proven difficult due to the fundamental cellular requirement for VPS34, exemplified by embryonic lethality in homozygous VPS34 -/- mice (Zhou et al. 2011). Tissue specific knock-out of VPS34 from sensory neurons generates mice that can survive gestation, however, all mice die within 2 weeks exhibiting severe movement defects (Zhou & Wang 2010). Similarly homozygous deletion of VPS34 from cardiomyocytes causes death in mice between week five and week thirteen due to heart failure (Jaber et al. 2012). Depletion of VPS34 acutely by RNAi has also been utilised and implicated VPS34 as a possible upstream regulator of mTOR based upon decreased phosphorylation of mTORC1 substrates (Nobukuni et al. 2005; Byfield et al. 2005). There are several drawbacks regarding the use of RNAi that include the possibility of incomplete depletion of the endogenous protein that may be permissive for some functions. Additionally the use of lipofectamine as a transfection reagent has been linked to autophagy induction which may lead to erroneous results when examining the role of VPS34 (Mo et al. 2012). Furthermore siRNA depletion of VPS34 leads to significant loss of other canonical interaction partners including BECLIN1, ATG14L and UVRAG that may affect VPS34 independent roles of these proteins (Itakura et al. 2008; Thoresen et al. 2010; Devereaux et al. 2013).

The use of ATP binding site inhibitors is a commonly used strategy for rapidly inhibiting kinase activity without affecting protein binding (Duong-Ly & Peterson 2013). Due to the conserved nature of the ATP binding site between kinases, many kinase inhibitors can act non-selectively

to bind and inhibit multiple kinases (Knight & Shokat 2005). Selectivity can be achieved and become therapeutically relevant as was demonstrated upon development of the first clinically approved kinase inhibitor Imatinib (Demetri & Mehren 2002).

Inhibitor based studies of VPS34 to date have been reliant on the PI3K inhibitor wortmannin or LY294002 (Carpentier et al. 2013). Whilst able to inhibit VPS34 (Stack & Emr 1994), these inhibitors have a much greater potency against class I PI3Ks (Arcaro & Wymann 1993). A specific inhibitor of VPS34 is therefore required to fully explore lipid kinase function with minimal off-target effects.

Recently developed inhibitors by Novartis, VPS34-IN1 and VPS34-IN2, are predicted to inhibit VPS34. This chapter examines the potency and specificity of these inhibitors towards VPS34 and the generation of cellular PI(3)P.

6.2 Results

6.2.1 *In vitro* inhibition of VPS34 and VPS15

VPS34-IN1 and VPS34-IN2 are structurally related bi-heteroaryl compunds that were originally reported in a patent by Novartis (WO 2012085815 A1), the structure of each is shown in Figure 6.1A&B. The potency of VPS34-IN1 and VPS34-IN2 against recombinant VPS34 was determined by titration of each inhibitor to determine the concentration at which kinase activity was inhibited by 50 %, the IC_{50} (Sebaugh 2011). The activity of recombinant His-VPS34-VPS15 was determined by reaction with phosphatidylinositol liposomes in the presence of ^{32}P γ-ATP and Mn^{2+} (Volinia et al. 1995; Whitman et al. 1988). VPS34-IN1 and VPS34-IN2 were both highly potent with IC_{50} values of 25 nM and 6 nM respectively (Figure 6.1C&D).

A common drawback of ATP-binding kinase inhibitors is the propensity to inhibit multiple kinases due to similarities that exist within the ATP binding pocket (Karaman et al. 2008; Knight & Shokat 2005). To determine the selectivity of VPS34-IN1 and VPS34-IN2, multiple commercial protein and lipid kinase inhibitor profiling services were utilised to characterise the inhibitors as reported in Bago et al. (2014). A panel of 140 protein kinases and 20 lipid kinases were tested at the International Centre for Kinase Profiling, University of Dundee using 1 µM of each inhibitor. VPS34-IN1 & 2 were highly selective with little off-target inhibition of either lipid kinases or protein kinases. VPS34-IN1 exhibited greater selectivity reducing activity of only three protein kinases to ≤ 50 compared to six kinases with VPS34-IN2. The average activity across all protein kinases tested was 106 % or 82.4 % for VPS34-IN1 and VPS34-IN2 respectively, demonstrating further that the majority of kinases were unaffected and that VPS34-IN1 was slightly more selective (Bago et al. 2014).

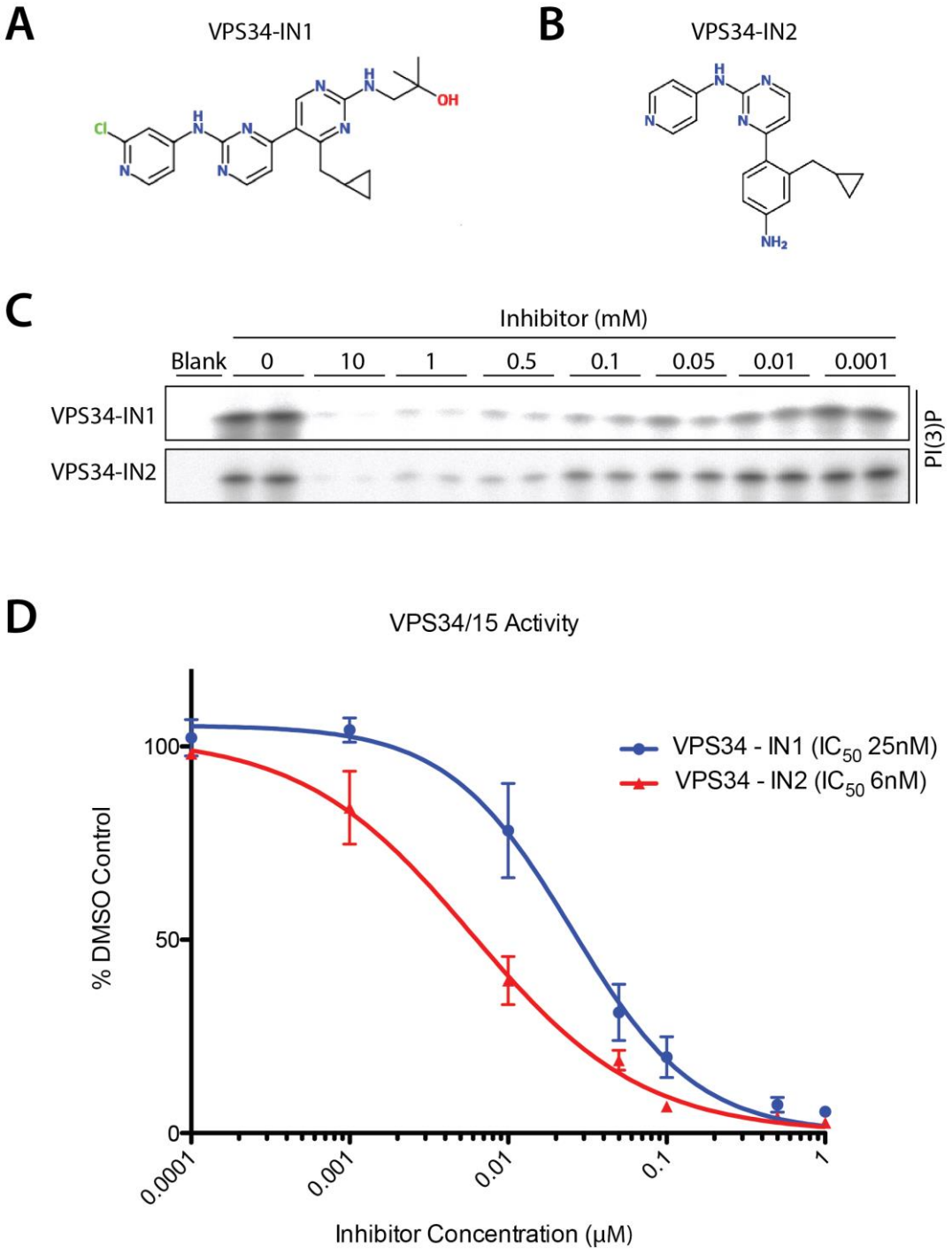

Figure 6.1 - IC_{50} of VPS34-IN1 and VPS34-IN2 *in vitro*

Chemical structure of the related compounds **(A)** VPS34-IN1 and **(B)** VPS34-IN2. **(C)** Recombinant His-VPS34-VPS15 (DU8692) was utilised for a radioactive *in vitro* lipid kinase assay with phosphatidylinositol liposomes. Lipid products were separated by thin layer chromatography and incorporation of ^{32}P γ-phosphate was calculated by using a phospho imager. **(D)** Quantitation of (C), points represent log inhibitor concentration relative to VPS34 kinase activity ± SEM from n= 3 independent experiments. IC_{50} curves were plotted by non-linear regression using Prism 5.0.

The IC_{50} of VPS34-IN1 was tested against a further panel of 13 lipid kinases at ProQinase, Tumor Biology Center, Freiburg and 8 lipid kinases by AstraZeneca. VPS34-IN1 demonstrated extreme selectivity towards PIK3C3 over other PI3K isoforms and the IC_{50} was between 15-130 fold lower than the second most inhibited lipid kinase PIP5K1C (Bago et al. 2014).

VPS34-IN1 and VPS34-IN2 are therefore highly potent and selective for VPS34 when tested *in vitro* and therefore the ability to inhibit cellular VPS34 was examined next. VPS34-IN1 & 2 were titrated from 0.01-10 µM in U2OS cells and the intensity of 2xFYVE-594 staining was used to determine cellular PI(3)P level. The level of response was comparable between inhibitors with ~30 % and ~10 % PI(3)P staining remaining at 1 µM and 10 µM respectively. VPS34-IN1 and VPS34-IN2 can therefore potently inhibit PI(3)P production in cells. Further analysis is required to fully confirm that this impairs VPS34 functions within cells.

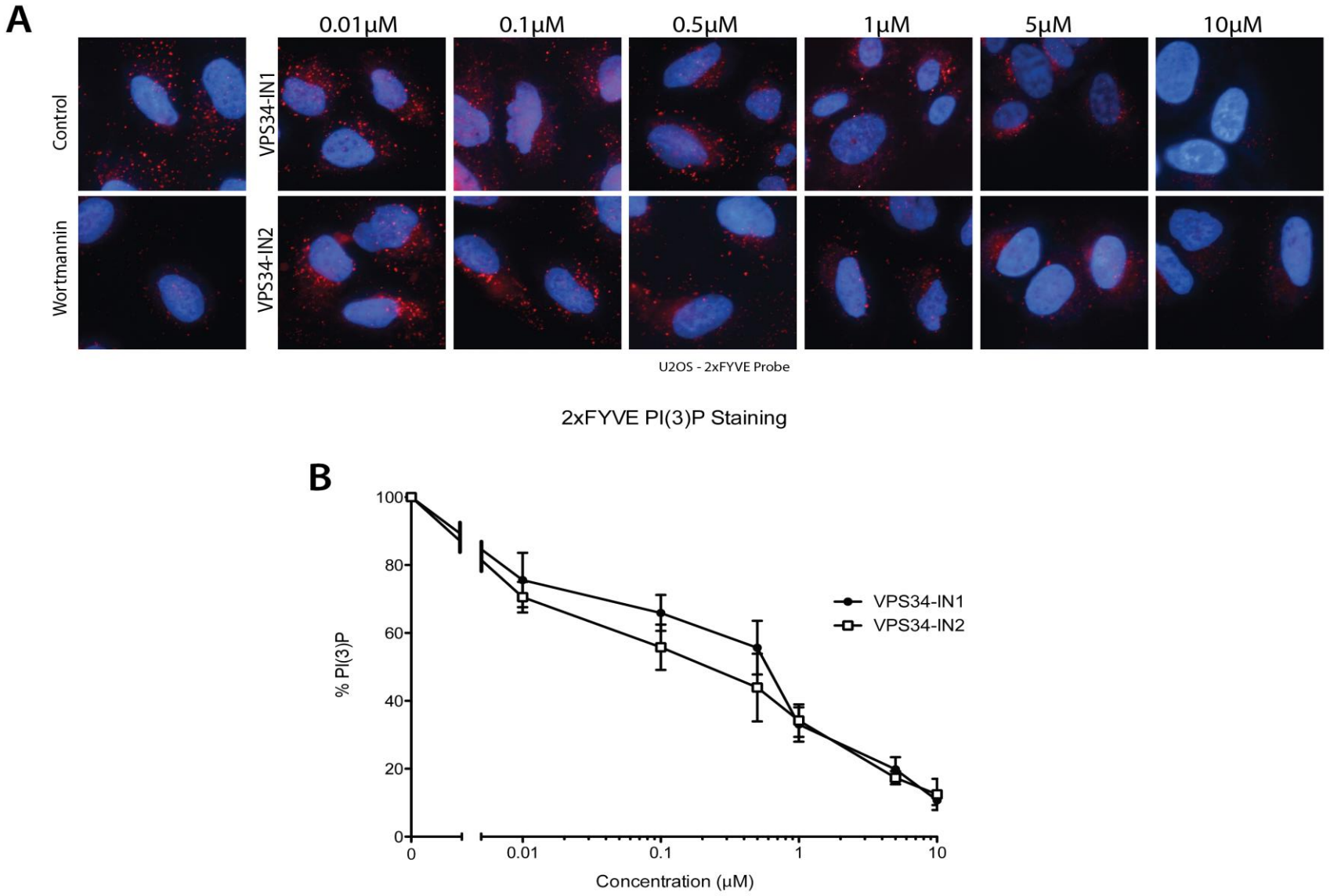

Figure 6.2 - Specific VPS34 Inhibitors block cellular PI(3)P production

(A) U2OS cells were treated for 1 h with the indicated concentration of inhibitor prior to freeze thaw formaldehyde fixation and staining with 2xFYVE-594. **(B)** Quantitation of (A), bars represent cellular PI(3)P relative to DMSO control ± SEM of n = 3 independent experiments.

6.3 Discussion

The data presented here demonstrates the potency and selectivity of the related compounds VPS34-IN1 and VPS34-IN2 for VPS34. The common drawback of previous VPS34 inhibitors has been the lack of selectivity over other PI3K classes (Stack & Emr 1994), this data now provides evidence for the first selective kinase inhibitor of VPS34.

Data gathered *in vitro* suggests low nanomolar IC_{50} values for both compounds (Figure 6.1C&D), however to reduce PI(3)P formation by ~90 % requires cells to be treated with 10 μM of inhibitor (Figure 6.2). The reason for this disparity may be due to limitations in the permeability or uptake of the compound. However treatment of U2OS cells with VPS34-IN1 causes inhibition of PI(3)P formation within 1 minute that could not occur if the drug were not freely permeable (Bago et al. 2014), alternatively the remaining PI(3)P may be attributed to VPS34-independent sources. Class I PI3Ks produce PI(3,4,5,)P_3 at the plasma membrane that undergoes sequential dephosphorylation via the SH2-containing inositol phosphatase (SHIP2) and inositol 4-phosphatase (INPP4β) to form PI(3)P (Lioubin et al. 1996; Gewinner & Wang 2009). As inhibitor treatments were carried out on cells growing in nutrient rich media it is likely that class I PI3Ks were active. In addition the class II PI3Ks are able to phosphorylate phosphatidylinositol *in vivo* to form PI(3)P similar to VPS34 (Falasca et al. 2007) . Conditional knock-out of VPS34 from MEFs has been demonstrated to reduce PI(3)P levels by ~70 %, RNAi directed against class II PI3K α/β reduces the total level of PI(3)P further. It is estimated that up to 20 % of cellular PI(3)P may be generated via class II PI3Kα/β and this may play important functional roles alongside VPS34 (Devereaux et al. 2013). The majority of VPS34 dependent PI(3)P is likely to be inhibited by treatment with 1 μM with the remaining likely to be generated from both class I (via dephosphorylation) and class II PI3Ks. It is important to characterise the effect of this inhibitor further in cells to confirm that it is sufficient to inhibit known VPS34 functions such as autophagy and endocytosis (Kihara, Noda, et al. 2001).

The ability to selectively inhibit VPS34 activity is an excellent tool that will allow VPS34 cellular function to be analysed more efficiently with fewer off-target effects, potentially avoiding artificial phenotypes. VPS34-IN1 has already proven beneficial for the study of VPS34, highlighting a potentially important and previously uncharacterised link between PI(3)P and the activation of serum and glucocorticoid-induced kinase 3 (SGK3) (Bago et al. 2014). Of particular interest will be further delineation of the reciprocal relationship between mTOR and VPS34, which has proved difficult to study so far with previous non-specific VPS34 inhibitors.

7 DISCUSSION

The data presented in this thesis highlights a novel and previously unanticipated role of mTOR in the regulation of lysosomes via phosphorylation of the protein UVRAG. This has been indicated through multiple lines of evidence.

Data shown here has characterised UVRAG as a novel mTORC1 substrate that is phosphorylated at S550 and S571 (Figure 3.7). The phosphorylation of UVRAG has no discernible effect upon the stoichiometry or localisation of the UVRAG-VPS34 complex (3.2.5 and 3.2.6), however, it mediates a ~2 fold increase in VPS34 lipid kinase activity that can be detected in cells utilising recombinant PI(3)P binding domain probes (Figure 4.13). UVRAG exhibits extensive co-localisation at LAMP1 positive structures that are established (Flinn et al. 2010) and demonstrated to be co-localised with mTORC1 (Figure 5.12). Mutation of the mTOR mediated phosphorylation sites in UVRAG induces a profound effect upon lysosomes, demonstrating increased small LAMP1 positive structures that are widely dispersed through the cytoplasm, even upon nutrient deprivation (Figure 5.9). Lysosomal reformation is dependent upon mTOR kinase activity for turnover (Yu et al. 2010) and it is possible that this effect is mediated via UVRAG.

The mechanism by which PI(3)P regulates lysosomes is unclear, however there are multiple possibilities that can be speculated upon and be subjected to further analysis. Treatment with the PIK3C3 inhibitor VPS34-IN1 rapidly causes a distended LAMP1 tubular phenotype similar to that observed upon inhibition of tubular scission (Schulze et al. 2013). It has previously been identified that Dynamin 2 is required for tubule scission at lysosomes and that use of the Dynamin inhibitor dynasore (Macia et al. 2006) rapidly induces a similar LAMP1 positive tubular phenotype (Schulze et al. 2013). The tubulated phenotype upon VPS34-IN1 administration would suggest that loss of PI(3)P or $PI(3,5)P_2$ prevents tubule scission. PIK_{FYVE} that utilises PI(3)P as a substrate to form $PI(3,5)P_2$ (Figure 1.6) has previously been associated with lysosome maturation (Nicot & Fares 2006). In contrast to VPS34-IN1 treatment, prevention of PIK_{FYVE}

activity by knock-out or by using the selective kinase inhibitor YM201636 causes accumulation of large late endosome/lysosome structures without tubule formation (Jefferies et al. 2008; Nicot & Fares 2006). Additionally, preliminary experiments suggest that treatment of either UVRAG wild-type or S550A+S571A rescue cells with YM201636 induces a similar swollen LAMP1 positive phenotype (Data not shown). This would indicate that the requirement of $PI(3,5)P_2$ precedes the regulatory step mediated by UVRAG, but this requires further analysis for confirmation. Whilst data presented here suggests many smaller structures are formed in the UVRAG S550A+S571A mutant, it is possible that they also represent fragmented tubules as a consequence of the fixation method. Preliminary examination by live cell suggests that tubules formed in UVRAG S550A+S571 mutant cells may persist for longer before scission.

Previous research examining the process of lysosomal reformation identified that PI4K and PI5K are localised to lysosomes and that this leads to formation of PI(4)P on lysosomes and $PI(4,5)P_2$ on budding tubular structures (Rong et al. 2012; Sridhar et al. 2013). $PI(4,5)P_2$ is well established to mediate the recruitment of clathrin to the plasma membrane for endocytosis (Ford et al. 2001) and it is assumed that membrane at lysosomes is turned over by an analogous mechanism (Rong et al. 2012). Dynamin is a small GTPase that forms a spiral around membranes and constricts by GTP hydrolysis to pinch off vesicles at the plasma membrane or lysosome tubules (Hinshaw & Schmid 1995; Schulze et al. 2013). Dynamin activity is modulated by phosphoinositides *in vitro,* however PI(4)P and $PI(4,5)P_2$ increased activity 1.5 and 3 fold respectively over PI(3)P (Yarar et al. 2008). Incubation of Dynamin with sorting nexin 9 (SNX9) synergises with multiple phosphoinositides to increase Dynamin activity further, in the presence of PI(3)P and SNX9 the activation of Dynamin is similar to that of $PI(4,5)P_2$ (Yarar et al. 2008). SNX9 belongs to the sub-family of SNX-BAR proteins that are characterised by containing a SNX-PX domain and a C-terminal BAR domain; there are 12 SNX-BAR proteins and this includes SNX1, SNX18, and SNX33 (Weering et al. 2010). The PX and BAR domains act together as co-incident detectors of membranes as mutation of the BAR domain in SNX1 abolishes membrane localisation despite retaining phosphoinositide binding ability (Carlton et al. 2004).

SNX9 is able to tubulate lipids (Shin et al. 2008) and is required for efficient CME at the plasma membrane (Soulet & Yarar 2005). This in part is due to the ability of SNX9 to recruit Dynamin 2 to tubular structures via SH3 domain-mediated interaction with the PRR in Dynamin (Lundmark & Carlsson 2004). Interestingly the PI3K inhibitor LY294002 (Vlahos et al. 1994) prevents tubular recycling from endosomes; removal of LY294002 causes rapid formation of tubular structures that subsequently recruit Dynamin 2 for tubule scission (Carpentier et al. 2013). This indicates that PI(3)P or PI(3,5)P_2 is sufficient and necessary for the recruitment of effectors that mediate tubulation and scission. Data obtained with VPS34-IN1 by contrast promotes distended tubule formation that appears deficient in scission (Figure 5.14). It is possible that a SNX-BAR protein may still be recruited to lysosomes via interaction of the PX domain with PI(4)P or PI(4,5)P_2 due to broad lipid binding ability (Yarar et al. 2007). At early endosomes however the recruitment of SNX-BAR proteins may be exclusively dependent upon PI(3)P or PI(3,5)P_2 as they are thought to be the major phosphoinositide species at this location (Di Paolo & De Camilli 2006). This could potentially explain why tubules only form following removal of LY294002 (Carpentier et al. 2013). Whilst a PX and BAR domain are required for lipid tubulation, an SH3 domain is essential for Dynamin 2 recruitment (Shin et al. 2008). Only SNX9, SNX18 and SNX33 from the SNX-BAR family contain SH3 domains (Weering et al. 2010). SNX18 is suggested to be functionally redundant with SNX9 to mediate CME with Adaptor protein-2 (AP-2) at the plasma membrane (Park et al. 2010). A separate study has indicated that SNX18 primarily functions via an analogous pathway but in combination with Adaptor protein 1 (AP-1) to mediate TGN to endosome trafficking (Håberg et al. 2008). The reported role of SNX18 in AP-1 trafficking (Håberg et al. 2008) is particularly interesting, as it would suggest that separate SNX-BAR proteins can combine with differing Adaptor proteins to mediate distinct clathrin mediated budding events. As yet the role of SNX33 has not been established. Recently, a fifth adaptor protein complex (AP-5) has been identified based upon structural similarity with APs 1-4 (Hirst et al. 2011). AP-5 has been demonstrated to interact with SPG11 and SPG15 (Słabicki et al. 2010), two of the most frequently mutated proteins in hereditary spastic paraplegia (Boukhris et al. 2008; Hanein et al.

2008). Together SPG11 and SPG15 form a coat-like complex that localises to LAMP1 positive structures by immunofluorescence (Hirst et al. 2013) and SPG15 has been identified by mass spectrometry in purified lysosome fractions (Chapel et al. 2013). SPG15 is also known as Spastizin, zFYVE26 or FYVE-CENT, due to the presence of a FYVE domain. The mechanistic role of SPG15 thus far has been established as a key mediator of cytokinesis, the final step of mitosis following chromatid separation that divides the membrane and forms two daughter cells (Sagona et al. 2010). PI(3)P Is critical in this process as depletion of VPS34 causes cytokinesis arrest and increased formation of multinucleate cells, an effect that is replicated upon SPG15 depletion (Sagona et al. 2010). Interestingly, knockdown of SNX9, SNX18 or SNX33 also cause cytokinesis failure and multinucleate cells formation (Ma & Chircop 2012). SPG15 is reported to immunoprecipitate with BECLIN1 and both BECLIN1 and UVRAG are demonstrated to localise to the midbody by immunofluorescence (Sagona et al. 2011; Thoresen et al. 2010). Importantly the localisation of SPG15 to LAMP1 structures is abolished by wortmannin suggesting it is recruited in a PI(3)P dependent manner (Khundadze et al. 2013). Additionally, a SPG15 knockout mouse model accumulates lysosomal enzymes (as seen in Figure 5.9D) and develops late-onset spastic paraplegia (Khundadze et al. 2013). Studies of the zebrafish SPG15 homologue *souffle* (Suf) identified that cortical granule maturation (a lysosome related organelle) is dependent upon Suf (Kanagaraj et al. 2014). Mutation of *suf* causes the accumulation of immature precursors that fail to pinch-off clathrin-coated buds, a phenotype that is also observed by inhibition of Dynamin with the inhibitor dynasore (Kanagaraj et al. 2014). Taken together this suggests that the recruitment of SPG15 to lysosomal structures occurs in a PI(3)P dependent manner and is critical for promoting scission and membrane turnover. Determining whether SPG15, Dynamin 2 and the SNX-BAR SH3 proteins are regulated downstream of UVRAG-dependent PI(3)P formation at the lysosome will be of critical importance. U2OS cell lines expressing Dynamin2-GFP, GFP-SPG15 or GFP-SNX9 are being generated to examine their localisation by immunofluorescence upon lysosomal tubulation. The effect of UVRAG S550A+S571A mutation will then subsequently be examined to determine whether this affects protein localisation.

The localisation of UVRAG to LAMP1 structures (Figure 5.10) is also interesting and it will be important to determine whether this is mediated directly via UVRAG or occurs via another component such as VPS15. UVRAG contains a C2 binding domain that has been demonstrated by lipid overlay to bind to PI(3)P, PI(4)P and PI(5)P (He et al. 2013). PI4K is present at the lysosome and forms PI(4)P (Sridhar et al. 2013) that could localise UVRAG via the C2 domain. Alternatively binding to PI(3)P would suggest a positive feedback loop for further recruitment of the UVRAG-VPS34 complex. This could be explored further by examining the localisation of UVRAG to LAMP1 structures in the presence of VPS34-IN1, additionally mutation of K78A/K82A in the UVRAG C2 domain abolishes phosphoinositide binding (He et al. 2013) and would determine whether recruitment is mediated by lipid binding.

One of the most intriguing and fundamental questions is why UVRAG is an mTORC1 substrate? Traditionally, substrates of mTORC1 are phosphorylated to promote growth pathways such as protein synthesis by 4E-BP1 and p70 S6K (Hara et al. 1997; Price et al. 1992). Alternately phosphorylation by mTORC1 acts to repress catabolic pathways and functions as has been observed with ULK1 and TFEB (Ganley et al. 2009; Roczniak-Ferguson & Petit 2012). Data presented in this thesis indicates a role for UVRAG in lysosomal turnover and consequently it is interesting to consider how UVRAG phosphorylation could impact upon this in a context that may promote growth or inhibit catabolism. Whilst the impact of completely impaired lysosomal turnover is apparent upon SPG15 knockout, the consequence of UVRAG phosphorylation is less clear. Analysis of EGFR degradation (Figure 5.3) or transferrin receptor recycling (Figure 5.5) demonstrated no obvious difference upon UVRAG phosphorylation, although it is possible that defects are managed by increasing the total level of lysosomes. Lysosomal reformation is suggested to be important to maintain a competent pool of lysosomes (Yu et al. 2010), as such it may be important to test trafficking and degradation rates in UVRAG S550A+S571A cells following prolonged periods of stress that may indicate a deficiency in prolonged lysosome maintenance. Given the intricate relationship of mTORC1 with the lysosome for activity (1.3.2), UVRAG phosphorylation may be important to maintain activation or promote downstream

substrate phosphorylation. Peripheral distribution of lysosomes is reported to assist with mTORC1 substrate phosphorylation (Korolchuk et al. 2011) and redistribution to the periphery also occurs during ALR upon mTOR activation (Yu et al. 2010). The Kinesin adaptor protein FYCO1 drives positive directed transport to the periphery in a PI(3)P dependent manner (Pankiv et al. 2010). FYCO1 has also been shown to reduce the formation of tubular lysosomes upon RNAi knockdown (Mrakovic et al. 2012). Increased production of PI(3)P at the lysosome upon UVRAG phosphorylation may act to enhance the association with FYCO1 and peripheral distribution and thereby promote mTORC1 signalling. However, mutation of UVRAG S550A+S571A elicits a diffuse punctate lysosomal staining upon fixation (Figure 5.9). This may represent other abnormalities that impede motor driven transport of lysosomes or may be a staining artefact of tubular structures. The effect of UVRAG upon basal mTOR signalling or recovery in ALR therefore requires further investigation.

UVRAG may promote growth and survival by assisting with efficient cytokinesis as PI(3)P is required for this process (Sagona et al. 2010), work is currently underway to examine whether the phosphorylation of UVRAG alters the rate or efficiency of this process. UVRAG has also been demonstrated to play a role distinct from the VPS34 complex in double-strand break repair pathways that is dependent upon interaction with DNA protein kinase (DNA-PK) via the protein KU-70 (Zhao et al. 2012). This interaction has been reported to occur under basal conditions however preliminary experiments have not been able to resolve an interaction with either UVRAG or VPS34 (data not shown). In addition SPG11 and SPG15 have been reported to interact with the helicase SPG48 and that SPG48 plays a role in double-strand break repair (Słabicki et al. 2010). Whether there is a possible interlinking role between SPG15, SPG48 and UVRAG in DNA damage repair remains to be seen.

The protein UVRAG therefore plays an important role in a myriad of cellular processes. Further work is still required to fully determine the functional consequences of lysosomal irregularities induced by UVRAG phosphorylation site mutations. Currently work has been dependent upon

the use of endogenous UVRAG siRNA and exogenous rescue constructs. This has certain limitations including residual incomplete knockout and limited time-frames for analysis. Work is ongoing to generate knock-in cell lines that express UVRAG S550A and S571A endogenously by utilising CRISPR site-specific nuclease technology (Cong et al. 2013). This would ensure endogenous protein comparison and improve data interpretation.

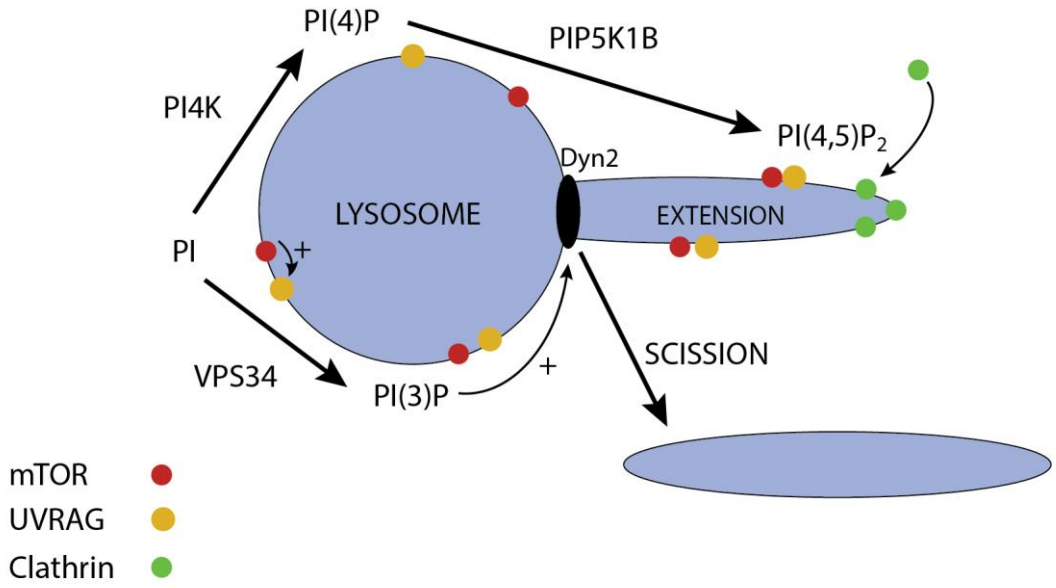

Figure 7.1 – Proposed Model for the Role of Phosphoinositides in Lysosome Reformation

The lysosome is regulated by multiple phosphoinositide species. PI4K forms PI(4)P that is sequentially converted to PI(4,5)P_2 by PIP5K1B that is important to recruit clathrin to the growing bud/extension (Rong et al. 2012). mTORC1 activity is required for tubule formation and can phosphorylate UVRAG to increase PI(3)P production. This has a positive effect upon scission mediated by Dynamin 2 (Dyn2) via a currently unknown pathway or regulator.

In conclusion, the VPS34 interacting protein UVRAG is phosphorylated in an mTOR dependent manner. Mutation of mTOR-mediated phosphorylation sites reduces VPS34 lipid kinase activity and consequently leads to aberrant LAMP1 staining, demonstrating a previously unanticipated link between the generation of PI(3)P and lysosome regulation. This study was originally intent on examination of VPS34 to identify regulatory mechanisms between intracellular trafficking pathways. Whilst the effect of UVRAG phosphorylation on trafficking rate is unclear, it has

unveiled a potentially fundamental aspect of lysosome regulation. This acts to redefine our current understanding of organelle identity and suggests that lysosomes in fact host multiple phosphoinositide species that are essential for function and regulation (Figure 7.1). Additionally this study adds further complexity to the current understanding of interactions between VPS34 and mTOR by suggesting that mTORC1 acts upstream of VPS34 via phosphorylation of UVRAG. One of the key areas to examine next shall be how lysosome regulation impacts upon mTORC1 signalling. mTOR and VPS34 feed into many similar pathways and this study has begun to reveal a reciprocal regulation of these two integral cellular components. This furthers our understanding of mTOR signalling and introduces additional implications for the utilisation of mTOR inhibitors in the clinic. The similarity of lysosome defect in UVRAG S550A+S571A mutants and SPG15 knockout is exciting and may suggest common elements. This study is the first to identify and characterise regulatory phosphorylation of the protein UVRAG and serves as a basis for future analysis. Further characterisation of UVRAG is essential for understanding its implicated role as a tumour suppressor and links to human disease, which could be critical for the development or improvement of future therapeutic strategies.

8 REFERENCES

Aasland, R. et al., 2002. Normalization of nomenclature for peptide motifs as ligands of modular protein domains. *FEBS letters*, 513(1), pp.141–4.

Achiriloaie, M., Barylko, B. & Albanesi, J.P., 1999. Essential Role of the Dynamin Pleckstrin Homology Domain in Receptor-Mediated Endocytosis Essential Role of the Dynamin Pleckstrin Homology Domain in Receptor-Mediated Endocytosis. , 19(2).

Aderem, A. & Underhill, D.M., 1999. Mechanisms of phagocytosis in macrophages. *Annual review of immunology*, 17, pp.593–623.

Alers, S. et al., 2012. The incredible ULKs. *Cell communication and signaling : CCS*, 10(1), p.7.

Alessi, D.R. et al., 1997. Characterization of a 3-phosphoinositide-dependent protein kinase which phosphorylates and activates protein kinase Bα. *Current Biology*, 7(4), pp.261–269.

Arcaro, A. & Wymann, M., 1993. Wortmannin is a potent phosphatidylinositol 3-kinase inhibitor. The role of phosphatidylinositol 3, 4, 5-triphosphate in neutrophil responses. *Biochem J*, 301, pp.297–301.

Axe, E.L. et al., 2008. Autophagosome formation from membrane compartments enriched in phosphatidylinositol 3-phosphate and dynamically connected to the endoplasmic reticulum. *Journal of Cell Biology*, 182, pp.685–701.

Back, J.H. et al., 2011. Cancer cell survival following DNA damage-mediated premature senescence is regulated by mammalian target of rapamycin (mTOR)-dependent Inhibition of sirtuin 1. *The Journal of biological chemistry*, 286(21), pp.19100–8.

Bago, R. et al., 2014. Characterisation of VPS34-IN1, a selective inhibitor of Vps34 reveals that the phosphatidylinositol 3-phosphate binding SGK3 protein kinase is a downstream target of. *The Biochemical Journal*, 34.

Bandyopadhyay, D. et al., 2014. Lysosome transport as a function of lysosome diameter. *PloS one*, 9(1), p.e86847.

Bankaitis, V. a, Johnson, L.M. & Emr, S.D., 1986. Isolation of yeast mutants defective in protein targeting to the vacuole. *Proceedings of the National Academy of Sciences of the United States of America*, 83(23), pp.9075–9.

Banta, L.M. et al., 1988. Organelle assembly in yeast: characterization of yeast mutants defective in vacuolar biogenesis and protein sorting. *The Journal of cell biology*, 107(4), pp.1369–83.

Bar-Peled, L. et al., 2012. Ragulator is a GEF for the rag GTPases that signal amino acid levels to mTORC1. *Cell*, 150(6), pp.1196–208.

Benjamin, D. et al., 2011. Rapamycin passes the torch: a new generation of mTOR inhibitors. *Nature Reviews Drug Discovery*, 10, pp.868–880.

Beretta, L. et al., 1996. Rapamycin blocks the phosphorylation of 4E-BP1 and inhibits cap-dependent initiation of translation. , 15(3), pp.658–664.

Besterman, J.M. & Low, R.B., 1983. Endocytosis: a review of mechanisms and plasma membrane dynamics. *The Biochemical journal*, 210(1), pp.1–13.

Bliek, A. van der & Redelmeier, T., 1993. Mutations in human dynamin block an intermediate stage in coated vesicle formation. *The Journal of cell biology*, 122(3), pp.553–563.

Boukhris, A., Stevanin, G. & Feki, I., 2008. Hereditary spastic paraplegia with mental impairment and thin corpus callosum in Tunisia: SPG11, SPG15, and further genetic heterogeneity. *Archives of biochemistry and biophysics*, 65(3), pp.393–402.

Boussif, O. et al., 1995. A versatile vector for gene and oligonucleotide transfer into cells in culture and in vivo: polyethylenimine. *Proceedings of the National Academy of Sciences of the United States of America*, 92(16), pp.7297–301.

Bradford, M.M., 1976. A rapid and sensitive method for the quantitation of microgram quantities of protein utilizing the principle of protein-dye binding. *Analytical biochemistry*, 72, pp.248–54.

Brown, C.L. et al., 2005. Kinesin-2 is a motor for late endosomes and lysosomes. *Traffic (Copenhagen, Denmark)*, 6(12), pp.1114–24.

Brown, W., Goodhouse, J. & Farquhar, M., 1986. Mannose-6-phosphate receptors for lysosomal enzymes cycle between the Golgi complex and endosomes. *The Journal of cell biology*, 103(October), pp.1235–1247.

Budovskaya, Y. V et al., 2002. The C terminus of the Vps34p phosphoinositide 3-kinase is necessary and sufficient for the interaction with the Vps15p protein kinase. *The Journal of biological chemistry*, 277(1), pp.287–94.

Butler, D. et al., 2011. Protective effects of positive lysosomal modulation in Alzheimer's disease transgenic mouse models. *PloS one*, 6(6), p.e20501.

Byfield, M.P., Murray, J.T. & Backer, J.M., 2005. hVps34 is a nutrient-regulated lipid kinase required for activation of p70 S6 kinase. *The Journal of biological chemistry*, 280(38), pp.33076–82.

Cai, H., Reinisch, K. & Ferro-Novick, S., 2007. Coats, tethers, Rabs, and SNAREs work together to mediate the intracellular destination of a transport vesicle. *Developmental cell*, 12(5), pp.671–82.

Carlsson, S.R. et al., 1988. Isolation and Characterization of Human Lysosomal Membrane Glycoproteins, h-lamp-1 and h-lamp-2. , 263(35), pp.18911–18919.

Carlton, J. et al., 2004. Sorting nexin-1 mediates tubular endosome-to-TGN transport through coincidence sensing of high- curvature membranes and 3-phosphoinositides. *Current biology : CB*, 14(20), pp.1791–800.

Carpentier, S. et al., 2013. Class III phosphoinositide 3-kinase/VPS34 and dynamin are critical for apical endocytic recycling. *Traffic*, 14, pp.933–948.

Carpten, J.D. et al., 2007. A transforming mutation in the pleckstrin homology domain of AKT1 in cancer. *Nature*, 448, pp.439–444.

Caviston, J.P. & Holzbaur, E.L.F., 2006. Microtubule motors at the intersection of trafficking and transport. *Trends in Cell Biology*, 16, pp.530–537.

Chan, E.Y.W., Kir, S. & Tooze, S. a, 2007. siRNA screening of the kinome identifies ULK1 as a multidomain modulator of autophagy. *The Journal of biological chemistry*, 282(35), pp.25464–74.

Chapel, A. et al., 2013. An extended proteome map of the lysosomal membrane reveals novel potential transporters. *Molecular & cellular proteomics : MCP*, 12(6), pp.1572–88.

Cheever, M.L. et al., 2001. Phox domain interaction with PtdIns(3)P targets the Vam7 t-SNARE to vacuole membranes. *Nature cell biology*, 3, pp.613–618.

Cheong, H. et al., 2005. Atg17 regulates the magnitude of the autophagic response. *Molecular biology of the cell*, 16(7), pp.3438–53.

Chiang, H.L. et al., 1989. A role for a 70-kilodalton heat shock protein in lysosomal degradation of intracellular proteins. *Science (New York, N.Y.)*, 246, pp.382–385.

Choo, A.Y. et al., 2008. Rapamycin differentially inhibits S6Ks and 4E-BP1 to mediate cell-type-specific repression of mRNA translation. *Proceedings of the National Academy of Sciences of the United States of America*, 105(45), pp.17414–9.

Christoforidis, S. et al., 1999. The Rab5 effector EEA1 is a core component of endosome docking. *Nature*, 397, pp.621–625.

Cohen, P.T. & Cohen, P., 1989. Discovery of a protein phosphatase activity encoded in the genome of bacteriophage lambda. Probable identity with open reading frame 221. *The Biochemical journal*, 260(3), pp.931–4.

Cohen, S.N., Chang, a C. & Hsu, L., 1972. Nonchromosomal antibiotic resistance in bacteria: genetic transformation of Escherichia coli by R-factor DNA. *Proceedings of the National Academy of Sciences of the United States of America*, 69(8), pp.2110–4.

Cong, L. et al., 2013. Multiplex genome engineering using CRISPR/Cas systems. *Science (New York, N.Y.)*, 339, pp.819–23.

Conner, S.D. & Schmid, S.L., 2003. Regulated portals of entry into the cell. *Nature*, 422(6927), pp.37–44.

Cook, N.R., Row, P.E. & Davidson, H.W., 2004. Lysosome associated membrane protein 1 (Lamp1) traffics directly from the TGN to early endosomes. *Traffic (Copenhagen, Denmark)*, 5(9), pp.685–99.

Csibi, A. et al., 2010. The translation regulatory subunit eIF3f controls the kinase-dependent mTOR signaling required for muscle differentiation and hypertrophy in mouse. *PloS one*, 5(2), p.e8994.

Dahms, N., Lobel, P. & Kornfeld, S., 1989. Mannose 6-phosphate receptors and lysosomal enzyme targeting. *J Biol Chem*, 264(21), pp.12115–12118.

Van Dam, E.M. et al., 2002. Endocytosed transferrin receptors recycle via distinct dynamin and phosphatidylinositol 3-kinase-dependent pathways. *The Journal of biological chemistry*, 277(50), pp.48876–83.

Daro, E. et al., 1996. Rab4 and cellubrevin define different early endosome populations on the pathway of transferrin receptor recycling. *Proceedings of the National Academy of Sciences of the United States of America*, 93(18), pp.9559–64.

Dautry-Varsat, a, Ciechanover, a & Lodish, H.F., 1983. pH and the recycling of transferrin during receptor-mediated endocytosis. *Proceedings of the National Academy of Sciences of the United States of America*, 80(8), pp.2258–62.

Demetri, G. & Mehren, M. von, 2002. Efficacy and safety of imatinib mesylate in advanced gastrointestinal stromal tumors. *… England Journal of …*, 347(7), pp.472–480.

Demetriades, C., Doumpas, N. & Teleman, A.A., 2014. Regulation of TORC1 in response to amino acid starvation via lysosomal recruitment of TSC2. *Cell*, 156, pp.786–799.

Devereaux, K. et al., 2013. Regulation of Mammalian Autophagy by Class II and III PI 3-Kinases through PI3P Synthesis. *PLoS ONE*, 8.

DiFiglia, M. et al., 1997. Aggregation of huntingtin in neuronal intranuclear inclusions and dystrophic neurites in brain. *Science (New York, N.Y.)*, 277, pp.1990–1993.

Doherty, G.J. & McMahon, H.T., 2009. Mechanisms of endocytosis. *Annual review of biochemistry*, 78, pp.857–902.

Dong, X. et al., 2010. PI (3, 5) P2 controls membrane trafficking by direct activation of mucolipin Ca2+ release channels in the endolysosome. *Nature …*, 1(4), pp.1–21.

Duncan, R. & Richardson, S.C.W., 2012. Endocytosis and intracellular trafficking as gateways for nanomedicine delivery: opportunities and challenges. *Molecular pharmaceutics*, 9(9), pp.2380–402.

Dunn, W.A., 1994. Autophagy and related mechanisms of lysosome-mediated protein degradation. *Trends in Cell Biology*, 4, pp.139–143.

Duong-Ly, K.C. & Peterson, J.R., 2013. The human kinome and kinase inhibition. *Current Protocols in Pharmacology*, (SUPPL.60).

Duve, C. de & Wattiaux, R., 1966. Functions of lysosomes. *Annual review of physiology*, (September).

Easton, J.B. & Houghton, P.J., 2006. mTOR and cancer therapy. *Oncogene*, 25(48), pp.6436–46.

Edman, P. & Begg, G., 1967. A protein sequenator. *European Journal of Biochemistry*, 1, pp.80–91.

Ennis, H.L. & Lubin, M., 1964. Cycloheximide: Aspects of Inhibition of Protein Synthesis in Mammalian Cells. *Science (New York, N.Y.)*, 146(3650), pp.1474–6.

Eyster, C. a et al., 2009. Discovery of new cargo proteins that enter cells through clathrin-independent endocytosis. *Traffic (Copenhagen, Denmark)*, 10(5), pp.590–9.

Falasca, M. et al., 2007. The role of phosphoinositide 3-kinase C2alpha in insulin signaling. *The Journal of biological chemistry*, 282(38), pp.28226–36.

Fan, W., Nassiri, A. & Zhong, Q., 2011. Autophagosome targeting and membrane curvature sensing by Barkor/Atg14(L). *Proceedings of the National Academy of Sciences*, 108(19), pp.7769–7774.

Farsad, K. et al., 2001. Generation of high curvature membranes mediated by direct endophilin bilayer interactions. *The Journal of cell biology*, 155(2), pp.193–200.

Fedorko, M., Hirsch, J. & Cohn, Z., 1968. Autophagic vacuoles produced in vitro I. Studies on cultured macrophages exposed to chloroquine. *The Journal of cell biology*, pp.377–391.

Di Fiore, P.P. et al., 1987. erbB-2 is a potent oncogene when overexpressed in NIH/3T3 cells. *Science (New York, N.Y.)*, 237, pp.178–182.

Flinn, R.J. et al., 2010. The late endosome is essential for mTORC1 signaling. *Molecular biology of the cell*, 21(5), pp.833–41.

Ford, M.G. et al., 2001. Simultaneous binding of PtdIns(4,5)P2 and clathrin by AP180 in the nucleation of clathrin lattices on membranes. *Science (New York, N.Y.)*, 291, pp.1051–1055.

Fruman, D. a, Meyers, R.E. & Cantley, L.C., 1998. Phosphoinositide kinases. *Annual review of biochemistry*, 67, pp.481–507.

Fukuda, M. et al., 2011. Genome-wide investigation of the Rab binding activity of RUN domains: development of a novel tool that specifically traps GTP-Rab35. *Cell structure and function*, 36(2), pp.155–70.

Funakoshi, T. et al., 1997. Analyses of APG13 gene involved in autophagy in yeast, Saccharomyces cerevisiae. *Gene*, 192(2), pp.207–213.

Furuya, N. et al., 2005. The Evolutionarily Conserved Domain of Beclin 1 is Required for Vps34 binding, autophagy and tumor suppressor function. , (June), pp.46–52.

Furuya, T. et al., 2010. Negative regulation of Vps34 by Cdk mediated phosphorylation. *Molecular cell*, 38(4), pp.500–511.

Futter, C.E. et al., 2001. Human VPS34 is required for internal vesicle formation within multivesicular endosomes. *The Journal of cell biology*, 155(7), pp.1251–64.

Gaidarov, I. & Keen, J., 1999. Phosphoinositide–AP-2 interactions required for targeting to plasma membrane clathrin-coated pits. *The Journal of cell biology*, 146(4), pp.755–764.

Ganley, I.G. et al., 2009. ULK1.ATG13.FIP200 complex mediates mTOR signaling and is essential for autophagy. *The Journal of biological chemistry*, 284(18), pp.12297–305.

Ganley, I.G., Espinosa, E. & Pfeffer, S.R., 2008. A syntaxin 10-SNARE complex distinguishes two distinct transport routes from endosomes to the trans-Golgi in human cells. *The Journal of cell biology*, 180(1), pp.159–72.

Garami, A. et al., 2003. Insulin activation of Rheb, a mediator of mTOR/S6K/4E-BP signaling, is inhibited by TSC1 and 2. *Molecular cell*, 11(6), pp.1457–66.

García-Martínez, J.M. et al., 2009. Ku-0063794 is a specific inhibitor of the mammalian target of rapamycin (mTOR). *The Biochemical journal*, 421(1), pp.29–42.

García-Martínez, J.M. & Alessi, D., 2008. mTOR complex 2 (mTORC2) controls hydrophobic motif phosphorylation and activation of serum- and glucocorticoid-induced protein kinase 1 (SGK1). *The Biochemical journal*, 416(3), pp.375–85.

Garza, A.M.S., Khan, S.H. & Kumar, R., 2010. Site-specific phosphorylation induces functionally active conformation in the intrinsically disordered N-terminal activation function (AF1) domain of the glucocorticoid receptor. *Molecular and cellular biology*, 30(1), pp.220–30.

Gaullier, J.M. et al., 1998. FYVE fingers bind PtdIns(3)P. *Nature*, 394(6692), pp.432–3.

Gewinner, C. & Wang, Z., 2009. Evidence that inositol polyphosphate 4-phosphatase type II is a tumor suppressor that inhibits PI3K signaling. *Cancer cell*, 16(2), pp.115–125.

Gillooly, D.J. et al., 2000. Localization of phosphatidylinositol 3-phosphate in yeast and mammalian cells. *The EMBO journal*, 19(17), pp.4577–88.

Gingras, A.C., Raught, B. & Sonenberg, N., 1999. eIF4 initiation factors: effectors of mRNA recruitment to ribosomes and regulators of translation. *Annual review of biochemistry*, 68, pp.913–963.

Godi, A. et al., 2004. FAPPs control Golgi-to-cell-surface membrane traffic by binding to ARF and PtdIns(4)P. *Nature cell biology*, 6, pp.393–404.

Goldberg, A.L. & St. John, A.C., 1976. Intracellular Protein Degradation in Mammalian and Bacterial Cells: Part 2. *Annual Review of Biochemistry*, 45(1), pp.747–804.

Gonzalez-Sastre, F. & Folch-Pi, J., 1968. Thin-layer chromatography of the phosphoinositides. *Journal of lipid research*, 9(4), pp.532–3.

Grabowski, G.A., 2008. Phenotype, diagnosis, and treatment of Gaucher's disease. *The Lancet*, 372, pp.1263–1271.

Graham, J., Ford, T. & Rickwood, D., 1994. The preparation of subcellular organelles from mouse liver in self-generated gradients of iodixanol. *Analytical biochemistry*, 220, pp.367–373.

Gray, A., Van Der Kaay, J. & Downes, C.P., 1999. The pleckstrin homology domains of protein kinase B and GRP1 (general receptor for phosphoinositides-1) are sensitive and selective probes for the cellular detection of phosphatidylinositol 3,4-bisphosphate and/or phosphatidylinositol 3,4,5-trisphosphate . *The Biochemical journal*, 344 Pt 3, pp.929–36.

Guertin, D. a et al., 2006. Ablation in mice of the mTORC components raptor, rictor, or mLST8 reveals that mTORC2 is required for signaling to Akt-FOXO and PKCalpha, but not S6K1. *Developmental cell*, 11(6), pp.859–71.

Gururaja, T.L. et al., 2003. Utility of peptide-protein affinity complexes in proteomics: identification of interaction partners of a tumor suppressor peptide. *The journal of peptide research : official journal of the American Peptide Society*, 61(4), pp.163–76.

Ha, S.H. et al., 2006. PLD2 forms a functional complex with mTOR/raptor to transduce mitogenic signals. *Cellular signalling*, 18(12), pp.2283–91.

Vander Haar, E. et al., 2007. Insulin signalling to mTOR mediated by the Akt/PKB substrate PRAS40. *Nature cell biology*, 9(3), pp.316–23.

Håberg, K., Lundmark, R. & Carlsson, S.R., 2008. SNX18 is an SNX9 paralog that acts as a membrane tubulator in AP-1-positive endosomal trafficking. *Journal of cell science*, 121(Pt 9), pp.1495–505.

Haft, C.R. et al., 1998. Identification of a family of sorting nexin molecules and characterization of their association with receptors. *Molecular and cellular biology*, 18(12), pp.7278–87.

Hammond, G.R. V, Schiavo, G. & Irvine, R.F., 2009. Immunocytochemical techniques reveal multiple, distinct cellular pools of PtdIns4P and PtdIns(4,5)P(2). *The Biochemical journal*, 422(1), pp.23–35.

Hanein, S. et al., 2008. Identification of the SPG15 gene, encoding spastizin, as a frequent cause of complicated autosomal-recessive spastic paraplegia, including Kjellin syndrome. *American journal of human genetics*, 82(4), pp.992–1002.

Hanks, S. & Hunter, T., 1995. Protein kinases 6. The eukaryotic protein kinase superfamily: kinase (catalytic) domain structure and classification. *The FASEB journal*.

Hara, K. et al., 2002. Raptor, a binding partner of target of rapamycin (TOR), mediates TOR action. *Cell*, 110(2), pp.177–89.

Hara, K. et al., 1997. Regulation of eIF-4E BP1 Phosphorylation by mTOR. *Journal of Biological Chemistry*, 272(42), pp.26457–26463.

Harada, A. et al., 1998. Golgi vesiculation and lysosome dispersion in cells lacking cytoplasmic dynein. *The Journal of cell biology*, 141(1), pp.51–9.

Hardie, D.G., 2011. AMP-activated protein kinase: an energy sensor that regulates all aspects of cell function. *Genes & development*, 25(18), pp.1895–908.

Harlan, J.E. et al., 1994. Pleckstrin homology domains bind to phosphatidylinositol-4,5-bisphosphate. *Nature*, 371, pp.168–170.

Haslam, R., Koide, H. & Hemmings, B., 1993. Pleckstrin domain homology. *Nature*.

Hayakawa, A. et al., 2006. The WD40 and FYVE domain containing protein 2 defines a class of early endosomes necessary for endocytosis. *Proceedings of the National Academy of Sciences of the United States of America*, 103(32), pp.11928–33.

He, B. et al., 2011. Differential functions of phospholipid binding and palmitoylation of tumour suppressor EWI2/PGRL. *The Biochemical journal*, 437(3), pp.399–411.

He, S. et al., 2013. PtdIns(3)P-bound UVRAG coordinates Golgi-ER retrograde and Atg9 transport by differential interactions with the ER tether and the beclin 1 complex. *Nature cell biology*, 15(10), pp.1206–19.

Herman, P.K. & Emr, S.D., 1990. Characterization of VPS34, a gene required for vacuolar protein sorting and vacuole segregation in Saccharomyces cerevisiae. *Molecular and cellular biology*, 10(12), pp.6742–54.

Herman, P.K., Stack, J.H. & Emr, S.D., 1991. A genetic and structural analysis of the yeast Vps15 protein kinase: evidence for a direct role of Vps15p in vacuolar protein delivery. *The EMBO journal*, 10(13), pp.4049–60.

Hershko, A. & Ciechanover, A., 1982. Mechanisms of Intracellular Protein Breakdown. *Annual Review of Biochemistry*, 51(1), pp.335–364.

Hesse, J., Ebbesen, P. & Kristensen, G., 1978. Correlation between polyion effect on cell susceptibility to in vitro infection with murine C-type viruses and polyion effect on some membrane-related functions. *Intervirology*, 9, pp.173–183.

Hinsby, A.M., Olsen, J. V & Mann, M., 2004. Tyrosine phosphoproteomics of fibroblast growth factor signaling: a role for insulin receptor substrate-4. *The Journal of biological chemistry*, 279(45), pp.46438–47.

Hinshaw, J.E. & Schmid, S.L., 1995. Dynamin self-assembles into rings suggesting a mechanism for coated vesicle budding. *Nature*, 374, pp.190–192.

Hirst, J. et al., 2013. Interaction between AP-5 and the hereditary spastic paraplegia proteins SPG11 and SPG15. *Molecular biology of the cell*, 24(16), pp.2558–69.

Hirst, J. et al., 2011. The fifth adaptor protein complex. *PLoS biology*, 9(10), p.e1001170.

Hoekenga, M.T., 1955. The Treatment of Malaria with Hydroxychloroquine. *The American Journal of Tropical Medicine and Hygiene*, 4(2), pp.221–223.

Hong, F. et al., 2008. mTOR-raptor binds and activates SGK1 to regulate p27 phosphorylation. *Molecular cell*, 30(6), pp.701–11.

Höning, S. et al., 1996. The tyrosine-based lysosomal targeting signal in lamp-1 mediates sorting into Golgi-derived clathrin-coated vesicles. *The EMBO journal*, 15(19), pp.5230–9.

Hosokawa, N. et al., 2009. Nutrient-dependent mTORC1 association with the ULK1-Atg13-FIP200 complex required for autophagy. *Molecular biology of the cell*, 20(7), pp.1981–91.

Hsu, P.P. et al., 2011. The mTOR-regulated phosphoproteome reveals a mechanism of mTORC1-mediated inhibition of growth factor signaling. *Science (New York, N.Y.)*, 332(6035), pp.1317–22.

Ikenoue, T. et al., 2008. Essential function of TORC2 in PKC and Akt turn motif phosphorylation, maturation and signalling. *The EMBO journal*, 27(14), pp.1919–31.

Ikonomov, O., Sbrissa, D. & Shisheva, a, 2001. Mammalian cell morphology and endocytic membrane homeostasis require enzymatically active phosphoinositide 5-kinase PIKfyve. *The Journal of biological chemistry*, 276(28), pp.26141–7.

Inoki, K. et al., 2003. Rheb GTPase is a direct target of TSC2 GAP activity and regulates mTOR signaling. *Genes & development*, 17(15), pp.1829–34.

Ionov, Y. et al., 2004. Manipulation of nonsense mediated decay identifies gene mutations in colon cancer Cells with microsatellite instability. *Oncogene*, 23, pp.639–645.

Ishihara, H. et al., 1999. Molecular cloning of rat SH2-containing inositol phosphatase 2 (SHIP2) and its role in the regulation of insulin signaling. *Biochemical and biophysical research communications*, 260, pp.265–272.

Itakura, E. et al., 2008. Beclin 1 forms two distinct phosphatidylinositol 3-kinase complexes with mammalian Atg14 and UVRAG. *Molecular biology of the cell*, 19, pp.5360–5372.

Jaber, N. et al., 2012. Class III PI3K Vps34 plays an essential role in autophagy and in heart and liver function. *Proc Natl Acad Sci U S A*, 109, pp.2003–2008.

Jacinto, E. et al., 2004. Mammalian TOR complex 2 controls the actin cytoskeleton and is rapamycin insensitive. *Nature cell biology*, 6(11), pp.1122–8.

Jacinto, E. et al., 2006. SIN1/MIP1 maintains rictor-mTOR complex integrity and regulates Akt phosphorylation and substrate specificity. *Cell*, 127(1), pp.125–37.

Jefferies, H.B.J. et al., 2008. A selective PIKfyve inhibitor blocks PtdIns(3,5)P(2) production and disrupts endomembrane transport and retroviral budding. *EMBO reports*, 9(2), pp.164–70.

Johnson, L.M., Bankaitis, V. a & Emr, S.D., 1987. Distinct sequence determinants direct intracellular sorting and modification of a yeast vacuolar protease. *Cell*, 48(5), pp.875–85.

Jones, a T. & Clague, M.J., 1995. Phosphatidylinositol 3-kinase activity is required for early endosome fusion. *The Biochemical journal*, 311 (Pt 1, pp.31–4.

Jones, E., 1977. Proteinase mutants of Saccharomyces cerevisiae. *Genetics*, pp.23–33.

Jung, C.H. et al., 2009. ULK-Atg13-FIP200 complexes mediate mTOR signaling to the autophagy machinery. *Molecular biology of the cell*, 20(7), pp.1992–2003.

Kabeya, Y. et al., 2005. Atg17 functions in cooperation with Atg1 and Atg13 in yeast autophagy. *Molecular biology of the cell*, 16(5), pp.2544–53.

Kabeya, Y. et al., 2000. LC3, a mammalian homologue of yeast Apg8p, is localized in autophagosome membranes after processing. *The EMBO journal*, 19(21), pp.5720–8.

Kamada, Y. et al., 2000. Tor-Mediated Induction of Autophagy via an Apg1 Protein Kinase Complex. *The Journal of Cell Biology*, 150(6), pp.1507–1513.

Kametaka, S. et al., 1998. Apg14p and Apg6/Vps30p Form a Protein Complex Essential for Autophagy in the Yeast, Saccharomyces cerevisiae. *Journal of Biological Chemistry*, 273(35), pp.22284–22291.

Kanagaraj, P. et al., 2014. Souffle/Spastizin controls secretory vesicle maturation during zebrafish oogenesis. *PLoS genetics*, 10(6), p.e1004449.

Kanai, F. et al., 2001. The PX domains of p47phox and p40phox bind to lipid products of PI (3) K. *Nature cell …*, 3(July).

Kang, S. et al., 2013. mTORC1 phosphorylation sites encode their sensitivity to starvation and rapamycin. *Science*, 341(6144), pp.1–16.

Karaman, M.W. et al., 2008. A quantitative analysis of kinase inhibitor selectivity. *Nature biotechnology*, 26, pp.127–132.

Karin, M. & Mintz, B., 1981. Receptor-mediated endocytosis of transferrin in developmentally totipotent mouse teratocarcinoma stem cells. *Journal of Biological Chemistry*, 256(7), pp.3245–3252.

Kenerson, H.L. et al., 2002. Activated Mammalian Target of Rapamycin Pathway in the Pathogenesis of Tuberous Sclerosis Complex Renal Tumors Advances in Brief Activated Mammalian Target of Rapamycin Pathway in the Pathogenesis of Tuberous Sclerosis Complex Renal Tumors 1. , pp.5645–5650.

Khundadze, M. et al., 2013. A hereditary spastic paraplegia mouse model supports a role of ZFYVE26/SPASTIZIN for the endolysosomal system. *PLoS genetics*, 9(12), p.e1003988.

Kihara, A., Kabeya, Y., et al., 2001. Beclin–phosphatidylinositol 3-kinase complex functions at the trans-Golgi network. *EMBO reports*, 2(4), pp.330–335.

Kihara, A., Noda, T., et al., 2001. Two Distinct Vps34 Phosphatidylinositol 3–Kinase Complexes Function in Autophagy and Carboxypeptidase Y Sorting inSaccharomyces cerevisiae. *The Journal of cell biology*, 152(3).

Kim, D.-H. et al., 2002. mTOR interacts with raptor to form a nutrient-sensitive complex that signals to the cell growth machinery. *Cell*, 110(2), pp.163–75.

Kim, J. et al., 2011. AMPK and mTOR regulate autophagy through direct phosphorylation of Ulk1. *Nature cell biology*, 13(2), pp.132–41.

Kim, J. et al., 2013. Differential regulation of distinct Vps34 complexes by AMPK in nutrient stress and autophagy. *Cell*, 152, pp.290–303.

Klionsky, D.J. & Abdalla, F., 2012. Guidelines for the use and interpretation of assays for monitoring autophagy. …, (April), pp.445–544.

Knævelsrud, H. et al., 2010. UVRAG mutations associated with microsatellite unstable colon cancer do not affect autophagy. *Autophagy*, 6, pp.863–870.

Knight, Z. a & Shokat, K.M., 2005. Features of selective kinase inhibitors. *Chemistry & biology*, 12(6), pp.621–37.

Kobayashi, T. & Cohen, P., 1999. glucocorticoid-regulated protein kinase by agonists that activate phosphatidylinositide 3-kinase is mediated by 3-phosphoinositide-dependent protein kinase-1 (PDK1. *Biochem. J*, 328, pp.319–328.

Komatsu, M. et al., 2005. Impairment of starvation-induced and constitutive autophagy in Atg7-deficient mice. *The Journal of cell biology*, 169(3), pp.425–34.

Kornfeld, S., 1987. Trafficking of lysosomal enzymes. *The FASEB journal*.

Korolchuk, V., Saiki, S. & Lichtenberg, M., 2011. Lysosomal positioning coordinates cellular nutrient responses. *Nature cell …*, 13(4), pp.453–460.

Kotoulas, O.B., Kalamidas, S.A. & Kondomerkos, D.J., 2006. Glycogen autophagy in glucose homeostasis. *Pathology - Research and Practice*, 202, pp.631–638.

Kuroyanagi, H. et al., 1998. Human ULK1, a novel serine/threonine kinase related to UNC-51 kinase of Caenorhabditis elegans: cDNA cloning, expression, and chromosomal assignment. *Genomics*, 51, pp.76–85.

Kurten, R.C., Cadena, D.L. & Gill, G.N., 1996. Enhanced degradation of EGF receptors by a sorting nexin, SNX1. *Science (New York, N.Y.)*, 272, pp.1008–1010.

Land, S.C. & Tee, A.R., 2007. Hypoxia-inducible factor 1alpha is regulated by the mammalian target of rapamycin (mTOR) via an mTOR signaling motif. *The Journal of biological chemistry*, 282(28), pp.20534–43.

Lawe, D.C. et al., 2000. The FYVE Domain of Early Endosome Antigen 1 Is Required for Both Phosphatidylinositol 3-Phosphate and Rab5 Binding. CRITICAL ROLE OF THIS DUAL INTERACTION FOR ENDOSOMAL LOCALIZATION. *Journal of Biological Chemistry*, 275(5), pp.3699–3705.

Lemmon, M.A., 2008. Membrane recognition by phospholipid-binding domains. *Nature reviews. Molecular cell biology*, 9(2), pp.99–111.

Lemmon, M.A., 2007. Pleckstrin homology (PH) domains and phosphoinositides. *Biochemical Society symposium*, (74), pp.81–93.

Li, J. et al., 1997. PTEN, a putative protein tyrosine phosphatase gene mutated in human brain, breast, and prostate cancer. *Science (New York, N.Y.)*, 275, pp.1943–1947.

Liang, C. et al., 2006. Autophagic and tumour suppressor activity of a novel Beclin1-binding protein UVRAG. *Nature cell biology*, 8, pp.688–699.

Liang, C. et al., 2008. Beclin1-binding UVRAG targets the class C Vps complex to coordinate autophagosome maturation and endocytic trafficking. *Nature cell biology*, 10, pp.776–787.

Liang, X.H. et al., 1999. Induction of autophagy and inhibition of tumorigenesis by beclin 1. *Nature*, 402, pp.672–676.

Lioubin, M., Algate, P. & Tsai, S., 1996. p150Ship, a signal transduction molecule with inositol polyphosphate-5-phosphatase activity. *Genes & …*, pp.1084–1095.

Lloyd, T. et al., 2002. Hrs Regulates Endosome Membrane Invagination and Tyrosine Kinase Receptor Signaling in Drosophila. *Cell*, 108, pp.261–269.

Loewith, R. et al., 2002. Two TOR complexes, only one of which is rapamycin sensitive, have distinct roles in cell growth control. *Molecular cell*, 10(3), pp.457–68.

Long, X. et al., 2005. Rheb binds and regulates the mTOR kinase. *Current biology : CB*, 15(8), pp.702–13.

Lowenstein, E.J. et al., 1992. The SH2 and SH3 domain-containing protein GRB2 links receptor tyrosine kinases to ras signaling. *Cell*, 70(3), pp.431–42.

Lund, K., Opresko, L. & Starbuck, C., 1990. Quantitative analysis of the endocytic system involved in hormone-induced receptor internalization. *Journal of Biological …*.

Lundmark, R. & Carlsson, S.R., 2004. Regulated membrane recruitment of dynamin-2 mediated by sorting nexin 9. *The Journal of biological chemistry*, 279(41), pp.42694–702.

Ma, M.P.C. & Chircop, M., 2012. SNX9, SNX18 and SNX33 are required for progression through and completion of mitosis. *Journal of cell science*, 125(Pt 18), pp.4372–82.

Macia, E. et al., 2006. Dynasore, a cell-permeable inhibitor of dynamin. *Developmental cell*, 10(6), pp.839–50.

Madsen, K.L. et al., 2010. BAR domains, amphipathic helices and membrane-anchored proteins use the same mechanism to sense membrane curvature. *FEBS letters*, 584(9), pp.1848–55.

Manders, E.M.M., Verbeek, F.J. & Aten, J.A., 1993. Measurement of Colocalization of Objects in Dual-Color Confocal Images. *Journal of Microscopy-Oxford*, 169, pp.375–382.

Masters, C. & Simms, G., 1985. Amyloid plaque core protein in Alzheimer disease and Down syndrome. *Proceedings of the …*, 82(June), pp.4245–4249.

Matsunaga, K. et al., 2010. Autophagy requires endoplasmic reticulum targeting of the PI3-kinase complex via Atg14L. *The Journal of cell biology*, 190(4), pp.511–21.

Matsunaga, K. et al., 2009. Two Beclin 1-binding proteins, Atg14L and Rubicon, reciprocally regulate autophagy at different stages. *Nature cell biology*, 11, pp.385–396.

Matsuura, A. et al., 1997. Apg1p, a novel protein kinase required for the autophagic process in Saccharomyces cerevisiae. *Gene*, 192, pp.245–250.

Mayor, S. & Pagano, R.E., 2007. Pathways of clathrin-independent endocytosis. *Nature reviews. Molecular cell biology*, 8, pp.603–612.

McCartney, A.J., Zhang, Y. & Weisman, L.S., 2014. Phosphatidylinositol 3,5-bisphosphate: low abundance, high significance. *BioEssays : news and reviews in molecular, cellular and developmental biology*, 36(1), pp.52–64.

Van Meer, G. & de Kroon, A.I.P.M., 2011. Lipid map of the mammalian cell. *Journal of cell science*, 124(Pt 1), pp.5–8.

Meikle, P. et al., 1999. Prevalence of lysosomal storage disorders. *Jama*, 281(3), pp.249–254.

Menon, S. et al., 2014. Spatial control of the TSC complex integrates insulin and nutrient regulation of mTORC1 at the lysosome. *Cell*, 156, pp.771–785.

Mijaljica, D., Prescott, M. & Devenish, R.J., 2011. Microautophagy in mammalian cells: Revisiting a 40-year-old conundrum. *Autophagy*, 7(7), pp.673–682.

Milne, S.B. et al., 2005. A targeted mass spectrometric analysis of phosphatidylinositol phosphate species. *Journal of lipid research*, 46(8), pp.1796–802.

Misawa, H. et al., 1998. Cloning and characterization of a novel class II phosphoinositide 3-kinase containing C2 domain. *Biochemical and biophysical research communications*, 244, pp.531–539.

Misra, S. & Hurley, J.H., 1999. Crystal structure of a phosphatidylinositol 3-phosphate-specific membrane-targeting motif, the FYVE domain of Vps27p. *Cell*, 97, pp.657–666.

Mo, R.H. et al., 2012. Effects of Lipofectamine 2000/siRNA complexes on autophagy in hepatoma cells. *Molecular Biotechnology*, 51, pp.1–8.

Mortimore, G.E. & Schworer, C.M., 1977. Induction of autophagy by amino-acid deprivation in perfused rat liver. *Nature*, 270(5633), pp.174–6.

Mrakovic, A. et al., 2012. Rab7 and Arl8 GTPases are necessary for lysosome tubulation in macrophages. *Traffic (Copenhagen, Denmark)*, 13(12), pp.1667–79.

Muller, P. a J. et al., 2009. Mutant p53 drives invasion by promoting integrin recycling. *Cell*, 139(7), pp.1327–41.

Muslin, a J. et al., 1996. Interaction of 14-3-3 with signaling proteins is mediated by the recognition of phosphoserine. *Cell*, 84(6), pp.889–97.

Nakamura, N. & Rabouille, C., 1995. Characterization of a cis-Golgi matrix protein, GM130. *The Journal of cell …*, 131(6), pp.1715–1726.

Nalefski, E. a & Falke, J.J., 1996. The C2 domain calcium-binding motif: structural and functional diversity. *Protein science : a publication of the Protein Society*, 5(12), pp.2375–90.

Neshat, M.S. et al., 2001. Enhanced sensitivity of PTEN-deficient tumors to inhibition of FRAP/mTOR. *Proceedings of the National Academy of Sciences of the United States of America*, 98(18), pp.10314–9.

Neufeld, E.F., 1991. Lysosomal storage diseases. *Annual review of biochemistry*, 60, pp.257–80.

Nicot, A. & Fares, H., 2006. The phosphoinositide kinase PIKfyve/Fab1p regulates terminal lysosome maturation in Caenorhabditis elegans. *Molecular biology of …*, 17(July), pp.3062–3074.

Nobukuni, T. et al., 2005. Amino acids mediate mTOR/raptor signaling through activation of class 3 phosphatidylinositol 3OH-kinase. *Proceedings of the National Academy of Sciences of the United States of America*, 102(40), pp.14238–43.

Noda, T. & Ohsumi, Y., 1998. Tor, a Phosphatidylinositol Kinase Homologue, Controls Autophagy in Yeast. *Journal of Biological Chemistry*, 273(7), pp.3963–3966.

Oshiro, N. et al., 2007. The proline-rich Akt substrate of 40 kDa (PRAS40) is a physiological substrate of mammalian target of rapamycin complex 1. *The Journal of biological chemistry*, 282(28), pp.20329–39.

Pankiv, S. et al., 2010. FYCO1 is a Rab7 effector that binds to LC3 and PI3P to mediate microtubule plus end-directed vesicle transport. *The Journal of cell biology*, 188(2), pp.253–69.

Di Paolo, G. & De Camilli, P., 2006. Phosphoinositides in cell regulation and membrane dynamics. *Nature*, 443(7112), pp.651–7.

Park, J. et al., 2010. SNX18 shares a redundant role with SNX9 and modulates endocytic trafficking at the plasma membrane. *Journal of cell science*, 123(Pt 10), pp.1742–50.

Patki, V. et al., 1997. Identification of an early endosomal protein regulated by phosphatidylinositol 3-kinase. *Proceedings of the National Academy of Sciences of the United States of America*, 94(14), pp.7326–30.

Pearce, L.R. et al., 2011. Protor-1 is required for efficient mTORC2-mediated activation of SGK1 in the kidney. *The Biochemical journal*, 436(1), pp.169–79.

Peña-Llopis, S. et al., 2011. Regulation of TFEB and V-ATPases by mTORC1. *The EMBO journal*, 30(16), pp.3242–58.

Peterson, T.R., Laplante, M. & Thoreen, C., 2009. DEPTOR is an mTOR Inhibitor frequently overexpressed in multiple myeloma cells and required for their survival. *Cell*, 137(5), pp.873–886.

Petiot, A. et al., 2000. Distinct Classes of Phosphatidylinositol 3'-Kinases Are Involved in Signaling Pathways That Control Macroautophagy in HT-29 Cells. *The Journal of Biological Chemistry*, 275(2), pp.992–998.

Van der Ploeg, A.T. & Reuser, A.J., 2008. Pompe's disease. *The Lancet*, 372, pp.1342–1353.

Podsypanina, K. et al., 2001. An inhibitor of mTOR reduces neoplasia and normalizes p70/S6 kinase activity in Pten+/- mice. *Proceedings of the National Academy of Sciences of the United States of America*, 98(18), pp.10320–5.

Polgár, J., Chung, S. & Reed, G., 2002. Vesicle-associated membrane protein 3 (VAMP-3) and VAMP-8 are present in human platelets and are required for granule secretion. *Blood*, 100(3), pp.1081–1083.

Polson, H.E.J. et al., 2010. Mammalian Atg18 (WIPI2) localizes to omegasome-anchored phagophores and positively regulates LC3 lipidation. *Autophagy*, 6(4), pp.506–22.

Potter, C.J., Pedraza, L.G. & Xu, T., 2002. Akt regulates growth by directly phosphorylating Tsc2. *Nature cell biology*, 4, pp.658–665.

Price, D.J. et al., 1992. Rapamycin-induced inhibition of the 70-kilodalton S6 protein kinase. *Science (New York, N.Y.)*, 257, pp.973–977.

Qu, X. et al., 2003. Promotion of tumorigenesis by heterozygous disruption of the beclin 1 autophagy gene. *The Journal of clinical investigation*, 112(12), pp.1809–20.

Rangwala, R. et al., 2014. Combined MTOR and autophagy inhibition: Phase I trial of hydroxychloroquine and temsirolimus in patients with advanced solid tumors and melanoma. …, 1(August), pp.1391–1402.

Ridley, S.H. et al., 2001. FENS-1 and DFCP1 are FYVE domain-containing proteins with distinct functions in the endosomal and Golgi compartments. *Journal of cell science*, 114(Pt 22), pp.3991–4000.

Riggs, K. a et al., 2012. Regulation of integrin endocytic recycling and chemotactic cell migration by syntaxin 6 and VAMP3 interaction. *Journal of cell science*, 125(Pt 16), pp.3827–39.

Roberts, D.J. et al., 2014. Hexokinase-II positively regulates glucose starvation-induced autophagy through TORC1 inhibition. *Molecular cell*, 53(4), pp.521–33.

Robinson, J.S. et al., 1988. Protein sorting in Saccharomyces cerevisiae: isolation of mutants defective in the delivery and processing of multiple vacuolar hydrolases. *Molecular and cellular biology*, 8(11), pp.4936–48.

Roczniak-Ferguson, A. & Petit, C., 2012. The transcription factor TFEB links mTORC1 signaling to transcriptional control of lysosome homeostasis. *Sci Signal*, 5(228).

Rohrer, J. et al., 1996. The targeting of Lamp1 to lysosomes is dependent on the spacing of its cytoplasmic tail tyrosine sorting motif relative to the membrane. *The Journal of cell biology*, 132(4), pp.565–76.

Rong, Y. et al., 2012. Clathrin and phosphatidylinositol-4,5-bisphosphate regulate autophagic lysosome reformation. *Nature Cell Biology*, 14, pp.924–934.

Rong, Y. et al., 2011. Spinster is required for autophagic lysosome reformation and mTOR reactivation following starvation. *Proceedings of the National Academy of Sciences*, 108(27), pp.11297–11297.

Rothman, J.H., Howald, I. & Stevens, T.H., 1989. Characterization of genes required for protein sorting and vacuolar function in the yeast Saccharomyces cerevisiae. *The EMBO journal*, 8(7), pp.2057–65.

Rothman, J.H. & Stevens, T.H., 1986. Protein sorting in yeast: mutants defective in vacuole biogenesis mislocalize vacuolar proteins into the late secretory pathway. *Cell*, 47(6), pp.1041–51.

Rousseau, D. et al., 1996. The eIF4E-binding proteins 1 and 2 are negative regulators of cell growth. *Oncogene*, 13, pp.2415–2420.

Russell, R.C. et al., 2013. ULK1 induces autophagy by phosphorylating Beclin-1 and activating VPS34 lipid kinase. *Nature Cell Biology*, 15, pp.741–750.

Sagona, A.P. et al., 2011. A tumor-associated mutation of FYVE-CENT prevents its interaction with Beclin 1 and interferes with cytokinesis. *PLoS ONE*, 6.

Sagona, A.P. et al., 2010. PtdIns(3)P controls cytokinesis through KIF13A-mediated recruitment of FYVE-CENT to the midbody. *Nature cell biology*, 12, pp.362–371.

Samuels, Y. et al., 2004. High frequency of mutations of the PIK3CA gene in human cancers. *Science (New York, N.Y.)*, 304, p.554.

Sancak, Y. et al., 2007. PRAS40 is an insulin-regulated inhibitor of the mTORC1 protein kinase. *Molecular cell*, 25(6), pp.903–15.

Sancak, Y. et al., 2010. Ragulator-Rag complex targets mTORC1 to the lysosomal surface and is necessary for its activation by amino acids. *Cell*, 141(2), pp.290–303.

Sancak, Y. et al., 2008. The Rag GTPases bind raptor and mediate amino acid signaling to mTORC1. *Science (New York, N.Y.)*, 320(5882), pp.1496–501.

Sarbassov, D.D. et al., 2004. Rictor, a novel binding partner of mTOR, defines a rapamycin-insensitive and raptor-independent pathway that regulates the cytoskeleton. *Current biology : CB*, 14(14), pp.1296–302.

Sardiello, M. et al., 2009. A gene network regulating lysosomal biogenesis and function. *Science (New York, N.Y.)*, 325(5939), pp.473–7.

Sbrissa, D., Ikonomov, O. & Shisheva, a., 1999. PIKfyve, a Mammalian Ortholog of Yeast Fab1p Lipid Kinase, Synthesizes 5-Phosphoinositides: EFFECT OF INSULIN. *Journal of Biological Chemistry*, 274(31), pp.21589–21597.

Schalm, S. et al., 2003. TOS motif-mediated raptor binding regulates 4E-BP1 multisite phosphorylation and function. *Current biology*, 13, pp.797–806.

Schalm, S.S. & Blenis, J., 2002. Identification of a conserved motif required for mTOR signaling. *Current biology : CB*, 12(8), pp.632–9.

Schindelin, J. et al., 2012. Fiji: an open-source platform for biological-image analysis. *Nature methods*, 9(7), pp.676–82.

Schlessinger, J., 1988. Signal transduction by allosteric receptor oligomerization. *Trends in biochemical sciences*, 13, pp.443–447.

Schmidt-Ullrich, R.K. et al., 1997. Radiation-induced proliferation of the human A431 squamous carcinoma cells is dependent on EGFR tyrosine phosphorylation. *Oncogene*, 15, pp.1191–1197.

Schnitzer, J.E. et al., 1994. Filipin-sensitive caveolae-mediated transport in endothelium: reduced transcytosis, scavenger endocytosis, and capillary permeability of select macromolecules. *The Journal of cell biology*, 127(5), pp.1217–32.

Schu, P. V et al., 1993. Phosphatidylinositol 3-kinase encoded by yeast VPS34 gene essential for protein sorting. *Science (New York, N.Y.)*, 260(5104), pp.88–91.

Schulze, R.J. et al., 2013. Lipid droplet breakdown requires dynamin 2 for vesiculation of autolysosomal tubules in hepatocytes. *The Journal of cell biology*, 203(2), pp.315–26.

Schulze, W.X. & Mann, M., 2004. A novel proteomic screen for peptide-protein interactions. *The Journal of biological chemistry*, 279(11), pp.10756–64.

Sebaugh, J.L., 2011. Guidelines for accurate EC50/IC50 estimation. *Pharmaceutical Statistics*, 10, pp.128–134.

Sengupta, S., Peterson, T.R. & Sabatini, D.M., 2010. Regulation of the mTOR complex 1 pathway by nutrients, growth factors, and stress. *Molecular cell*, 40(2), pp.310–22.

Settembre, C. et al., 2012. A lysosome-to-nucleus signalling mechanism senses and regulates the lysosome via mTOR and TFEB. *The EMBO journal*, 31(5), pp.1095–108.

Settembre, C., Malta, C. Di & Polito, V., 2011. TFEB links autophagy to lysosomal biogenesis. *Science*, 332(6036), pp.1429–1433.

Shang, L. et al., 2011. Nutrient starvation elicits an acute autophagic response mediated by Ulk1 dephosphorylation and its subsequent dissociation from AMPK. *Proceedings of the National Academy of Sciences of the United States of America*, 108(12), pp.4788–93.

Shayesteh, L. et al., 1999. PIK3CA is implicated as an oncogene in ovarian cancer. *Nature genetics*, 21, pp.99–102.

Shin, N. et al., 2008. SNX9 regulates tubular invagination of the plasma membrane through interaction with actin cytoskeleton and dynamin 2. *Journal of cell science*, 121(Pt 8), pp.1252–63.

Siddhanta, U., McIlroy, J. & Shah, A., 1998. Distinct roles for the p110α and hVPS34 phosphatidylinositol 3'-kinases in vesicular trafficking, regulation of the actin cytoskeleton, and mitogenesis. *The Journal of cell …*, 143(6), pp.1647–1659.

Sigismund, S. et al., 2005. Clathrin-independent endocytosis of ubiquitinated cargos. *Proceedings of the National Academy of Sciences of the United States of America*, 102(8), pp.2760–5.

Sigismund, S. et al., 2008. Clathrin-mediated internalization is essential for sustained EGFR signaling but dispensable for degradation. *Developmental cell*, 15(2), pp.209–19.

Sigismund, S. et al., 2012. Endocytosis and signaling: cell logistics shape the eukaryotic cell plan. *Physiological reviews*, 92(1), pp.273–366.

Simonsen, A., Lippe, R. & Christoforidis, S., 1998. EEA1 links PI(3)K function to Rab5 regulation of endosome fusion. *Nature*, 394(JULY), pp.2–6.

Słabicki, M. et al., 2010. A genome-scale DNA repair RNAi screen identifies SPG48 as a novel gene associated with hereditary spastic paraplegia. *PLoS biology*, 8(6), p.e1000408.

Slamon, D.J. et al., 1987. Human breast cancer: correlation of relapse and survival with amplification of the HER-2/neu oncogene. *Science (New York, N.Y.)*, 235, pp.177–182.

Smith, E.M. et al., 2005. The tuberous sclerosis protein TSC2 is not required for the regulation of the mammalian target of rapamycin by amino acids and certain cellular stresses. *The Journal of biological chemistry*, 280(19), pp.18717–27.

Söllner, T. et al., 1993. SNAP receptors implicated in vesicle targeting and fusion. *Nature*, 362, pp.318–324.

Song, X. et al., 2001. Phox homology domains specifically bind phosphatidylinositol phosphates. *Biochemistry*, 40, pp.8940–8944.

Soulet, F. & Yarar, D., 2005. SNX9 regulates dynamin assembly and is required for efficient clathrin-mediated endocytosis. *Molecular biology of the …*, 16(April), pp.2058–2067.

Sridhar, S. et al., 2013. The lipid kinase PI4KIIIβ preserves lysosomal identity. *The EMBO journal*, 32(3), pp.324–39.

Stack, J.H. et al., 1993. A membrane-associated complex containing the Vps15 protein kinase and the Vps34 PI 3-kinase is essential for protein sorting to the yeast lysosome-like vacuole. *The EMBO journal*, 12(5), pp.2195–204.

Stack, J.H. et al., 1995. Vesicle-mediated protein transport: regulatory interactions between the Vps15 protein kinase and the Vps34 PtdIns 3-kinase essential for protein sorting to the vacuole in yeast. *The Journal of cell biology*, 129(2), pp.321–34.

Stack, J.H. & Emr, S.D., 1994. Vps34p required for yeast vacuolar protein sorting is a multiple specificity kinase that exhibits both protein kinase and phosphatidylinositol-specific PI 3-kinase activities. *The Journal of biological chemistry*, 269(50), pp.31552–62.

Steck, P.A. et al., 1997. Identification of a candidate tumour suppressor gene, MMAC1, at chromosome 10q23.3 that is mutated in multiple advanced cancers. *Nature genetics*, 15, pp.356–362.

Steinman, R.M. et al., 1983. Endocytosis and the recycling of plasma membrane. *The Journal of cell biology*, 96(1), pp.1–27.

Stenmark, H. et al., 1996. Endosomal Localization of the Autoantigen EEA1 Is Mediated by a Zinc-binding FYVE Finger. *Journal of Biological Chemistry*, 271(39), pp.24048–24054.

Stephens, L., Eguinoa, A. & Corey, S., 1993. Receptor stimulated accumulation of phosphatidylinositol (3, 4, 5)-trisphosphate by G-protein mediated pathways in human myeloid derived cells. *The EMBO …*, 12(6), pp.2265–2273.

Stevens, T., Esmon, B. & Schekman, R., 1982. Early stages in the yeast secretory pathway are required for transport of carboxypeptidase Y to the vacuole. *Cell*, 30, pp.439–448.

Stevens, T.H. et al., 1986. Gene dosage-dependent secretion of yeast vacuolar carboxypeptidase Y. *The Journal of cell biology*, 102(5), pp.1551–7.

Sullivan, A., Grasso, J. & Weintraub, L., 1976. Micropinocytosis of transferrin by developing red cells: an electron-microscopic study utilizing ferritin-conjugated transferrin and ferritin-conjugated antibodies to. *Blood*, 47(1), pp.133–143.

Sun et al., 2010. The RUN Domain of Rubicon Is Important for hVps34 Binding, Lipid Kinase Inhibition, and Autophagy Suppression. *Journal of Biological Chemistry*, 286(1), pp.185–191.

Sun, Q. et al., 2008. Identification of Barkor as a mammalian autophagy-specific factor for Beclin 1 and class III phosphatidylinositol 3-kinase. *Proceedings of the National Academy of Sciences of the United States of America*, 105, pp.19211–19216.

Sutton, R.B. et al., 1995. Structure of the first C2 domain of synaptotagmin I: a novel Ca2+/phospholipid-binding fold. *Cell*, 80(6), pp.929–38.

Suzuki, T. et al., 2007. Differential regulation of caspase-1 activation, pyroptosis, and autophagy via Ipaf and ASC in Shigella-infected macrophages. *PLoS pathogens*, 3(8), p.e111.

Takahashi, Y. et al., 2007. Bif-1 interacts with Beclin 1 through UVRAG and regulates autophagy and tumorigenesis. *Nature cell biology*, 9, pp.1142–1151.

Takahashi, Y., Meyerkord, C.L. & Wang, H.-G., 2009. Bif-1/endophilin B1: a candidate for crescent driving force in autophagy. *Cell death and differentiation*, 16, pp.947–955.

Takeshige, K. et al., 1992. Autophagy in yeast demonstrated with proteinase-deficient mutants and conditions for its induction. *The Journal of cell biology*, 119(2), pp.301–11.

Taylor, G.S., Maehama, T. & Dixon, J.E., 2000. Myotubularin, a protein tyrosine phosphatase mutated in myotubular myopathy, dephosphorylates the lipid second messenger, phosphatidylinositol 3-phosphate. *Proceedings of the National Academy of Sciences of the United States of America*, 97(16), pp.8910–5.

Tee, A.R. et al., 2003. Tuberous sclerosis complex gene products, Tuberin and Hamartin, control mTOR signaling by acting as a GTPase-activating protein complex toward Rheb. *Current biology : CB*, 13(15), pp.1259–68.

Teitz, T. et al., 1990. Isolation by polymerase chain reaction of a cDNA whose product partially complements the ultraviolet sensitivity of xeroderma pigmentosum group C cells. *Gene*, 87(2), pp.295–8.

Thomas, C.C. et al., 2002. High-resolution structure of the pleckstrin homology domain of protein kinase b/akt bound to phosphatidylinositol (3,4,5)-trisphosphate. *Current biology : CB*, 12(14), pp.1256–62.

Thoreen, C.C. et al., 2009. An ATP-competitive mammalian target of rapamycin inhibitor reveals rapamycin-resistant functions of mTORC1. *The Journal of biological chemistry*, 284(12), pp.8023–32.

Thoresen, S.B. et al., 2010. A phosphatidylinositol 3-kinase class III sub-complex containing VPS15, VPS34, Beclin 1, UVRAG and BIF-1 regulates cytokinesis and degradative endocytic traffic. *Experimental Cell Research*, 316, pp.3368–3378.

Thumm, M., Egner, R. & Koch, B., 1994. Isolation of autophagocytosis mutants of Saccharomyces cerevisiae. *FEBS letters*, 349, pp.275–280.

Tracy, K. et al., 2007. BNIP3 is an RB/E2F target gene required for hypoxia-induced autophagy. *Molecular and cellular biology*, 27(17), pp.6229–42.

Traub, L., Ostrom, J. & Kornfeld, S., 1993. Biochemical dissection of AP-1 recruitment onto Golgi membranes. *The Journal of cell biology*, 123(3), pp.561–573.

Traub, L.M., 2003. Sorting it out: AP-2 and alternate clathrin adaptors in endocytic cargo selection. *The Journal of cell biology*, 163(2), pp.203–8.

Tsukada, M. & Ohsumi, Y., 1993. Isolation and characterization of autophagy-defective mutants of saccharomyces cerevisiae. *FEBS letters*, 333(1), pp.169–174.

Ullrich, O., Reinsch, S. & Urbé, S., 1996. Rab11 regulates recycling through the pericentriolar recycling endosome. *The Journal of cell …*, 135(4), pp.913–924.

Vasquez, R.J. et al., 1997. Nanomolar concentrations of nocodazole alter microtubule dynamic instability in vivo and in vitro. *Molecular biology of the cell*, 8(6), pp.973–85.

Vivanco, I. & Sawyers, C.L., 2002. The phosphatidylinositol 3-Kinase AKT pathway in human cancer. *Nat Rev Cancer*, 2, pp.489–501.

Vlahos, C.J. et al., 1994. A specific inhibitor of phosphatidylinositol 3-kinase, 2-(4-morpholinyl)-8-phenyl-4H-1-benzopyran-4-one (LY294002). *Journal of Biological Chemistry*, 269(7), pp.5241–5248.

Vogelstein, B., Lane, D. & Levine, A.J., 2000. Surfing the p53 network. *Nature*, 408, pp.307–310.

Volinia, S. et al., 1995. A human phosphatidylinositol 3-kinase complex related to the yeast Vps34p-Vps15p protein sorting system. *The EMBO journal*, 14(14), pp.3339–48.

Walker, D. et al., 2001. Characterization of MTMR3: an inositol lipid 3-phosphatase with novel substrate specificity. *Current Biology*, 3, pp.1600–1605.

Weering, J. van, Verkade, P. & Cullen, P.J., 2010. SNX–BAR proteins in phosphoinositide-mediated, tubular-based endosomal sorting. *Seminars in cell & developmental …*, 21(4), pp.371–380.

Wells, A. et al., 1990. Ligand-induced transformation by a noninternalizing epidermal growth factor receptor. *Science (New York, N.Y.)*, 247, pp.962–964.

Whitman, M. et al., 1988. Type I phosphatidylinositol kinase makes a novel inositol phospholipid, phosphatidylinositol-3-phosphate. *Nature*.

Williamson, M.P., 1994. The structure and function of proline-rich regions in proteins. *The Biochemical journal*, 297 (Pt 2, pp.249–60.

Wong, A.S.L. et al., 2011. Cdk5-mediated phosphorylation of endophilin B1 is required for induced autophagy in models of Parkinson's disease. *Nature cell biology*, 13(5), pp.568–79.

Xia, P. et al., 2014. RNF2 is recruited by WASH to ubiquitinate AMBRA1 leading to downregulation of autophagy. *Cell research*, 24(8), pp.943–58.

Xia, P. et al., 2013. WASH inhibits autophagy through suppression of Beclin 1 ubiquitination. *The EMBO journal*, 32(20), pp.2685–96.

Xie, X., White, E.P. & Mehnert, J.M., 2013. Coordinate autophagy and mTOR pathway inhibition enhances cell death in melanoma. *PloS one*, 8(1), p.e55096.

Xu, Y. et al., 2013. Protein charge and mass contribute to the spatio-temporal dynamics of protein–protein interactions in a minimal proteome. *Proteomics*, 13(8), pp.1339–1351.

Yaffe, M. et al., 1997. The structural basis for 14-3-3: phosphopeptide binding specificity. *Cell*, 91, pp.961–971.

Yamamoto, A. & Tagawa, Y., 1998. Bafilomycin A1 Prevents Maturation of Autophagic Vacuoles by Inhibiting Fusion between Autophagosomes and Lysosomes in Rat Hepatoma Cell Line. *Cell structure and …*, 42, pp.33–42.

Yamamoto, H. et al., 2010. Functional cross-talk between Rab14 and Rab4 through a dual effector, RUFY1/Rabip4. *Molecular biology of the cell*, 21(15), pp.2746–55.

Yamazaki, T. et al., 2002. Role of Grb2 in EGF-stimulated EGFR internalization. *Journal of cell science*, 115(Pt 9), pp.1791–802.

Yan, J. et al., 1998. Identification of mouse ULK1, a novel protein kinase structurally related to C. elegans UNC-51. *Biochemical and biophysical research communications*, 246, pp.222–227.

Yang, Q. et al., 2006. Identification of Sin1 as an essential TORC2 component required for complex formation and kinase activity. *Genes & development*, 20(20), pp.2820–32.

Yarar, D. et al., 2008. SNX9 activities are regulated by multiple phosphoinositides through both PX and BAR domains. *Traffic (Copenhagen, Denmark)*, 9(1), pp.133–46.

Yarar, D., Waterman-Storer, C.M. & Schmid, S.L., 2007. SNX9 couples actin assembly to phosphoinositide signals and is required for membrane remodeling during endocytosis. *Developmental cell*, 13(1), pp.43–56.

Yoshimori, T. et al., 1991. Bafilomycin A1, a specific inhibitor of vacuolar-type H(+)-ATPase, inhibits acidification and protein degradation in lysosomes of cultured cells. *The Journal of biological chemistry*, 266(26), pp.17707–12.

Yu, L. et al., 2010. Termination of autophagy and reformation of lysosomes regulated by mTOR. *Nature*, 465, pp.942–946.

Yu, Y. et al., 2011. Phosphoproteomic analysis identifies Grb10 as an mTORC1 substrate that negatively regulates insulin signaling. *Science (New York, N.Y.)*, 332(6035), pp.1322–6.

Yuan, H.-X., Russell, R.C. & Guan, K.-L., 2013. Regulation of PIK3C3/VPS34 complexes by MTOR in nutrient stress-induced autophagy. *Autophagy*, 9, pp.1983–95.

Yue, Z. et al., 2003. Beclin 1, an autophagy gene essential for early embryonic development, is a haploinsufficient tumor suppressor. *Proceedings of the National Academy of Sciences of the United States of America*, 100(25), pp.15077–82.

Zarate, Y.A. & Hopkin, R.J., 2008. Fabry's disease. *The Lancet*, 372, pp.1427–1435.

Zhao, Z. et al., 2012. A Dual Role for UVRAG in Maintaining Chromosomal Stability Independent of Autophagy. *Developmental Cell*, 22, pp.1001–1016.

Zhong, Q. et al., 2002. Endosomal localization and function of sorting nexin 1. *Proceedings of the National Academy of Sciences of the United States of America*, 99(10), pp.6767–72.

Zhong, Y. et al., 2009. Distinct regulation of autophagic activity by Atg14L and Rubicon associated with Beclin 1-phosphatidylinositol-3-kinase complex. *Nature cell biology*, 11, pp.468–476.

Zhou, X., Takatoh, J. & Wang, F., 2011. The mammalian class 3 PI3K (PIK3C3) is required for early embryogenesis and cell proliferation. *PloS one*, 6(1), p.e16358.

Zhou, X. & Wang, L., 2010. Deletion of PIK3C3/Vps34 in sensory neurons causes rapid neurodegeneration by disrupting the endosomal but not the autophagic pathway. *Proceedings of the …*, pp.1–6.

Zhuo, S. et al., 1993. Expression, purification, crystallization, and biochemical characterization of a recombinant protein phosphatase. *The Journal of biological chemistry*, 268(24), pp.17754–61.

Zolov, S. et al., 2012. In vivo, Pikfyve generates PI (3, 5) P2, which serves as both a signaling lipid and the major precursor for PI5P. *Proceedings of the …*, 109(43), pp.17472–17477.

Zoncu, R. et al., 2009. A phosphoinositide switch controls the maturation and signaling properties of APPL endosomes. *Cell*, 136(6), pp.1110–21.

Zoncu, R. et al., 2011. mTORC1 senses lysosomal amino acids through an inside-out mechanism that requires the vacuolar H(+)-ATPase. *Science (New York, N.Y.)*, 334(6056), pp.678–83.

9 APPENDIX

9.1 APPENDIX A

Appendix A - – GST-UVRAG wild-type interacting proteins from experiment described in (Table 11), hits marked with an asterisk (*) are included on the curated list.

REF		Score	Peptides	Coverage	Gene	Name
Q9P2Y5	*	3391	253	71%	UVRAG	UV radiation resistance-associated gene protein
P68363	*	1150	53	54%	TUBA1B	Tubulin alpha-1B chain
Q9BVA1	*	589	28	46%	TUBB2B	Tubulin beta-2B chain
Q13509		457	19	25%	TUBB3	Tubulin beta-3 chain
Q6S8J3		376	18	9%	POTEE	POTE ankyrin domain family member E
Q02878		358	18	34%	RPL6	60S ribosomal protein L6
P26373		298	27	45%	RPL13	60S ribosomal protein L13
P12235		296	27	26%	SLC25A4	ADP/ATP translocase 1
P57721		284	9	15%	PCBP3	Poly(rC)-binding protein 3
P55884		214	12	10%	EIF3B	Eukaryotic translation initiation factor 3 subunit B
Q6S8J3		203	8	3%	POTEE	POTE ankyrin domain family member E
Q13200		198	12	7%	PSMD2	26S proteasome non-ATPase regulatory subunit 2
P42677		177	13	14%	RPS27	40S ribosomal protein S27
Q8N122	*	173	13	9%	RPTOR	Regulatory-associated protein of mTOR
P63167	*	170	5	37%	DYNLL1	Dynein light chain 1, cytoplasmic
P83731		168	5	13%	RPL24	60S ribosomal protein L24
P62306		157	2	7%*	SNRPF	Small nuclear ribonucleoprotein F
P13929		143	3	9%	ENO3	Beta-enolase
Q15019		135	7	14%	Sep-02	Septin-2
Q99570	*	135	16	9%	PIK3R4	Phosphoinositide 3-kinase regulatory subunit 4
O95071	*	132	9	3%	UBR5	E3 ubiquitin-protein ligase UBR5
P60900		132	2	5%	PSMA6	Proteasome subunit alpha type-6
P62829		126	12	37%	RPL23	60S ribosomal protein L23
P36542		115	6	11%	ATP5C1	ATP synthase subunit gamma, mitochondrial
P63220		113	7	33%	RPS21	40S ribosomal protein S21
Q13347		113	8	28%	EIF3I	Eukaryotic translation initiation factor 3 subunit I
P61981	*	108	3	8%	YWHAG	14-3-3 protein gamma
P53675	*	102	8	4%	CLTCL1	Clathrin heavy chain 2
P10809		98	7	14%	HSPD1	60 kDa heat shock protein, mitochondrial
P60468		98	6	37%	SEC61B	Protein transport protein Sec61 subunit beta
P14618		96	4	5%	PKM2	Pyruvate kinase isozymes M1/M2
Q9H853		95	5	21%	TUBA4B	Putative tubulin-like protein alpha-4B
Q15836	*	94	3	24%	VAMP3	Vesicle-associated membrane protein 3
P62753		88	13	30%	RPS6	40S ribosomal protein S6
Q6S8J3		85	4	2%	POTEE	POTE ankyrin domain family member E
Q14240		84	3	8%	EIF4A2	Eukaryotic initiation factor 4A-II
P05109		83	2	11%	S100A8	Protein S100-A8
Q14257		83	5	7%	RCN2	Reticulocalbin-2
O95816		81	8	19%	BAG2	BAG family molecular chaperone regulator 2
Q58FG0		81	6	13%	HSP90AA5P	Putative heat shock protein HSP 90-alpha A5
Q96L21		79	6	16%	RPL10L	60S ribosomal protein L10-like
Q14157		77	3	4%	UBAP2L	Ubiquitin-associated protein 2-like
O15027		76	5	3%	SEC16A	Protein transport protein Sec16A
P12004		76	3	7%	PCNA	Proliferating cell nuclear antigen
Q07020		76	7	11%	RPL18	60S ribosomal protein L18
O00410		75	2	2%	IPO5	Importin-5
P18124		74	4	20%	RPL7	60S ribosomal protein L7
P49207		74	6	16%	RPL34	60S ribosomal protein L34
P58546		73	2	14%	MTPN	Myotrophin
P06703		71	2	8%	S100A6	Protein S100-A6
P46779		71	18	54%	RPL28	60S ribosomal protein L28
P62942		68	2	8%	FKBP1A	Peptidyl-prolyl cis-trans isomerase FKBP1A
Q8NEB9	*	68	6	6%	PIK3C3	Phosphatidylinositol 3-kinase catalytic subunit type 3

P33176	*	65	8	8%	KIF5B	Kinesin-1 heavy chain
Q14839		65	3	1%	CHD4	Chromodomain-helicase-DNA-binding protein 4
P55209		64	4	11%	NAP1L1	Nucleosome assembly protein 1-like 1
P31943		62	4	8%	HNRNPH1	Heterogeneous nuclear ribonucleoprotein H
P11586		59	9	9%	MTHFD1	C-1-tetrahydrofolate synthase, cytoplasmic
P35580		59	8	3%	MYH10	Myosin-10
P39019		59	3	20%	RPS19	40S ribosomal protein S19
P14136		58	3	9%	GFAP	Glial fibrillary acidic protein
P55795		58	4	5%	HNRNPH2	Heterogeneous nuclear ribonucleoprotein H2
O60282		57	3	3%	KIF5C	Kinesin heavy chain isoform 5C
Q12840		57	3	3%	KIF5A	Kinesin heavy chain isoform 5A
Q9Y490		57	6	2%	TLN1	Talin-1
P62263		56	3	15%	RPS14	40S ribosomal protein S14
P62424		56	14	32%	RPL7A	60S ribosomal protein L7a
P41252		55	5	1%	IARS	Isoleucyl-tRNA synthetase, cytoplasmic
P55786		55	2	2%	NPEPPS	Puromycin-sensitive aminopeptidase
Q9Y281		55	2	6%	CFL2	Cofilin-2
P35268		54	1	10%	RPL22	60S ribosomal protein L22
P55072		53	3	2%	VCP	Transitional endoplasmic reticulum ATPase
Q15154		53	5	1%	PCM1	Pericentriolar material 1 protein
P23246		52	10	15%	SFPQ	Splicing factor, proline- and glutamine-rich
P40429		52	8	17%	RPL13A	60S ribosomal protein L13a
Q5JNZ5		52	6	7%	RPS26P11	Putative 40S ribosomal protein S26-like 1
Q9Y277	*	52	4	10%	VDAC3	Voltage-dependent anion-selective channel protein 3
P61289		51	1	5%	PSME3	Proteasome activator complex subunit 3
A5A3E0		50	5	7%	POTEF	POTE ankyrin domain family member F
Q92538		50	4	1%	GBF1	Golgi-specific brefeldin A-resistance guanine nucleotide exchange factor 1
Q9UBP0	*	32	4	3%	SPAST	Spastin

9.2 APPENDIX B

Appendix B - GST-UVRAG S550A interacting proteins from experiment described in (Table 11), hits marked with an asterisk (*) are included on the curated list.

REF		Score	Peptides	Coverage	Gene	Name
Q9P2Y5	*	6405	434	72%	UVRAG	UV radiation resistance-associated gene protein
Q9BVA1	*	2046	88	58%	TUBB2B	Tubulin beta-2B chain
P68363	*	2010	85	62%	TUBA1B	Tubulin alpha-1B chain
Q13509		1461	48	30%	TUBB3	Tubulin beta-3 chain
Q05639		1173	69	32%	EEF1A2	Elongation factor 1-alpha 2
P68032		790	60	34%	ACTC1	Actin, alpha cardiac muscle 1
Q6S8J3		556	21	9%	POTEE	POTE ankyrin domain family member E
Q71U36		389	16	30%	TUBA1A	Tubulin alpha-1A chain
P55735		385	11	20%	SEC13	Protein SEC13 homolog
Q14257		345	17	29%	RCN2	Reticulocalbin-2
A6NKZ8		314	17	10%		Putative tubulin beta chain-like protein ENSP00000290377
Q8TEB1	*	312	14	22%	DCAF11	DDB1- and CUL4-associated factor 11
Q6PEY2		287	16	24%	TUBA3E	Tubulin alpha-3E chain
Q8NHW5		279	16	29%	RPLP0P6	60S acidic ribosomal protein P0-like
P62829		264	14	37%	RPL23	60S ribosomal protein L23
O95816		237	16	40%	BAG2	BAG family molecular chaperone regulator 2
P31943		236	12	18%	HNRNPH1	Heterogeneous nuclear ribonucleoprotein H
P13929		232	5	7%	ENO3	Beta-enolase
Q8N122	*	227	19	14%	RPTOR	Regulatory-associated protein of mTOR
Q9H853		220	6	10%	TUBA4B	Putative tubulin-like protein alpha-4B
P42677		208	14	14%	RPS27	40S ribosomal protein S27
Q9H4B7		197	8	7%	TUBB1	Tubulin beta-1 chain
O95831		193	17	26%	AIFM1	Apoptosis-inducing factor 1, mitochondrial
Q99570	*	193	15	10%	PIK3R4	Phosphoinositide 3-kinase regulatory subunit 4
P10809		188	16	21%	HSPD1	60 kDa heat shock protein, mitochondrial
O14654	*	185	13	12%	IRS4	Insulin receptor substrate 4
P55884		179	4	5%	EIF3B	Eukaryotic translation initiation factor 3 subunit B
Q13263	*	176	10	8%	TRIM28	Transcription intermediary factor 1-beta
P63167	*	161	5	37%	DYNLL1	Dynein light chain 1, cytoplasmic
P83731		160	13	32%	RPL24	60S ribosomal protein L24
P26373		158	18	36%	RPL13	60S ribosomal protein L13
P62306		151	3	9%	SNRPF	Small nuclear ribonucleoprotein F
Q02878		149	6	22%	RPL6	60S ribosomal protein L6
P46736		143	3	3%	BRCC3	Lys-63-specific deubiquitinase BRCC36
Q96IX5		143	4	43%	USMG5	Up-regulated during skeletal muscle growth protein 5
P52597		126	13	17%	HNRNPF	Heterogeneous nuclear ribonucleoprotein F
P33176	*	119	5	5%	KIF5B	Kinesin-1 heavy chain
O15372		111	7	14%	EIF3H	Eukaryotic translation initiation factor 3 subunit H
P46782		111	8	16%	RPS5	40S ribosomal protein S5
P14136		110	4	5%	GFAP	Glial fibrillary acidic protein
Q6ZMR3		109	3	7%	LDHAL6A	L-lactate dehydrogenase A-like 6A
Q13347		107	11	33%	EIF3I	Eukaryotic translation initiation factor 3 subunit I
P62195		106	6	7%	PSMC5	26S protease regulatory subunit 8
Q16718		104	2	8%	NDUFA5	NADH dehydrogenase [ubiquinone] 1 alpha subcomplex subunit 5
P60468		103	4	37%	SEC61B	Protein transport protein Sec61 subunit beta
P43243		102	16	14%	MATR3	Matrin-3
P53675	*	95	5	1%	CLTCL1	Clathrin heavy chain 2
Q96EY1		93	4	6%	DNAJA3	DnaJ homolog subfamily A member 3, mitochondrial
Q6ZMR3		90	4	3%	LDHAL6A	L-lactate dehydrogenase A-like 6A
P27635		86	15	35%	RPL10	60S ribosomal protein L10
Q15390		84	4	11%	MTFR1	Mitochondrial fission regulator 1
Q96L21		84	14	38%	RPL10L	60S ribosomal protein L10-like
Q13155		82	3	7%	AIMP2	Aminoacyl tRNA synthase complex-interacting multifunctional protein 2
O00743		80	7	17%	PPP6C	Serine/threonine-protein phosphatase 6 catalytic subunit
Q8NEB9	*	78	4	3%	PIK3C3	Phosphatidylinositol 3-kinase catalytic subunit type 3
P05109		76	2	11%	S100A8	Protein S100-A8
P62942		76	2	8%	FKBP1A	Peptidyl-prolyl cis-trans isomerase FKBP1A
Q9P253		76	2	2%	VPS18	Vacuolar protein sorting-associated protein 18 homolog
P62249		72	8	30%	RPS16	40S ribosomal protein S16

P04844		71	3	3%	RPN2	Dolichyl-diphosphooligosaccharide--protein glycosyltransferase subunit 2
P53618	*	69	7	6%	COPB1	Coatomer subunit beta
Q12904		69	7	29%	AIMP1	Aminoacyl tRNA synthase complex-interacting multifunctional protein 1
Q9Y5A9		66	2	2%	YTHDF2	YTH domain family protein 2
P62829		65	4	32%	RPL23	60S ribosomal protein L23
O00165		63	2	8%	HAX1	HCLS1-associated protein X-1
Q96S19		63	6	12%	C16orf13	UPF0585 protein C16orf13
O43175		60	4	6%	PHGDH	D-3-phosphoglycerate dehydrogenase
Q14157		57	3	2%	UBAP2L	Ubiquitin-associated protein 2-like
Q8TCT9		57	2	5%	HM13	Minor histocompatibility antigen H13
Q8NC51		54	1	3%	SERBP1	Plasminogen activator inhibitor 1 RNA-binding protein
P25705		52	12	15%	ATP5A1	ATP synthase subunit alpha, mitochondrial
P46779		52	13	45%	RPL28	60S ribosomal protein L28
P63220		52	3	33%	RPS21	40S ribosomal protein S21
P58546		51	1	14%	MTPN	Myotrophin
Q9Y266		51	2	10%	NUDC	Nuclear migration protein nudC
O15160		50	3	10%	POLR1C	DNA-directed RNA polymerases I and III subunit RPAC1
O75190		50	4	9%	DNAJB6	DnaJ homolog subfamily B member 6
P36578		50	3	8%	RPL4	60S ribosomal protein L4
P49207		50	5	16%	RPL34	60S ribosomal protein L34
Q9Y2R0		45	4	17%	CCDC56	Coiled-coil domain-containing protein 56
Q8N4V1		44	2	18%	MMGT1	Membrane magnesium transporter 1
Q9NYH9		44	4	1%	UTP6	U3 small nucleolar RNA-associated protein 6 homolog
P46821		43	3	1%	MAP1B	Microtubule-associated protein 1B
P78559		43	3	1%	MAP1A	Microtubule-associated protein 1A
Q86U44		43	2	N/A	METTL3	N6-adenosine-methyltransferase 70 kDa subunit
Q9H269		43	1	1%	VPS16	Vacuolar protein sorting-associated protein 16 homolog
Q9UBP0	*	39	6	6%	SPAST	Spastin
Q9BV73		31	2	0%	CEP250	Centrosome-associated protein CEP250
Q9NQT8		23	5	1%	KIF13B	Kinesin-like protein KIF13B
Q9Y2H2		18	2		INPP5F	Phosphatidylinositide phosphatase SAC2

9.3 APPENDIX C

Appendix C – UVRAG non-phospho biotin peptide interacting proteins from experiment described in Table 12. all proteins with over 2 unique peptides shown.

REF	Score	Peptides (Unique)	Gene	Name
P20029	2568	96 (79)	GRP78	78 kDa glucose-regulated protein
P17879	366	10 (8)	HS71B	Heat shock 70 kDa protein 1B
P38647	1290	47 (36)	GRP75	Stress-70 protein
P11499	155	6 (3)	HS90B	Heat shock protein HSP 90-beta
Q61545	137	14 (3)	EWS	RNA-binding protein EWS

9.4 APPENDIX D

Appendix D – UVRAG phospho biotin peptide interacting proteins from experiment described in Table 12, all proteins with over 2 unique peptides shown.

REF	Score	Peptides (Unique)	Gene	Name
P62259	2097	102 (78)	1433E	14-3-3 protein epsilon
Q9CQV8	1770	88 (60)	1433B	14-3-3 protein beta/alpha
P61982	1631	89 (65)	1433G	14-3-3 protein gamma
P68510	1547	67 (56)	1433F	14-3-3 protein eta
P63101	1233	50 (40)	1433Z	14-3-3 protein zeta/delta
P68254	696	38 (25)	1433T	14-3-3 protein theta
P20029	1419	58 (44)	GRP78	78 kDa glucose-regulated protein
P17879	258	7 (5)	HS71B	Heat shock 70 kDa protein 1B
P38647	991	45 (31)	GRP75	Stress-70 protein, mitochondrial
P11499	463	20 (14)	HS90B	Heat shock protein HSP 90-beta
P07901	358	11 (10)	HS90A	Heat shock protein HSP 90-alpha
P08113E	130	7 (5)	ENPL	Endoplasmin
Q61545	184	10 (4)	EWS	RNA-binding protein EWS
P58252	146	9 (6)	EF2	Elongation factor 2
P63038	89	4 (3)	CH60	60 kDa heat shock protein, mitochondrial
P52480	78	5 (2)	KPYM	Pyruvate kinase isozymes M1/M2
P16381	74	5 (2)	DDX3L	Putative ATP-dependent RNA helicase Pl10
Q99PT1	71	2 (2)	GDIR1	Rho GDP-dissociation inhibitor 1
Q61753	67	4 (2)	SERA	D-3-phosphoglycerate dehydrogenase
P17182	61	5 (2)	ENOA	Alpha-enolase
E9Q557	56	17 (3)	DESP	Desmoplakin
P01631	51	2 (2)	KV2A7	Ig kappa chain V-II region 26-10
P10630	47	2 (2)	IF4A2	Eukaryotic initiation factor 4A-II
Q8C120	33	6 (2)	SH3R3	SH3 domain-containing RING finger protein 3
Q8BIJ7	29	6 (2)	RUFY1	RUN and FYVE domain-containing protein 1
Q8VDD5	25	4 (2)	MYH9	Myosin-9
Q7TN37	22	4 (2)	TRPM4	Transient receptor potential cation channel subfamily M member 4